

**Establishment of the body axes in *Xenopus laevis*  
through *goosecoid*, *myosin 1d* and *bicaudal c***

Dissertation for Obtaining the Doctoral Degree  
of Natural Sciences (Dr. rer. nat.)

Faculty of Natural Sciences  
University of Hohenheim

Institute of Biology, Dept. of Zoology (190z)

submitted by

**Markus Ferdinand Maerker**

from Stuttgart-Bad Cannstatt

2021

Dean: Prof. Dr. Uwe Beifuss

1st reviewer: apl. Prof. Dr. Axel Schweickert

2nd reviewer: Prof. Dr. Heinz Breer

Submitted on: April 14<sup>th</sup>, 2021

Oral examination on: July 1<sup>st</sup>, 2021

The present work was accepted by the faculty of Natural Science as “Dissertation for obtaining the Doctoral Degree of Natural Science (Dr.rer.nat.)” on April 16<sup>th</sup>, 2021.

**Affidavit according to Sec. 7(7) of the University of Hohenheim doctoral degree regulations for Dr. rer. nat.**

1. For the dissertation submitted on the topic

Establishment of the body axes in *Xenopus laevis* through *goosecoid*, *myosin 1d* and *bicaudal c*

I hereby declare that I independently completed the work.

2. I only used the sources and aids documented and only made use of permissible assistance by third parties. In particular, I properly documented any contents which I used - either by directly quoting or paraphrasing - from other works.

3. I did not accept any assistance from a commercial doctoral agency or consulting firm.

4. I am aware of the meaning of this affidavit and the criminal penalties of an incorrect or incomplete affidavit.

I hereby confirm the correctness of the above declaration: I hereby affirm in lieu of oath that I have, to the best of my knowledge, declared nothing but the truth and have not omitted any information.

Kirchheim/Teck, 13.04.2021

**Place and Date**

**Signature**

## Abstract

The bilaterian body plan consists of three body axes: the anteroposterior (AP; head-trunk/tail), the dorsoventral (DV; back-belly) and the left-right (LR; placement of inner organs) axis. Axis formation occurs during early embryogenesis and is critical for further development and viability of the embryo. In this comprehensive study three highly conserved determinants were functionally analyzed in the context of axis development.

The first chapter of this work covers the autoregulatory, homeodomain containing, repressor gene *gooseoid* (*gsc*), whose most prominent expression marks the Spemann-(Mangold) organizer (SO). The SO is the primary dorsal signaling center and is instructive for tissue patterning along the DV and AP axes. Transplanting the SO or misexpressing *gsc* on the opposite ventral side of an embryo is sufficient to establish a new/secondary AP axis.

However, its function during normal development in the SO remained enigmatic as the *gsc* loss of function (LOF) lead to no severe early developmental defects. To elucidate the function of *gsc*, timed gain of function (GOF) experiments were performed. Gsc efficiently repressed the planar cell polarity (PCP)/Wnt signaling pathway leading to severe gastrulation and neurulation defects. This novel Gsc function was correlated with two vertebrate specific domains, suggesting an evolutionary new function of Gsc with the emergence of jaws/neural crests in vertebrates.

The second chapter of this study addresses the functions of Myosin1d (Myo1d) and Bicaudal c1 (Bicc1) during the LR axis determination in vertebrates. In this group LR symmetry breakage takes place at a ciliated epithelium called LR organizer (LRO). The initial cue for the asymmetric LR axis development is a cilia-driven leftward fluid flow. These cilia have to be correctly polarized through PCP/Wnt signaling. Interestingly, the invertebrate *Drosophila melanogaster* also displays a distinct LR axis but uses a cilia independent, yet not fully understood, mechanism. It depends on a *myo1d* homologous gene, *myo31DF*, and PCP. To unravel a potential common evolutionary origin of the bilaterian LR axis *myo1d* was analyzed during *Xenopus laevis* lateralization. Myo1d LOF experiments disturbed LR axis formation by compromising PCP dependent outgrowth and polarization of LRO cilia. These experiments link the PCP/Myosin based mechanism of flies to the newly evolved cilia/flow dependent mode of vertebrate LR axis determination suggesting actomyosin as common ancestral LR determinant.

Contrary to Myo1d, Bicc1 was already described for its function during polarization of flow producing LRO cilia. However *bicc1*'s expression is most prominent in the sensory LRO cells (sLRO). These cells detect the fluid flow and translate it into left-sided signaling of the morphogen Nodal1 and consequently asymmetric LR axis formation. These cells



downregulate the expression of the secreted Nodal1 antagonist *DAN domain family member 5 (dand5)* in response to flow.

Bicc1`s function was re-evaluated with respect to its function in sLRO cells. *Ex vivo* and *in vivo* experiments involving GOF as well as LOF experiments showed that Bicc1 regulates both *dand5* and *nodal1* via a direct and indirect post-transcriptional mechanism, respectively. In the process of *dand5* regulation several other LR determinants and regulatory events were linked with the Bicc1 dependent mechanism: Dicer1 dependent microRNA repression of *dand5* and a proposed cation channel Polycystin 2 mediated Bicc1 modification. These results highlight the importance of a tightly controlled Dand5 protein level as decisive for the overall outcome of the LR symmetry breakage in vertebrates.

## Zusammenfassung

Der Körperbauplan von Bilateria setzt sich aus drei Körperachsen zusammen: Der anteroposterioren (AP; Längsachse), der dorsoventralen (DV; Rücken-Bauch) und der links-rechts (LR, Anordnung der inneren Organe) Achse. Die Körperachsenbildung findet während der frühen Embryonalentwicklung statt und ist entscheidend für die weitere Entwicklung und die Lebensfähigkeit des Embryos. In dieser umfassenden Arbeit wurden drei hoch konservierte Determinanten auf ihre Funktion während der Achsenentwicklung analysiert.

Das erste Kapitel dieser Arbeit beschreibt die Funktion des autoregulatorischen Repressors und Homeoboxgens *gooseoid* (*gsc*), dessen bekannteste Expression den Spemann- (Mangold) Organisator (SO) markiert. Der SO ist das primäre dorsale Signalzentrum und bekannt für seine instruktive gewebespezifizierende Funktion entlang der AP- und der DV-Achse. Transplantation des SO oder Missexpression von *gsc* auf der gegenüberliegenden, ventralen, Seite des Embryos, ist ausreichend, um eine neue/zweite AP Körperachse zu erzeugen. Trotzdem blieb seine Funktion im SO während der normalen Entwicklung rätselhaft, da ein Funktionsverlust zu keinen massiven frühen Entwicklungsproblemen führte. Um die Funktion von *gsc* herauszufinden wurden zeitlich und räumlich terminierte Überexpressionen durchgeführt. *Gsc* reprimierte effizient den Planaren Zellpolaritäts (PCP)/Wnt Signalweg was zu ernsthaften Gastrulations- und Neurulationsdefekten führte. Die neu beschriebene Funktion von *Gsc* konnte mit zwei Wirbeltier-spezifischen Domänen korreliert werden. Dies suggerierte eine evolutionär neue Funktion von *Gsc* mit der Entstehung von Kiefern und Neuralleistenzellen in Wirbeltieren.

Das zweite Kapitel dieser Arbeit behandelt die Funktion von Myosin1d (*Myo1d*) und Bicaudal c1 (*Bicc1*) während der LR Achsenentwicklung in Wirbeltieren. In dieser Tiergruppe wird die LR Symmetrie durch ein ciliertes Epithel, den sogenannten LR Organisator (LRO), gebrochen. Das erste Signal für die asymmetrische LR Entwicklung ist ein durch Cilien erzeugter linksgerichteter Flüssigkeitsstrom. Dafür müssen diese Cilien durch den PCP Signalweg korrekt polarisiert sein. Interessanterweise zeigt das wirbellose Tier *Drosophila melanogaster* auch eine eindeutige LR-Achse, für die sie allerdings einen Zilien-unabhängigen Mechanismus verwenden. Dieser ist bis heute noch nicht eindeutig geklärt, beruht aber auf dem *myo1d* orthologen Gen *myo31DF* und dem PCP Signalweg. Um einen potentiellen evolutionären Ursprung der LR Achsenentwicklung in Bilateria zu entschlüsseln, wurde *myo1d* während der Lateralisierung in *Xenopus laevis* analysiert. Funktionsverlust Experimente von *Myo1d* resultierten dabei in einer gestörten LR Achsenentwicklung, basierend auf einer Störung des PCP abhängigen Auswachsens und der Polarisierung der LRO-Cilien. Diese Experimente verbinden den PCP/Myosin abhängigen Mechanismus von Fliegen mit dem neu evolvierten Cilien/Flüssigkeitsstrom abhängigen Mechanismus der LR

Achsenentwicklung in Wirbeltieren. Somit wird ein Actomyosin abhängiger Mechanismus als gemeinsamer ursprünglicher LR Achsendeterminant für Bilateria impliziert.

Im Gegensatz zu *Myo1d* wurde für *Bicc1* schon eine Funktion während der Polarisierung der LRO Cilien beschrieben. Dennoch ist die markanteste Expression von *bicc1* in den sensorischen LRO Zellen (sLRO), welche den Flüssigkeitsstrom detektieren und in ein linksseitiges Signal des Morphogens *Nodal1* umwandeln. Dieses Signal resultiert dann in der Entstehung der asymmetrischen LR Achse. Als Antwort auf den Flüssigkeitsstrom wird die Expression von dem sekretierten *Nodal1*-Antagonisten *DAN domain family member 5* (*dand5*) in den sLRO Zellen runter reguliert. Die Funktion von *Bicc1* sollte im Bezug auf die Funktion in den sLRO Zellen reevaluiert werden. *Ex vivo* und *in vivo* Funktionsverlust und Funktionsgewinn Experimente zeigten, dass *Bicc1* sowohl *dand5* direkt als auch *nodal1* indirekt post-transkriptional reguliert. Desweiteren wurden auch andere LR Determinanten mit dem Mechanismus der *Bicc1* abhängigen *dand5* Regulation vernetzt: Die *Dicer1* abhängige microRNA vermittelte Repression von *dand5* und die mögliche Modifikation von *Bicc1* in Abhängigkeit vom Kationen-Kanal *Polycystin 2* (*Pkd2*). Diese Ergebnisse verdeutlichen maßgeblich die Bedeutung eines engmaschig kontrollierten *Dand5* Proteinlevels für das Ergebnis des LR Symmetriebruchs in Wirbeltieren.

## Table of contents

Affidavit .....	I
Abstract .....	II
Zusammenfassung.....	IV
Table of contents.....	VI
Abbreviations .....	VIII
1. Introduction.....	1
1.1 Axes development in vertebrates .....	1
1.1.1 Fertilization, cortical rotation and cleavage stages: establishment of the first body axis, the DV axis. ....	1
1.1.2 Spemann organizer and pre-specification of the three germ layers.....	2
1.1.3 Gastrulation: determination of the second body axis, the DV axis, and germ layer positioning.....	2
1.2 Neurulation and determination of the last body axis, the LR axis .....	4
1.2.1 Neurulation .....	4
1.2.2 Breaking the LR symmetry: The left-right organizer .....	4
1.2.3 Breaking the LR symmetry: The Nodal signaling cascade .....	5
1.3 The TGF- $\beta$ superfamily .....	5
1.3.1 TGF- $\beta$ subfamily: Nodal signaling pathway .....	6
1.4 Wnt signaling pathway .....	6
1.4.1 Canonical Wnt pathway .....	6
1.4.2 Planar cell polarity pathway .....	7
1.5 MicroRNA pathway .....	8
1.6 Aim of this work .....	9
2. Original research chapter .....	11
2.1 Anteroposterior and dorsoventral -axis development.....	11
A novel role of the organizer gene Goosecoid as an inhibitor of Wnt/PCP-mediated convergent extension in Xenopus and mouse .....	11
2.2 Left-right axis development .....	39
A Conserved Role of the Unconventional Myosin1d in Laterality Determination.....	39
Bicc1 and Dicer regulate left-right patterning through post-transcriptional control of the Nodal-inhibitor Dand5.....	56
2.3 Author's contribution .....	99

3. Discussion .....	101
3.1 The novel function of <i>gsc</i> during the evolution of vertebrates .....	101
3.2 Myo1d: An ancestral effector of the cytoskeleton based mechanism for the LR axis determination .....	102
3.3 Bicc1 as key regulator of LR axis determinants .....	103
3.4 Conclusion .....	105
References .....	106
Curriculum vitae .....	129
Danksagung .....	132

### Abbreviations

3'UTR	3'untranslated region
AA	amino acids
ActRIIA/B	Activin A/B receptor type II
AC	apical constriction
Ago	Argonaute
AP	anteroposterior
APC	Adenomatous polyposis coli
BMP	Bone morphogenetic protein
CaMK II	Ca <sup>2+</sup> /calmodulin-dependent protein kinase II
CE	convergent extension
Cdc42	Cell division control protein 42 homolog
CK1	Casein kinase 1
coSmad	common Smad
cLRO	central LRO
Ctnnb1	CaMK II catenin beta 1
Daam1	Disheveled-associated activator of morphogenesis 1
Dand5	DAN domain family member 5
Dgo	Diego
Dia1	Diaphanous related formin 1
<i>D. melanogaster</i>	<i>Drosophila melanogaster</i>
DV	dorsoventral
Dvl/Dsh	Dishevelled
eh-1	En homology region 1
e.g.	example given
Fmi	Flamingo
Fz	Frizzled
GBP	GSK3-binding protein
Gdf3	Growth differentiation factor 3
GOF	gain of function
GRP	gastrocoel roof plate
Gsc	Gooseoid
GSK3	Glycogen synthase kinase 3
HD	homeodomain
JNK	c-Jun N-terminal kinases
LEF	Lymphoid enhancer binding factor
LOF	loss of function

LPM	lateral plate mesoderm
LR	left-right
LRO	left-right organizer
LRP	low-density lipoprotein receptor related protein
MAPK	Mitogen-activated protein kinase
MBT	midblastula transition
miR	microRNA
Mixer	Mix-like endodermal regulator
Myo1d	Myosin 1d
nt	nucleotide
Pitx2	Paired like homeodomain 2
Pk	Prickle
Pkd2	Polycystin 2
pre-miR	precursor miR
pri-miR	primary miR
R-Smad	receptor regulated Smad
Rac1	Rac family small GTPase 1
Rhoa	Ras homolog family member A
RI	radial intercalation
RISC	RNA-induced silencing complex
siRNA	small interfering RNA
SM	superficial mesoderm
sLRO	sensing LRO
Stbm	Strabismus
SO	Spemann-(Mangold) organizer
Tbxt	T-box gene t
TGF- $\beta$	Transforming-growth factor- $\beta$
TBMO	translation blocking morpholino oligomere
tpMO	target protector morpholino oligomere
<i>X. laevis</i>	<i>Xenopus laevis</i>

## 1. Introduction

### 1.1 Axes development in vertebrates

The generation of the three primary body axes is one of the first and most important steps during early development of all vertebrates. These axes, termed as anteroposterior (AP; head-trunk/tail), the dorsoventral (DV; back-belly) and the left-right (LR; arrangement of many inner organs) axis, share similar overlapping mechanisms and genes to establish the proper body plan (Bénazéraf and Pourquié, 2013; Blum et al., 2014a; Durston, 2015; Meinhardt, 2006). Therefore it can be assumed if you cover a mechanism in several model organisms among e.g. anamniotic and amniotic vertebrates it is likely a conserved feature of these phyla. As the main part of this thesis focuses on axis determination in the model organism *Xenopus laevis* (Daudin, 1802), the introduction is mainly restricted to the development of *X. laevis* and only briefly covers other organisms.

#### 1.1.1 Fertilization, cortical rotation and cleavage stages: establishment of the first body axis, the DV axis.

The oocyte of *X. laevis* already has an intrinsic axis, the animal-vegetal axis. This axis is defined by pigmented granules at the animal pole and an asymmetric distribution of yolk, mRNAs and proteins, favoring the vegetal pole. The sperm entry takes place at the animal hemisphere through asymmetrically localized glycoproteins (Kubo et al., 2010; Nagai et al., 2009; Sindelka et al., 2018). As consequence of the sperm entry (later ventral side), the nucleus and the centriole are intaken in the oocyte, which initiates the cortical rotation. This rearrangement of the cytoskeleton, emanating from the centriole, leads to a microtubule based rotation of the outer/cortical cytoplasm and associated proteins/mRNAs (approximately 30 °; (Elinson and Rowning, 1988; Houliston and Elinson, 1991; Vincent and Gerhart, 1987). The shift of maternal determinants like the mRNAs *vegt* and *vg1* as well as proteins like Dishevelled (Dsh/Dvl) and the GSK3-binding protein (GBP) determines the later dorsal side of the embryo (He et al., 1995; Weaver and Kimelman, 2004; Yost et al., 1998). These components belong to two main signaling pathways, namely the transforming-growth factor- $\beta$  (TGF- $\beta$ ) signaling pathway (more information on TGF- $\beta$  in 1.3) and the canonical Wnt pathway (more information on Wnt signaling in 1.4.1). Both are required to induce the Nieuwkoop centre, which is a dorsal signaling centre (Larabell et al., 1997; Manes and Elinson, 1980; Schneider et al., 1996; Vincent, Oster and Gerhart, 1986). After the first cleavage, the embryo undergoes fast unequal radial holoblastic cleavages with a low level of gene transcription until the midblastula transition (MBT) at the 12<sup>th</sup> cell cycle. The MBT is accompanied by not only a name shift from morula to a blastula embryo, but also by a cell cycle shift and an activation of the zygotic genome (Newport and Kirschner, 1982; Valles et al., 2002; Yang et al., 2002).



### 1.1.2 Spemann organizer and pre-specification of the three germ layers

During blastula stages the embryo pre-patterns the three germ layers: The ectoderm, which will give rise to the nervous system and the skin; the mesoderm, which will give rise to e.g. heart muscles and the notochord (a flexible, mostly transient, embryonic rod); and the endoderm, which will form most of the gastrointestinal tract except e.g. the pharynx (Urry et al., 2019). The Nieuwkoop center, part of the dorsal endoderm, induces the so called Spemann-(Mangold) organizer (SO). This endo-/mesoderm induction is accomplished by the previously mentioned Wnt- and TGF- $\beta$  signals, which induce the transcription of specific homeobox genes like *nieuwkoid*, *lhx1* (previously *lim1*) and the autoregulatory homeobox gene *gooseoid* (*gsc*) (Bae, Reid and Kessler, 2011; Fan and Sokol, 1997; Koos and Ho, 1998; Spemann and Mangold, 1924; Taira et al., 1992). Other genes like the ventral mesodermal repressor Tcf3 switch to an activator function when combined with active Wnt signals in the dorsal mesoderm. Conversely, family members of microRNA-15 (miR-; more information on miRs in 1.5), which control the TGF- $\beta$  signal in the ventral mesoderm, are inhibited by the Wnt signals and therefore an additional TGF- $\beta$  gradient (ventral to dorsal mesoderm) is established. The ectoderm is secured against these endo-/mesoderm signals by the blastocoel a fluid filled cavity which ensures distance between endoderm (vegetal pole) and ectoderm (animal pole; (Gerhart, 1999; Martello et al., 2007; Smithers and Jones, 2002; Vonica and Gumbiner, 2007; Zhang et al., 1998). The function of the SO is to control the Wnt- and the Bone morphogenetic protein (BMP)-signaling pathways to induce dorsal structures along the AP-axis. This is ensured by expressing BMP antagonists like *chordin*, *noggin*, *folliculin* and Wnt antagonists like *cerberus* (also a BMP and TGF- $\beta$  antagonist) and *dickkopf*. Secretion of these components leads to repression of both pathways (BMP and Wnt) which leads to a differentiation of anterior head structures. Inhibition of the BMP-pathway alone in a more posterior region leads to trunk structures. Meanwhile, the activation of both pathways in the most posterior region specifies posterior dorsal structures and epidermis (Gawantka et al., 1995; Kiecker and Niehrs, 2001; Petersen and Reddien, 2009; Piccolo et al., 1996; Piccolo et al., 1997; Piccolo et al., 1999; Silva et al., 2003).

### 1.1.3 Gastrulation: determination of the second body axis, the DV axis, and germ layer positioning

The embryonic induction emanating from the SO goes hand in hand with the induction of the process of gastrulation and the correct positioning of all three germ layers in the body cavity. Four distinct mechanisms are indispensable for this process.

1. Epiboly: The animal pole cells (ectoderm) have to spread over the vegetal hemisphere. This is accomplished by thinning through radial intercalation (RI): cells elongate and migrate from the inner into the outer cell layer, thereby transforming the three to two cell layers. Part

of this spreading also involves proliferation (Keller and Miksis, 1980; Keller and Schoenwolf, 1977; Saka and Smith, 2001).

2. The vegetal rotation: Shortly before gastrulation starts, vegetal cells press asymmetrically against the dorsal side of the blastocoel and replace it to form the archenteron (gastrocoel or primitive gut; (Gilbert and Barresi, 2020; Nieuwkoop and Faber, 1994).

3. Bottle cell formation, migration and involution: localized apical constriction (AC) of cells at the dorsal marginal zone leads to formation of the blastopore lip at the SO. The cells that invaginate first represent the leading edge. They crawl/migrate into the archenteron through lamellipodia. This generates a traction force for the intercalation of the mediolateral cells (Hardin and Keller, 1988; Keller et al., 2000; Lee and Harland, 2007; Wallingford, Fraser and Harland, 2002). Even though the endoderm and the mesoderm are connected they are always separated by a tight extracellular space (Brachet's cleft; (Gorny and Steinbeisser, 2012). This separation and the timing of involution (endoderm followed by mesoderm) leads to the correct establishment of the AP axis. When the first endodermal cells come to rest under the prospective head ectoderm they are potent enough to stimulate the head and heart gene expression.

Mesodermal cells which migrate right after the leading edge will later give rise to the prechordal plate (precursor of the head mesoderm). These cells express *gsc* to induce head expression. This is accomplished by repressing head repressor genes and is therefore a double repressor function, which is a common feature in early development (like the inhibition of miR-15 in the dorsal mesoderm above). Finally, the future notochordal and somitic cells, which are important to pattern the nervous system, involute while the ventral lip appears and more meso-/endodermal precursor cells involute (Gilbert and Barresi, 2020; Rankin et al., 2011; Winklbauer and Schürfeld, 1999).

4. Convergence and extension: The intercalation of lateral cells in the midline through RI (convergence) narrows the embryo in respect to the LR axis. This drives the AP axis elongation and thereby elongates the notochord of the embryo (extension).

Important signaling processes which are involved in this include, but are not limited to, the Wnt planar cell polarity pathway (Wnt/PCP signaling; more information on PCP in 1.4.2),  $Ca^{2+}$  waves and cadherin mediated adhesion (Keller et al., 2008; Shindo et al., 2019; Shindo and Wallingford, 2014).

## 1.2 Neurulation and determination of the last body axis, the LR axis

### 1.2.1 Neurulation

Following the process of gastrulation is the neurulation. Included in the process of neurulation is the closure of the neural tube laying the foundation for the central nervous system. The floorplate of the neural plate, which was specified during gastrulation, gets further specified by the underlying notochord. The flat neural plate then forms lateral neural folds through AC (Gilbert and Barresi, 2020; Sokol, 2016). After the neural plate folding, the basal cells elongate basolaterally and thereby promote fold elevation and convergence at the midline. This, together with RI to flatten the neural plate and the fusion of the neural fold tips at the dorsal midline, gives rise to the single-layered neural tube covered by epithelial cells (Davidson and Keller, 1999; Edlund, Davidson and Keller, 2013; Schroeder, 1970; Schroeder, 1973; Shih and Keller, 1992; Sokol, 2016). In the anterior region that forms the fore- and hindbrain, neural tube closure occurs without mediolateral convergent extension (CE) and is driven by RI through AC (Prager et al., 2017; Shih and Keller, 1992; Wallingford and Harland, 2002). After the formation of the neural tube, cells of its floor plate give rise to the neural crest (sometimes called the fourth germ layer). These cells delaminate and migrate into the body to give rise to various cell types e.g. craniofacial cartilage/bone, smooth muscle and glia cells (Gilbert and Barresi, 2020; Shyamala et al., 2015).

### 1.2.2 Breaking the LR symmetry: The left-right organizer

In contrast to the other two body axes the left right axis is only visible in the asymmetric arrangement of inner organs e.g. the heart and the liver (Blum et al., 2014a). The LR symmetry is broken by the left-right organizer (LRO; in *Xenopus* the gastrocoel roof plate, GRP). The notochordal/somitic cells which are part of the LRO come to lie at the posterior archenteron roof and are derivations from the superficial (dorsal) mesoderm (SM) during late blastula/early gastrula stages. It is a transient structure, which detaches later on, composed of hypochordal and notochordal cells (central; cLRO), which are bilaterally flanked by somitic more lateral sensing cells (sLRO; (Antic et al., 2010; Schweickert et al., 2007; Shook, Majer and Keller, 2004). The LRO cells are ciliated due to the prepatterning of the SM at the onset of gastrulation, which occurs through the master control gene of motile cilia, *forkhead box j1* (*foxj1*). While the cLRO cells harbor posterior polarized motile cilia, the sLRO cells have shorter, unpolarized, immotile, supposedly sensory cilia (Blum et al., 2014a; Boskovski et al., 2013; Shook, Majer and Keller, 2004; Stubbs et al., 2008). Recent findings implicated not only the Wnt/PCP signaling pathway, through proteins like the RNA binding protein Bicaudal c1 (Bicc1), but also strain through gastrulation as an important factor for ciliogenesis and polarization of these cells (Chien et al., 2018; Maisonneuve et al., 2009). Through beating in a counterclockwise manner the cLRO cilia produce an extracellular leftward fluid flow which is then sensed by the left sLRO. How sensing occurs at the sLRO is not fully understood yet,

but it supposedly is through the sLRO cilia. Currently two models try to approach this by implicating mechanosensitive cilia and/or by sensing morphogens which are distributed from the cLRO to the sLRO by flow (McGrath et al., 2003; Nonaka et al., 1998; Okada and Hirokawa, 1999; Tabin and Vogan, 2003). In the process of sensing, the importance of  $\text{Ca}^{2+}$  is heavily implied through cilia cation channels like Polycystin 2 (Pkd2; (Takao et al., 2013; Yoshida et al., 2012; Yuan et al., 2015)). Breaking the bilateral symmetry of the LR axis through a cilia based LRO also seems to be the ancestral mechanism in chordates, maybe even in deuterostomes, and therefore can be found in ancestral clades like sturgeons (Blum and Ott, 2018c; Bolker, 1993).

### 1.2.3 Breaking the LR symmetry: The Nodal signaling cascade

On a molecular level, there are several bilaterally symmetrically expressed genes in the sLRO cells like *growth differentiation factor 3* (*gdf3* previously *derrière*), the TGF- $\beta$  morphogen *nodal1* and the BMP/TGF/Wnt antagonist *DAN domain family member 5* (*dand5* previously *coco*). *Dand5* represses *Nodal1* in pre-flow stages (Bell et al., 2003; Schweickert et al., 2007; Vonica and Brivanlou, 2007). After the flow sensing event, *dand5* mRNA is downregulated on the left sLRO while *nodal1*, which is normally repressed by *Dand5*, is still symmetrically expressed. *Nodal1* is then released from the sLRO to the left lateral plate mesoderm (LPM), where it induces the Nodal signaling cascade resulting in expressing *nodal1*, *lefty2* (the extracellular antagonist of *Nodal1*) and the *paired like homeodomain 2* (*pitx2*). *pitx2* continues expression long after the Nodal signaling pathway in the organ anlage and is crucial for the asymmetric organogenesis. For the transport of *Nodal1* into the LPM, *Nodal1* has to dimerize with the symmetrically expressed *Gdf3* (equivalent to *gdf1* in mouse), enabling long range signaling to transfer *Nodal1* via sulfated proteoglycans in the extracellular matrix (Eimon and Harland, 2002; Lohr, Danos and Yost, 1997; Marjoram and Wright, 2011; Oki et al., 2007; Sampath et al., 1997; Schweickert et al., 2010; Vonica and Brivanlou, 2007).

### 1.3 The TGF- $\beta$ superfamily

The first TGF- $\beta$  family member was first described 1983. Since then, the superfamily members were separated in three distinct branches: the TGF- $\beta$  subfamily, the BMP and growth differentiation factor subfamily and the activin and inhibin subfamily (Assoian et al., 1983; Burt, 1992; Burt and Law, 1994). All family members have in common that they are cytokines important for proliferation and differentiation and bind to a type II TGF- $\beta$  receptor. This leads to the binding and activation of a type I TGF- $\beta$  receptor which then activates through phosphorylation various Smad proteins, which act as signal transducers and transcription factors for target genes (Faure et al., 2000; Gilbert and Barresi, 2020; Reissmann et al., 2001; Yan et al., 2002; Yeo and Whitman, 2001).

### 1.3.1 TGF- $\beta$ subfamily: Nodal signaling pathway

The first nodal ligand of the TGF- $\beta$  subfamily was found 1993 in mouse (Zhou et al., 1993). While higher vertebrates (human, mouse and chicken) only have a single Nodal ligand, lower vertebrates like fishes and frogs have multiple ligands (6 in *X. laevis*) which can act in a tissue and context dependent manner (Schier, 2003). The secreting Nodal ligand can emit long-range signals acting in a dose-dependent manner. Binding of the Nodal ligand to the complex of the serine-threonine kinase receptors ActRIIA/B (Activin A/B receptor type II) and the ActRIB/ALK4/7 receptor promotes binding of the co-receptor Cripto or Cryptic. This leads to the canonical Smad-cascade, resulting in a heterodimeric complex of receptor regulated Smad2 and Smad3 with the common Smad 4. This complex, together with co-transcription factors like Foxh1 and Mix-like endodermal regulator (Mixer), activates the Nodal signaling cascade (Dickmeis et al., 2001; Germain et al., 2000; Papanayotou et al., 2014; Reissmann et al., 2001; Schier, 2003; Yan et al., 2002; Yeo and Whitman, 2001).

### 1.4 Wnt signaling pathway

*wnt*, a composite of *wg* (*wingless*; *Drosophila melanogaster*, Meigen, 1830) and *int-1* (*integrated-1*; mouse), was found and described in non-vertebrates and vertebrates alike which reflects its conserved evolutionary nature. Wnt pathways are important for embryonic development from cell fate specification to cell migration and proliferation and have a well-characterized role in carcinogenesis. Wnt proteins are secreted glycosylated and palmitoylated signaling molecules of approximately 20 family members in vertebrates (19 in human, 20 in *X. laevis*) and approximately 15 different receptors and co-receptors (Hikasa and Sokol, 2013; MacDonald, Tamai and He, 2009; Nusse and Varmus, 2012; Willert and Nusse, 2012; <http://wnt.stanford.edu>) Generally, they are distinguished into three branches: the canonical Wnt/ $\beta$ -catenin pathway, the non-canonical Wnt/Frizzled (Fz) PCP pathway and the non-canonical Wnt/ $\text{Ca}^{2+}$  pathway (MacDonald, Tamai and He, 2009; Seifert and Mlodzik, 2007). They all underlie the same general mechanism for pathway induction: The secreted Wnt molecule binds a Fz-receptor and a pathway dependent co-receptor to transduce the signal to the cytoplasmic phosphoprotein Dvl. Dvl is dynamically controlled by phosphorylation, ubiquitination and degradation, which is the basis of the branches of the Wnt pathway that even antagonize each other (Axelrod et al., 1998; Bryja et al., 2009; Gao and Chen, 2010; Komiya and Habas, 2008; Torres et al., 1996).

#### 1.4.1 Canonical Wnt pathway

The canonical Wnt pathway is important for a large variety of cellular processes from proliferation and specification to cell survival (MacDonald, Tamai and He, 2009). In the absence of canonical Wnt ligands (e.g. Wnt3), Catenin beta 1 (Ctnnb1; previously  $\beta$ -catenin) is constantly ubiquitinated and therefore proteasomally degraded by the destruction/Axin

complex. This complex is composed of e.g. the scaffolding protein Axin, the tumor suppressor adenomatous polyposis coli (APC) gene product, casein kinase 1 (CK1), glycogen synthase kinase 3 (GSK3) (He et al., 2004; MacDonald, Tamai and He, 2009; Niehrs, 2012). When the Wnt ligand binds the Fz receptor and the co-receptor low-density lipoprotein receptor related protein (LRP) 6 or LRP5, the scaffold protein Dvl is recruited and LRP is phosphorylated. The Axin complex is then recruited to the Fz/LRP complex and inhibited, resulting in a stabilization and accumulation of Ctnnb1 in the cytoplasm. In the nucleus it forms complexes with TCF/lymphoid enhancer binding factor (LEF) and activates the expression of genes like *nodal3*, *bmp4* and *siamois* (Bilic et al., 2007; Brannon et al., 1997; Kimelman and Xu, 2006; MacDonald, Tamai and He, 2009; McKendry et al., 1997; Metcalfe and Bienz, 2011; Zheng et al., 2008). These complexes can be composed of different factors which include among others Fox transcription factors and Smad proteins. In absence of Ctnnb1 TCF/LEF inherit no transcriptional activity and exhibit a repressor function through binding the co-repressor Groucho (Eastman and Grosschedl, 1999; Funa et al., 2015; Gan et al., 2008; van den Bosch et al., 2015).

#### 1.4.2 Planar cell polarity pathway

In contrast to the canonical Wnt pathway, the PCP pathway mostly results in a direct response of the cytoskeleton, rather than a transcriptional response. It is important e.g. for gastrulation, ciliation, mitotic spindle orientation and polarity of a cell in general (Bellaïche et al., 2001; Park et al., 2006; Seifert and Mlodzik, 2007; Wallingford, Fraser and Harland, 2002). To accomplish this, PCP components are polarized/activated in different subregions of the cell, building a gradient of clues upon signaling. The core PCP proteins involved in this are Fz and Dvl but also Flamingo (Fmi, also known as Stan), Strabismus (Stbm, also known as Vang), Diego (Dgo), and Prickle (Pk; (Feiguin et al., 2001; Gubb et al., 1999; Taylor et al., 1998; Theisen et al., 1994; Usui et al., 1999; Vladar, Antic and Axelrod, 2009). Downstream of these core components the cytoskeleton is often regulated through modulation of small GTPases, specifically Ras homolog family member A (Rhoa), Rac family small GTPase 1 (Rac1) and Cell division control protein 42 homolog (Cdc42) eventually mediated through Disheveled-associated activator of morphogenesis 1 (Daam1; (Gao and Chen, 2010; Habas, Kato and He, 2001; Jaffe and Hall, 2005; Schlessinger, Hall and Tolwinski, 2009). In order to fully exhibit the PCP signal, the cell has to interpret not only long-range ligand driven PCP signaling through Vang and Fz but also short-range signaling without Wnt ligands through direct cell-cell transmembrane interactions (Strutt, 2003; Yang and Mlodzik, 2015). In some cases, the PCP pathway acts additionally through transcriptional responses through Rac1 and JNK (c-Jun N-terminal kinases; (Kirsch et al., 2020; Zeke et al., 2016).

### 1.5 MicroRNA pathway

Originally derived from small interfering RNA (siRNA), miRs are non-coding RNAs which degrade complementary RNA to protect against RNA viruses (Malone and Hannon, 2009; Shabalina and Koonin, 2008). In contrast to siRNA, miRs do not have to bind completely which gives them a huge subset of sequences to bind and repress. This is reflected by their importance during embryogenetic processes from the activation of the zygotic genome, germ layer differentiation, ciliogenesis to the interplay with important signaling pathways like the Nodal signaling pathway and the canonical Wnt pathway (Giraldez et al., 2006; Ma et al., 2016; Martello et al., 2007; Song et al., 2014; Wang et al., 2014). The primary miR (pri-miR), like other mRNAs, is transcribed and has a CAP and a poly-A tail. Then it is cleaved by a processor complex involving Drosha and double strand RNA-binding protein DiGeorge syndrome critical region gene 8 (Dgcr8 or pasha) resulting in a 70-80 nucleotide (nt) precursor miR (pre-miR) with a hairpin structure. Upon release into the cytoplasm the pre-miR gets matured to a 19-25 nt single-stranded miR by the RNase III family member Dicer. After that the mature miR is loaded onto the RNA binding protein Argonaute (Ago) 1, a core protein from the RNP which is part of the RNA-induced silencing complex (RISC) to repress the complementary mRNA (Bartel, 2018; Cai, Hagedorn and Cullen, 2004; Lee et al., 2002; Nguyen et al., 2015). While this is the canonical synthesis of miRs, it is only a percentage of all active miRs. miRs derived from introns or other small non-coding RNAs bypass the processing steps of Drosha/Dgcr8 or Dicer and feed into the active miR pool (Babiarz et al., 2008; Okamura et al., 2007; Ruby, Jan and Bartel, 2007; Xie and Steitz, 2014). The active cellular complement in which miRs are active is known as processing bodies (p-bodies or pi/gw-bodies). Upon binding of the RISC to an mRNA with the seed sequence (complementary sequence important to find the target mRNA) there are two possible modes of repression: 1. Degradation through endonucleolytic cleavage with a sufficient binding via the seed sequence, which is not as common in higher vertebrates as deadenylation as it is an ancestral mechanism in e.g. cnidaria or plants. 2. Silencing through imperfect binding of the seed sequence and sometimes reengagement into translation again (Brenques, Teixeira and Parker, 2005; Hubstenberger et al., 2017; Jones-Rhoades, Bartel and Bartel, 2006; Kulkarni, Ozgur and Stoecklin, 2010; Moran et al., 2014).

### 1.6 Aim of this work

The establishment of the three body axes is an important step during the development of bilateria. While there are similarities among phyla, overall ancestral conserved mechanisms are sometimes hard to determine among derived mechanisms. Even though many processes and genes which are involved in the establishment of the three body axes are known, the precise function and mechanism of many of them have yet to be discovered. Based on this the aim of this work was to define the function of *gsc* in AP and DV axes development as well as the function of *myosin 1d* (*myo1d*) and *bicc1* during the establishment of the LR axis.

The DV and AP axes development is linked to the formation of the SO. An important regulator in the SO is the homeodomain box gene *gsc*, which is able to induce a secondary axis upon misexpression/gain of function (GOF) in the ventral side of an embryo, showed no early developmental defects upon loss of function (LOF) in mice and *X. laevis*. This was despite its expression in the SO. Surprisingly the GOF of *gsc* in the dorsal tissues leads to gastrulation and neurulation defects, based on migratory defects (Cho et al., 1991; Rivera-Pérez et al., 1995; Ulmer, 2008; Ulmer, 2012; Yamada et al., 1995). Earlier publications also stated a role of *gsc* in various migratory cells such as explanted head mesenchymal cells and metastatic tumor cells (Hartwell et al., 2006; Luu et al., 2008; Niehrs et al., 1993). This lead to the assumption that *gsc* may play an important role in the establishment of the AP and DV axis, through most likely PCP mediated CE, which should be further investigated in this work.

LR asymmetries are known for protostomes and deuterostomes alike but while deuterostomes seem to use a nodal/cilia/flow based ancestral mechanism, protostomes seem to have different modes to break the LR symmetry, awaiting a clarification on an ancestral mode. While it is an exception that some derived vertebrates break LR symmetry without cilia, the fruit fly *D. melanogaster* breaks the bilateral LR symmetry with a non-cilia based mechanism and without Nodal signaling. It is known that *D. melanogaster*'s hindgut and genitalia rotate asymmetrically in respect to the LR axis, which depends on a PCP-based mechanism (Blum et al., 2014a; Boorman and Shimeld, 2002; Grande and Patel, 2009; Hozumi et al., 2006; Spéder, Adám and Noselli, 2006). An important protein for this mechanism is the unconventional Myo31DF (ortholog in *X. laevis* Myo1d) which interferes with adherens junctions and PCP pathway components (Fernandez-Gonzalez et al., 2009; Hozumi et al., 2006). In this work it should be analyzed if *myo1d* also interferes with the LR symmetry breakage in vertebrates, which rely on a cilia/Nodal based mechanism.

Concerning LR axis determination another factor which has an important role in PCP dependent LRO formation should be re-evaluated in terms of a new role. Remarkably *Bicc1*, an important factor for cilia polarization of the cLRO cells, shows the strongest expression



not in the cLRO but rather in the sLRO cells. This observation was not addressed during the initial publication and should be further addressed in this work for several reasons (Maisonneuve et al., 2009): The expression pattern of *bicc1* overlaps in the sLRO cells with *dand5*. Additionally, *dand5* mRNA degradation only occurs in up to 75 % of specimens, while over 95 % show a normal LR axis. Together, these two occurrences fit a general theme where post-transcriptional regulation leads to a discrepancy between number of transcripts and protein level (Becker et al., 2018; Keene, 2007). Being an RNA binding protein, Bicc1 was shown to bind the 3' untranslated region (3'UTR) of *dand5* and post-transcriptionally downregulate *dand5* translation, which could also be true in the context of the sLRO (Zhang et al., 2013). This lead to the postulation that *dand5* may be post-transcriptionally regulated through Bicc1 in the sLRO cells (Schweickert et al., 2010). In this work, this question and the involvement of miRs in the process will be followed up on.

## **2. Original research chapter**

### **2.1 Anteroposterior and dorsoventral axis development**

**A novel role of the organizer gene Goosecoid as an inhibitor of Wnt/PCP-mediated convergent extension in *Xenopus* and mouse**

<https://doi.org/10.1038/srep43010>

Reproduced with permission from Springer Nature

# SCIENTIFIC REPORTS

OPEN

## A novel role of the organizer gene *Gooseoid* as an inhibitor of Wnt/PCP-mediated convergent extension in *Xenopus* and mouse

Received: 01 August 2016  
Accepted: 18 January 2017  
Published: 21 February 2017

Bärbel Ulmer<sup>1,\*,\*</sup>, Melanie Tingler<sup>1,\*</sup>, Sabrina Kurz<sup>1,\*,\*</sup>, Markus Maerker<sup>1,\*,\*</sup>, Philipp Andre<sup>1</sup>, Dina Mönch<sup>1</sup>, Marina Campione<sup>1,2,3</sup>, Kirsten Deißler<sup>1</sup>, Mark Lewandoski<sup>2</sup>, Thomas Thumberger<sup>1,5</sup>, Axel Schweickert<sup>1</sup>, Abraham Fainsod<sup>3</sup>, Herbert Steinbeißer<sup>4</sup> & Martin Blum<sup>1</sup>

*Gooseoid* (*Gsc*) expression marks the primary embryonic organizer in vertebrates and beyond. While functions have been assigned during later embryogenesis, the role of *Gsc* in the organizer has remained enigmatic. Using conditional gain-of-function approaches in *Xenopus* and mouse to maintain *Gsc* expression in the organizer and along the axial midline, neural tube closure defects (NTDs) arose and dorsal extension was compromised. Both phenotypes represent convergent extension (CE) defects, arising from impaired Wnt/planar cell polarity (PCP) signaling. Dvl2 recruitment to the cell membrane was inhibited by *Gsc* in *Xenopus* animal cap assays and key Wnt/PCP factors (*RhoA*, *Vangl2*, *Prickle*, *Wnt11*) rescued *Gsc*-mediated NTDs. Re-evaluation of endogenous *Gsc* functions in MO-mediated gene knockdown frog and knockout mouse embryos unearthed PCP/CE-related phenotypes as well, including cartilage defects in *Xenopus* and misalignment of inner ear hair cells in mouse. Our results assign a novel function to *Gsc* as an inhibitor of Wnt/PCP-mediated CE. We propose that in the organizer *Gsc* represses CE as well: *Gsc*-expressing prechordal cells, which leave the organizer first, migrate and do not undergo CE like the *Gsc*-negative notochordal cells, which subsequently emerge from the organizer. In this model, *Gsc* provides a switch between cell migration and CE, i.e. cell intercalation.

During development, invertebrate and vertebrate embryos alike elongate and narrow their anterior-posterior (AP) axis by convergent extension (CE). CE is driven by intercalation of bipolar cells perpendicular to the previously established AP axis, necessitating a perfect coordination between spatial cues and cellular behavior. In *Drosophila* it has been shown that positional AP information, encoded by *Eve*, *Runt* and localized *Toll*-receptor expression, is directly translated into germ band CE<sup>1</sup>. Likewise, AP-patterning was shown to be directly linked to CE movements in explanted chordamesoderm of *Xenopus* embryos<sup>2</sup>. Molecular cues, which control and orient CE relative to the AP axis, have not been described in vertebrate embryos. How the spatial patterning is maintained and reinforced in the highly dynamic environment of the elongating and developing vertebrate embryo has yet to be defined.

The vertebrate body plan is established during gastrulation through the activity of the primary embryonic organizer (Spemann organizer), a specialized group of cells located at the amphibian dorsal lip of the blastopore

<sup>1</sup>University of Hohenheim, Garbenstr. 30, 70599 Stuttgart, Germany. <sup>2</sup>Genetics of Vertebrate Development Section, Cancer and Developmental Biology Lab, National Cancer Institute, National Institutes of Health, Frederick, MD 21702, USA. <sup>3</sup>Department of Developmental Biology and Cancer Research, Institute for Medical Research Israel-Canada, Hebrew University, Jerusalem 9112102, Israel. <sup>4</sup>Institute of Human Genetics, University Hospital Heidelberg, Im Neuenheimer Feld 366, 69120 Heidelberg, Germany. <sup>5</sup>Present address: Department of Experimental Pharmacology and Toxicology, Cardiovascular Research Center, University Medical Center Hamburg-Eppendorf, 20246 Hamburg, Germany. <sup>\*</sup>Present address: CNR-Neuroscience Institute, Department of Biomedical Sciences, University of Padova, Italy. <sup>\*\*</sup>Present address: Centre for Organismal Studies (COS) Heidelberg, Heidelberg University, Im Neuenheimer Feld 230, 69120 Heidelberg, Germany. <sup>†</sup>These authors contributed equally to this work. Correspondence and requests for materials should be addressed to M.B. (email: martin.blum@uni-hohenheim.de)

or homologous structures in other vertebrates (node in birds and mammals, embryonic shield in fish<sup>3</sup>). Organizer transplantation to the opposite, ventral side of the gastrula embryo induces the formation of a secondary axis, in which neighboring ventral cells adopt both a dorsal fate and undergo gastrulation movements<sup>4</sup>. Expression of the homeobox transcription factor gene *Gooseoid* (*Gsc*) marks Spemann's organizer in vertebrates and beyond<sup>5,6</sup>. Upon ectopic expression on the ventral side, i.e. opposite to its normal site of action, *Gsc* efficiently induces the formation of secondary embryonic axes in *Xenopus*<sup>7</sup>. This remarkable ability to mimic Spemann's organizer in gain-of-function experiments is readily explained by its well characterized ability to transcriptionally repress target genes identified in mouse, frog and zebrafish, including *Wnt8a* and *BMP4* pathway components<sup>8–18</sup>. In stark contrast, *Gsc* knockout mouse embryos lack gastrulation defects<sup>19,20</sup>, as do frog and fish embryos with impaired *Gsc* function<sup>15,16,21,22</sup>. This lack of a gastrulation phenotype is likely explained by functional redundancy with other factors expressed in the organizer, which await identification.

Yet there may be additional *Gsc* functions in the organizer. A number of studies suggested a general role of *Gsc* in cell migration during development and disease that is not explained by its role as a transcriptional repressor of BMP4 and Wnt8 targets. Lineage labeling and video microscopy of *Gsc*-injected embryos revealed enhanced anterior migration of posterior cells<sup>23</sup>. *Gsc* was also able to enhance the migratory behavior of cultured embryonic frog head mesenchymal cells<sup>24</sup>. In tumor cells, *Gsc* expression correlated with enhanced migratory activity as well<sup>25</sup>. Together these data point to a possible role of *Gsc* in mediating cellular behavior.

The early embryonic expression pattern of *Gsc* in vertebrate embryos is in agreement with such a function. The initial transcription in the organizer tissue itself is very transient. As axial mesodermal cells (prechordal plate and notochord) begin to leave the organizer in rostral direction, *Gsc* expression remains active in prechordal cells but ceases in the resident organizer tissue and the notochord<sup>10,26,27</sup>. Segregation of organizer-derived cells into these two cell populations is accompanied by differences in cell behavior and gene expression: *Gsc* marks the prechordal cells, characterized by single cell migration, while *Brachyury* is expressed and instrumental for CE in the notochord<sup>28–31</sup>.

Based on this dichotomy we hypothesize that *Gsc* plays a role in prechordal cells to promote migration and to inhibit CE. In order to test this hypothesis, we performed conditional gain-of-function experiments in mouse and *Xenopus*. Our experiments resulted in CE-phenotypes in both species, including neural tube closure and axial elongation defects. Rescue of *Gsc*-induced CE phenotypes by co-expression of planar cell polarity (PCP) pathway components suggested a novel function of *Gsc* as a negative regulator of PCP-mediated CE. Loss-of-function experiments showed that *Gsc* impaired bipolar elongation of cells in Meckel's cartilage in *Xenopus* and affected the alignment of hair cells in the inner ear of *Gsc* knockout mouse embryos. Based on these results we propose a novel role of *Gsc* as inhibitor of PCP-mediated CE.

## Results

**Sustained *Gsc* expression along the axial midline interferes with CE and causes neural tube and blastopore closure defects in *Xenopus*.** *Gsc* expression in the organizer ceases with the exit of the first cell population, which migrates anteriorly and constitutes the prechordal mesoderm. Our hypothesis predicts that a sustained activity of *Gsc* along the subsequently emerging notochord interferes with the cellular behavior of these cells, namely CE. In order to ectopically express *Gsc* in a tightly controlled temporal and spatial manner, we employed a previously described inducible *Gsc* protein<sup>32</sup>. In short, a construct was used, in which the *Gsc* coding sequence was fused to the ligand binding domain of the glucocorticoid receptor (GR). In the absence of the synthetic ligand dexamethasone (dex), *Gsc*-GR localizes to the cytoplasm and remains inactive, while ligand addition results in a conformational change, nuclear entry and onset of *Gsc* function as a transcriptional repressor<sup>32</sup>. Functionality of the construct was demonstrated by dex treatment of ventrally injected specimens, which led to double axis induction in 14/24 cases, i.e. at frequencies described previously<sup>32</sup> (not shown).

Targeting of *Gsc*-GR to the dorsal midline was achieved by microinjection of synthetic mRNA into the marginal region of the two dorsal blastomeres of the 4-cell embryo (Fig. 1A). Analysis of a co-injected lineage tracer confirmed delivery to the notochord and floor plate, which cannot be targeted separately in such experiments (not shown). No phenotypic changes were observed in the absence of dex (Fig. 1B,E), while ligand addition between cleavage and blastula stages (st. 6–9) resulted in a high percentage of embryos with neural tube closure defects (NTDs; Fig. 1C,E; Table S1). More severe blastopore closure defects (BPD<sup>33</sup>) were observed as well (Fig. 1D,E; Table S1). In these cases, the dorsal midline was disrupted, which resulted in cup-shaped morphologies (Fig. 1D). The overall percentage of affected embryos dropped when dex was added during gastrulation, and very few malformations were recorded when *Gsc*-GR was activated during late gastrula/early neurula stages (Fig. 1E; Table S1 and data not shown). Development of BPD and NTD depended on the presence of the homeodomain (HD) as well as the paired-type DNA binding specificity of *Gsc* (lysine in position 50 of the HD), while the repression domain (eh1/GEH) was not required for NTD/BPD induction (Fig. 1E). A slight but non-significant delay in neural tube closure was observed in a proportion of specimens (not shown). Sustained *Gsc* expression along the dorsal midline thus interfered with blastopore and neural tube closure, processes known to depend on CE<sup>34,35</sup>.

*Xbra* mRNA transcription serves as a readout of CE in the notochord, which narrows and lengthens concomitantly with neural tube closure<sup>36</sup>. In order to assess whether notochordal CE was affected by sustained *Gsc* expression as well, we analyzed *Xbra* in less severely affected dex-treated specimens without BPD. In the absence of dex, the notochord was elongated and narrow during neurula stages. Activation of ectopic *Gsc* activity, however, resulted in shortened and widened *Xbra* expression domains (Fig. 1F–I), in agreement with CE defects in the notochord. While the expression level of *Xbra* in the notochord was not affected, we expected a repression of *Xbra* transcription by *Gsc* during gastrulation, in line with the reported role of *Gsc* as a repressor of *Brachyury* in the prechordal mesoderm<sup>10,11,13</sup>. Analysis at late gastrula (stage 11) demonstrated that repression of *Xbra* in dex-treated specimens took place but was restricted to the injection site (Fig. 1K; 35/74, 47.3%). In the absence of

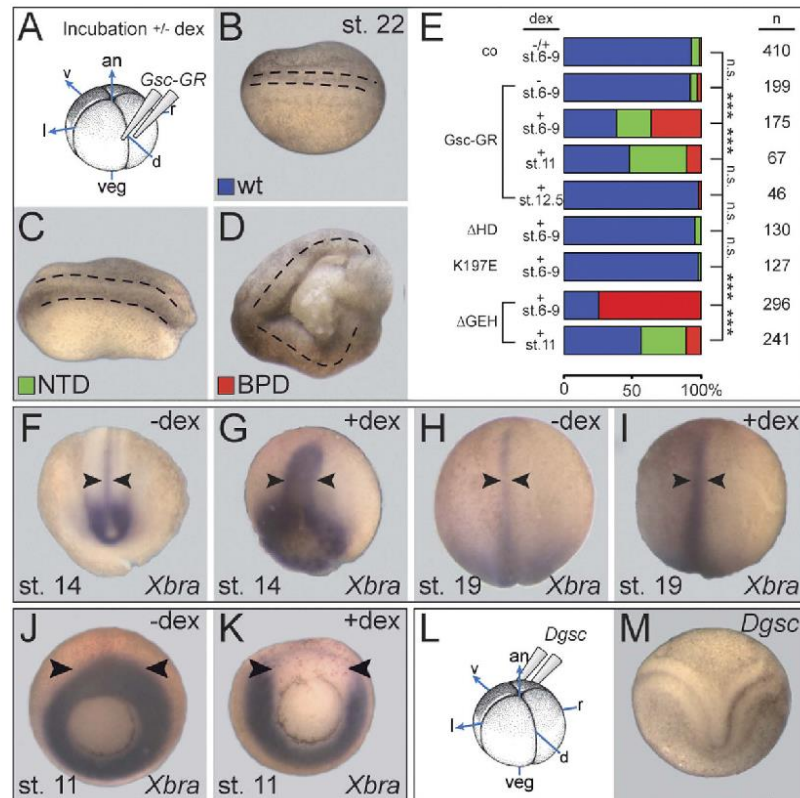


**Figure 1.** Gsc-mediated CE phenotypes in *Xenopus*. (A) Experimental design. Specimens were injected with Gsc-GR into the dorsal marginal region of the 4-cell embryo and cultured to the stages indicated, with or without addition of dex. (B–E) Gsc-GR induced BPD and NTD in whole embryos. Specimens were scored for wt appearance (blue; B), NTD (green; C) and BPD (red; D). Anterior is to the left in (B–D). (E) Compilation of results. Note that Gsc-GR caused CE phenotypes in a highly significant proportion of embryos, but only when activated before and during gastrulation. Note also that deletion of the homeodomain ( $\Delta$ HD) or altering the DNA-binding specificity (K197E) prevented BPD/NTD-induction, while the repression domain GEH was not required for BPD/NTD. (F–I) Impaired CE of the notochord upon sustained dorsal Gsc-GR expression. Note that the notochord was wider and shorter in dex-treated (G,I) as opposed to untreated (F,H) specimens, both at stage 14 (F,G) and stage 19 (H,I). (J,K) Repression of *Xbra* transcription on the dorsal side upon Gsc-GR activation. (L,M) Double axis formation (M) following ventral injections of *Dgsc* mRNA into 4-cell *Xenopus* embryos (L).

dex, Gsc-GR injected embryos showed wildtype (wt) *Xbra* expression around the blastopore (arrowheads, Fig. 1J; 48/51, 94.1%).

In order to assess the effects of Gsc on CE in a semi-quantitative manner, we turned to Keller open-face explants, which have been used in the past to investigate notochord CE in *ex vivo* assays<sup>37</sup> (Fig. 2A). Dorsal marginal zone tissue was isolated at stage 10–10.5 from Gsc-GR-injected embryos, which were incubated in the presence or absence of dex from stage 6/7 onwards, and scored for CE when un-injected siblings reached stage 22 (Fig. 2A–C). CE was classified into three categories<sup>38</sup>, with class 0 representing explants without elongation, class 1 containing elongated specimens, and class 2 explants which in addition displayed a constriction (Fig. 2B). In the absence of dex, more than 90% of explants elongated, with the majority of specimens falling into class 2 (36/51; 70.6%). In contrast, CE in dex-treated explants was severely compromised, with significantly reduced class 2 extensions (19/75), the relative majority of specimens elongating without constriction and about 25% not elongating at all (class 1; 36/75, 48%; Fig. 2C).

In order to investigate if and how sustained Gsc expression along the dorsal midline interfered with cell fate determination, i.e. with neural induction and mesodermal patterning, mRNA transcription of neural (*Ncam*) and



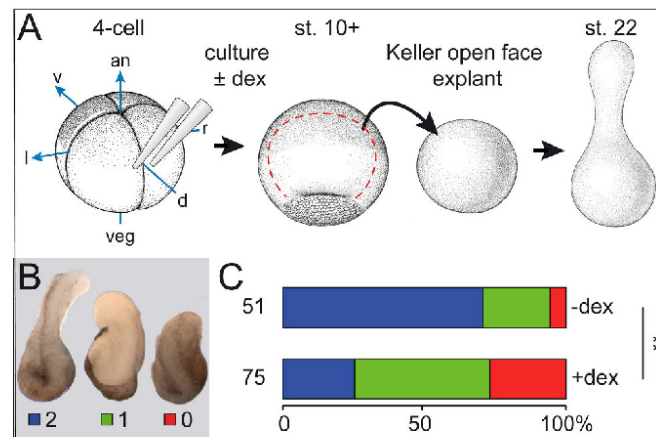


**Figure 2. Gsc inhibits CE in Keller open face explants.** (A–C) CE defects in Keller open face explants (schematically depicted in (A) upon activation of *Gsc-GR*. (B) Explants were classified as class 2 (blue) when extensions showed a constriction (left), as class 1 (green) when elongation occurred without constriction (middle), and as class 0 (red) when no elongation ensued (right)<sup>38</sup>. an, animal; uninj., uninjected control; d, dorsal; l, left; r, right; v, ventral; veg, vegetal. (C) Summary of results.

somatic (*MyoD*) marker genes was analyzed. Both genes were expressed in specimens displaying BPDs upon dex treatment, even though somites did not epithelialize into the typical chevron-shaped patterns of control specimens (Fig. S1A–D). Sustained expression of *Gsc* on the dorsal side of *Xenopus* embryos thus did not interfere with specification of neural and mesodermal tissue, but inhibited CE in the notochord.

To analyze whether NTDs were caused by impaired CE as well, we investigated a potential role of *Gsc* in cell shape changes in the neuroectoderm. A prerequisite of CE is that cells polarize, i.e. elongate and adopt a bipolar morphology. *Gsc-GR* was targeted to the neuroectoderm by microinjecting synthetic mRNA to the A1 lineage of 8-cell embryos. Rhodamine dextran was co-injected as a lineage tracer, and injections were performed unilaterally in order to provide for an internal control on the un-injected contralateral side (Fig. 3A). Injected specimens were incubated until mid-neurula stages (stage 16), fixed and processed for cell shape assessment via phalloidin-staining of the actin cytoskeleton. In the absence of dex, cell morphologies appeared indistinguishable on both sides, while *Gsc* activation resulted in less elongated, rounder cells (Fig. 3B–D). To quantitate this effect, the length-to-width ratio was determined and expressed as elongation score, with a value of 1 representing a round cell and 0 a hypothetical elongated cell without width. The results from a representative specimen are depicted in Fig. 3E. On the *Gsc-GR* side a significant decrease of cells displaying a score of  $<0.5$  was observed (14/105 or 13% on the *Gsc-GR* injected side, and 55/173 or 32% on the control side). In addition, unlabeled cells in between the injected rhodamine dextran-positive cells, which likely represent intercalation events, were observed on un-injected and untreated control sides (asterisks in Fig. 3B). Upon *Gsc* activation, no such unlabeled cells were found (Fig. 3C). In some explants, cell numbers were slightly (and non-significantly) reduced (not shown), however, cell proliferation and apoptosis were not affected by *Gsc-GR* activation (Fig. S2). The occasionally observed alterations of cell numbers may be caused by dex treatment, as previously reported<sup>39</sup>. These results strongly suggest that NTDs in frog tadpoles were due to impaired CE as well, caused by a lack of bipolar cell polarization in *Gsc*-misexpressing neuroectodermal cells.

Finally, we wondered whether this novel function of *Gsc* as an inhibitor of CE was evolutionary conserved. *Gsc* represents an ancient member of the metazoan toolkit of animal embryogenesis which is present from radiata (cnidarians; hydra<sup>6,40</sup>) to lophotrochozoans<sup>41</sup>, ecdysozoans (e.g. *Drosophila*) and deuterostomians alike. In all cases, the homeodomain and the N-terminal repression domain are highly conserved<sup>42,43</sup>. We chose to analyze *Drosophila Gsc*, which was previously shown to be able to rescue the dorsal axis of UV-treated ventralized *Xenopus* embryos<sup>44</sup>. In line with these experiments, *Dgsc* was able to induce double axis formation upon ventral injection (Fig. 1L, M; 24/25, 96%). Dorsal injections of *Dgsc*, however, had no effect on neural tube or blastopore closure (100/100, not shown), indicating that the novel function of *Gsc* described here as a repressor of CE arose later in evolution and may be independent of its function as a transcriptional repressor.

**Expression of *Gsc* in the entire mouse primitive streak results in NTD and compromises axial extension.** Next we wondered whether this novel role of *Gsc* to repress CE was conserved among the vertebrates. To investigate this possibility, we expressed *Gsc* in the entire primitive streak of mouse embryos using a conditional approach<sup>45</sup>. Construct *T-Gsc* contained the 650 bp primitive streak enhancer of the mouse *Brachyury (T)* gene<sup>46</sup>, followed by a floxed LacZ gene and the mouse *Gsc* coding sequence (Fig. 4A). Construct *mT-Gsc* was

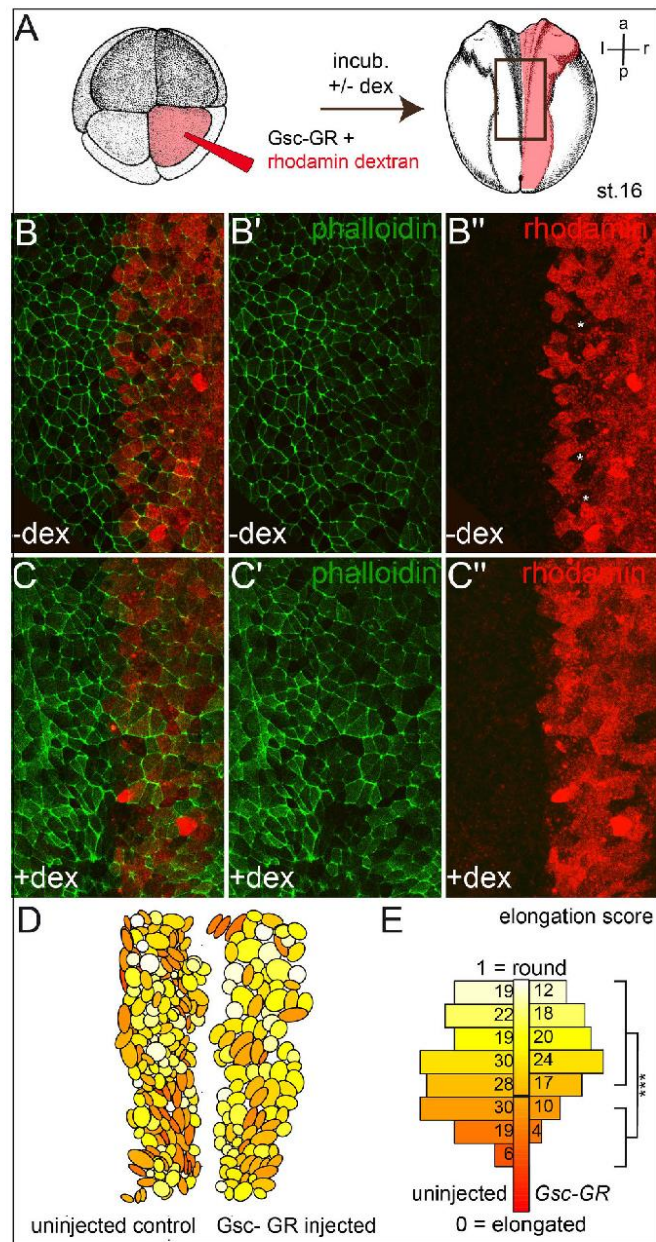


**Figure 3. Gsc compromises bipolar elongation of neural plate cells.** (A) Targeted injection scheme of *Gsc-GR* and lineage tracer (rhodamine red) into the right side of the neural plate (B,C). Drawings taken from Xenbase ([www.xenbase.org/anatomy/alldevo.do](http://www.xenbase.org/anatomy/alldevo.do))<sup>37</sup>. (D,E) Analysis of cell elongation. The color gradient ranging from pale yellow (round, width = length, 1) to dark red (elongated, 0) exemplifies the change from bipolar cells on the uninjected (right) side towards rounded cells upon activation of *Gsc-GR* (D). (E) Significant decrease of percentage of elongated cells (elongation score < 1/2) after *Gsc-GR* misexpression. a, anterior; l, left; p, posterior; r, right.

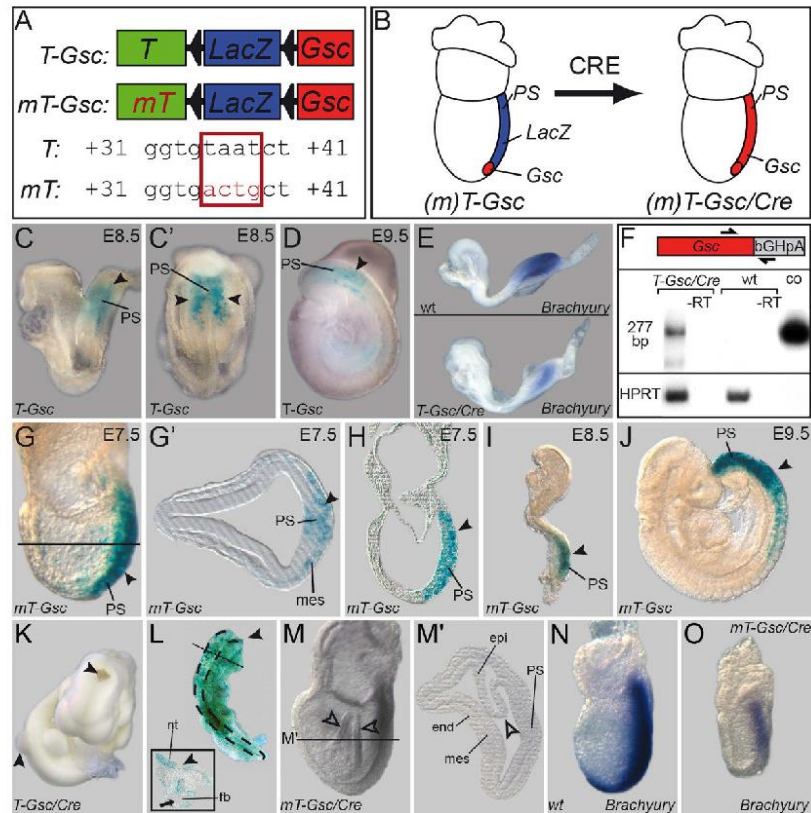


**Figure 4. Gsc-mediated CE phenotypes in the mouse.** Conditional misexpression of *Gsc* in the entire primitive streak of the mouse. (A) Constructs used to generate transgenic mouse lines. *T*, wt *Brachyury* streak enhancer; *mT*, mutant enhancer not repressed by *Gsc*; triangles, loxP sites. (B) Schematic depiction of *Gsc* (red) and *LacZ* (blue) expression at E7.5 before (left) and after (right) Cre-mediated recombination. (C,D) *LacZ* expression (arrowheads) in the primitive streak (PS) mesoderm of E8.5 (lateral view in C, posterior view in C') and E9.5 (D) *T-Gsc* embryos. (E) Reduced *Brachyury* mRNA expression upon transgene activation (*T-Gsc/Cre*, lower panel) compared to wt embryo (upper panel). (F) Detection of transgenic *Gsc* mRNA by RT-PCR from *T-Gsc/Cre* and wt E8.5 embryos. A 277 bp fragment specific for transgenic *Gsc* mRNA was amplified using a *Gsc* primer and a primer derived from the bovine growth hormone polyadenylation (bGHpA) signal present in the construct. Note that no signal was detected in wt embryos, and that a band identical in size to one amplified from the *T-Gsc* control plasmid was seen in *T-Gsc/Cre* embryos. (G–J) *LacZ* expression (arrowheads) in the PS mesoderm of E7.5 (G,H) plane of histological section *G'* indicated in (G), E8.5 (I) and E9.5 (J) *mT-Gsc* embryos. (K) Cranial and caudal NTD (arrowheads) in E10.5 *T-Gsc/Cre* embryo. (L) Craniorachischisis in chimeric E10.5 embryo generated from ES cells expressing *LacZ* and *Gsc*. Note that, except for the forebrain region (arrow; cross section shown in inset), the entire neural tube stayed open (arrowheads). (M) Malformation of *mT-Gsc/Cre* gastrula embryo. Note irregular folding of epiblast (open arrowheads). (M') Histological section at level indicated in (M). (N,O) Repression of *Brachyury* transcription in *mT-Gsc/Cre* (O) compared to wt (N) E7.5 embryos. end, endoderm; epi, epiblast; fb, forebrain; mes, mesoderm; nt, neural tube; PS, primitive streak.

identical, except that the *Gsc*-binding site in the *Brachyury* streak enhancer was mutated to prevent *Gsc*-mediated transgene repression<sup>11</sup>. Thus, *T-Gsc* should result in moderate transgene expression, creating a scenario resembling the endogenous *Gsc* gene, where *Gsc* negatively autoregulates its own expression<sup>47</sup>. *mT-Gsc*, in contrast, should allow for pronounced and sustained ectopic *Gsc* expression in the primitive streak mesoderm and descendants thereof. Transgenic *T-Gsc* mouse lines moderately expressed the *LacZ* reporter gene in the nascent primitive streak mesoderm from E7.5 onwards (Fig. 4C,D and data not shown). Much stronger *LacZ* staining was found in embryos of *mT-Gsc* lines, as expected (Fig. 4G–J).



To study the phenotypes induced by ectopic *Gsc* activity, mice were mated to the *deleter* line, which expresses the CRE-recombinase ubiquitously from blastocyst stages onwards<sup>48</sup> (Fig. 4B). First, the effects of moderate *Gsc* misexpression were assessed. Transgenic *T-Gsc* embryos analyzed from E7.0–E9.0 were morphologically indistinguishable from wt specimens (not shown). *Brachyury* expression in the primitive streak was reduced (Fig. 4E), demonstrating that the transgenic *Gsc* protein was functional. Transgenic *Gsc* expression was verified by RT-PCR (Fig. 4F). Phenotypic effects, however, were encountered in 44/197 (22.3%) of transgenic embryos analyzed at E9.5–E10.5. Affected specimens in all cases were characterized by cranial NTDs, while 10/44 in addition showed spina bifida (Fig. 4K). In order to prove the specificity of *Gsc*-induced NTDs, we generated chimeric mouse embryos by blastocyst injection of ES cells stably expressing *Gsc* and *LacZ*. Embryos were analyzed at E9.5–E10.5 to assess NTDs. In control chimeric embryos, derived from injection of ES cells expressing only *LacZ*, no NTDs were observed (not shown). *Gsc/LacZ* chimeras, in contrast, were characterized by a high percentage of NTDs which were encountered in 22/27 specimens (81.5%) generated in five experiments. Of these, two chimeric embryos were characterized by a lack of closure along the entire cranio-caudal axis except for the fore-brain region (craniorachischisis; Fig. 4L). Together these data demonstrated that NTDs induced from moderate level overexpression of *Gsc* in the primitive streak of transgenic *T-Gsc/Cre* embryos represented a *Gsc*-specific gain-of-function phenotype.

High level ectopic *Gsc* expression from Cre-mediated activation of *mT-Gsc* resulted in much earlier phenotypes. At E8.5 only very few but severely malformed embryos were recovered (not shown). E7.5 *mT-Gsc/Cre* embryos expressed various levels of *Gsc* transcripts. Compared to wt embryos, *mT-Gsc* specimens generally revealed *Gsc* expression domains that were more intensely stained and extended towards the caudal primitive streak (Fig. S3A–D). E7.5 specimens displayed a range of deficiencies that can roughly be grouped into two categories. A typical example of a mildly affected embryo, which was seen in about 60% of cases, is shown in Fig. 4M. The overall size did not differ significantly from wt, however, the epiblast appeared folded-up, which was more obvious in sections (arrowhead in Fig. 4M'). Primitive streak and mesoderm were clearly discernible. Severely affected embryos, in contrast, were characterized by egg cylinders that appeared hardly elongated at all and were approximately half the size of wt specimens (Fig. S3J,L).

The lack of axial elongation suggested that notochordal cells did not form or did not undergo CE. To investigate these options, E7.5 *mT-Gsc/Cre* embryos were analyzed morphologically, histologically and for marker gene expression. Scanning electron microscopy demonstrated that mutant embryos lacked the ciliated epithelium of the posterior notochord (PNC) at the distal tip of the egg cylinder, that is also known as ventral node<sup>26</sup> (Fig. S3E,F). The notochordal plate, i.e. the anterior extension of the PNC from which the notochord develops, was consistently absent in severely affected embryos as well (Fig. S3F and data not shown). To analyze axial mesoderm formation, the notochordal marker genes *Brachyury* and *Noto* were studied (Fig. 4N,O; Fig. S3G,H). Both genes were clearly down-regulated. Residual mRNAs were found in the primitive streak (*Brachyury*; Fig. 4O) and at the distal tip of the egg cylinder (*Noto*; Fig. S3H). No signals were observed anterior to the primitive streak. Thus, although mesoderm clearly arose in transgenic embryos (Fig. 4N), cells did not organize into PNC and notochordal plate during the course of gastrulation. Next, axis specification was analyzed, as *Gsc* acts as a potent inducer of secondary axes in *Xenopus*. Transcripts of *Otx2*, which marks the anterior pole (Fig. S3I), and *Fgf8*, which is expressed in the posterior part of the embryo (Fig. S3K), were found localized in the anterior and posterior half of the mutant egg cylinders as well (Fig. S3J,L). The AP-axis, therefore, was correctly specified in transgenic embryos, even in the most severe cases (Fig. S3J,L, and data not shown). Taken together, *Gsc* expression along the entire primitive streak of the mouse gastrula embryo impaired axial elongation, without affecting the patterning of embryonic tissues, and caused NTDs comparable to the BPDs and NTDs seen in *Xenopus*.

**Gsc inhibits Wnt/PCP.** CE in frog and mouse is regulated by non-canonical Wnt signaling, specifically the PCP pathway<sup>49–51</sup>. One of the hallmarks of PCP signaling is the recruitment of Dvl2 to the plasma membrane<sup>52,53</sup>, which is compromised when PCP signaling is impaired<sup>54,55</sup>. We therefore wondered whether *Gsc* was able to interfere with Dvl2 localization. In *Xenopus*, a Dvl2-GFP fusion protein serves to investigate the subcellular localization in animal cap explant cultures<sup>56</sup>. Upon expression of the Wnt receptor Fz7, Dvl2-GFP translocated from the cytoplasm to the plasma membrane (Fig. 5C,E). Animal caps represent a naïve stem cell-like tissue that can be differentiated into descendants of all three germ layers<sup>57</sup>. As *Gsc* expression in the early vertebrate embryo is limited to mesodermal tissues<sup>58,59</sup>, animal cap explants were injected with the mesoderm-inducing isoform of *Fgf8*, *Fgf8b*, which was verified by germ layer-specific marker gene expression<sup>60</sup> (Fig. S4). In order to assess whether *Gsc* impacted on Dvl2 subcellular localization, *Dvl2-GFP*, *fz7*, *fgf8* and *Gsc-GR* were coinjected into the animal region of 4–8 cell embryos, specimens were cultured in the presence or absence of dex until control embryos reached stage 10.5, when animal caps were excised and imaged (Fig. 5A). In the absence of dex, Dvl2-GFP relocated from the cytoplasm to the plasma membrane (Fig. 5B,E). When *Gsc* activity was induced following dex treatment, Dvl2-recruitment to the cell membrane was severely compromised (Fig. 5D,E;  $p = 0.002$ ). *Gsc-GR* acted in a cell-autonomous manner, as Dvl2 membrane localization was not affected in neighboring cells when *Gsc-GR* was only injected and activated in a subset of animal cap cells (Fig. 5F,G). These data demonstrated that in overexpression assays *Gsc* was clearly able to interfere with the recruitment of Dvl2 to the membrane as a prerequisite of non-canonical Wnt signaling and CE, in agreement with the observed gain-of-function phenotypes in mouse and frog.

**Wnt/PCP pathway components rescue Gsc-induced NTD/BPD.** Our hypothesis that *Gsc* interferes with Wnt/PCP signaling predicted that pathway components should be able to rescue the *Gsc-GR* induced gain-of-function phenotypes NTD and BPD *in vivo*. The downstream effector *RhoA* was assessed, which regulates CE by reorganization of the actin cytoskeleton<sup>61</sup>. A constitutively active (ca) construct was used as well as a dominant-negative (dn) form of *RhoA* (Paterson *et al.*<sup>90</sup>). Both have been shown to induce BPD and NTD<sup>61</sup>, like

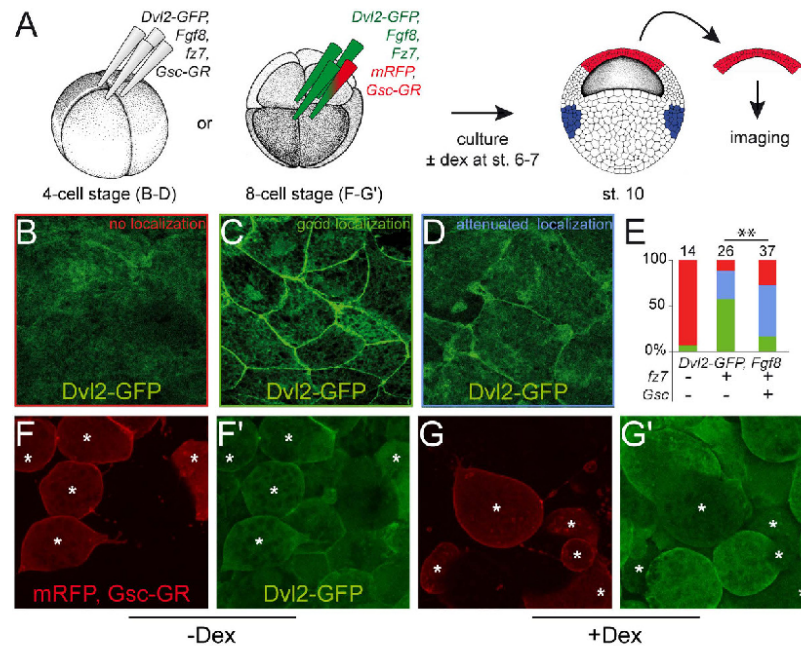


**Figure 5.** *Gsc-GR* inhibits membrane recruitment of *Dvl2*. (A) Co-injection of mRNAs as indicated into the animal region of all cells at the 4-cell stage or of selected cells at the 8-cell stage. Embryos were cultured  $\pm$  dex (added at st. 6/7), animal cap tissues were excised at stage 10 and subjected to live imaging. (B–E) Membrane localization of *Dvl2*-GFP was significantly impaired upon *Gsc-GR* activation. (B–D) Examples of specimens from the same batch of embryos and photographed with the same exposure times showing lack of localization (B; red), good (C; green) and attenuated localization (D; blue). (E) Quantification of results ( $p = 0.002$ ). (F, G) Cell-autonomous effect of *Gsc-GR*. Injection of *Gsc-GR* in 1/4 animal cap cells at the 8-cell stage (cf. A) resulted in attenuation of *Dvl2*-GFP membrane recruitment upon dex treatment (cf. F' and G'). \*mark *Gsc-GR*-injected cells, as revealed by fluorescence of lineage tracer mRFP.

most PCP components, which give rise to similar phenotypes upon gain- and loss-of-function<sup>63</sup>. In addition, the core PCP components *Vangl2* and *Prickle* were investigated, as they are required for subcellular localization of *Dvl2*<sup>63,64</sup>. In addition, the potential of *Wnt11* and *Xbra* to rescue *Gsc*-mediated phenotypes was analyzed, as both are known to induce CE in *Xenopus*<sup>65,66</sup>.

NTD and BPD were observed when *Gsc-GR* or any of the PCP components were injected into the dorsal marginal zone (Fig. 6). To test if and how *Gsc* interacted with PCP signaling, co-injection experiments were performed. *caRhoA* significantly decreased the percentage of malformed embryos induced by *Gsc-GR* (Fig. 6A; Table S1). In order to analyze whether *dnRhoA* enhanced the *Gsc* effects accordingly, both were co-expressed. High lethality of embryos prevented the quantitative analysis of the experiment (not shown). When the dosage of the injected *Gsc-GR* construct was lowered 2.5-fold, *dnRhoA* co-injection resulted in a significantly higher percentage of affected specimens as compared to the injection of *dnRhoA* alone (Fig. 6B; Table S1). As *RhoA* is a general modifier of actin cytoskeleton dynamics, we extended our study to core PCP pathway components. Co-injections of *Prickle* and *Vangl2* partially rescued the *Gsc*-induced phenotypes (Fig. 6C,D; Table S1). In addition, mouse *Brachyury* and *Xenopus Wnt11* were also able to partially revert *Gsc-GR* induced NTD and BPD (Fig. 6E,F; Table S1). In summary, these gain-of-function experiments demonstrated the potential of *Gsc* to act as a negative regulator of PCP-mediated CE, at least in the context of gain-of-function induced phenotypes.

**Wnt/PCP phenotypes in *Gsc* morphant frog and mutant mouse embryos.** In order to analyze whether the endogenous *Gsc* is involved in inhibition of Wnt/PCP-mediated CE as well, we re-investigated *Gsc* morphant frog embryos and knockout mouse specimens. In *Xenopus* we used a previously characterized *Gsc* MO<sup>21</sup>. Analysis of morphant tadpoles revealed that the eye distance was significantly reduced at stage 45 compared to uninjected control specimens (Fig. 7A,B). Co-injection of a full-length mouse *Gsc* cDNA construct, which was not targeted by the MO, partially rescued this phenotype, demonstrating the specificity of the MO (Fig. 7C). As during development the eye field is split by the prechordal plate, which expresses *Gsc*, we hypothesized that this population of migrating cells was affected in morphants. *Shh* mRNA transcription was analyzed,

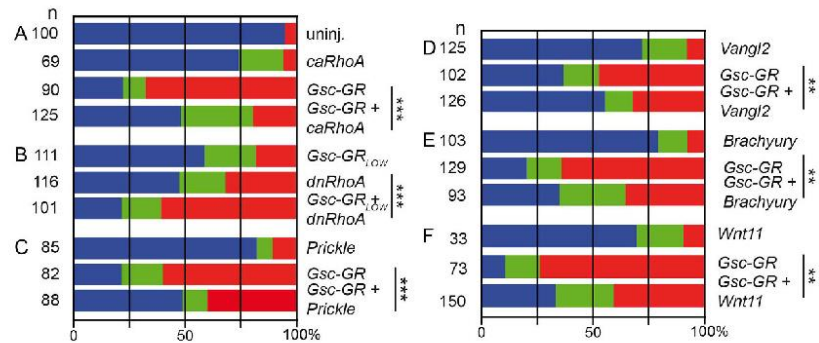


**Figure 6. Rescue of Gsc-GR mediated NTD/BPD by Wnt/PCP pathway components.** *Xenopus* embryos were injected with the indicated mRNAs into the dorsal marginal region of all cells at the 4-cell and cultured to stage 22. Dex was added when *Gsc-GR* was used. Specimens were scored for normal appearance (blue bars), NTD (green) and BPD (red). (A) constitutively active *RhoA*; (ca; A) dominant-negative (dn) *RhoA*; (C) *Prickle*; (D) *Vangl2*; (E) *Brachyury*; (F) *Wnt11*. Uninjected embryos (uninj.) served as controls. Note that rescue was observed upon co-injection of *Gsc-GR* with *ca-RhoA*, *Prickle*, *Vangl2*, *Brachyury* and *Wnt11*, while enhanced phenotypes were seen with co-injected *dn-RhoA*. As embryos in the latter combination showed high rates of lethality, the dose of injected *Gsc-GR* was reduced from 400 pg to 160 pg. Cf. Table S1 for numbers and statistics.

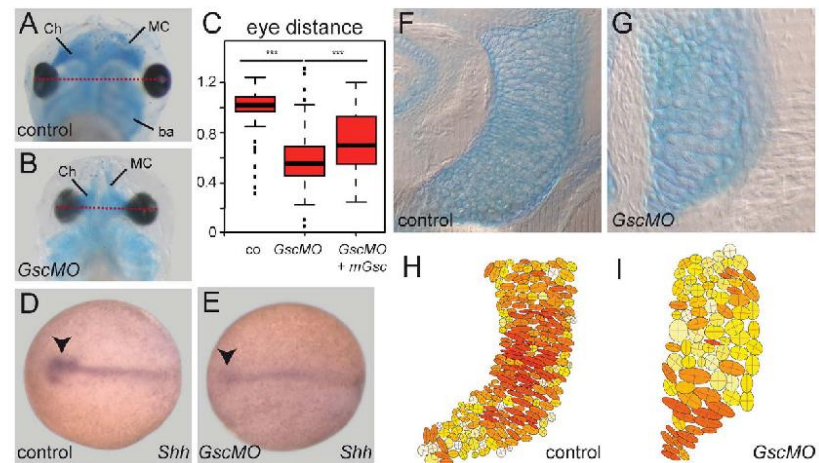


**Figure 7. Prechordal plate and cartilage defects in *Gsc* morphant *Xenopus* tadpoles.** (A–E) Prechordal plate defects. (A–C) Close-set eyes in *Gsc* morphants. Distance between left and right eye (red lines) was reduced in morphants. Arithmetic mean of control specimens was set to 1.0 in (C). Note that this phenotype was rescued by co-injection of a mouse *Gsc* cDNA construct. (D,E) *Shh* mRNA expression in control (D) and high dose *Gsc* morphant (E). Note that the prechordal plate (arrowheads) was severely reduced in morphants. (F–I) Cartilage phenotypes in *Gsc* morphant frog tadpoles. Cartilage was stained with alcian blue in wt (F,H) or *Gsc* morphant (G,I) tadpoles at stage 45. Shape of cartilage cells was analyzed in frontal sections of embryos (E,G). (H,I) Cells were outlined with ImageJ and aspect ratios were calculated and visualized. Cell shapes are indicated by a color gradient from yellow to red, with round cells depicted in light yellow and elongated bipolar cells in deep red. Note that the majority of cartilage cells in *Gsc* morphants had lost their bipolar appearance.

which along the axial midline is expressed in the prechordal plate mesoderm and the floorplate of the neural tube. Figure 7(D,E) shows that the width of the anteriormost *Shh* expression domain, i.e. the expression in or above the prechordal plate, was narrowed, in line with the observed close-set eyes.



To analyze whether the notochord was expanded at the expense of the prechordal plate, which was previously suggested in experiments using antisense *Gsc* DNA expression constructs<sup>16</sup>, *Xbra* mRNA expression was investigated in morphant specimens. Surprisingly, the notochord appeared wider and shorter, as compared to wt specimen (Fig. S5). The aspect ratio, which was set to 1.0 in control specimens, was significantly reduced to 0.61 in morphants (Fig. S5C). As we had noted this particular phenotype in *Gsc* gain-of-function specimens (Fig. 1F–I), we wondered whether *Gsc* transcription was affected in *Gsc* morphants. The *Gsc* expression domain in morphants was indeed stronger and expanded both laterally and posteriorly towards the blastopore (Fig. S5G,H). This at first glance paradoxical finding, however, is in good agreement with our previous finding of a negative auto-regulatory feedback loop of *Gsc* on its own transcription<sup>67</sup>. The analysis of MO-mediated *Gsc* loss-of-function phenotypes thus might be hampered by limiting MO-doses, which might be insufficient to prevent the translation of additional transcripts generated by the release of the negative autoregulatory *Gsc* feedback loop. When the MO doses were increased to counteract this possible effect, the length of the notochord was slightly expanded to an aspect ratio of 1.14 in morphants ( $p = 0.0193$ ), an effect which was partially (and non-significantly) reversed by co-injection of the mouse rescue cDNA construct (aspect ratio 1.07; Fig. S5D–F). These tendencies may suggest that MO doses have, indeed, been limiting.

In addition to a reduced eye distance we noted that the morphology of the head cartilage was altered in *Gsc* morphant tadpoles at stage 45, in particular Meckel's cartilage and the ceratohyale (Fig. 7A,B,F–I). In mouse, *Gsc* is expressed in undifferentiated branchial arch mesenchyme and persists as these tissues undergo differentiation into head cartilage<sup>68</sup>. Re-evaluating *Gsc* expression during late tadpole development revealed a like expression pattern in *Xenopus* as well (Fig. S6). As cartilage condensation involves CE<sup>69,70</sup>, we wondered whether morphological alterations in morphants were reminiscent of PCP phenotypes. To that end we analyzed cellular morphologies of cartilage cells. While wt cells displayed predominantly bipolar morphologies (Fig. 7F,H), evaluation of length vs. width aspect ratios demonstrated loss of elongated cell shapes in morphants (Fig. 7G,I). This phenotype strikingly resembled the failure of Meckel's cartilage cells to elongate and intercalate in morphants of the PCP effectors *inturned* and *fuzzy*<sup>70</sup>, suggesting that the cartilage phenotype in *Gsc* morphant tadpoles represented a PCP-phenotype as well.

Finally, we re-investigated *Gsc*-knockout mouse embryos for potential PCP/CE phenotypes. Besides the above-mentioned expression around condensing cartilage, the inner ear is the organ that has been particularly well characterized with respect to PCP in the mouse. As previously described, *Gsc* was expressed in the inner ear opposite the organ of Corti<sup>71</sup> (Fig. 8A,B), and opposite the expression domain of the non-canonical Wnt ligand *Wnt5a*<sup>72</sup> (Fig. 8B). Stereo- and kinocilia of outer and inner hair cells (OHC/IHC) display a distinctive planar cell polarity and are a well-known target of PCP-signaling<sup>73</sup>. To investigate whether PCP of inner ear hair cells was altered in *Gsc* knockout embryos, E18.5 cochleas were isolated from wt and knockout specimens and analyzed for stereo- and kinocilia orientation. Phalloidin staining was used to highlight the actin cytoskeleton of the V-shaped stereocilia, and tubulin staining to visualize the axoneme of the kinocilium. In wt and heterozygous E18.5 specimens, stereo- and kinocilia of IHCs and OHCs align and point towards the periphery of the cochlea (Fig. 8C,E). In *Gsc* knock-out embryos, however, this orientation was disrupted (Fig. 8D,F). A quantification of average deviations from the normal perpendicular orientation revealed higher values in *Gsc* knockout specimens, which was significantly pronounced in outer hair cell row 3 (Fig. 8G,  $p = 0.03$ ,  $n = 390$ ) compared to wt littermates ( $n = 308$ ). This result unequivocally demonstrated that *Gsc* knockout mouse embryos displayed a well-characterized Wnt/PCP phenotype as well. Taken together, our *Gsc* gain- and loss-of-function studies in frog and mouse embryos revealed a novel role of *Gsc* as an inhibitor of Wnt/PCP-mediated cell morphogenesis and behavior, in particular CE.

## Discussion

A quarter of a century ago, the first description of *Gsc*'s potential to induce secondary axis formation set the starting point for an extremely productive molecular analysis of Spemann's organizer<sup>7</sup>. The apparent lack of gastrulation phenotypes in mutants and morphants reduced the perceived relevance of *Gsc* to being the best available marker of organizer tissue across the animal kingdom. Our present report of a novel function of *Gsc* as transcriptional inhibitor of Wnt/PCP-mediated CE not only offers a potential mechanism to understanding the various malformations of bone and cartilage in *Gsc* knockout mice (and human patients<sup>74</sup>). It may as well assign a role for *Gsc* in the organizer-derived prechordal plate, namely to restrict CE to the notochord and to facilitate or enable the migration of the prechordal mesodermal cells. Our conditional gain-of-function analyses in frog and mouse clearly demonstrate the potential of *Gsc* to act as an inhibitor of Wnt/PCP-mediated CE. The analysis of loss-of-function phenotypes in both model systems supports such a role during embryonic development, although - admittedly - they represent in parts initial and preliminary characterizations. A key question, that remains unanswered, relates to the molecular mechanism of *Gsc* function in inhibiting Wnt/PCP. Two aspects, which our experiments touch upon, deserve further elaboration, namely whether this effect is cell- or non-cell autonomous and how novel target genes were recruited under the control of *Gsc*.

As mentioned in passing, it is not possible to target the axial mesoderm/notochord in *Xenopus* without at the same time delivering constructs to the floorplate of the neural tube. Thus, the observed NTDs could represent a cell-autonomous effect of ectopic *Gsc* expression. The cell-autonomous interference of *Gsc*-GR with Dvl2 membrane recruitment in animal caps (cf. Fig. 5F,G) supports this notion. In the conditional mouse experiments, however, ectopic *Gsc* expression was strictly limited to the primitive streak mesoderm, as the *Brachyury* streak enhancer is only active there<sup>16</sup>. NTDs in mouse, therefore, cannot be caused by a cell-autonomous *Gsc* function. The same reasoning holds true for the inner ear: here *Gsc* is expressed opposite to the IHCs/OHCs at the organ of Corti that undergo PCP. Further, *Gsc* and the Wnt ligand *Wnt5a*, which has been shown to be the decisive ligand for the arrangement of these cells<sup>75</sup>, are expressed in adjacent rather than the same cells, demonstrating that the

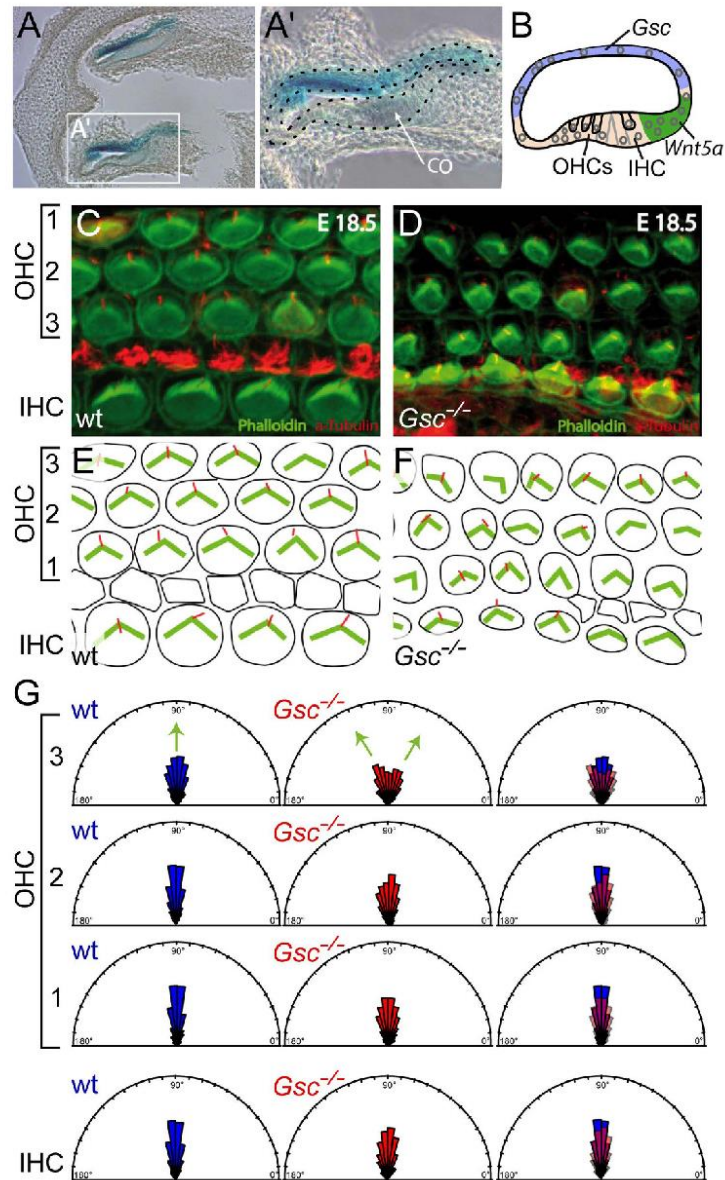


**Figure 8.** Disrupted alignment of outer hair cells (OHCs) in the cortical organ of *Gsc* knockout embryos. (A) *Gsc* transcription (blue) locates opposite of the cortical organ (CO). (B) Schematic depiction of *Gsc* expression in blue and *Wnt5a* expression in green. OHCs and inner hair cells (IHC) are highlighted by arrows. (C–G) Confocal imaging of kinocilia (red, tubulin) and stereocilia (green, phalloidin) in the cortical organ of *Gsc* knockout mouse embryos (D,F), compared to wt littermates (C,E) schematically depicted in (E,F). (G) Quantification of alignments, depicted as rose plots. According to the angle of deviations from the normal perpendicular orientation ( $90^\circ$ ), vectors were plotted in  $11.25^\circ$  sectors. The area of a sector represents the number of cells with this directionality. Note that significantly higher deviations from the normal perpendicular orientation ( $90^\circ$ ) were observed in OHC3 of *Gsc* knockout specimens (middle, red,  $n = 390$ ) compared to wildtype littermates (left, blue,  $n = 308$ ,  $p = 0.03$ ).

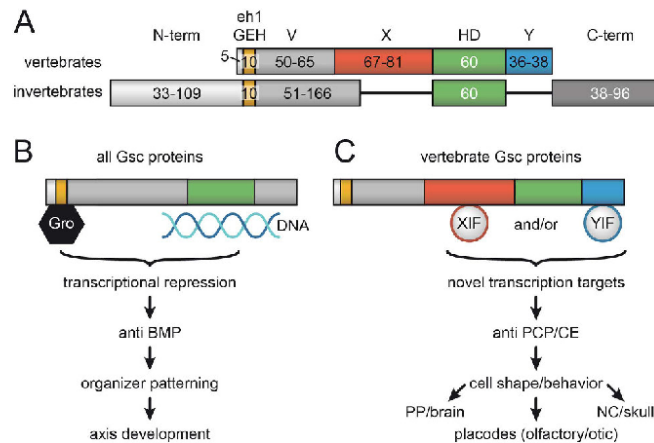


**Figure 9. Vertebrate-specific Gsc functions: a model.** (A) Domain structure of invertebrate and vertebrate Gsc proteins; numbers indicate ranges of amino acids. The engrailed homology (eh1/GEF) repression domain and the homeodomain (HD) are common to all Gsc proteins. Two highly conserved domains (X, Y) flanking the HD emerged at the base of the vertebrates. Note that invertebrates, besides lacking X/Y, possess variable length N- and C-terminal sequences and that the linker region between eh1/GEF and HD also varies greatly in length. (B) All Gsc proteins have the potential to act as transcriptional repressors through HD-binding to DNA and Groucho-recruitment to eh1/GEF. When assayed in *Xenopus*, *Drosophila* and vertebrate Gsc proteins act in organizer patterning and axis development through their conserved anti-BMP function. (C) Vertebrate Gsc proteins in addition affect cell shape and behavior through their anti PCP/CE function. We propose that X- and Y-domain interacting factors XIF and YIF function in recruiting novel transcriptional target genes under Gsc control. We further propose that this novel function of Gsc co-evolved with the vertebrate-specific novelties of an enlarged brain, skull and placodes, as vertebrate Gsc is expressed in the prechordal plate/floor plate of the diencephalon, neural crest mesenchyme and derivatives as well as otic vesicle/nasal cavity.

inner ear phenotype in the genetic knockout situation is the result of a non-cell autonomous effect of Gsc. It thus appears that context-dependently Gsc acts in a cell or non-cell autonomous manner to repress PCP/CE.

The inability of *Drosophila* Gsc to interfere with PCP/CE (while inducing double axis formation even more efficiently than *Xenopus* or mouse Gsc) indicates that this function either arose during vertebrate evolution or was lost in *Drosophila*. To approach this question, we compared Gsc protein sequences across the animal kingdom. In invertebrates, no conserved regions besides the highly conserved eh1/GEH domain and a basically invariant homeodomain (HD) were found, arguing against a loss of anti-PCP/CE activity in *Drosophila* (Fig. 9A, Fig. S7). The presence of eh1/GEH and HD in all Gsc sequences in addition suggests that all proteins should have the potential to act as transcriptional repressors in organizer patterning and axis development, at least when assayed in *Xenopus*, a function which is mediated through Gsc's well-documented anti-BMP function (Fig. 9B)<sup>16,76</sup>. Vertebrate Gsc proteins in contrast possess two novel highly conserved domains flanking the HD, which we address as "X" and "Y" (Fig. 9A, Fig. S7). Interestingly, both domains are absent in the cephalochordate amphioxus, in which neither a cranium nor neural crest have evolved yet<sup>77-79</sup>, as well as in the lamprey, a primitive agnathan vertebrate that has neural crest but lacks jaws<sup>80</sup> (not shown). When databases were screened for sequences related to X and Y, exclusively vertebrate Gsc sequences were picked up (not shown). These data indicate that the anti-PCP/CE function evolved at the base of the vertebrates, likely together with the acquisition of domains X and/or Y (or parts thereof). We like to propose that X- and/or Y-interacting factors (XIF and YIF in Fig. 8C) recruited Gsc to novel target promoters, either by direct DNA-binding of XIF/YIF or through interaction with other DNA-binding proteins. Vertebrate-specific target genes could function directly upstream of PCP components. Alternatively, they may act in a parallel pathway that controls competence for Wnt/PCP signaling. Elucidating the molecular mechanisms will involve the identification of (1) target genes; (2) peptides mediating the vertebrate anti-PCP/CE function, for example by introducing X/Y sequences and fragments thereof into *Drosophila* Gsc and assaying recombinant genes in *Xenopus*; (3) XIF/YIF, for example through the identification of the interactome of identified peptides.

Relating the emergence of the anti-PCP/CE function at the base of the vertebrates to post-gastrulation expression patterns in the vertebrates reveals a potentially highly relevant coincidence: Gsc transcripts are found in (1) the prechordal plate and floor plate of the diencephalon; (2) branchial arch mesenchyme and derivatives (skull cartilage, tongue, etc.<sup>68</sup>); (3) placodal derivatives (otic vesicle/organ of Corti, olfactory pit/nasal passage<sup>71</sup>, i.e. in tissues representing evolutionary novelties of the vertebrates<sup>81</sup>). It is tempting to speculate that Gsc was recruited into gene regulatory networks specific to these tissues to shape their morphogenesis by regulating cellular morphology and behavior.



In the light of this reasoning, an in-depth re-evaluation of the endogenous *Gsc* functions in the various vertebrates is in demand. While this manuscript was under review, two relevant studies were published. The analysis of otic vesicle differentiation in zebrafish morphants and TALEN-induced mutants revealed a function for *Gsc* in the delamination of neuroblasts, i.e. a process involving epithelial-to-mesenchymal transitions associated with cell shape changes and delamination/migration behavior<sup>82</sup>. Inner ear hair cell PCP was not investigated in this study. In *Xenopus*, a CRISPR/Cas9 approach to genome-editing of - among others - *Gsc* was reported and specimens were shown to display massive head defects, that were not further characterized<sup>83</sup> but in perfect agreement with the neural crest/skull phenotypes reported here. Genome editing should provide a powerful complementing means to the use of MOs for studying *Gsc* function, as applicable MO-doses may be the limiting factor in such experiments, based on the observed gain-of-function by loss-of-function, i.e. interference with the negative auto-regulatory feedback loop (cf. Fig. S5G,H). Even antisense RNA may prove useful in the future. The late Herbert Steinbeißer and colleagues previously injected such RNAs into the axial midline and noted that the notochord was expanded at the expense of the prechordal plate<sup>16</sup>. Unfortunately, this loss-of-function approach fell in disgrace<sup>84</sup> and the prechordal plate phenotype was never fully characterized.

The knockout mouse in any case deserves to be re-evaluated. When we analyzed *Gsc* expression domains during organogenesis stages, we found transcripts adjacent to tissues that elongate during development, which might involve PCP-mediated convergent extension. *Gsc* mRNA was for example found at the anterior tip of the tongue, in the arytoid swellings and the palatal shelves<sup>71</sup> (Fig. S8). The previously described limb bud expression fits to this proposal as well, as limb bud differentiation was identified as a PCP-dependent process as well<sup>85,86</sup>.

Finally, the early embryonic expression pattern of *Gsc* in vertebrate embryos is in agreement with such a function. The first transcription in the organizer tissue itself is very transient. As axial mesodermal cells (prechordal plate and notochord) migrate out in rostral direction, *Gsc* is downregulated in the organizer, maintained in the prechordal cells and absent in the notochord<sup>10,26,27</sup>. Segregation of organizer-derived cells into these two populations is accompanied by differences in cell behavior (single cell migration of the prechordal cells and CE in the notochord) and gene expression (*Gsc* in the prechordal and *Brachyury* in the notochordal mesoderm<sup>28-30,87,88</sup>). *Gsc*, thus, may provide the switch between cell intercalation and cell migration by limiting CE to the notochord. 25 years after the first characterization of *Gsc* in the organizer, the fascination for this gene continues. Much has to be learned about its function in development and disease.

## Methods

All methods were performed in accordance with the relevant guidelines and regulations.

**Statement of approval of animal experimentation.** Handling, care and experimental manipulations of were approved by the Regional Government Stuttgart, Germany (Vorhaben A379/12 ZO "Molekulare Embryologie"), according to German regulations and laws (§6, article 1, sentence 2, nr. 4 of the animal protection act).

**Plasmids and construction of *Xenopus* expression vectors.** K197E<sup>17</sup> was obtained from Dan Kessler, Wnt11 constructs were from Kristen Kwan, Vangl2 from Ray Keller, and Prickle1 from Naoto Ueno. *Gsc*-GR has been described in ref. 89. Fgf8, Fz7, Dvl2-GFP, dnRhoA and caRhoA constructs were provided by the Steinbeißer laboratory.

The following PCR primers were used for cloning of deletion constructs  $\Delta$ HD and  $\Delta$ GEH:  $\Delta$ HDfor 5'-ATATCGATGCGCTGCAAGGAGTCGCTGCTG-3',  $\Delta$ HDrev 5'-CTGGACTCTGACAGTGGTCCTCGAGAT-3',  $\Delta$ GEHfor 5'-ATATCGATGCGCTGCAAGGAGTCGCTGCTG-3',  $\Delta$ GEHrev 5'-CTGGACTCTGACAGTGGTCCTCGAGAT-3'. The starting construct to clone T-*Gsc* was PML129 (vector backbone PGEM3, Promega), which contained the 658 bp *Brachyury* streak promoter, followed by a floxed LacZ cassette with triplicate polyadenylation signals to ensure that the downstream open reading frame is not part of the mRNA. To create construct T-*Gsc* the 771 bp *Gsc* coding sequence was inserted downstream, flanked by a 231 bp polyadenylation signal from the bovine growth hormone gene (from pRc/CMV, Invitrogen). Construct mT-*Gsc* was generated by mutating the *Brachyury* streak promoter 35bp downstream of the transcriptional start site from TAAT into ACTG<sup>11</sup>.

**Generation of transient chimeric embryos.** Two constructs were used to transfect mouse ES cells (line E14-KPA, kindly provided by Klaus Peter Knobloch, FMP, Berlin, Germany), a *Gsc* and a LacZ expression construct, which both used the human ubiquitin promoter. Stable lines were selected by co-transfection of the selection plasmid containing the PGK-neo cassette. Individual clones were characterized for transgene expression by RT-PCR analysis (pcubi-*Gsc* primer; see below). A clone displaying high expression levels was used in blastocyst injection experiments to derive transgenic embryos which were harvested at E9.5 and E10.5.

**Generation of T-*Gsc* and mT-*Gsc* mouse lines and Cre-mediated transgene activation.** Inserts of vectors were isolated by KpnI enzyme digestion and introduced by electroporation into E14-KPA and CJ7 cells (kindly provided by Thomas Gridley, Jackson Laboratory, USA), and cultured following standard procedures. After G418 selection (250 µg/ml), four transgenic clones were identified with T-*Gsc* and 28 clones with mT-*Gsc*, each containing single copy gene integration verified by Southern blot analysis. Reporter gene activity was tested by X-gal staining of mesodermally differentiated clones, which express *Brachyury*. Mesodermal differentiation was performed in hanging drop cultures in the presence of DMSO. Clones showing strong reporter gene activity were used to generate transgenic mice, which were derived from C57BL/6J blastocyst injections. Offspring of germ line-transmitting chimeric mice were screened for the presence of the T-*Gsc* transgene. Heterozygous mice were kept on a mixed background and mated to obtain homozygous animals. One line was obtained with T-*Gsc* and two lines with mT-*Gsc*. Transgenes were activated by crossing homozygous deleter females with homozygous T-*Gsc* or mT-*Gsc* males.

**Genotyping of transgenic mice and embryos.** DNA from embryos and tail biopsies was isolated using standard protocols. Primers and PCR conditions were as follows:

LoxP primer: a) 5'-TCAATCCGCGTTTGTTC; 3'-CCGCCACATATCCTGATCTTC; 280 bp, 55 °C b) 5'-GCAGTGCACGGCAGATACACACTT; 3'-CCCCATATGGAAACCGTCG; 510 bp, 55 °C; c) 5'-GGGACGCGCAATTGAATGAATTA; 3'-CCCCATATGGAAACCGTCG; 160 bp, 55 °C;

Cre primer: a) 5'-CGCATAACCAGTAAAACAGCAT; 3'-GAAAGTCGAGTAGGCGTGTACG; 550 bp, 55 °C b) 5'-TAATCGCCATCTTCCAGCAG; 3'-GCTGGCTGGTGGCAGATGGCG; 650 bp, 55 °C; c) 5'-CAATTTACTGACCGTACAC; 3'-GCTGGCTGGTGGCAGATGGCG; 751 bp, 55 °C; Gsc-bGHPa primer: 5'-GTTCTGTACTGGTGTCTCG (in Exon3 of Gsc); 3'-GGCACCTTCCAGGGTCAAGG (in the polyadenylation signal of the bovine growth hormone); 277 bp, 63.5 °C; pcubi-Gsc 5'-CCACTAGTCCAGTGTGGTGG; 3'-GACGCAGGGCTGCGGGGTC; 385 bp, 65 °C.

**Manipulations of *Xenopus* embryos.** For microinjections, drop size was calibrated to about 8 nl/injection. Embryo culture and microinjection followed standard procedures. mRNAs were prepared using the Ambion message machine kit. DsRed mRNA (1.6 ng mRNA/embryo) and rhodamine-B dextran (0.5–1.0 µg/µl; Molecular Probes) were used as lineage tracers. Unless indicated otherwise, 400 pg Xgsc-GR mRNA/embryo was injected<sup>32</sup>. Gsc-GR fusion protein was activated by the addition of 10 µg/ml dexamethasone at stage 6–8 (unless specified otherwise). Concentrations of injected mRNAs (transcribed from CS2<sup>+</sup>-expression vectors) were: constitutive active RhoA V14 (32–64 pg mRNA/embryo), dominant negative RhoA N19<sup>90</sup> (320 pg mRNA/embryo), *Prickle1*<sup>91</sup> (1.8 ng/embryo), *Vangl2/Strb*<sup>53</sup> (400 pg/embryo), *T* (800 pg mRNA/embryo; cds of mouse *Brachyury*), and *Wnt11*<sup>29</sup> (80 pg mRNA/embryo). For Knock-down experiments a coding morpholino was used (5'-GCTGAACATGCCAGAAGGCATCACC-3, Gene Tools LLC<sup>21</sup>). Statistical calculations were performed using Pearson's chi-square test comparing the number of affected embryos against the number of wt embryos (Statpages.com).

**Manipulations of *Xenopus* explants.** Keller open face explants were prepared as described<sup>37,87</sup>, except that DFA medium was used. Animal cap assays were conducted according to Green, 1999. All cells of the 4-cell embryo were injected into the animal pole, dex was added at stage 6, where indicated, and the animal caps were cut at stage 9. Recombinant human Activin A (R&D Systems) was added immediately after cutting and the embryos were cultured until control specimens reached stage 22–30. For the Dvl2 localization assay, the following mRNAs, transcribed with the Ambion message machine from CS2<sup>+</sup> vectors, were injected: a construct containing the C-terminal DEP-domain of Dvl2 fused to GFP (400 pg/cell; D9<sup>56</sup>), *Frizzled7*<sup>92</sup> (400 pg/cell), *Fgf8* (8.8 pg/cell), *Gsc-GR*<sup>32</sup> (560 pg/cell). Explants were cultured until control siblings reached stage 10.5.

**RT-PCR.** Total RNA was isolated from animal cap explants at stage 10.5, and cDNAs were prepared using standard protocols. Primers used for amplification where from different exons to avoid genomic contamination. *EFlalpha* served as loading control. EFlα: for 5'-ACTGCCTTGATGATGATCCTCTAG rev 5'-CAGATTGGTGCTGGATATGC; *Wnt11*: for 5-TGACGGTCTAGTCCCTGACCA, rev 5'-GGT TGCAGCTGTACCTACCA; *Xbra*: for 5'-CACAGTTCATAGCAGTGACCG, rev 5'-TTCTGTG AGTGACGGACTGG.

**Analysis of cell proliferation and apoptosis.** Immunofluorescence was performed on whole-mount embryos, fixed for 1–2 hours at room temperature in 4% PFA for cell proliferation or in methanol/DMSO (4:1; Dent's solution) for assessment of apoptosis. Embryos were processed as previously published and according to standard procedures<sup>93,94</sup>. Ethanol treatment (2.5%) served as positive control for the apoptosis assay. Primary antibodies: polyclonal rabbit anti-phospho-Histone H3 (Ser10; 1:700; Merck), monoclonal rabbit anti-caspase-3 Ab (1:150; 9665, Cell Signaling Technologies). Secondary antibody: Alexa Fluor 488-conjugated goat anti-rabbit (1:750, Invitrogen).

**RNA *in situ* hybridization and histological analysis.** *Xenopus* and mouse embryos were fixed in 4% PFA for 2 hrs and processed following standard protocols. Digoxigenin-labelled (Roche) RNA probes were prepared from linearized plasmids using SP6 or T7 RNA polymerase (Promega). *In situ* hybridization was performed as described<sup>95</sup>. Cartilage was stained with 0.05% alcian blue followed by bleaching. For histological analysis embryos were embedded in gelatine-albumin and sectioned on a vibratome (30 µm).

**Analysis of cell shape and gene expression domains.** Aspect ratios of cell shape and gene expression domains as well as statistical significances were calculated by Mann-Whitney-U test in statistical R (R-Development-Core-Team, 2008). The whiskers of the box plots extend to maximal 1.5 × IQR, outliers are displayed as dots. Aspect ratio = major axis/minor axis. Major and minor are the primary and secondary axis of the best fitting ellipse.

**Scanning Electron Microscopy.** SEM analysis was performed following published protocols<sup>96</sup>. In brief, embryos were dissected and immediately fixed in 2.5% glutaraldehyde in Soerensen's buffer (0.1 M sodium phosphate buffer; pH 7.4). Specimens were postfixed in 1% OsO<sub>4</sub>, critical point dried, sputter coated, and examined using a Zeiss DSM 940 A SEM (Oberkochen, Germany).

**Analysis of the cortical organ.** The inner ear of E18.5 embryos was dissected and fixed in 4% PFA for 2 days at 4 °C. Cochleae were opened for better accessibility and stained with a mouse monoclonal antibody directed against acetylated alpha tubulin (1:700; Sigma), Cy3-conjugated secondary polyclonal rabbit sheep anti



mouse antibodies (Sigma; 1:250) and Alexa Fluor® 488 Phalloidin (Molecular probes, 1:40) following standard procedures, and imaged using a Zeiss LSM Pascal 5 Confocal Laser Scanning Microscope.

To determine stereociliary bundle orientation, we used the angle measurement tool in ImageJ, measuring the angle between the line from the position of the kinocilium through the middle of the “V”-shaped stereocilia and a line parallel to the mediolateral axis. In perfectly aligned cells, this angle is 90°. A Wilcoxon rank sum test with continuity correction in statistical R (R-Development-Core-Team, 2008) was used for statistical analyses.

## References

1. Paré, A. C. *et al.* A positional Toll receptor code directs convergent extension in *Drosophila*. *Nature* **515**, 523–527 (2014).
2. Ninomiya, H., Elinson, R. P. & Winklbauer, R. Antero-posterior tissue polarity links mesoderm convergent extension to axial patterning. *Nature* **430**, 364–367 (2004).
3. Blum, M. *et al.* Ciliation and gene expression distinguish between node and posterior notochord in the mammalian embryo. *Differentiation* **75**, 133–146 (2007).
4. Spemann, H. & Mangold, H. Über Induktion von Embryonalanlagen durch Implantation artfremder Organisatoren. *Archiv für Entwicklungsmechanik der Organismen* **100**, 599–638 (1924).
5. Blum, M. *et al.* Gastrulation in the mouse: the role of the homeobox gene *goosecoid*. *Cell* **69**, 1097–1106 (1992).
6. Broun, M., Sokol, S. & Bode, H. R. *Cngsc*, a homologue of *goosecoid*, participates in the patterning of the head, and is expressed in the organizer region of *Hydra*. *Development* **126**, 5245–5254 (1999).
7. Cho, K. W., Blumberg, B., Steinbeisser, H. & de Robertis, E. M. Molecular nature of Spemann's organizer: the role of the *Xenopus* homeobox gene *goosecoid*. *Cell* **67**, 1111–1120 (1991).
8. Christian, J. L. & Moon, R. T. Interactions between *Xwnt-8* and Spemann organizer signaling pathways generate dorsoventral pattern in the embryonic mesoderm of *Xenopus*. *Genes Dev* **7**, 13–28 (1993).
9. Fainsod, A., Steinbeisser, H. & de Robertis, E. M. On the function of BMP-4 in patterning the marginal zone of the *Xenopus* embryo. *EMBO J.* **13**, 5015–5025 (1994).
10. Artinger, M., Blitz, I., Inoue, K., Tran, U. & Cho, K. W. Interaction of *goosecoid* and *brachyury* in *Xenopus* mesoderm patterning. *Mech. Dev.* **65**, 187–196 (1997).
11. Boucher, D. M. *et al.* *Goosecoid* expression represses *Brachyury* in embryonic stem cells and affects craniofacial development in chimeric mice. **44**, 279–288 (2000).
12. Dixon Fox, M. & Bruce, A. E. E. Short- and long-range functions of *Goosecoid* in zebrafish axis formation are independent of Chordin, Noggin 1 and Follistatin-like 1b. *Development* **136**, 1675–1685 (2009).
13. Latinkic, B. V. & Smith, J. C. *Goosecoid* and *mix.1* repress *Brachyury* expression and are required for head formation in *Xenopus*. *Development* **126**, 1769–1779 (1999).
14. Latinkic, B. V. *et al.* The *Xenopus* *Brachyury* promoter is activated by FGF and low concentrations of activin and suppressed by high concentrations of activin and by paired-type homeodomain proteins. *Genes Dev* **11**, 3265–3276 (1997).
15. Seiliez, I., Thisse, B. & Thisse, C. *FoxA3* and *goosecoid* promote anterior neural fate through inhibition of *Wnt8a* activity before the onset of gastrulation. *Dev Biol* **290**, 152–163 (2006).
16. Steinbeisser, H., Fainsod, A., Niehrs, C., Sasai, Y. & de Robertis, E. M. The role of *gsc* and BMP-4 in dorsal-ventral patterning of the marginal zone in *Xenopus*: a loss-of-function study using antisense RNA. *EMBO J.* **14**, 5230–5243 (1995).
17. Yao, J. & Kessler, D. S. *Goosecoid* promotes head organizer activity by direct repression of *Xwnt8* in Spemann's organizer. *Development* **128**, 2975–2987 (2001).
18. Yasuo, H. & Lemaire, P. Role of *Goosecoid*, *Xnot* and *Wnt* antagonists in the maintenance of the notochord genetic programme in *Xenopus* gastrulae. *Development* **128**, 3783–3793 (2001).
19. Rivera-Pérez, J. A., Mallo, M., Gendron-Maguire, M., Gridley, T. & Behringer, R. R. *Goosecoid* is not an essential component of the mouse gastrula organizer but is required for craniofacial and rib development. *Development* **121**, 3005–3012 (1995).
20. Yamada, G. *et al.* Targeted mutation of the murine *goosecoid* gene results in craniofacial defects and neonatal death. *Development* **121**, 2917–2922 (1995).
21. Sander, V., Reversade, B. & de Robertis, E. M. The opposing homeobox genes *Goosecoid* and *Vent1/2* self-regulate *Xenopus* patterning. *EMBO J.* **26**, 2955–2965 (2007).
22. Ferreira, B., Artinger, M., Cho, K. & Niehrs, C. Antimorphic *goosecoids*. *Development* **125**, 1347–1359 (1998).
23. Niehrs, C., Keller, R., Cho, K. W. & de Robertis, E. M. The homeobox gene *goosecoid* controls cell migration in *Xenopus* embryos. *Cell* **72**, 491–503 (1993).
24. Luu, O., Nagel, M., Wacker, S., Lemaire, P. & Winklbauer, R. Control of gastrula cell motility by the *Goosecoid/Mix.1/Siamois* network: basic patterns and paradoxical effects. *Dev Dyn.* **237**, 1307–1320 (2008).
25. Hartwell, K. A. *et al.* The Spemann organizer gene, *Goosecoid*, promotes tumor metastasis. *Proc Natl Acad Sci USA* **103**, 18969–18974 (2006).
26. Blum, M. *et al.* Ciliation and gene expression distinguish between node and posterior notochord in the mammalian embryo. *Differentiation* **75**, 133–146 (2007).
27. Schulte-Merker, S. *et al.* Expression of zebrafish *goosecoid* and no tail gene products in wild-type and mutant no tail embryos. *Development* **120**, 843–852 (1994).
28. Winklbauer, R. Mesodermal cell migration during *Xenopus* gastrulation. *Dev Biol* **142**, 155–168 (1990).
29. Kwan, K. M. *Xbra* functions as a switch between cell migration and convergent extension in the *Xenopus* gastrula. *Development* **130**, 1961–1972 (2003).
30. Domingo, C. & Keller, R. Induction of notochord cell intercalation behavior and differentiation by progressive signals in the gastrula of *Xenopus laevis*. *Development* **121**, 3311–3321 (1995).
31. Yamada, T. Caudalization by the amphibian organizer: *brachyury*, convergent extension and retinoic acid. *Development* **120**, 3051–3062 (1994).
32. Shapira, E., Marom, K., Yelin, R., Levy, A. & Fainsod, A. A role for the homeobox gene *Xvex-1* as part of the BMP-4 ventral signaling pathway. *Mech. Dev.* **86**, 99–111 (1999).
33. Ewald, A. J., Peyrot, S. M., Tyszk, J. M., Fraser, S. E. & Wallingford, J. B. Regional requirements for Dishevelled signaling during *Xenopus* gastrulation: separable effects on blastopore closure, mesendoderm internalization and archenteron formation. *Development* **131**, 6195–6209 (2004).
34. Shih, J. & Keller, R. The epithelium of the dorsal marginal zone of *Xenopus* has organizer properties. *Development* **116**, 887–899 (1992).
35. Keller, R., Shook, D. & Skoglund, P. The forces that shape embryos: physical aspects of convergent extension by cell intercalation. *Phys Biol* **5**, 015007 (2008).
36. Keller, R. & Tibbetts, P. Mediolateral cell intercalation in the dorsal, axial mesoderm of *Xenopus laevis*. *Dev Biol* **131**, 539–549 (1989).
37. Sive, H. L., Grainger, R. M. & Harland, R. M. *Xenopus laevis* Keller Explants. *CSH Protoc* **2007**, pdb.prot4749–pdb.prot4749 (2007).

38. Kühl, M. *et al.* Antagonistic regulation of convergent extension movements in *Xenopus* by Wnt/ $\beta$ -catenin and Wnt/Ca<sup>2+</sup> signaling. *Mech. Dev.* **106**, 61–76 (2001).
39. McCulloch, C. A. & Tenenbaum, H. C. Dexamethasone induces proliferation and terminal differentiation of osteogenic cells in tissue culture. *Anat Rec* **215**, 397–402 (1986).
40. Matus, D. Q. *et al.* Molecular evidence for deep evolutionary roots of bilaterality in animal development. *Proc Natl Acad Sci USA* **103**, 11195–11200 (2006).
41. Lartillot, N., Le Gouar, M. & Adoutte, A. Expression patterns of fork head and gooseoid homologues in the mollusc *Patella vulgata* supports the ancestry of the anterior mesendoderm across Bilateria. *Dev. Genes Evol.* **212**, 551–561 (2002).
42. Mailhos, C. *et al.* *Drosophila* Gooseoid requires a conserved heptapeptide for repression of paired-class homeoprotein activators. *Development* **125**, 937–947 (1998).
43. Tessmar-Raible, K. & Arendt, D. Emerging systems: between vertebrates and arthropods, the Lophotrochozoa. *Curr. Opin. Genet. Dev.* **13**, 331–340 (2003).
44. Goriely, A. *et al.* A functional homologue of gooseoid in *Drosophila*. *Development* **122**, 1641–1650 (1996).
45. Lewandoski, M. Conditional control of gene expression in the mouse. *Nat. Rev. Genet.* **2**, 743–755 (2001).
46. Clements, D., Taylor, H. C., Herrmann, B. G. & Stott, D. Distinct regulatory control of the Brachyury gene in axial and non-axial mesoderm suggests separation of mesoderm lineages early in mouse gastrulation. *Mech. Dev.* **56**, 139–149 (1996).
47. Danilov, V., Blum, M., Schweickert, A., Campione, M. & Steinbeisser, H. Negative autoregulation of the organizer-specific homeobox gene gooseoid. *J. Biol. Chem.* **273**, 627–635 (1998).
48. Schwenk, F., Baron, U. & Rajewsky, K. A cre-transgenic mouse strain for the ubiquitous deletion of loxP-flanked gene segments including deletion in germ cells. *Nucleic Acids Res* **23**, 5080–5081 (1995).
49. Park, T. J., Gray, R. S., Sato, A., Habas, R. & Wallingford, J. B. Subcellular localization and signaling properties of Dishevelled in developing vertebrate embryos. *Current Biology* **15**, 1039–1044 (2005).
50. Wallingford, J. B. & Harland, R. M. Neural tube closure requires Dishevelled-dependent convergent extension of the midline. *Development* **129**, 5815–5825 (2002).
51. Ybot-Gonzalez, P. *et al.* Convergent extension, planar-cell-polarity signalling and initiation of mouse neural tube closure. *Development* **134**, 789–799 (2007).
52. Axelrod, J. D., Miller, J. R., Shulman, J. M., Moon, R. T. & Perrimon, N. Differential recruitment of Dishevelled provides signaling specificity in the planar cell polarity and Wingless signaling pathways. *Genes Dev* **12**, 2610–2622 (1998).
53. Wallingford, J. B. *et al.* Dishevelled controls cell polarity during *Xenopus* gastrulation. *Nature* **405**, 81–85 (2000).
54. Carreira-Barbosa, F. *et al.* Prickle 1 regulates cell movements during gastrulation and neuronal migration in zebrafish. *Development* **130**, 4037–4046 (2003).
55. Park, M. & Moon, R. T. The planar cell-polarity gene *stbm* regulates cell behaviour and cell fate in vertebrate embryos. *Nat Cell Biol* **4**, 20–25 (2002).
56. Rothbacher, U. *et al.* Dishevelled phosphorylation, subcellular localization and multimerization regulate its role in early embryogenesis. *EMBO J.* **19**, 1010–1022 (2000).
57. Green, J. In *Molecular Methods in Developmental Biology* 127, 1–14 (Humana Press, 1999).
58. Blum, M. *et al.* Gastrulation in the mouse: the role of the homeobox gene gooseoid. *Cell* **69**, 1097–1106 (1992).
59. Blumberg, B., Wright, C. V., De Robertis, E. M. & Cho, K. W. Organizer-specific homeobox genes in *Xenopus laevis* embryos. *Science* **253**, 194–196 (1991).
60. Fletcher, R. B., Baker, J. C. & Harland, R. M. FGF8 spliceforms mediate early mesoderm and posterior neural tissue formation in *Xenopus*. *Development* **133**, 1703–1714 (2006).
61. Tahinci, E. & Symes, K. Distinct functions of Rho and Rac are required for convergent extension during *Xenopus* gastrulation. *Dev Biol* **259**, 318–335 (2003).
62. Wang, Y. & Nathans, J. Tissue/planar cell polarity in vertebrates: new insights and new questions. *Development* **134**, 647–658 (2007).
63. Goto, T. & Keller, R. The planar cell polarity gene *strabismus* regulates convergence and extension and neural fold closure in *Xenopus*. *Dev Biol* **247**, 165–181 (2002).
64. Wallingford, J. B., Goto, T., Keller, R. & Harland, R. M. Cloning and expression of *Xenopus* Prickle, an orthologue of a *Drosophila* planar cell polarity gene. *Mech. Dev.* **116**, 183–186 (2002).
65. Conlon, F. L. & Smith, J. C. Interference with brachyury function inhibits convergent extension, causes apoptosis, and reveals separate requirements in the FGF and activin signalling pathways. *Dev Biol* **213**, 85–100 (1999).
66. Tada, M. & Smith, J. C. *Xwnt11* is a target of *Xenopus* Brachyury: regulation of gastrulation movements via Dishevelled, but not through the canonical Wnt pathway. *Development* **127**, 2227–2238 (2000).
67. Danilov, V., Blum, M., Schweickert, A., Campione, M. & Steinbeisser, H. Negative Autoregulation of the Organizer-specific Homeobox Gene gooseoid. *Journal of Biological ...* (1998).
68. Gaunt, S. J., Blum, M. & de Robertis, E. M. Expression of the mouse gooseoid gene during mid-embryogenesis may mark mesenchymal cell lineages in the developing head, limbs and body wall. *Development* **117**, 769–778 (1993).
69. Ahrens, M. J., Li, Y., Jiang, H. & Dudley, A. T. Convergent extension movements in growth plate chondrocytes require gpi-anchored cell surface proteins. *Development* **136**, 3463–3474 (2009).
70. Park, T. J., Haigo, S. L. & Wallingford, J. B. Ciliogenesis defects in embryos lacking *inturned* or *fuzzy* function are associated with failure of planar cell polarity and Hedgehog signaling. *Nat Genet* **38**, 303–311 (2006).
71. Gaunt, S. J., Blum, M. & de Robertis, E. M. Expression of the mouse gooseoid gene during mid-embryogenesis may mark mesenchymal cell lineages in the developing head, limbs and body wall. *Development* **117**, 769–778 (1993).
72. Munnamalai, V. & Fekete, D. M. Wnt signaling during cochlear development. *Semin Cell Dev Biol* **24**, 480–489 (2013).
73. Kelly, M. & Chen, P. Shaping the mammalian auditory sensory organ by the planar cell polarity pathway. *Int J Dev Biol* **51**, 535–547 (2007).
74. Parry, D. A. *et al.* SAMS, a syndrome of short stature, auditory-canal atresia, mandibular hypoplasia, and skeletal abnormalities is a unique neurocristopathy caused by mutations in Gooseoid. *Am. J. Hum. Genet.* **93**, 1135–1142 (2013).
75. Qian, D. *et al.* Wnt5a functions in planar cell polarity regulation in mice. *Dev Biol* **306**, 121–133 (2007).
76. Onichtchouk, D. *et al.* The *Xvent-2* homeobox gene is part of the BMP-4 signalling pathway controlling [correction of controlling] dorsoventral patterning of *Xenopus* mesoderm. *Development* **122**, 3045–3053 (1996).
77. Putnam, N. H. *et al.* The amphioxus genome and the evolution of the chordate karyotype. *Nature* **453**, 1064–1071 (2008).
78. Yu, J.-K. S. The evolutionary origin of the vertebrate neural crest and its developmental gene regulatory network – insights from amphioxus. *Zoology (Jena)* **113**, 1–9 (2010).
79. Yu, J.-K., Meulemans, D., McKeown, S. J. & Bronner-Fraser, M. Insights from the amphioxus genome on the origin of vertebrate neural crest. *Genome Res.* **18**, 1127–1132 (2008).
80. Shimeid, S. M. & Donoghue, P. C. J. Evolutionary crossroads in developmental biology: cyclostomes (lamprey and hagfish). *Development* **139**, 2091–2099 (2012).
81. Gans, C. & Northcutt, R. G. Neural crest and the origin of vertebrates: a new head. *Science* **220**, 268–273 (1983).
82. Kantarci, H., Gerberding, A. & Riley, B. B. Spemann organizer gene Gooseoid promotes delamination of neuroblasts from the otic vesicle. *Proc Natl Acad Sci USA* 201609146–16, doi: 10.1073/pnas.1609146113 (2016).

83. Blitz, I. L., Fish, M. B. & Cho, K. W. Y. Leapfrogging: primordial germ cell transplantation permits recovery of CRISPR/Cas9-induced mutations in essential genes. *Development* **143**, 2868–2875 (2016).
84. Blum, M., De Robertis, E. M., Wallingford, J. B. & Niehrs, C. Morpholinos: Antisense and Sensibility. *Dev. Cell* **35**, 145–149 (2015).
85. Gao, B. *et al.* Wnt signaling gradients establish planar cell polarity by inducing Vangl2 phosphorylation through Ror2. *Dev. Cell* **20**, 163–176 (2011).
86. Gros, J. *et al.* WNT5A/JNK and FGF/MAPK pathways regulate the cellular events shaping the vertebrate limb bud. *Curr. Biol.* **20**, 1993–2002 (2010).
87. Keller, R. & Winklbauer, R. In **27**, 39–89 (Elsevier, 1992).
88. Yamada, G. *et al.* Targeted mutation of the murine gooseoid gene results in craniofacial defects and neonatal death. *Development* **121**, 2917–2922 (1995).
89. Shapira, E., Marom I, K., Levy, V., Yelin, R. & Fainsod, A. The Xvex-1 antimorph reveals the temporal competence for organizer formation and an early role for ventral homeobox genes. *Mech. Dev.* **90**, 77–87 (2000).
90. Paterson, H. F. *et al.* Microinjection of recombinant p21rho induces rapid changes in cell morphology. *J. Cell Biol.* **111**, 1001–1007 (1990).
91. Takeuchi, M. *et al.* The prickle-related gene in vertebrates is essential for gastrulation cell movements. *Current Biology* **13**, 674–679 (2003).
92. Medina, A., Reintsch, W. & Steinbeisser, H. Xenopus frizzled 7 can act in canonical and non-canonical Wnt signaling pathways: implications on early patterning and morphogenesis. *Mech. Dev.* **92**, 227–237 (2000).
93. Tözser, J. *et al.* TGF- $\beta$  Signaling Regulates the Differentiation of Motile Cilia. *CellReports* **11**, 1000–1007 (2015).
94. Sive, H. L., Grainger, R. M. & Harland, R. M. *Early development of Xenopus laevis* (2000).
95. Belo, J. A. *et al.* Cerberus-like is a secreted factor with neutralizing activity expressed in the anterior primitive endoderm of the mouse gastrula. *Mech. Dev.* **68**, 45–57 (1997).
96. Sulik, K. *et al.* Morphogenesis of the murine node and notochordal plate. *Dev. Dyn.* **201**, 260–278 (1994).
97. Karpinka, J. B. *et al.* Xenbase, the Xenopus model organism database, new virtualized system, data types and genomes. *Nucleic Acids Res.* **43**, D756–63 (2015).

### Acknowledgements

This paper is dedicated to the memory of the late Herbert Steinbeißer, who passed away in 2014. He was involved in this project from its beginning in the 1990s; the Dvl2 membrane recruitment experiments in animal caps were performed in his laboratory. We thank all members of the Blum lab for continuous support and suggestions. Verena Andre, Andreas Faissler, Simone Kienle, Anna Schäfer and Susanne Seitz helped with some of the experiments. This work was supported by a grant from the Volkswagen Foundation to MB and a fellowship from the Landesgraduiertenförderung Baden-Württemberg to BU.

### Author Contributions

M.B. conceived the project and supervised it throughout. B.U. performed the *Xenopus* experiments except for the Gsc mutant analysis in whole embryos, the apoptosis and proliferation analysis in Gsc-GR injected neural plates, the Dvl2 membrane localization assay to investigate the cell-autonomous Gsc function in animal caps, the expression analysis of *Xenopus Gsc* during organogenesis and the protein alignments of invertebrate and vertebrate Gsc sequences, which were performed by M.T., S.K. and M.M.; D.M. analyzed the inner ear phenotype in Gsc knockout mice; M.C. generated the T-Gsc mouse line; K.D. generated and analyzed the mT-Gsc mouse line together with P.A.; M.L. provided the conditional mouse expression system; T.T. analyzed the cartilage phenotype in Gsc morphants; A.F. suggested important experiments and helped with the interpretation of results; A.S. provided constant advice and helped with the interpretation and evaluation of data. H.S. was an invaluable advisor throughout the project; he suggested the animal cap experiments, which B.U. performed in his laboratory. M.B. and B.U. wrote the manuscript with input from A.F., A.S., M.T., S.K., M.M., M.C., M.L.

### Additional Information

**Supplementary information** accompanies this paper at <http://www.nature.com/srep>

**Competing financial interests:** The authors declare no competing financial interests.

**How to cite this article:** Ulmer, B. *et al.* A novel role of the organizer gene *Gooseoid* as an inhibitor of Wnt/PCP-mediated convergent extension in *Xenopus* and mouse. *Sci. Rep.* **7**, 43010; doi: 10.1038/srep43010 (2017).

**Publisher's note:** Springer Nature remains neutral with regard to jurisdictional claims in published maps and institutional affiliations.



This work is licensed under a Creative Commons Attribution 4.0 International License. The images or other third party material in this article are included in the article's Creative Commons license, unless indicated otherwise in the credit line; if the material is not included under the Creative Commons license, users will need to obtain permission from the license holder to reproduce the material. To view a copy of this license, visit <http://creativecommons.org/licenses/by/4.0/>

© The Author(s) 2017

## Supplementary Information

### **A novel role of the organizer gene *Gooseoid* as an inhibitor of Wnt/PCP-mediated convergent extension in *Xenopus* and mouse**

Bärbel Ulmer<sup>1§+</sup>, Melanie Tingler<sup>1§</sup>, Sabrina Kurz<sup>1§</sup>, Markus Maerker<sup>1§</sup>, Philipp Andre<sup>1</sup>, Dina Mönch<sup>1</sup>, Marina Campione<sup>1\*</sup>, Kirsten Deißler<sup>1</sup>, Mark Lewandoski<sup>2</sup>, Thomas Thumberger<sup>1&</sup>, Axel Schweickert<sup>1</sup>, Abraham Fainsod<sup>3</sup>, Herbert Steinbeißer<sup>4</sup> and Martin Blum<sup>1#</sup>

<sup>1</sup>University of Hohenheim, Garbenstr. 30, 70599 Stuttgart, Germany

<sup>2</sup>Genetics of Vertebrate Development Section, Cancer and Developmental Biology Lab, National Cancer Institute, National Institutes of Health, Frederick, MD 21702, USA

<sup>3</sup>Department of Developmental Biology and Cancer Research, Institute for Medical Research Israel-Canada, Hebrew University, Jerusalem 9112102, Israel

<sup>4</sup>Institute of Human Genetics, University Hospital Heidelberg, Im Neuenheimer Feld 366, 69120 Heidelberg, Germany

<sup>+</sup>Present address: Department of Experimental Pharmacology and Toxicology, Cardiovascular Research Center, University Medical Center Hamburg-Eppendorf, 20246 Hamburg, Germany.

<sup>\*</sup>Present address: CNR-Neuroscience Institute, Department of Biomedical Sciences, University of Padova, Italy

<sup>&</sup>Present address: Centre for Organismal Studies (COS) Heidelberg, Heidelberg University, Im Neuenheimer Feld 230, 69120 Heidelberg, Germany

<sup>§</sup>These authors contributed equally to the present work

<sup>#</sup>Corresponding author: martin.blum@uni-hohenheim.de

## SUPPLEMENTARY INFORMATION

## Supplemental Figures and Tables

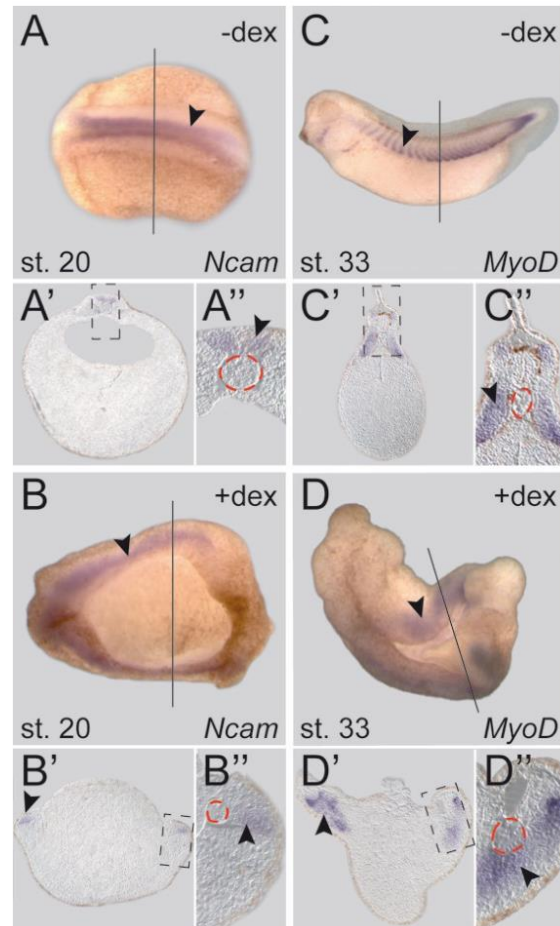


**Fig. S1. Characterization of *Gsc-GR* mediated CE phenotypes in *Xenopus* embryos.** Analysis of neural (*Ncam*; A, B) and paraxial mesodermal (somite; *MyoD*; C, D) marker gene expression in wildtype (-dex; A, C) and *Gsc-GR* expressing (+dex; B, D) embryos. Dex was added at stage 6-9, and embryos were analyzed for marker gene expression by whole-mount in situ hybridization following fixation at the stages indicated. Note that specification of examined tissues (arrowheads) was not affected. Solid lines indicate planes of sections, dashed boxes mark regions shown in higher magnification. Red dashed lines outline notochord.



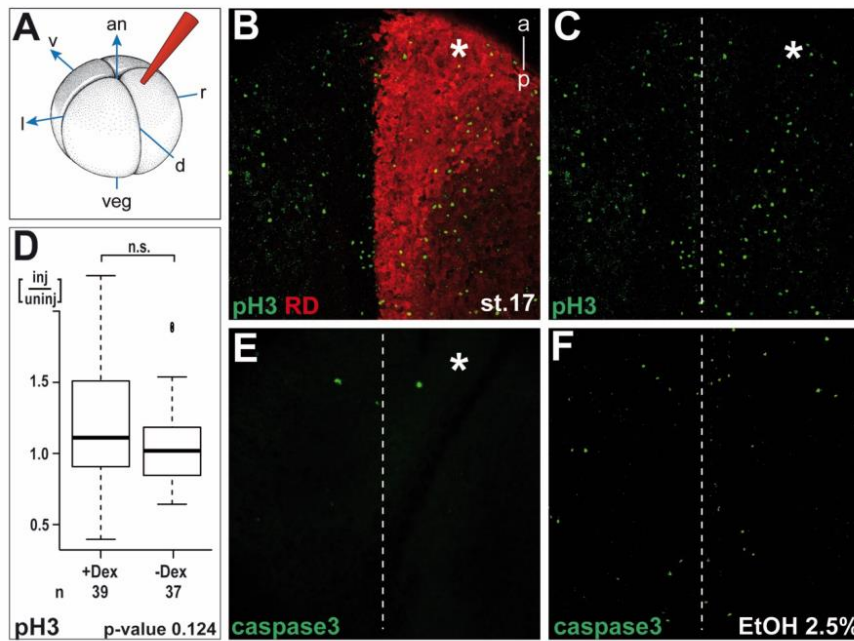
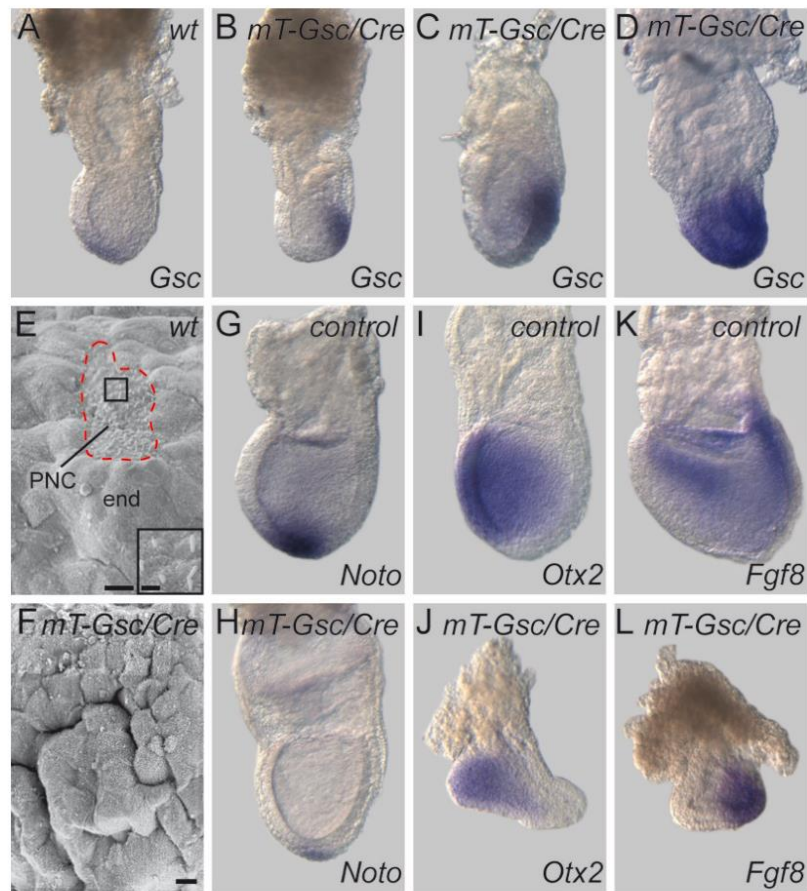


Fig. S2. Proliferation (A-D) and apoptosis (A, E, F) were unaffected upon Gsc-GR activation in the neuroectoderm. Embryos were unilaterally injected with *Gsc-GR* and lineage tracer rhodamine dextrane into the neuroectodermal (dorsal-animal) lineage at the 4-cell stage, dex was added (+Dex) or omitted (-Dex) between st. 6-8, and specimens were cultured until stage 17. \*, injected side. Proliferation and apoptosis were assessed by IF using an anti-pH3 (B, C) and anti-caspase3 antibodies (E, F), respectively. (D) Evaluation of proliferation. (F) Ethanol treatment at stage 13 (2.5%) served as a positive control for induction of apoptosis. Note that neither proliferation nor apoptosis were affected by Gsc-GR activation.



**Fig. S3. Characterization of E7.5 *mt-Gsc/Cre* embryos.**

(A-D) Variable degree of ectopic *Gsc* mRNA expression in E7.5 *mt-Gsc/Cre* embryos (B-D) compared to wildtype (A; wt).

(E, F) Scanning electron micrographs, revealing absence of ciliated epithelium of posterior notochord (PNC; outlined by dashed red line), and deep furrows in endodermal cell layer of *mt-Gsc/Cre* specimen (F) as compared to wt embryo (E). Detail of ciliated epithelium shown in higher magnification in inset of (E).

(G, H) Reduced *Noto* mRNA transcription in *mt-Gsc/Cre* (H) compared to wt (G) embryo.

(I-L) *Otx2* (I, J) and *Fgf8* (K, L) gene expression demonstrate normal anterior-posterior axis specification in *mt-Gsc/Cre* (J, L) compared to wt (I, K) embryos.

Scale bars in (E, F) represent 10  $\mu\text{m}$  and 2  $\mu\text{m}$  in inset of (E).

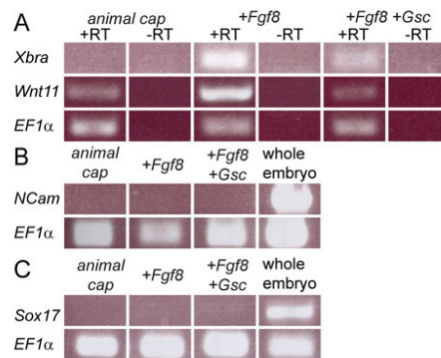


**Fig. S4. Mesodermal differentiation of *Fgf8*-injected animal cap explants.**

Semi-quantitative RT-PCR analysis of animal cap explants injected with *Gsc-GR* and/or *Fgf8*.

(A) *Fgf8* induces transcription of mesodermal marker genes *Xbra* and *Wnt11*.

(B, C) No induction of the neural marker *Ncam* (B) or the endoderm gene *Sox17* (C). Elongation factor 1 $\alpha$  (*EF1 $\alpha$* ) served as loading control.



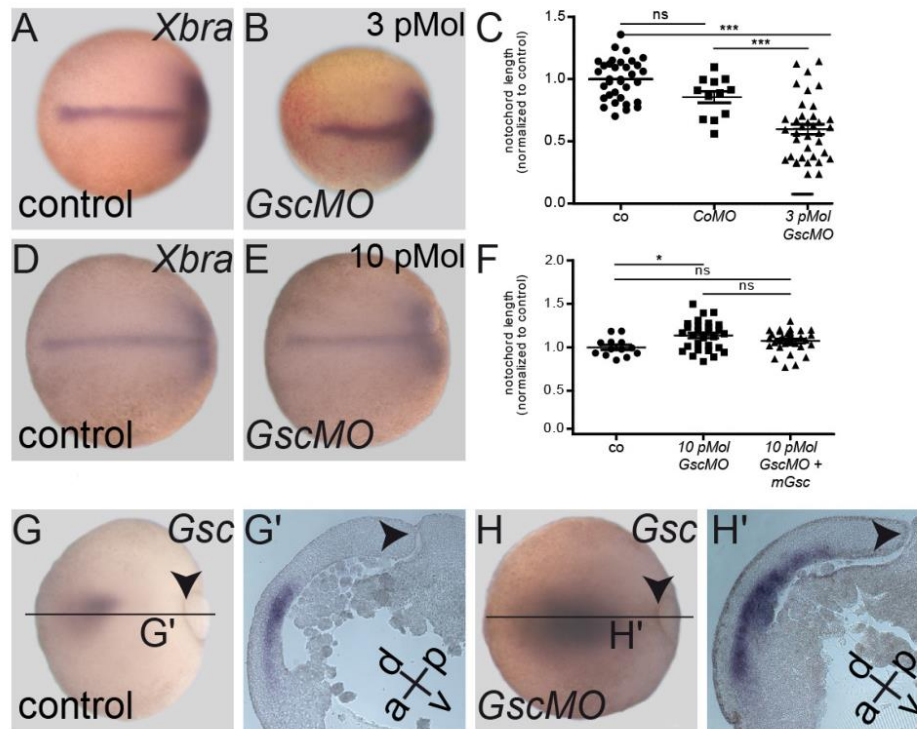


**Fig. S5. CE phenotypes in *Gsc* morphant *Xenopus* embryos.**

(A-C) Shorter and widened notochord as judged by *Xbra* mRNA expression in low dose *Gsc* morphant (B) as compared to control MO injected specimen (A). (C) Quantitative assessment of notochord lengths (normalized to control which was set to 1.0 in uninjected specimens).

(D-F) High dose injections of *GscMO* enhanced axis elongation. (D, E) *Xbra* mRNA expression in control un-injected embryo (co, D) and high dose *Gsc* morphant (E). (F) Quantification of notochord lengths in controls, high dose *Gsc* morphants and morphant specimens co-injected with a mouse *Gsc* cDNA construct.

(G, H) *Gsc* mRNA expression in low-dose *Gsc* morphants. (G, G') *Gsc* mRNA expression in control MO-injected neurula stage embryo. (H, H') Upregulated and expanded *Gsc* expression levels in *Gsc* morphant. Note that *Gsc* expression in morphant almost extended to the blastopore (arrowheads in G', H'). a, anterior; co, control un-injected; CoMO; control MO-injected; d, dorsal; p, posterior; v, ventral. Embryos shown with anterior to the left.

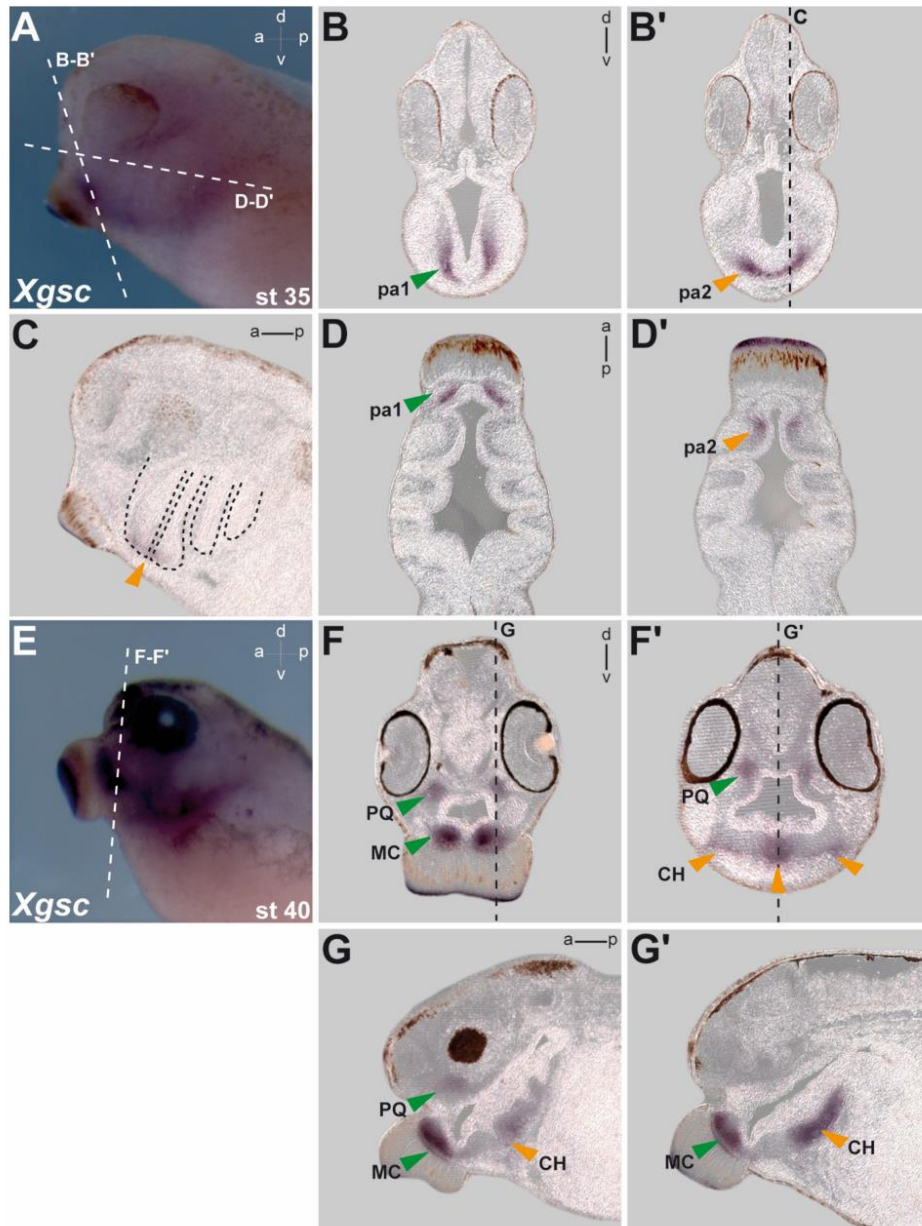


Fig. S6. *Gsc* expression in cranial neural crest and derived head cartilage. Whole-mount *in situ* hybridization of st. 35 (A-D) and st. 40 (E-G) tadpoles with a *Gsc*-specific antisense probe. Planes of histological vibratome sections are indicated by dashed lines. *Gsc* transcripts were found in pharyngeal arch (pa) mesenchyme and in differentiating cranial cartilage. Green arrowheads, pa1 and its derivatives palatoquadrate (PQ) and Meckel's cartilage (MC); orange arrowheads, pa2 and its derivative ceratohyale (CH).

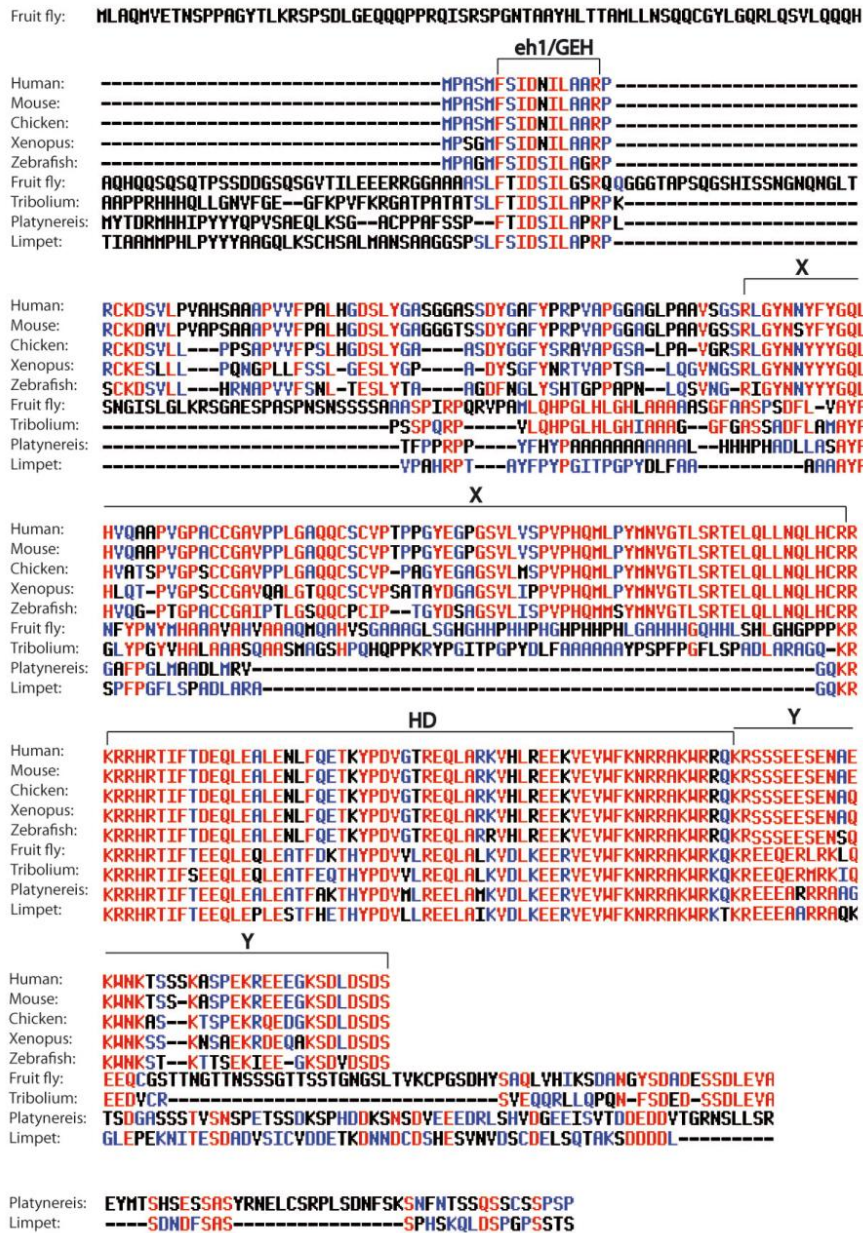
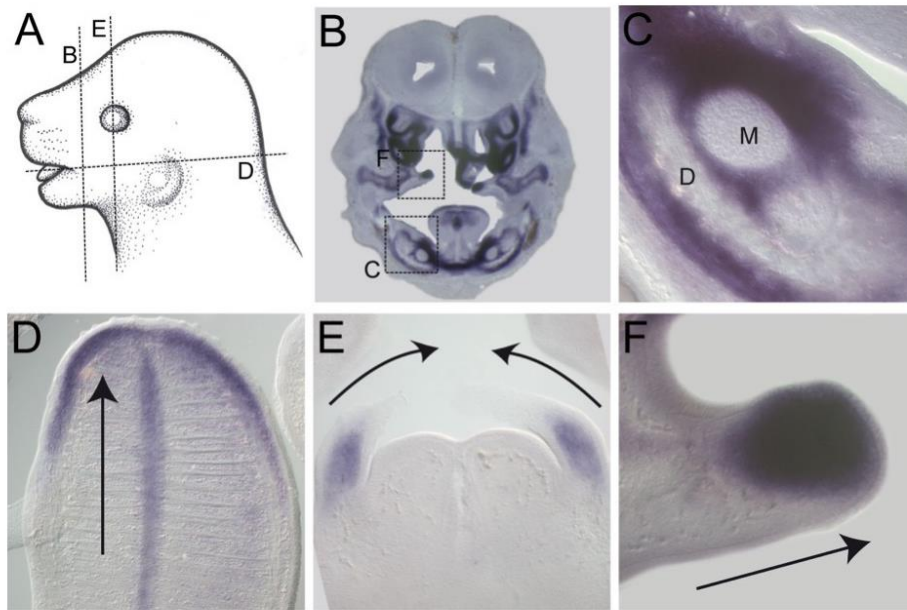


Fig. S7. Multiple sequence alignment of Gsc proteins. Note that the eh1- and homeodomains are very highly conserved throughout the animal kingdom. Two similarly highly conserved domains N- and C-terminal of the homeodomain, marked “X” and “Y”, are specific for vertebrate Gsc protein sequences. The following sequences were used: human (NM\_173849.2), mouse (NM\_010351.1), chicken (NP\_990662.1), *Xenopus* (XM\_018231890.1), zebrafish (NM\_131017.1), fruit fly (CAA64699.1), tribolium (XP\_008198241.1), *Platynereis* (AJ289023.1), limpet (AJ507423.1). Alignments were generated using multalin (<http://multalin.toulouse.inra.fr/multalin/>).





**Fig. S8. *Gsc* expression adjacent to tissues undergoing elongation in E14.5 mouse embryos.**

*In situ* hybridisation using a mouse *Gsc* antisense RNA probe on frontal and transversal vibratome section of E14.5 wildtype mouse embryos.

(A) Schematic depiction of sectional planes.

(B, C) *Gsc* transcripts localize to regions around Meckel's (M) cartilage and the developing *dentale*.

(D) *Gsc* was expressed at the tip of the tongue and the developing *septum linguae*. (E) *Gsc* transcript localization to the arytenoid swellings before fusion.

(F) *Gsc* expression in the mesenchyme of the palatal shelves.

	wt		BPD		NTD		n	n defects	p wt-defects Chi-Square
	n	%	n	%	n	%			
<b>GscGR, 10 experiments</b>									
uninjected controls with/without dex	267	93,0	3	1,0	17	5,9	287	20	
<i>GscGR</i> without dex	183	92,0	6	3,0	10	5,0	199	16	
<i>GscGR</i> + dex st 6-8	67	38,3	64	36,6	44	25,1	175	108	<10-4
<i>GscGR</i> + dex st 11	32	47,8	7	10,4	28	41,8	67	35	<10-4
<i>GscGR</i> + dex st 12,5	46	97,9	1	2,1		0,0	47	1	0,080
<b>RhoAca, 4 experiments</b>									
uninjected controls with/without dex	95	95,0	5	5,0	0	0,0	100	5	
<i>GscGR</i> without dex	20	80,0	1	4,0	4	16,0	25	5	
<i>GscGR</i> and <i>RhoAca</i> without dex	51	73,9	4	5,8	14	20,3	69	18	
<i>GscGr</i> with dex	20	22,2	61	67,8	9	10,0	90	70	
Rescue ( <i>GscGR</i> and <i>RhoAca</i> with dex)	60	48,0	24	19,2	41	32,8	125	65	<10-4
<b>RhoAdn, 4 experiments</b>									
uninjected controls with dex	149	96,1	3	1,9	3	1,9	155	6	
<i>GscGR</i> 160 pg without dex	85	88,5	4	4,2	7	7,3	96	11	
<i>GscGr</i> 160 pg with dex	65	58,6	20	18,0	26	23,4	111	46	
<i>GscGR</i> and <i>RhoAdn</i> without dex	55	47,4	37	31,9	24	20,7	116	61	
Rescue ( <i>GscGR</i> and <i>RhoAdn</i> with dex)	22	21,8	61	60,4	18	17,8	101	79	<10-4
<b>Prickle, 4 experiments</b>									
uninjected controls without dex	137	95,8	2	1,4	4	2,8	143	6	
<i>GscGR</i> without dex	70	93,3	5	6,7	0	0,0	75	5	
<i>GscGR</i> and <i>Prickle</i> without dex	70	82,4	9	10,6	6	7,1	85	15	
<i>GscGr</i> with dex	18	22,0	49	59,8	15	18,3	82	64	
Rescue ( <i>GscGR</i> and <i>Prickle</i> with dex)	43	48,9	35	39,8	10	11,4	88	45	<10-4
<b>Vangl2, 6 experiments</b>									
uninjected controls without dex	115	95,8	0	0,0	5	4,2	120	5	
<i>GscGR</i> without dex	55	94,8	2	3,4	1	1,7	58	3	
<i>GscGR</i> and <i>Vangl2</i> without dex	90	72,0	10	8,0	25	20,0	125	35	
<i>GscGr</i> with dex	38	37,3	48	47,1	16	15,7	102	64	
Rescue ( <i>GscGR</i> and <i>Vangl2</i> with dex)	70	55,6	40	31,7	16	12,7	126	56	0,006
<b>T, 6 experiments</b>									
uninjected controls without dex	131	94,9	2	1,4	5	3,6	138	7	
<i>GscGR</i> without dex	37	90,2	2	4,9	2	4,9	41	4	
<i>GscGR</i> and <i>T</i> without dex	82	79,6	8	7,8	13	12,6	103	21	
<i>GscGr</i> with dex	27	20,9	82	63,6	20	15,5	129	102	
Rescue ( <i>GscGR</i> and <i>T</i> with dex)	53	35,3	44	29,3	53	35,3	150	97	0,008
<b>Wnt11, 3 experiments</b>									
uninjected controls	45	90,0	1	2,0	4	8,0	50	5	
<i>GscGR</i> without dex	20	80,0	4	16,0	1	4,0	25	5	
<i>GscGR</i> and <i>Wnt11</i> without dex	23	69,7	3	9,1	7	21,2	33	10	
<i>GscGR</i> with dex	8	11,0	54	74,0	11	15,1	73	65	
Rescue ( <i>GscGR</i> and <i>Wnt11</i> with dex)	31	33,3	38	40,9	24	25,8	93	62	0,007

**Table S1. *Gsc-GR* induced CE phenotypes and rescue by PCP components.**

Raw data of experiments summarized in Figure 2. BPD, blastopore closure defect; NTD, neural tube closure defect. Statistical analyses were performed using StatPages.org.

## **2.2 Left-right axis development**

### **A Conserved Role of the Unconventional Myosin1d in Laterality Determination**

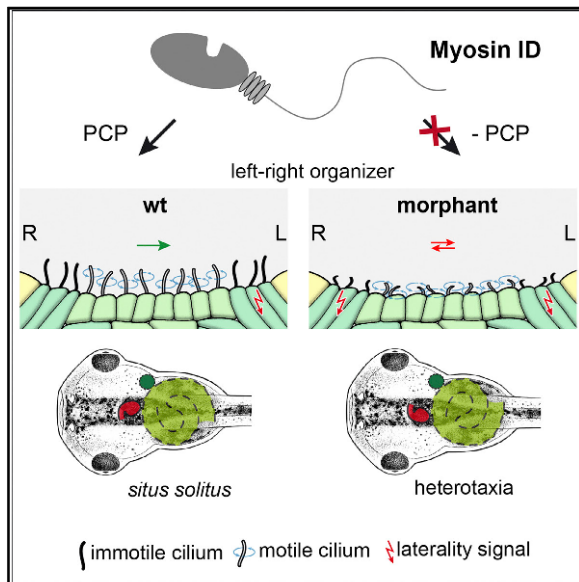
<https://doi.org/10.1016/j.cub.2018.01.075>

Reproduced with permission from CellPress

# Current Biology

## A Conserved Role of the Unconventional Myosin 1d in Laterality Determination

### Graphical Abstract



### Authors

Melanie Tingler, Sabrina Kurz, Markus Maerker, ..., Janine M. LeBlanc-Straceski, Stéphane Noselli, Martin Blum

### Correspondence

martin.blum@uni-hohenheim.de

### In Brief

Tingler et al. show that myosin 1D is required for laterality in the frog *Xenopus*, namely for left-asymmetric gene expression and leftward flow. Myosin 1D acts through the planar cell polarity pathway, a key feature of asymmetric gonad and gut morphogenesis in *Drosophila*, suggesting a common evolutionary origin of arthropod and chordate laterality.

### Highlights

- The unconventional myosin 1D is required for vertebrate left-right asymmetry
- Loss of *myo1d* causes aberrant leftward flow and laterality defects in *Xenopus*
- The function of myosin1D is mediated through the planar cell polarity pathway
- Myosin 1D links laterality in arthropods and chordates



Tingler et al., 2018, Current Biology 28, 810–816  
March 5, 2018 © 2018 Elsevier Ltd.  
<https://doi.org/10.1016/j.cub.2018.01.075>

CellPress

## A Conserved Role of the Unconventional Myosin 1d in Laterality Determination

Melanie Tingler,<sup>1,4</sup> Sabrina Kurz,<sup>1,4</sup> Markus Maerker,<sup>1,4</sup> Tim Ott,<sup>1,4</sup> Franziska Fuhl,<sup>1,4</sup> Axel Schweickert,<sup>1</sup> Janine M. LeBlanc-Straceski,<sup>2</sup> Stéphane Noselli,<sup>3</sup> and Martin Blum<sup>1,5,\*</sup>

<sup>1</sup>University of Hohenheim, Institute of Zoology, Garbenstrasse 30, 70593 Stuttgart, Germany

<sup>2</sup>Department of Biology, Merrimack College, 315 Turnpike Street, North Andover, MA 01845, USA

<sup>3</sup>Université Côte d'Azur, CNRS, INSERM, Institut de Biologie Valrose, Parc Valrose, 06108 Nice, France

<sup>4</sup>These authors contributed equally

<sup>5</sup>Lead Contact

\*Correspondence: [martin.blum@uni-hohenheim.de](mailto:martin.blum@uni-hohenheim.de)

<https://doi.org/10.1016/j.cub.2018.01.075>

### SUMMARY

Anatomical and functional asymmetries are widespread in the animal kingdom [1, 2]. In vertebrates, many visceral organs are asymmetrically placed [3]. In snails, shells and inner organs coil asymmetrically, and in *Drosophila*, genitalia and hindgut undergo a chiral rotation during development. The evolutionary origin of these asymmetries remains an open question [1]. Nodal signaling is widely used [4], and many, but not all, vertebrates use cilia for symmetry breaking [5]. In *Drosophila*, which lacks both cilia and Nodal, the unconventional myosin 1D (*myo1d*) gene controls dextral rotation of chiral organs [6, 7]. Here, we studied the role of *myo1d* in left-right (LR) axis formation in *Xenopus*. Morpholino oligomer-mediated *myo1d* downregulation affected organ placement in >50% of morphant tadpoles. Induction of the left-asymmetric Nodal cascade was aberrant in >70% of cases. Expression of the flow-target gene *dand5* was compromised, as was flow itself, due to shorter, fewer, and non-polarized cilia at the LR organizer. Additional phenotypes pinpointed Wnt/planar cell polarity signaling and suggested that *myo1d*, like in *Drosophila* [8], acted in the context of the planar cell polarity pathway. Indeed, convergent extension of gastrula explant cultures was inhibited in *myo1d* morphants, and the *ATF2* reporter gene for non-canonical Wnt signaling was downregulated. Finally, genetic interference experiments demonstrated a functional interaction between the core planar cell polarity signaling gene *vangl2* and *myo1d* in LR axis formation. Thus, our data identified *myo1d* as a common denominator of arthropod and chordate asymmetry, in agreement with a monophyletic origin of animal asymmetry.

### RESULTS AND DISCUSSION

#### The Unconventional myosin1D Gene Is Required for LR Axis Formation in *Xenopus laevis*

We have previously shown that maternal and zygotic Myo1d is present in the *Xenopus* egg cell and throughout the first 3 days of embryogenesis [9], i.e., before, during, and after left-right (LR) symmetry breaking [5]. Zygotic mRNA expression was predominantly found in presomitic mesoderm and somites [9], tissues related to the *Xenopus* LR organizer (LRO) [5]. To assess a possible function of *myo1d* in *Xenopus* LR axis formation, an antisense morpholino oligomer (MO) was designed that targeted sequences overlapping the translational start site (AUG-MO). AUG-MO was injected at the 4-cell stage and targeted toward the LRO. Specimens were cultivated until they reached stages 24, 32, or 45 to investigate *nodal1* or *pitx2* expression and organ situs, respectively. Organ placement, as assessed by heart and gut looping as well as positioning of the gall bladder (Figure 1A), was significantly disturbed in specimens injected with AUG-MO (Figures 1B–1D). Likewise, left-asymmetric expression of *nodal1* and *pitx2* were disturbed in >70% of AUG-MO-injected morphants, with bilateral expression in the left and right lateral plate mesoderm (LPM) representing the most commonly observed defective pattern (Figures 1E and 1F; Figures S1A–S1H). Remarkably, AUG-MO caused phenotypes at very low doses (0.2 pmol or 3.3 ng per embryo). Furthermore, a scrambled mismatch MO (MM-MO) did not affect the laterality of injected embryos (Figures 1E and 1F). In addition, Myo1d protein was downregulated in morphant embryos, as shown by western blot analysis (Figure S1I). A full-length *myo1d* expression construct [10] that was not targeted by AUG-MO partially rescued left-asymmetric *nodal1* expression in the LPM (Figure 1E). Together, these experiments argue for MO specificity. Bilateral *nodal1/pitx2* expression, observed in the majority of LR-altered *myo1d* morphants (75%; cf. Figures 1E and 1F), also occurs when the midline barrier function is disturbed [11], i.e., when Nodal1 protein crosses from the left to the right side. However, the midline in *myo1d* morphants was normal, as shown by the wild-type expression pattern of the midline barrier gene *lefty1* (Figures S1J and S1K).

To confirm the MO-derived LR phenotypes, we created CRISPR/Cas9 F0 mutants in *Xenopus laevis*. Two guide RNAs were designed, targeting subdomains of the ATP-binding site





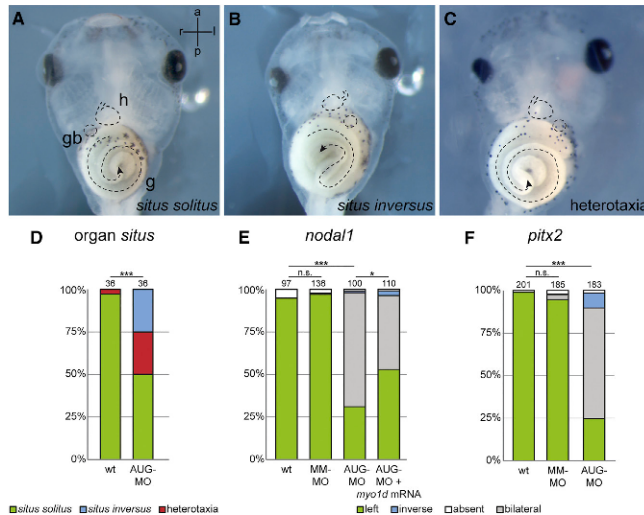


**Figure 1. *myo1d* Is Required for LR Axis Formation in *Xenopus laevis***

(A–D) Organ situs in wild-type (A) and *myo1d* morphant tadpoles displaying situs inversus (B) and heterotaxia (C) at stage 45. g, gut; gb, gall bladder, h, heart.

(D) Quantification of organ situs analysis.

(E and F) Quantification of *nodal1* (E) and *pitx2* (F) expression patterns in wildtype embryos and specimens injected with MM-MO, AUG-MO or co-injected with AUG-MO and rescue mRNA. Numbers represent analyzed specimens, which were derived from 3 (D and E) and 5 (F) independent experiments. See also Figure S1.

(Figure 2A), which were separately co-injected together with Cas9 protein into 1-cell-stage embryos [12]. Both resulted in identical ranges of phenotypes (Figures 2B and 2C): at least half the embryos were severely malformed, with gastrulation and blastopore closure defects, preventing the analysis of marker gene expression. Importantly, these phenotypes were encountered upon the injection of high doses of AUG-MO as well (data not shown). The remaining injected F0 specimens were evaluated for *pitx2* expression. About 60% lacked asymmetry and showed absent or bilateral *pitx2* expression (Figure 2D); remarkably, these embryos were also stunted, i.e., revealed a convergence extension phenotype (Figure 2C). The remaining specimens appeared normal and displayed left-asymmetric *pitx2* expression (Figures 2C and 2D). F0 *myo1d* mutants thus closely resembled *myo1d* morphants, as in both cases asymmetric marker gene expression was lost. Differences were recorded, however, namely that in morphants, Nodal cascade gene expression was bilateral in the vast majority of cases, while it was absent or bilateral in mutants. Although we lack a conclusive explanation at this time, beyond realizing that gene knockdowns differ from mosaic F0 mutants, genome editing provided additional proof of MO specificity, as in both cases the same quality of LR defect was observed, i.e., loss of asymmetry. In summary, these experiments demonstrated a role for *myo1d* in LR axis formation in *Xenopus*.

#### ***myo1d* Is Required for LRO Morphogenesis and Leftward Flow**

Induction of the left-asymmetric Nodal cascade in the LPM of the 2-day embryo is preceded by several well-defined morphogenetic and molecular steps, beginning with the specification of the LRO precursor, the so-called superficial mesoderm (SM), which forms caudal to the Spemann organizer at mid-gastrula stages [5, 13] (Figure S2A). The SM was not affected in *myo1d*

morphants, as demonstrated by the expression of marker genes *foxj1* and *wnt11b* [14] (Figures S2B–S2E). The LRO in the frog is represented by the transient ciliated epithelium of the gastrocoel roof plate (GRP), which forms at the dorsal-posterior end of the primitive gut when SM cells involute during gastrulation [13, 15] (Figure S2A). We investigated whether the GRP had correctly formed in *myo1d* morphants using a Tektin isoform marker gene; *tekt2* expression was unaffected (Figures S2F and S2G), indicating that a GRP had formed. LRO function of the GRP arises when cilia develop and polarize in the central region of the GRP. As they become motile, they produce a leftward flow of extracellular fluids [16], which, presumably, is sensed by peripheral GRP cells harboring non-polarized and immotile cilia [1, 5].

To assess GRP morphogenesis, dorsal explants were prepared and analyzed for cilia by immunofluorescence (IF) using an antibody against acetylated alpha-tubulin. Figures 3A–3E show that, although cilia were present in morphant GRPs, ciliation was markedly altered. Cilia were significantly shorter, showed reduced polarization to the posterior pole of cells (a prerequisite of leftward flow), and were reduced in number (Figures 3F–3H). To determine if the flow itself was compromised, the transport of fluorescent microbeads was assessed using high-speed videography [16]. Time-lapse movies of GRPs show that flow was indeed disordered in *myo1d* morphants compared to wild-type specimens (Movie S1). Evaluation of flow parameters confirmed this disruption, with significantly reduced flow velocity and directionality in *myo1d* morphant specimens (Figures 3I and 3J). Importantly, some individual beads showed inverted movement, i.e., from left to right (Movie S1), in agreement with the observed predominant bilateral induction of asymmetric LPM marker genes (cf. Figures 1E and 1F). Leftward flow induces asymmetric LPM gene expression by downregulating the Nodal repressor *dand5* in lateral GRP cells (i.e., the purported flow sensor cells), where this gene is co-expressed with *nodal1* [17]. Expression of both genes was analyzed in dorsal explants isolated at post-flow stages (stage 19). Figures 3K–3O show that *nodal1* was unaffected in morphants, while *dand5* asymmetries were lost due to bilateral downregulation of mRNA expression. Expression of the

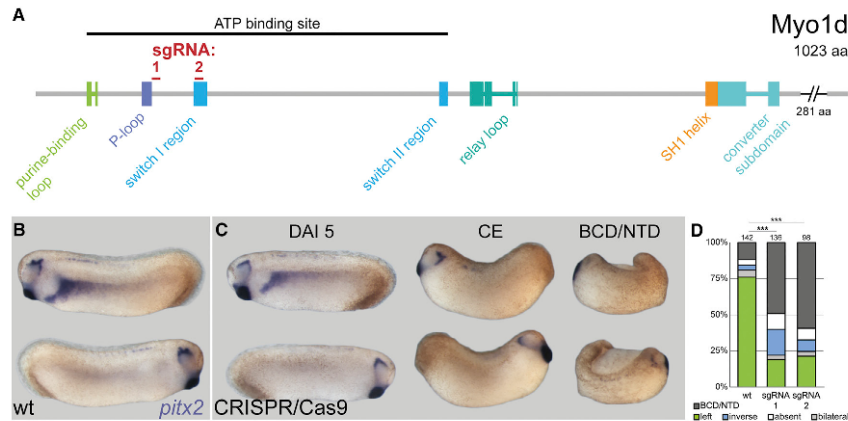


**Figure 2. Laterality Defects in Genome-Edited F0 *myo1d* Mutant Tadpoles**

(A) Schematic depicting Myo1d protein structure (sgRNA sites indicated). (B and C) Appearance and *pitx2* gene expression in WT (B) and F0 *myo1d* mutant (C) tadpoles. (D) Compilation of *pitx2* expression patterns. BCD, blastopore closure defect; NTD, neural tube closure defect. Note that mutant embryos with WT appearance showed WT *pitx2* expression in the left LPM, while stunted specimens with a convergent extension (CE) phenotype lacked expression or displayed mRNA expression on both sides.

transforming growth factor  $\beta$  (TGF- $\beta$ ) gene *gdf3*, the functional frog homolog of the Nodal agonist *Gdf1* in mouse, was unaltered in morphants (Figures S2H and S2I). In summary, these results demonstrated that *myo1d* was required for GRP morphogenesis and leftward flow and that downregulation of this conserved unconventional myosin resulted in a loss of molecular asymmetries and, consequently, a high frequency of heterotaxia (*situs ambiguus*) and *situs inversus* in morphant tadpoles (Figure 1).

#### PCP Defects in *myo1d* Morphant Frog Embryos

In *Drosophila*, *myo1d* interacts with both the global (Dachsous/Fat) and core (Frizzled/Wnt) PCP pathways to control chiral morphogenesis of the adult hindgut [8]. In the course of analyzing *myo1d* morphant *Xenopus* embryos, we noted a number of LR-unrelated developmental defects that have been linked to altered PCP signaling. First, the apical surface of GRP cells appeared enlarged in morphants as compared to wild-type (WT), suggesting a defect in apical constriction of involuting SM cells (cf. Figures 2A–2E). Apical constriction during gastrulation and neural tube closure is under the control of PCP [18]. Quantification of 25 cells each from 15 WT and 15 morphant embryos revealed that, on average, the cell surface in *myo1d* morphants was increased by 25% (Figure 4A). Second, neural tube closure was delayed in morphant embryos, i.e., the neural tube was still open at stage 18 when it had just closed in wild-type specimens (Figure 4B; Figures S3A and S3B; Movie S2). Delayed neural tube closure has been reported in the frog upon knockdown of *dishevelled2* (*dsh2*) and characterized as a convergent-extension (CE) defect that fails to narrow the midline [19]. In mouse embryos lacking one or both copies of the core PCP gene *vangl2*, the same phenotype was described [20]. Third, the ciliation of

multi-ciliated cells (MCCs) in the larval skin of *myo1d* morphants was delayed. Ciliation of MCCs was much reduced on the morphant side of unilaterally injected stage 24 embryos, compared to the uninjected contralateral side (Figure S3C). No differences were recorded at stage 32, i.e., this phenotype represented a transient delay in MCC differentiation and apical intercalation (data not shown). MCC function was directly assessed by tracking fluorescent microbeads added to tadpoles. Figure 4C and Movies S3 and S4 demonstrate that defects observed at stage 24 were no longer present at stage 32 (data not shown). Such a transient delay in cilia extension of MCCs has previously been described upon *Foxn4* loss of function in *Xenopus* [21], and radial cell intercalation of MCC has been linked to PCP proteins Vangl2, Prickle3, and Dishevelled [22]. Finally, the stunted appearance of F0 mutants with disturbed *pitx2* expression was reminiscent of a CE phenotype as well (cf. Figure 2C). Together, this evidence hinted at a more general role of *myo1d* in PCP signaling and CE.

To investigate *myo1d* function in the context of a well-established CE-Wnt/PCP assay, we employed Keller open-face explants [23]. Dorsal marginal zone tissue was isolated at stage 10–10.5 from WT and *myo1d* morphant embryos, and it was scored for CE when un-manipulated siblings reached stage 22 (Figure 4C). CE was classified into three categories, with class 0 representing explants without elongation, class 1 containing elongated specimens, and class 2 explants being those that were elongated and displayed a constriction (Figure 4C). While more than 90% of WT explants elongated, with the relative majority of specimens falling into class 2 (23/54, 43%), CE was severely compromised in *myo1d* morphants, with significantly reduced class 2 extensions (6/44), the relative majority of specimens elongating without constriction, and about 25% not

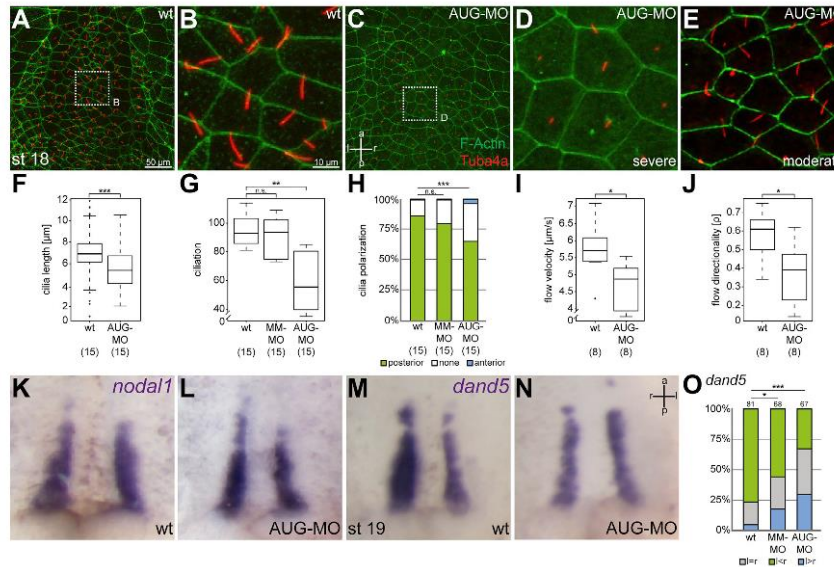


**Figure 3. *myo1d* Is Required for GRP Morphogenesis and Leftward Flow**

(A–E) GRP ciliation. Dorsal explants were prepared and analyzed for the presence and polarization of cilia by immunofluorescence using an antibody against acetylated alpha-tubulin. Counterstaining of actin using Phalloidin highlighted cell boundaries.

(A) Wild-type (blow-up shown in B).

(C) *myo1d* morphant.

(D and E) Blowups of severe phenotype shown in (D) and of moderate phenotype shown in (E).

(F–J) Quantification of cilia lengths (F), ciliation rate (G), cilia polarization (H), flow velocity (I), and flow directionality (J).

(K and L) Wild-type expression of *nodal1* in control (K) and *myo1d* morphant (L) stage 19 embryo.

(M–O) Asymmetrical *dand5* expression in lateral GRP cells of wild-type control embryo (M) was lost in *myo1d* morphant specimen (N).

(O) Quantification of *dand5* expression patterns.

(K)–(N) are shown at the same magnification.

Numbers represent analyzed specimens, which were derived from 3 (A–H), 2 (I and J), and 5 (K–O) independent experiments. For the assessment of cilia polarization, 15 cilia were analyzed per explant, for cilia lengths 30 cilia per GRP, and the ciliation rate was determined upon evaluating the entire GRP. See also Figure S2 and Movie S1.

elongating at all (class 1, 24/44, 61%; Figure 4C). Finally, an *ATF2*-based luciferase reporter was analyzed to monitor non-canonical Wnt signaling in *Xenopus* [24]. The reporter gene, alone or in combination with different concentrations of *myo1d* AUG-MO, was injected into the neural lineage at the 4-cell stage, neural plate explants were prepared at stage 14/15, and luciferase activity was recorded (Figure S3D). Compared to WT specimens, the reporter gene activity was dose-dependently downregulated in morphants (Figure S3D). In summary, these analyses of LR-unrelated phenotypes demonstrated that *myo1d* acted on non-canonical Wnt/PCP signaling and CE in the broader sense.

#### Functional Interaction between the Core PCP Signaling Gene *vangl2* and *myo1d* in LR Axis Formation in *Xenopus*

Finally, we asked whether PCP signaling and *myo1d* interacted during LR axis specification. Knockdown of the core PCP gene *vangl2* in *Xenopus* has been shown to disrupt cilia polarization

and LPM *nodal1* expression [25]. For gene knockdown of *vangl2*, a combination of two previously characterized antisense MOs was injected [26]. To analyze the potential genetic interaction of *vangl2* and *myo1d*, MO doses were reduced such that individual knockdowns resulted in greatly attenuated phenotypes. When MOs were co-injected, LR phenotypes were observed, as documented for the expression of LPM *pitx2* (Figure 4D). These experiments unequivocally showed that *myo1d* was required for PCP-dependent determination of the LR axis in *Xenopus* in much the same way as in the fruit fly *Drosophila* [8]. A possible role of *myo1d* has been previously addressed by overexpression of a full-length expression construct [10]. Injections of high amounts of synthetic *myo1d* mRNAs ( $\geq 5$  ng) resulted in 15% of specimens with heterotaxia, but the mechanism of action was not addressed in this study [10]. We were not able to reproduce this result; it is a hallmark of non-canonical Wnt signaling and PCP, however, that both gain- and loss-of-function manipulations result in qualitatively similar phenotypes [27].



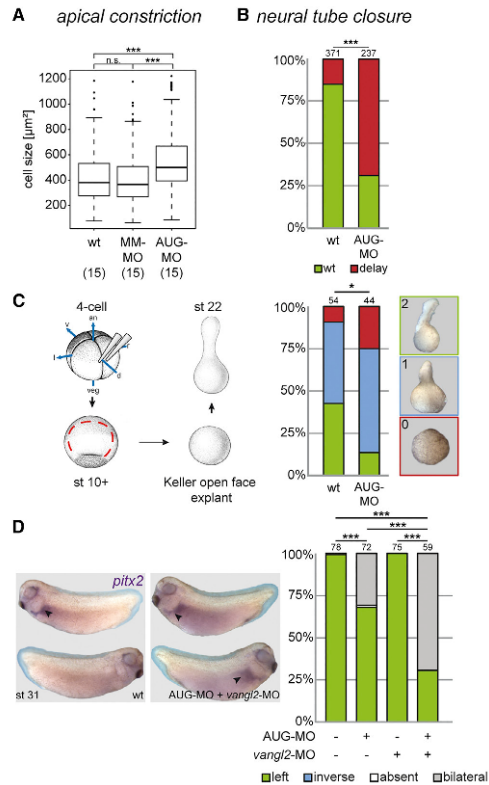


**Figure 4. Functional Interaction between *myo1d* and PCP**

(A and B) Morphant specimens displayed enhanced apical surfaces of GRP cells at stage 18 (A) and delayed neural tube closure at stage 18 (B). (C) Convergent extension defects in Keller open-face explants of *myo1d* morphants at stage 22. (D) Co-injection of *myo1d* AUG-MO with two antisense MOs directed against *vangl2* (at sub-phenotypic doses each) disrupted LR axis formation, as determined by expression of *pitx2* in the LPM. Numbers represent analyzed specimens, which were derived from 3 independent experiments for apical constriction defects of GRP cells, 7 experiments for neural tube closure delay, and 4 experiments for *myo1d* and *vangl2* interaction during LR axis formation. To determine the cell surface area, 25 cells from a central part of the GRP were analyzed in each case. See also Figure S3 and Movies S2, S3, and S4.

The evolutionary origin of animal asymmetries has been controversially discussed in recent years [1, 28–30]. While morphological and functional asymmetries have been described in most phyla [1], there is no single common mechanism that accounts for asymmetric development. The Nodal cascade genes *nodal*, *lefty*, and *pitx2* are present and required for asymmetric development in lophotrochozoans (such as snails) and deuterostomes (sea urchins, uro- and cephalochordates as well as vertebrates), but they have not been described in ecdy-

sozoans [1]. Cilia-driven leftward fluid flow at the LR organizer is a hallmark of some, but not all, chordates [1], and *Drosophila* as the sole ecdysozoan species studied in depth lacks Nodal and cilia but uses *Myo1d*, PCP, and the Hox gene *Abd-B* [7, 8] to achieve laterality. This diversity has been taken as evidence of multiple independent evolutionary pathways to establish LR asymmetry [31, 32].

Our finding of a role of *myo1d* in *Xenopus* LR development represents the first demonstration of a common denominator of ecdysozoan and deuterostome/chordate asymmetries. Interestingly, actomyosin-dependent asymmetric heart morphogenesis has recently been shown to depend on a right-sided instructive pathway that involves BMP signaling and, as a target, the homeobox gene *prx1* [33]. It has been proposed that this BMP-*Prx1*-actomyosin pathway is suggestive of a conserved role in laterality determination during bilaterian evolution [33], a notion that is fully supported by our data. Future studies will address the question of whether or not *myo1d* is involved in this pathway. Additionally, we uncovered a conserved link between PCP and *myo1d* in establishing LR asymmetry in flies and frogs. Interestingly, these results can be further generalized, as LR defects were also encountered in morphant and mutant CRISPR/Cas9 zebrafish embryos (S.N. and Max Furthauer, personal communication). Defects in zebrafish included shorter and mispolarized cilia, LRO morphogenetic defects, and aberrant leftward flow, resulting in absent Nodal cascade gene induction and organ situs distortions, and, most significantly, a genetic interaction with *vangl2* as well (S.N. and Max Furthauer, personal communication).

In conclusion, our data are consistent with a monophyletic origin of animal organ asymmetries. It may be beneficial to investigate other mechanisms of invertebrate asymmetries in vertebrate model organisms in the future (for which the frog *Xenopus* is particularly well suited [34]), such as the role of Hox genes, which may be involved in placing the LRO at the correct anterior-posterior position during development.

#### STAR★METHODS

Detailed methods are provided in the online version of this paper and include the following:

- KEY RESOURCES TABLE
- CONTACT FOR REAGENT AND RESOURCE SHARING
- EXPERIMENTAL MODEL AND SUBJECT DETAIL
- METHOD DETAILS
  - Plasmid construction
  - Immunofluorescence staining
  - Flow-analysis
  - Luciferase Assay
  - CRISPR/Cas9 mediated genome editing
  - Monoclonal Antibody Preparation
  - Western blot analysis
- QUANTIFICATION AND STATISTICAL ANALYSIS
  - Statistical analysis

#### SUPPLEMENTAL INFORMATION

Supplemental Information includes three figures and four movies and can be found with this article online at <https://doi.org/10.1016/j.cub.2018.01.075>.

**ACKNOWLEDGMENTS**

We are grateful to Michael Levin for sharing a full-length *myo1d* expression construct and to Susanne Bogusch, whose expert help was instrumental to cloning the rescue vector. Work in the Blum lab has been supported by DFG grants BL-285/9 and BL-285/10. S.K. and T.O. have been recipients of fellowships from the Landesgraduiertenförderung Baden-Württemberg. S.K. was also funded by the Federal Ministry of Education and Research (01PL11003), project Humboldt reloaded. J.M.L.-S. gratefully acknowledges several students in her 1998–2015 Molecular Biology and Biotechnology and Directed Research courses, especially G. Angelini, K. Ganser, S. Saldi, N. McIver, and B. Sickler; the Merrimack College Faculty Development Grant Program; Murray Fellowship; Yassini Award; NSF-RUI 0077516; and B. Bement, A. Sokac, S. Sokol, and members of his laboratory. Work in the Noselli lab was supported by grants from ANR (DRO-ASY ANR-13-BSV2-006, DroZeMyo, and LABEX SIGNALIFE ANR-11-LABX-0028-01).

**AUTHOR CONTRIBUTIONS**

M.B., M.T., A.S., and S.N. designed experiments. M.T., S.K., M.M., F.F., and J.M.L.-S. conducted experiments, with T.O. performing the CRISPR/Cas9 genome editing. M.B. wrote the manuscript with help from M.T., A.S., S.N., and J.M.L.-S.

**DECLARATION OF INTERESTS**

The authors declare no competing interests.

Received: October 19, 2017  
Revised: January 1, 2018  
Accepted: January 24, 2018  
Published: February 22, 2018

**REFERENCES**

- Blum, M., Feistel, K., Thumberger, T., and Schweickert, A. (2014a). The evolution and conservation of left-right patterning mechanisms. *Development* 141, 1603–1613.
- Coutelis, J.B., González-Morales, N., Géminard, C., and Noselli, S. (2014). Diversity and convergence in the mechanisms establishing L/R asymmetry in metazoa. *EMBO Rep.* 15, 926–937.
- Grimes, D.T., and Burdine, R.D. (2017). Left-Right Patterning: Breaking Symmetry to Asymmetric Morphogenesis. *Trends Genet.* 33, 616–628.
- Shiratori, H., and Hamada, H. (2014). TGF $\beta$  signaling in establishing left-right asymmetry. *Semin. Cell Dev. Biol.* 32, 80–84.
- Blum, M., Schweickert, A., Vick, P., Wright, C.V.E., and Danilchik, M.V. (2014b). Symmetry breakage in the vertebrate embryo: when does it happen and how does it work? *Dev. Biol.* 393, 109–123.
- Hozumi, S., Maeda, R., Taniguchi, K., Kanai, M., Shirakabe, S., Sasamura, T., Spéder, P., Noselli, S., Aigaki, T., Murakami, R., and Matsuno, K. (2006). An unconventional myosin in *Drosophila* reverses the default handedness in visceral organs. *Nature* 440, 798–802.
- Spéder, P., Adám, G., and Noselli, S. (2006). Type ID unconventional myosin controls left-right asymmetry in *Drosophila*. *Nature* 440, 803–807.
- González-Morales, N., Géminard, C., Lebreton, G., Cerezo, D., Coutelis, J.-B., and Noselli, S. (2015). The Atypical Cadherin Dachsous Controls Left-Right Asymmetry in *Drosophila*. *Dev. Cell* 33, 675–689.
- LeBlanc-Straceski, J.M., Sokac, A., Bement, W., Sobrado, P., and Lemoine, L. (2009). Developmental expression of *Xenopus* myosin 1d and identification of a *myo1d* tail homology that overlaps TH1. *Dev. Growth Differ.* 51, 443–451.
- McDowell, G.S., Lemire, J.M., Paré, J.-F., Cammarata, G., Lowery, L.A., and Levin, M. (2016). Conserved roles for cytoskeletal components in determining laterality. *Integr. Biol.* 8, 267–286.
- Meno, C., Shiono, A., Saijoh, Y., Yashiro, K., Mochida, K., Ohishi, S., Noji, S., Kondoh, H., and Hamada, H. (1998). *lefty-1* is required for left-right determination as a regulator of *lefty-2* and nodal. *Cell* 94, 287–297.
- Nakayama, T., Blitz, I.L., Fish, M.B., Odeleye, A.O., Manohar, S., Cho, K.W.Y., and Grainger, R.M. (2014). Cas9-based genome editing in *Xenopus tropicalis*. *Methods Enzymol.* 546, 355–375.
- Shook, D.R., Majer, C., and Keller, R. (2004). Pattern and morphogenesis of presumptive superficial mesoderm in two closely related species, *Xenopus laevis* and *Xenopus tropicalis*. *Dev. Biol.* 270, 163–185.
- Walentek, P., Schneider, I., Schweickert, A., and Blum, M. (2013). *Wnt11b* is involved in cilia-mediated symmetry breakage during *Xenopus* left-right development. *PLoS ONE* 8, e73646.
- Blum, M., Andre, P., Muters, S., Schweickert, A., Fischer, A., Bitzer, E., Bogusch, S., Beyer, T., van Straaten, H.W.M., and Viebahn, C. (2007). Ciliation and gene expression distinguish between node and posterior notochord in the mammalian embryo. *Differentiation* 75, 133–146.
- Schweickert, A., Weber, T., Beyer, T., Vick, P., Bogusch, S., Feistel, K., and Blum, M. (2007). Cilia-driven leftward flow determines laterality in *Xenopus*. *Curr. Biol.* 17, 60–66.
- Schweickert, A., Vick, P., Getwan, M., Weber, T., Schneider, I., Eberhardt, M., Beyer, T., Pachur, A., and Blum, M. (2010). The nodal inhibitor *Coco* is a critical target of leftward flow in *Xenopus*. *Curr. Biol.* 20, 738–743.
- Ossipova, O., Chuykin, I., Chu, C.-W., and Sokol, S.Y. (2015b). *Vangl2* cooperates with *Rab11* and *Myosin V* to regulate apical constriction during vertebrate gastrulation. *Development* 142, 99–107.
- Wallingford, J.B., and Harland, R.M. (2002). Neural tube closure requires *Dishevelled*-dependent convergent extension of the midline. *Development* 129, 5815–5825.
- Ybot-Gonzalez, P., Savery, D., Gerrelli, D., Signore, M., Mitchell, C.E., Faux, C.H., Greene, N.D.E., and Copp, A.J. (2007). Convergent extension, planar-cell-polarity signalling and initiation of mouse neural tube closure. *Development* 134, 789–799.
- Campbell, E.P., Quigley, I.K., and Kintner, C. (2016). *Foxn4* promotes gene expression required for the formation of multiple motile cilia. *Development* 143, 4654–4664.
- Ossipova, O., Chu, C.-W., Filatre, J., Brott, B.K., Itoh, K., and Sokol, S.Y. (2015a). The involvement of PCP proteins in radial cell intercalations during *Xenopus* embryonic development. *Dev. Biol.* 408, 316–327.
- Sive, H.L., Grainger, R.M., and Harland, R.M. (2007). *Xenopus laevis* Keller Explants. *CSH Protoc.* 2007, pdb.prot4749.
- Ohkawara, B., and Niehrs, C. (2011). An ATF2-based luciferase reporter to monitor non-canonical Wnt signaling in *Xenopus* embryos. *Dev. Dyn.* 240, 188–194.
- Antic, D., Stubbs, J.L., Suyama, K., Kintner, C., Scott, M.P., and Axelrod, J.D. (2010). Planar cell polarity enables posterior localization of nodal cilia and left-right axis determination during mouse and *Xenopus* embryogenesis. *PLoS ONE* 5, e8999.
- Prager, A., Hagenlocher, C., Ott, T., Schambony, A., and Feistel, K. (2017). *hmmr* mediates anterior neural tube closure and morphogenesis in the frog *Xenopus*. *Dev. Biol.* 430, 188–201.
- Wang, Y., and Nathans, J. (2007). Tissue/planar cell polarity in vertebrates: new insights and new questions. *Development* 134, 647–658.
- Booman, C.J., and Shimeld, S.M. (2002). The evolution of left-right asymmetry in chordates. *BioEssays* 24, 1004–1011.
- Thompson, H., Shaw, M.K., Dawe, H.R., and Shimeld, S.M. (2012). The formation and positioning of cilia in *Ciona intestinalis* embryos in relation to the generation and evolution of chordate left-right asymmetry. *Dev. Biol.* 364, 214–223.
- Nakamura, T., and Hamada, H. (2012). Left-right patterning: conserved and divergent mechanisms. *Development* 139, 3257–3262.



31. Okumura, T., Utsuno, H., Kuroda, J., Gittenberger, E., Asami, T., and Matsuno, K. (2008). The development and evolution of left-right asymmetry in invertebrates: lessons from *Drosophila* and snails. *Dev. Dyn.* 237, 3497–3515.
32. Vandenberg, L.N., and Levin, M. (2013). A unified model for left-right asymmetry? Comparison and synthesis of molecular models of embryonic laterality. *Dev. Biol.* 379, 1–15.
33. Ocaña, O.H., Coskun, H., Minguillón, C., Murawala, P., Tanaka, E.M., Galcerán, J., Muñoz-Chápuli, R., and Nieto, M.A. (2017). A right-handed signalling pathway drives heart looping in vertebrates. *Nature* 549, 86–90.
34. Duncan, A.R., and Khokha, M.K. (2016). *Xenopus* as a model organism for birth defects—Congenital heart disease and heterotaxy. *Semin. Cell Dev. Biol.* 51, 73–79.



## STAR★METHODS

## KEY RESOURCES TABLE

REAGENT or RESOURCE	SOURCE	IDENTIFIER
<b>Antibodies</b>		
Mouse monoclonal anti acetylated $\alpha$ -tubulin	Sigma	T6793
Anti-mouse IgG (whole molecule) F(ab') <sub>2</sub> fragment-Cy3	Sigma	C2181
Anti-mouse IgG (H+L), CF 405S	Sigma	SAB4600023
Alexa Fluor 488 Phalloidin	Invitrogen	A12379
Alexa Fluor 555 Phalloidin	Invitrogen	A34055
<b>Chemicals, Peptides, and Recombinant Proteins</b>		
Pfu DNA Polymerase	Promega	M7745
Cas9 with NLS	PNA BIO	CP01-50
FluoSpheres Carboxylate-Modified Microspheres, 0.5 $\mu$ m, yellow-green fluorescent (505/515)	Invitrogen	F8813
Human chorionic gonadotropin (hCG)	Sigma	C0809-1VL
PureProteome NHS Flexibind Magnetic Beads	Milipore	LSKMAGA02
Laemmli sample buffer 2x	Sigma	S3401
<b>Critical Commercial Assays</b>		
MEGAscript T7 Transcription Kit	Thermo Fisher Scientific	AM1354
MEGAclean Transcription Clean-Up Kit	Thermo Fisher Scientific	AM1908
innuPREP DOUBLEpure Kit	Analytik Jena	845-KS-5050050
Ni-NTA affinity purification column	QIAGEN	N/A
EDTA-free Protease Inhibitor Cocktail	Roche	00000011873580001
Dual-Luciferase® Reporter Assay System	Promega	E1910
<b>Experimental Models: Cell Lines</b>		
BL21 Star One Shot cells	Invitrogen	C602003
<b>Experimental Models: Organisms/Strains</b>		
<i>Xenopus laevis</i> (female, male)	Nasco	<a href="https://www.enasco.com/xenopus/">https://www.enasco.com/xenopus/</a>
<b>Oligonucleotides</b>		
sgRNA-RO: AAAAGCACCGACTCGGTGCCACTTTTTCAAGT TGATAACGGACTAGCCTTATTTAACTTGCTATTCTAGCT CTAAAAC	Merck	N/A
T7:sgRNA 1-FO: GCAGCTAATACGACTCACTATAGGTACT GCATGATGTACTTACGTTTTAGAGCTAGAAATAGCAAG	Merck	N/A
T7:sgRNA 2-FO: GCAGCTAATACGACTCACTATAGGGTT GTCGTTACGATTCTGCTGTTTTAGAGCTAGAAATAGCAAG	Merck	N/A
myo1d forward primer [5' ATCCATGGCGGAACAAAGAGG GGCTGC 3']	Sigma	N/A
myo1d reverse primer [5' ATTCTAGATTAATTGGCTGGAAC ACTGAG 3']	Sigma	N/A
<b>Software and Algorithms</b>		
Adobe Suite CS6: Photoshop and Illustrator	Adobe	N/A
ImageJ/Fiji	N/A	<a href="https://fiji.sc/">https://fiji.sc/</a>
AxioVision 4.6	Zeiss	N/A
Zen 2012 Blue edition	Zeiss	<a href="https://www.zeiss.com">https://www.zeiss.com</a>
Statistical R-Gui	N/A	<a href="https://www.r-project.org/">https://www.r-project.org/</a>
RStudio	N/A	<a href="https://www.rstudio.com/">https://www.rstudio.com/</a>

(Continued on next page)

<b>Continued</b>		
REAGENT or RESOURCE	SOURCE	IDENTIFIER
Other		
pET100/D-TOPO vector	Invitrogen	N/A
myo1d AUG-MO [5' TGCAGCCCTCTGTCCGCCATGT 3']	GeneTools	N/A
myo1d mismatch-MO [5' TGGACCCCGTCTTCTCCCC CATGT 3']	GeneTools	N/A
Axioplan2 imaging microscope	Zeiss	N/A
Zeiss LSM 700	Zeiss	N/A
GloMax® Explorer System	Promega	N/A
AxioCam HSm video camera	Zeiss	N/A
Xenbase	N/A	<a href="https://xenbase.org">https://xenbase.org</a>
PubMed	N/A	<a href="https://www.ncbi.nlm.nih.gov/pubmed/">https://www.ncbi.nlm.nih.gov/pubmed/</a>

#### CONTACT FOR REAGENT AND RESOURCE SHARING

Further information and requests for resources and reagents should be directed to and will be fulfilled by the Lead Contact, Martin Blum ([martin.blum@uni-hohenheim.de](mailto:martin.blum@uni-hohenheim.de)).

#### EXPERIMENTAL MODEL AND SUBJECT DETAIL

For *in vivo* studies, *Xenopus laevis* was used as model organism. Frogs were obtained from Nasco (901 Janesville Avenue PO Box 901 Fort Atkinson). Handling, care and experimental manipulations of animals was approved by the Regional Government Stuttgart, Germany (Vorhaben A379/12 ZO "Molekulare Embryologie"), according to German regulations and laws (§6, article 1, sentence 2, nr. 4 of the animal protection act). Animals were kept at the appropriate condition (pH=7.7, 20°C) at a 12 h light cycle in the animal facility of the Institute of Zoology of the University of Hohenheim. Female frogs (4-20 years old) were stimulated with 25-75 units of human chorionic gonadotropin (hCG; Sigma), depending on weight and age, that was injected subcutaneously one week prior to oviposition. On the day prior to ovulation, female frogs were injected with 300-700 units of hCG. Eggs were collected into a petri dish by careful squeezing of the females, followed by *in vitro* fertilization. Sperm of male frogs was gained by dissecting of testes that were stored at 4°C in 1x MBSH (Modified Barth's Saline with HEPES).

#### METHOD DETAILS

##### Plasmid construction

The *myo1d*-CS2+ construct was a gift of Dr. Michael Levin (Tufts University). For generation of a rescue construct, *myo1d* was cloned into the CS2+ myc-tag vector that contained 5 myc sequences at the N terminus. The following primers were used for cloning:

*myo1d* forward primer: 5' ATCCATGGCGGAACAAGAGGGGCTGC 3'  
*myo1d* reverse primer: 5' ATTCTAGATTAATTGGCTGGAACACTGAG 3'

For *in vitro* synthesis of mRNA using the Ambion sp6 message kit, the plasmid was linearized with NotI.

##### Immunofluorescence staining

For immunofluorescence staining, embryos were fixed in 4% PFA for 1h at RT on a rocking platform, followed by 2 washes in calcium- and magnesium-free PBS (PBS<sup>-</sup>) for 15 min each. For staining of GRP explants, embryos were dissected using a scalpel into anterior and posterior halves. Posterior halves (GRP explants) were collected and transferred to a 24 well plate and washed twice for 15 min in PBS<sup>-</sup>. GRP-explants and whole embryos were blocked for 2h at RT in CAS-Block diluted 1:10 in PBS<sup>-</sup>. The blocking reagent was replaced by antibody solution (anti acetylated tubulin antibody, diluted 1:700 in CAS-Block) and incubated overnight at 4°C. In the morning, the antibody solution was removed and explants/embryos were washed twice for 15 min in PBS<sup>-</sup>. Finally, the secondary antibody (diluted 1:1000 in CAS-Block) was added together with Phalloidin (1:200) and incubated for a minimum of 3h at RT. Before photo documentation, embryos or explants were shortly washed in PBS<sup>-</sup> and transferred onto a microscope slide.

##### Flow-analysis

For analysis of leftward flow, dorsal posterior GRP-explants were dissected from stage 16/17 embryos in 1x MBSH [16]. GRP-explants were placed in a Petri dish containing fluorescent microbeads (diameter 0.5 µm; diluted 1:2500 in 1xMBSH) and incubated for a few seconds. Explants were transferred to a microscope slide which was prepared with Vaseline to create a small chamber



that contained fluorescent microbead solution; a coverslip was carefully pressed on to seal the chamber. Time lapse movies of leftward flow were recorded using an AxioCam HSm video camera (Zeiss) at 2 frames per second for 1 min using an AxioPlan2 imaging microscope (Zeiss). For flow analysis, two open-source programs, ImageJ and statistical-R, were used. Using the Particle-Tracker plug-in from ImageJ, leftward flow was analyzed and particle movement was measured. Directionality and velocity of fluorescent microbeads were calculated using statistical-R.

#### Luciferase Assay

Luciferase reporter assays were carried out using the Promega Dual-Luciferase® Reporter Assay System. Embryos were injected at the 4-cell stage with AUG-MO, ATF2-luciferase DNA and Renilla DNA into the dorsal animal blastomeres, and neural tissue was dissected at stage 14/15 (cf. Figure S3D for a schematic depiction of the procedure [24]). Neural tissue was transferred into a 1.5 mL Eppendorf tube and the 0.1xMBSH buffer was removed, leaving the tissue moistened. The tissue was lysed and homogenized in 100  $\mu$ l 1x passive lysis-buffer by pipetting the suspension up and down, followed by a 15 min incubation at RT. The lysate was centrifuged for 2 minutes at 14 000 rpm and the upper phase was transferred into a new tube. The lysate was re-centrifuged and two 25  $\mu$ l aliquots (technical duplicates) were transferred into a 96well plate. 75  $\mu$ l 1x Luciferase assay substrate was added through the GloMax® Explorer System and the luminescence was measured. This step was repeated with 75  $\mu$ l 1x Stop and Glow reagents. To calculate the relative luciferase units (RLU in [%]) the ratio between luciferase and Renilla values was calculated and correlated to the wt control, which we set to 100%.

#### CRISPR/Cas9 mediated genome editing

sgRNA templates (under T7 promoter control) were generated using Pfu polymerase-mediated primer extension following *in vitro* synthesis (4 h) of the sgRNAs [12]. Prior to use, sgRNAs were denatured at 70°C for 2 min and immediately chilled on ice. Cas9 protein and sgRNAs were mixed and incubated at 37°C for 5 min to allow RNP formation. Zygotes were dejellied 20 min post fertilization and immediately injected with 8 nL of RNP mix. Injected embryos were cultivated for 12 h at 25°C to enhance cutting efficiency, followed by transfer to ambient temperature (20°C) until stage 28 was reached, when specimens were fixed for phenotype analysis.

#### Monoclonal Antibody Preparation

A monoclonal antibody, Mab4E12, was raised against the tail polypeptide NARNSNQFVSRNSNE (aa834-847) of the *Xenopus laevis* myosin 1d L homolog (GenBank Accession Number AF540952.1) by AbPro, Woburn, MA, USA. A 828 bp tail region that included amino acids R729-N1007 was amplified by PCR from a cDNA clone optimized for expression in *E. coli* (GenScript), pXIMyo1d-opt, using the primers (Forward: CACCGCCGTTATAAAGTTAAAAGT; Reverse: TTATTAGTTTGCCGGAACAGACAG), and cloned into the pET100/D-TOPO vector (Invitrogen) to create pXIMyo1d-optTail2D. BL21 Star One Shot cells (Invitrogen) were transformed with this vector and expression of the 35 kDa fusion protein consisting of the myo1d tail and N terminus 6X His-tag was induced with IPTG. Cells were harvested after 1.5 hr of induction and the fusion protein was affinity purified using Ni-NTA affinity purification column from a cleared lysate under denaturing conditions (QIAGEN). The affinity purified tail polypeptide was cross-linked to PureProteome NHS Flexibind Magnetic Beads (Milipore), and Mab4E12 was purified following the manufacturer's instructions.

#### Western blot analysis

Embryos were injected at the 1-4 cell stage with 1 ng of MO and cultivated until stage 28. The antisense morpholino, AUG-MO, [5' TGCAGCCCCTCTTGTTCCGCATGT 3'] overlapped the start codon (underlined) of *myo1d*. The control mismatch morpholino MM-MO, [5' TGGACCCCTCTTCTCCCCCATGT 3'] was identical to the AUG-MO except for the five C/G mismatches (underlined and indicated by bold lettering). Embryo lysates were made by homogenizing 1 embryo in 20  $\mu$ l of 4°C lysis buffer (50 mM Tris pH 8.0, 150 mM NaCl, 0.5% NP40 0.5 ml, 0.5% Triton X-100 0.5 ml, 1 mM EGTA) plus cOmplete, Mini, EDTA-free Protease Inhibitor Cocktail (Roche) and centrifuging at 13,000 x g for 10 min to remove cellular debris followed immediately by mixing the supernatant 1:1 with 2x Laemmli SDS sample buffer (SIGMA). Embryo lysates in Laemmli sample buffer were boiled for 5 min, snap cooled on ice, and spun to remove debris before loading onto gels. Bio-Rad Precision Plus Kaleidoscope markers and half-embryo equivalents were loaded per lane on Bio-Rad 4%–20% polyacrylamide precast gels at 100 V. Western blots were prepared using the Trans-Blot SD. Semi-Dry Transfer Cell at 15 V for 45 min. Blots were air-dried, blocked in 5% non-fat dry milk in TBS, rinsed and incubated in the affinity purified 4E12 monoclonal antibody at a concentration of 5  $\mu$ g in 10 mL TBS overnight at 4°C. Blots were washed in TBS, re-blocked in 10% non-fat dry milk in TBS, rinsed and incubated with goat anti-mouse horseradish peroxidase (HRP) conjugated anti-mouse IgG (Jackson Labs) at 1:10,000 dilution for 1 hr at RT. After rinsing with TBS, chemiluminescent detection was performed using a peroxide-luminol/enhancer solution (Pierce) and GeneSnap image acquisition software on a SynGene gel documentation system.

#### QUANTIFICATION AND STATISTICAL ANALYSIS

##### Statistical analysis

Statistical calculations of marker gene expression patterns and cilia distribution were performed using Pearson's chi-square test (Bonferroni corrected) in statistical R. For statistical calculation of ciliation, cilia length, cell size, flow velocity and directionality Wilcoxon-Match-Pair test was used (RStudio).

Current Biology, Volume 28

**Supplemental Information**

**A Conserved Role of the Unconventional**

**Myosin 1d in Laterality Determination**

Melanie Tingler, Sabrina Kurz, Markus Maerker, Tim Ott, Franziska Fuhl, Axel Schweickert, Janine M. LeBlanc-Straceski, Stéphane Noselli, and Martin Blum

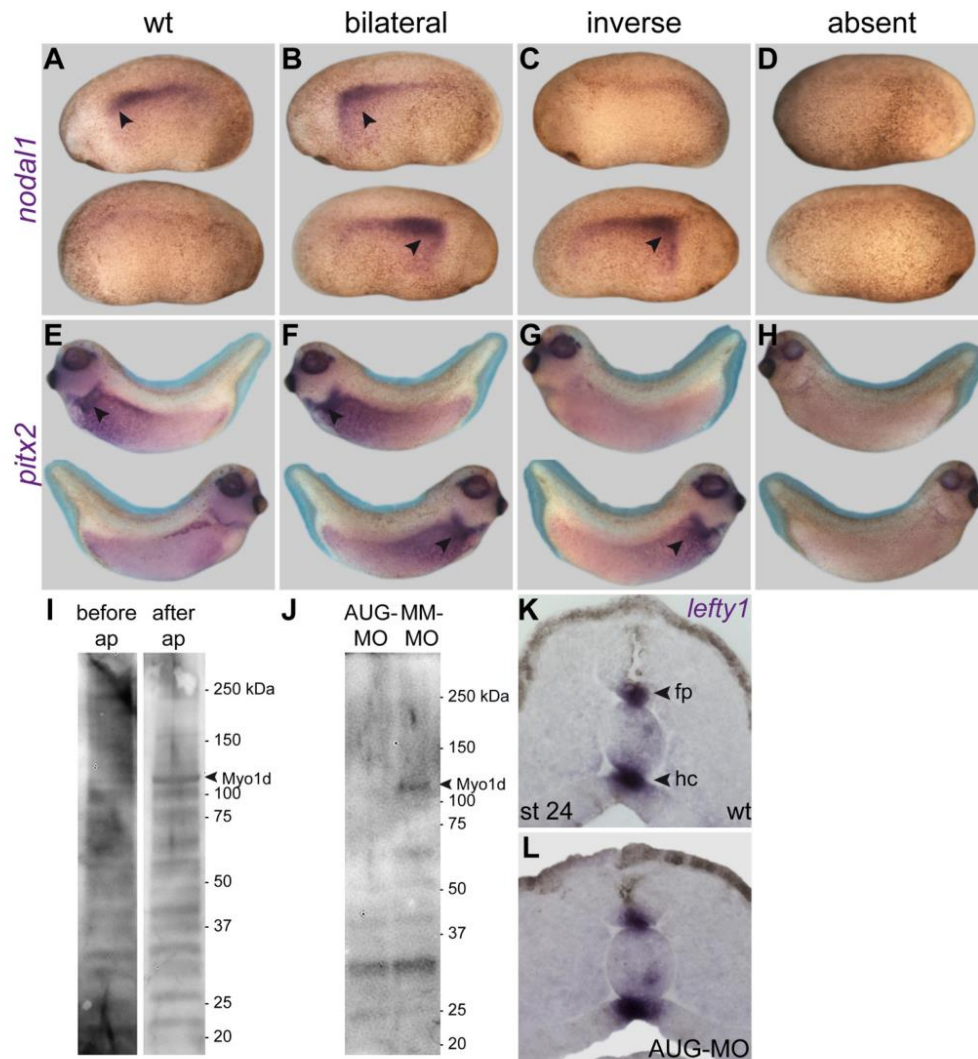


**Figure S1. *Myo1d* is required for LR axis formation, Related to Figure 1.**

(A-H) *nodal1* (A-D) and *pitx2* (E-H) expression in wildtype (A, E) and *myo1d* morphant (B-D, F-H) embryos, as determined by WM-ISH with antisense probes for *nodal1* (A-D) and *pitx2* (E-H).

(I, J) Downregulation of *Myo1d* protein in *myo1d* morphants. (I) Tadpole lysates were probed with Mab4E12 before (left) and after (right) affinity purification (ap). (J) Embryos were injected at the 2-4 cell stage with 1 ng of AUG-MO or an antisense MO containing 5 mismatches (MM-MO). Affinity purified Mab4E12 was used to probe western blots containing lysates from stage 28 embryos.

(K, L) *Lefty1* mRNA expression in wildtype (K) and *myo1d* morphant (L) specimen, as shown by transversal histological sections of WM-ISH stained embryos at stage 24. fp, floor plate; hc, hypochord; MM-MO, mismatch MO.



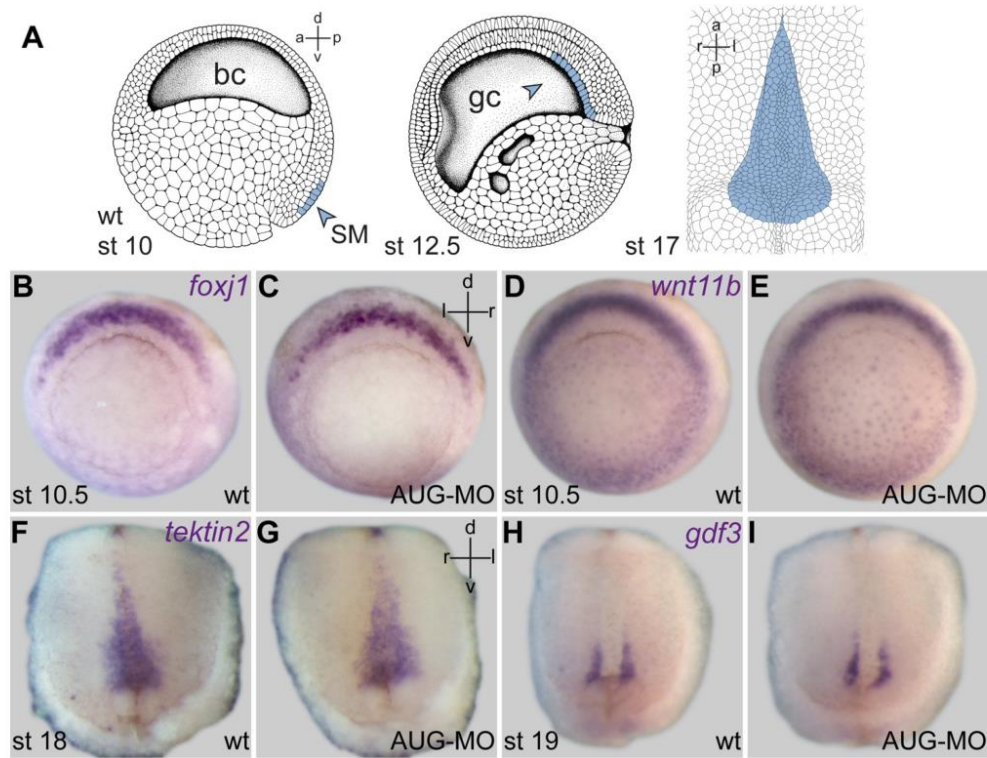


**Figure S2. Marker gene expression in the superficial mesoderm (SM) and gastrocoel roof plate (GRP) of wildtype and *myo1d* morphant embryos, Related to Figure 3.**

(A) Development of the LRO at the *Xenopus* gastrocoel roof: the SM involutes during gastrulation to give rise to the GRP during early neurulation, which is shown in a dorsal explant in a ventral view on the right (blue); modified from [S1]. (B-E) Expression of *foxj1* (B, C) and *wnt11b* (D, E) in the SM of wt (B, D) and *myo1d* morphant (C, E) embryos at stage 10.5. (F-I) Expression of *tektin2* (F, G) and *gdf3* (H, I) in the GRP of dorsal explants isolated from wt (F, H) and *myo1d* morphant embryos (G, I) at stage 18 (G, H) and 19 (H, I).



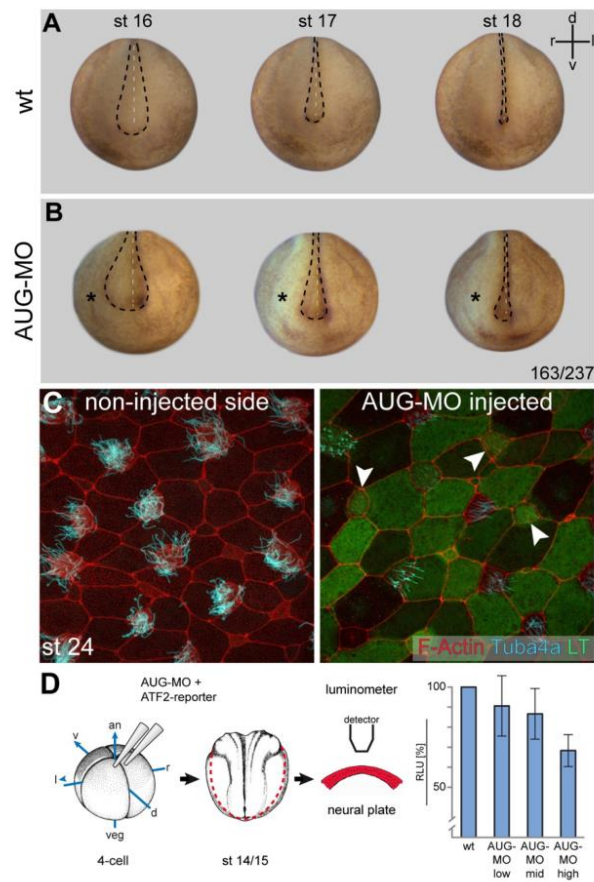


**Figure S3. PCP defects in *myo1d* morphant *Xenopus* embryos, Related to Figure 4.**

(A, B) Neural tube closure delay. Embryos were injected with AUG-MO at the 4-cell stage on the right side. Progress of neural tube closure in unilaterally injected embryos (B) was recorded at stages 16, 17 and 18, when the neural tube in wildtype uninjected specimens (A) had closed. \*, injected side. Dashed lines outline neural folds. Please cf. also Movie S3.

(C) Ciliation of skin multi-ciliated cells (MCCs) at stage 24 in specimen unilaterally injected with AUG-MO at the 4-cell stage. Left: control side; right: MO-injected side. LT, lineage tracer fluorescein dextrane. Please cf. also Movies S4 +5.

(D) Dose-dependent inhibition of the ATF2-based luciferase reporter to monitor non-canonical Wnt signaling. AUG-MO, the ATF2-reporter gene and Renilla luciferase were injected into the neural lineage at the 4-cell stage, and specimens were cultured until stage 14/15. Neural plate tissue was dissected and analyzed for reporter gene activity. RLU, relative luciferase units ( $\pm$  standard error).

#### Supplemental References

[S1] Tisler, M., Thumberger, T., Schneider, I., Schweickert, A., and Blum, M. (2017). Leftward Flow Determines Laterality in Conjoined Twins. *Curr. Biol.* 27, 543–548.

## **Original Movie legends from Current Biology**

### **Movie S1. Leftward Flow in WT and *myo1d* Morphant Embryos, Related to Figure 3**

Dorsal explant was prepared at stage 16/17, fluorescent microbeads were added and cilia-driven bead transport was recorded at a frame rate of 2 frames per second. Left: wildtype embryo; right: morphant specimen. Movie plays at 5 x real time. Note that in the morphant, individual beads were also transported from left to right

### **Movie S2. Delay of Neural Tube Closure in *myo1d* Morphants, Related to Figure 4**

Embryos were unilaterally injected with AUG-MO at the 4-cell stage. Time lapse movie was recorded from stage 14 to stage 19 at 2 frames per minute. Injected side is marked by an asterisk. Jerks in the middle of the sequence were caused by manual re-positioning of the specimens. Movie plays at 900 x real time. Note that neural tube closure in the morphant specimen proceeds at reduced velocity on the injected sides.

### **Movie S3. Bead Transport along the Larval Skin of a WT Specimen at Stage 24, Related to Figure 4**

Bead transport along the anterior-posterior axis of a wildtype embryo, incubated in culture medium containing fluorescent microbeads, was recorded at 10 frames per second. Movie plays at real time.

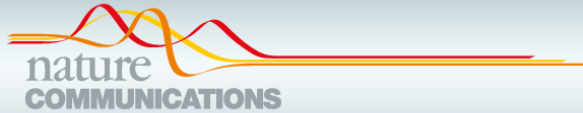
### **Movie S4. Compromised Bead Transport along the Larval Skin of a *myo1d* Morphant Specimen at Stage 24, Related to Figure 4**

AUG-MO was injected into the ventral right blastomere at the 4-cell stage and embryos were cultured until stage 24. Bead transport along the anterior-posterior axis, incubated in culture medium containing fluorescent microbeads, was recorded at 10 frames per second. Note that bead transport on the injected side (\*) was slowed down. Movie plays at real time.

**Bicc1 and Dicer regulate left-right patterning through post-transcriptional control of the Nodal-inhibitor Dand5**

<https://doi.org/10.1038/s41467-021-25464-z>

Reproduced with permission from Springer Nature



## ARTICLE


<https://doi.org/10.1038/s41467-021-25464-z>

OPEN

# Bicc1 and Dicer regulate left-right patterning through post-transcriptional control of the Nodal inhibitor Dand5

Markus Maerker<sup>1,7</sup>, Maïke Getwan<sup>6,7</sup>, Megan E. Dowdle<sup>2</sup>, Jason C. McSheene<sup>3</sup>, Vanessa Gonzalez<sup>3</sup>, José L. Pelliccia<sup>3</sup>, Danielle S. Hamilton<sup>3</sup>, Valeria Yartseva<sup>4</sup>, Charles Vejnár<sup>4</sup>, Melanie Tingler<sup>1</sup>, Katsura Minegishi<sup>5</sup>, Philipp Vick<sup>1</sup>, Antonio J. Giraldez<sup>4</sup>, Hiroshi Hamada<sup>5</sup>, Rebecca D. Burdine<sup>3</sup>, Michael D. Sheets<sup>2</sup>, Martin Blum<sup>1</sup> & Axel Schweickert<sup>1</sup>✉

Rotating cilia at the vertebrate left-right organizer (LRO) generate an asymmetric leftward flow, which is sensed by cells at the left LRO margin. Ciliary activity of the calcium channel Pkd2 is crucial for flow sensing. How this flow signal is further processed and relayed to the laterality-determining Nodal cascade in the left lateral plate mesoderm (LPM) is largely unknown. We previously showed that flow down-regulates mRNA expression of the Nodal inhibitor Dand5 in left sensory cells. De-repression of the co-expressed Nodal, complexed with the TGFβ growth factor Gdf3, drives LPM Nodal cascade induction. Here, we show that post-transcriptional repression of *dand5* is a central process in symmetry breaking of *Xenopus*, zebrafish and mouse. The RNA binding protein Bicc1 was identified as a post-transcriptional regulator of *dand5* and *gdf3* via their 3'-UTRs. Two distinct Bicc1 functions on *dand5* mRNA were observed at pre- and post-flow stages, affecting mRNA stability or flow induced translational inhibition, respectively. To repress *dand5*, Bicc1 co-operates with Dicer1, placing both proteins in the process of flow sensing. Intriguingly, Bicc1 mediated translational repression of a *dand5* 3'-UTR mRNA reporter was responsive to *pkd2*, suggesting that a flow induced Pkd2 signal triggers Bicc1 mediated *dand5* inhibition during symmetry breakage.

<sup>1</sup>University of Hohenheim, Institute of Biology, Department of Zoology, Stuttgart, Germany. <sup>2</sup>Department of Biomolecular Chemistry, University of Wisconsin, Madison, WI, USA. <sup>3</sup>Department of Molecular Biology, Princeton University, Princeton, NJ, USA. <sup>4</sup>Department of Genetics, Yale University School of Medicine, New Haven, CT, USA. <sup>5</sup>Laboratory for Organismal Patterning, RIKEN Center for Biosystems Dynamics Research, Hyogo, Japan. <sup>6</sup>Present address: University of Zurich, Institute of Anatomy, Zurich, Switzerland. <sup>7</sup>These authors contributed equally: Markus Maerker, Maïke Getwan. ✉email: [axel.schweickert@uni-hohenheim.de](mailto:axel.schweickert@uni-hohenheim.de)

The Nodal signaling cascade is central in setting up organ situs during embryonic development<sup>1,2</sup>. In *Xenopus*, the Tgfb $\beta$  ligand Nodal1 is activated in the LPM of the neurula embryo, where it induces its own transcription, that of its feedback inhibitor *lefty* and the homeobox transcription factor *pitx2*. Cilia are required for Nodal cascade induction<sup>3–5</sup> in fish, amphibian and mammalian embryos, but not in reptiles and birds<sup>1,6,7</sup>. The archenteron (primitive gut or remnants thereof) transiently harbors the ciliated epithelium of the left-right organizer (LRO) during neurula stages. In frogs, the gastrocoel roof plate (GRP<sup>8</sup>) develops from precursor cells, i.e., superficial mesoderm, which is specified during the early gastrula stages. GRP cells have different fates, which correlate with specific properties. They are notochordal (cLRO) at the midline or somitic (sLRO) more laterally. The GRP, like other vertebrate LROs, is typically characterized by motile cilia at its center and immotile, supposedly sensory cilia at its lateral borders<sup>5</sup>. The posterior orientation and tilt of motile cilia, and their intrinsic clockwise rotation, give rise to a leftward fluid flow in the extracellular space that is sensed at the left LRO margin by a ciliary complex containing the ion-channel Pkd2 (TRPP2/Polycystin2). It is generally believed that the cation channel Pkd2, which we initially characterized as an LR determinant in a *pkd2* knockout mouse<sup>9</sup>, is central to flow sensing. In mice and fish, left-asymmetric calcium spikes in lateral LRO cells were reported, which were depending on a ciliary Pkd2 function. Calcium influx, therefore, seems to represent the initial response to flow sensing<sup>10,11</sup>.

The decisive molecular target of leftward flow is the repression of the Nodal inhibitor *dand5* (former *coco* in frog; *Cert2* in mouse; *charon* in fish) at the left LRO margin<sup>12–14</sup>. *nodal* is co-expressed with *dand5* in time and/or space and thereby inhibition of Dand5 protein synthesis results in de-repression of Nodal signaling. As a consequence, Nodal bound to the Gdf3 protein (former *derrière* in frog; *Gdf1* in mouse) is transferred to the left LPM, where it induces the left-asymmetric Nodal signaling cascade<sup>15,16</sup>. A critical component of LR patterning is the flow-dependent repression of Dand5, manifested partially by a left-sided reduction of *dand5* mRNA in vertebrate embryos. In mice, *dand5* mRNA is destabilized via its 3'-UTR in a flow-dependent manner<sup>13</sup>. However, the timing of *dand5* asymmetry raises the possibility that post-transcriptional mRNA decay might be insufficient for reducing Dand5 protein levels and suggests that additional mechanisms contribute to repression. In frog, *dand5* mRNA asymmetry is most pronounced at late neurula, i.e., the very stages (st. 19–21) in which *nodal1* is already expressed in the left LPM<sup>12</sup>. In addition, left-sided *dand5* mRNA decay in *Xenopus* is observed in a maximum of ~80% of wt specimens, whereas left Nodal cascade induction and the arrangement of inner organs were undisturbed in 95% of cases. Thus, the frequency of *dand5* asymmetry is insufficient to explain the robust occurrence of wildtype organ asymmetry (situs solitus). The data indicates that detectable *dand5* mRNA asymmetry occurs too late and infrequently to be functionally relevant and suggests that flow-dependent *dand5* repression might also include translational inhibition.

A protein that could exert both proposed post-transcriptional functions is Bic1 (Bic family RNA-binding protein 1). Bic1 binds to selected mRNAs and modifies translation post-transcriptionally, in a positive<sup>17</sup> or negative context-dependent manner<sup>18,19</sup>. Further, Bic1 localizes to P-bodies, cytoplasmic complexes involved in mRNA stability and turnover<sup>17,20,21</sup>. Interestingly, Bic1 interacts with microRNAs (miRs), which function in post-transcriptional regulation of mRNA translation and integrity<sup>22</sup>. Previous studies indicated Bic1 functions are important for LR patterning. *bic1* in frogs and mice is expressed in the LRO. *bic1* loss-of-function (LoF) impacts Wnt/planar cell

polarity (PCP) signaling, resulting in unpolarized LRO cilia and perturbed leftward flow<sup>20</sup>. However, *bic1* expression in the frog LRO revealed strong enrichment of mRNA in *nodal1* and *dand5* positive sLRO cells (cf. Figure 3 in ref. <sup>20</sup>), indicative of a separate, specific function in these cells, which was not addressed at the time.

Here, we show that the RNA-binding protein Bic1 regulates *dand5* mRNA stability and translation in LRO sensor cells. Approximately 139 nucleotides of the proximal *dand5* 3'-UTR are required and sufficient for Bic1-mediated translational repression. Furthermore, within this small sequence, we identify distinct sub-regions specific for *dand5* mRNA stability and translational repression. In addition, we show that Bic1 also regulates the translation of *gdf3*, thereby influencing Nodal signaling directly. Finally, our data indicate that *bic1* functions together with *dicer1* (the enzyme catalyzing the final step of miR biosynthesis) and *pkd2* to mediate *dand5* repression, and this function is evolutionary conserved in other organisms.

## Results

**Bic1 represses *dand5* translation.** Because of the allotetraploid genome of *Xenopus laevis*, 3'-UTRs of *dand5* alleles were compared. Sequence conservation between S and L-alleles is low, except for the proximal 230 nucleotides downstream of the Stop-codon, which show 84% sequence identity (Supplementary Fig. 1A, B). Asymmetric *dand5* mRNA expression was found for both alleles, as visualized by in situ hybridization (ISH) of dorsal explants at stages 18 and 20 with antisense RNA probes specific for the 3'-UTRs of S- and L-alleles (Supplementary Fig. 1C, D).

Based on our previous identification of *dand5* mRNA as a target of Bic1 binding<sup>18</sup> we wondered whether Bic1 regulates *dand5*, the critical effector downstream of leftward flow<sup>1</sup>. To directly test this, an assay in animal cap explants was set up (AC assay; Fig. 1A) which specifically analyzed Bic1's capacity to interfere with mRNA translation. We used mRNAs of our previously published *dand5.S* 3'-UTR and newly cloned L 3'-UTR luciferase reporters (Supplementary Fig. 1B<sup>18</sup>). Because *bic1* is not present in AC cells<sup>23</sup>, gain-of-function (GoF) experiments do not unravel any in vivo functions but reflect a somewhat artificial assay. *dand5* mRNA, however, is maternally deposited at the animal pole<sup>24</sup> and thus post-transcriptional regulation might be active in AC cells. Injections were targeted to the animal region of the four-cell embryo and AC tissue was excised at the early gastrula stage 10 (Fig. 1A). Reporter mRNAs harboring the full-length 3'-UTRs of the respective S and L-alleles of *dand5* were translated, subsequently resulting in luciferase activity (Fig. 1B). Co-injection of *bic1* mRNA, however, repressed luciferase activity of both reporters to ~20%. A full-length mouse *bic1* mRNA also repressed reporter activities, though less efficiently (Fig. 1B). These experiments demonstrate a repressive effect of Bic1 on a reporter protein expressed from an mRNA construct harboring the *dand5* 3'-UTR.

Next, we asked which sequences in the 3'-UTR were required for translational inhibition by Bic1. To do so, different regions of the 1818 nucleotides of *dand5.S* 3'-UTR were deleted (Fig. 1C). Deleting the proximal 568 nucleotides abrogated the repressing effect of Bic1 (Fig. 1D). This proximal sequence alone enabled translational repression to ~30% of wt, i.e., slightly less than the full-length 3'-UTR. Further narrowing down to nucleotides 1–139 allowed repression at wt levels while deleting additional 26 nucleotides (construct 1–103) abolished translational inhibition, suggesting that nucleotides 103–139 could be particularly important. For validation, a *cyclin B1* reporter was used as negative, and a *tdgfl* (*cripto*) reporter as a positive control, as previously reported<sup>18</sup>.

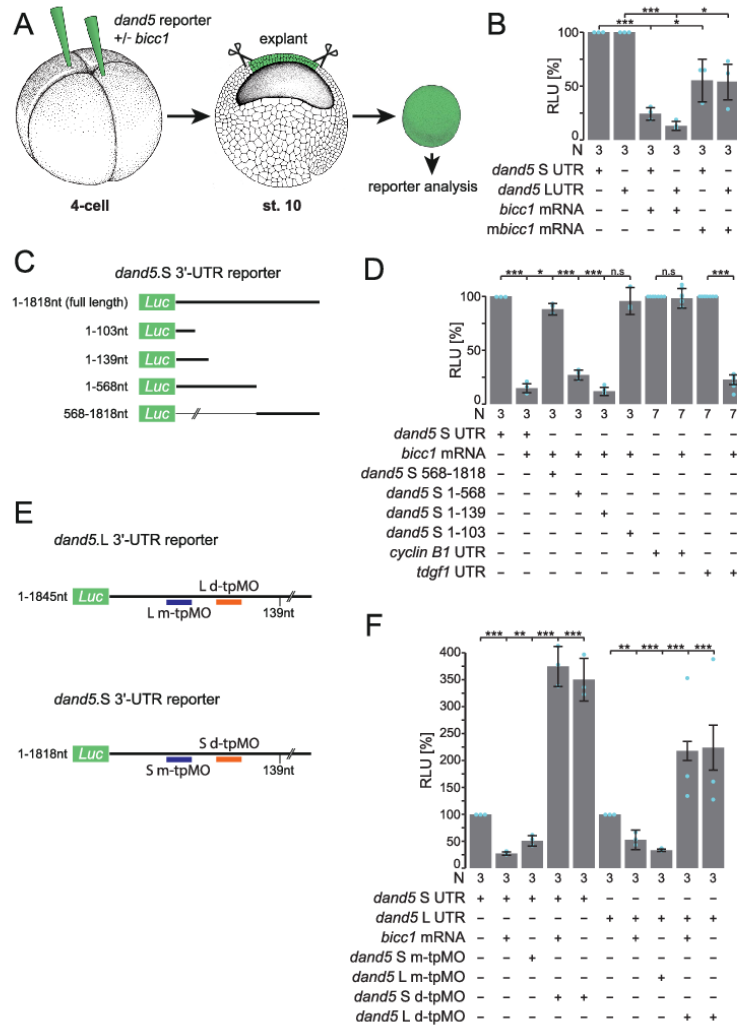


**Fig. 1** Bicc1 represses *dand5* mRNA translation via its proximal 3'-UTR. **A** Schematic depiction of *dand5* reporter assay. *dand5* 3'-UTR sequences fused to luciferase coding were injected either with or without *bicc1* mRNA into the animal region of four-cell embryos. At st. 10, the animal cap region was excised and assayed for luciferase activity. Adapted from refs. 65 and 66. **B** Animal cap reporter assay following injections of *dand5* S- or L 3'-UTRs alone or together with *Xenopus* (*bicc1*) or mouse *Bicc1* (*mbicc1*) effector mRNAs. Note that both alleles were equally repressed. Note also that *mbicc1* was efficient as a repressor as well. **C** Luciferase reporter constructs harboring different regions of the *dand5* (S-allele) 3'-UTR. **D** Repression of translation is mediated through a proximal 139 nucleotides (nt) sequence element in the *dand5* 3'-UTR. **E** Schematic depiction of medial and distal target protector MOs (m-tpMOs or d-tpMOs) binding to the minimal Bicc1 responsive element (Bicc1RE) in the *dand5* 3'-UTR (L or S). **F** m- and d-tpMOs (0.4 or 0.5 pmol/embryo, respectively) interact differently with the luciferase reporter expression. m-tpMO blocked and d-tpMO boosted luciferase activity. Co-injection of d-tpMOs prevented Bicc1-dependent repression of the full-length *dand5* reporters (L and S) and further enhanced their expressivity. N in **B**, **D**, and **F** represents the number of independent experiments. A pool of 10 animal caps was analyzed per experiment and treatment. Results from reporter mRNAs alone served as reference and were set to 100% RLU. Relative values of single experiments are depicted as blue dots. Data of at least three experiments are presented as mean value (bar)  $\pm$  standard deviation (error bar, SD). Statistical analyses were done with a one-sided Student's *t* test for two independent means (Bonferroni corrected) using the values of at least three individual experiments. *p* values, values for individual experiments, the mean values, and standard deviations are found in the source data file. n.s. not significant  $p > 0.05$ ; \* significant,  $p < 0.05$ ; \*\* highly significant  $p < 0.01$ ; \*\*\*, very highly significant  $p < 0.001$ ; RLU relative luciferase units; *Luc* Luciferase.



To test whether the proximal element of the *dand5* 3'-UTR was instrumental in mediating Bicc1-dependent translational repression, antisense target protector morpholino oligomers (tpMOs) were designed. tpMOs have been recently used to block specific sequences in UTRs, i.e., miRNA or protein-binding sites, to analyze post-transcriptional regulation<sup>25</sup>. We specifically targeted the distal 103–139 region (d-tpMO) and 5' adjacent medial sequences (m-tpMO) of the identified minimal Bicc1 responsive 3'-UTR in S and L. The medial tpMOs were complementary to nucleotides 65–89 for the L and S alleles (*dand5.L* m-tpMO; *dand5.S* m-tpMO). The distal tpMOs were complementary to nucleotides 91–116 of the L (*dand5.L* d-tpMO) and 107–132 of the S (*dand5.S* d-tpMO) allele (Fig. 1E; Supplementary Fig. 1B). m-tpMOs alone efficiently repressed reporter mRNA translation, suggesting that the blocked sequence is critical for general expressivity (Fig. 1F). Co-injection of the d-tpMOs with the full-length 3'-UTR *dand5* reporter and *bicc1* mRNA prevented repression (Fig. 1F). The reporter activity was about two- to threefold enhanced by d-tpMOs, as was the reporter activity upon co-injection with d-tpMO in the absence of *bicc1* (Fig. 1F). These data show that additional components restrict *dand5* reporter activity through interaction with its 3'-UTR, suggesting that the endogenous *dand5* mRNA is under post-transcriptional control independently of Bicc1. Taken together the reporter assays confirm the role of the proximal 3'-UTR *dand5* sequences in Bicc1-dependent repression, which we, therefore, termed “Bicc1 responsive element” (Bicc1RE; Supplementary Fig. 1B).

**Bicc1 responsive element is required for LR asymmetry.** To underscore the functional relevance of our AC assays, we examined the in vivo effect of tpMOs on LR asymmetry. Injections were performed in a unilateral manner at the 4–8 cell stage and thereby the effects on flow receiving, left or right sLRO cells were analyzed separately. Targeting m-tpMOs (L or S) to left sLRO cells did not change *pitx2* asymmetry at tadpole stages, whereas on the right, m-tpMOs induced ectopic *pitx2* expression in the right LPM (Fig. 2A, B). In contrast, right-sided injections of d-tpMOs (either L or S allele) had no effect, whereas left application prevented *pitx2* induction in the left LPM in close to 50% of specimens (Fig. 2A, C), suggesting that Bicc1RE is also required for *dand5* repression in vivo. Importantly, co-injection of *dand5* translation blocking morpholino (TBMO) rescued asymmetric *pitx2* induction (Fig. 2C), emphasizing d-tpMO specificity. These results suggest that medial and distal sub-regions of the Bicc1RE in the *dand5* 3'-UTR mediate different aspects of *dand5* post-transcriptional regulation and therefore both impact on LR asymmetry.

We then analyzed *dand5* expression patterns following tpMO treatment. *dand5* mRNA expression at post-flow stages (st. 20) was considerably reduced by m-tpMO irrespective of whether the right or left sLRO lineage was targeted (Fig. 2D, E). Sided *dand5* downregulation by m-tpMO was in agreement with either ectopic *pitx2* induction in the right LPM or its wildtype expression in left injected specimens. Importantly, loss of *dand5* mRNA was already observed in pre-flow stages (Fig. 2F, Supplementary Fig. 2A), indicating independence of flow. Toxic effects by m-tpMOs were excluded because targeted sLRO cells depicted wt *nodal1* expression (Supplementary Fig. 2A). Thus, we identified a medially localized sub-region in the Bicc1RE, likely required for *dand5* mRNA stability. Intriguingly, left-sided d-tpMO injections did not alter flow-induced downregulation of *dand5* mRNA (Fig. 2G, H), although *pitx2* asymmetry was lost. Irrespective of which side was targeted, the frequency of stronger right-sided *dand5* signals compared with left sLRO (R>L) in post-flow stages

did not differ between untreated controls and d-tpMO injected specimens (Fig. 2G, H). In pre-flow embryos (st. 16) no changes in *dand5* expression were observed either (Fig. 2I, Supplementary Fig. 2C). *nodal1* expression was also not altered, showing that d-tpMOs did not cause unspecific detrimental effects (Supplementary Fig. 2D). Our results suggest that the distal sub-region conveys flow-dependent repression specifically via *dand5* translation but does not impair mRNA decay.

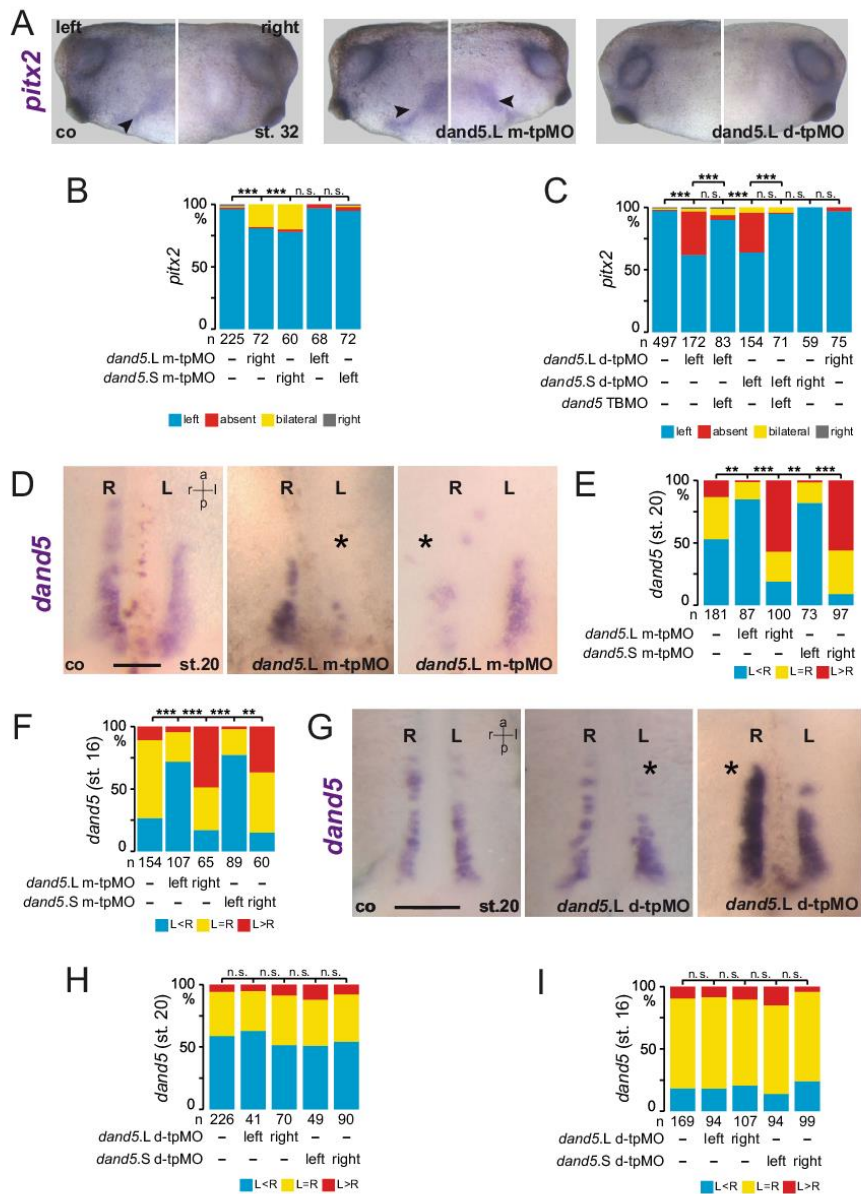
#### Bicc1 regulates *dand5* and *nodal1* expression at pre-flow stages.

To connect our observed tpMO effects on the *dand5* Bicc1RE to Bicc1 function, we performed *bicc1* LoF experiments. *X. laevis* offers precise targeting of sLRO cells by microinjection of the left or right C2-lineage<sup>26–28</sup>, whereas avoiding the flow-generating cLRO (Supplementary Fig. 3A). This injection setup circumvents described defects in cilia polarization. To knockdown *bicc1*, a previously published TBMO<sup>20</sup> was used as well as a designed splice-blocking MO (SBMO). In both cases, two MOs were used which specifically targeted the S- or L-allele, which are both expressed during embryogenesis and encode identical proteins<sup>29</sup>. Injecting either MO separately did not affect laterality (Supplementary Fig. 3B).

In morphants, in which the sLRO was targeted by co-injection of S- and L-MOs, the LRO morphology and cilia polarization in cLRO and sLRO cells was unaffected, demonstrating proper targeting (Supplementary Fig. 3C, C', D). *pitx2* expression, however, was predominately absent in morphants injected unilaterally on the left side (Fig. 3A; Supplementary Fig. 2E). Right-sided *bicc1* LoF had no effect on *pitx2* expression. MO-specificity was demonstrated by co-injecting full-length *bicc1* mRNA that was not targeted by either MO (mouse *Bicc1*, *mbicc1*, in case of TBMO, and *Xenopus bicc1* in case of SBMO), which rescued *pitx2* expression in a significant proportion of specimens (Fig. 3A; Supplementary Fig. 3E). In addition, splicing of *bicc1* pre-mRNA was affected in SBMO-treated specimens, shown by RT-PCR (Supplementary Fig. 3F). Interestingly, GoF alone did not affect *pitx2* (Fig. 3A), which indicates that an excess of Bicc1 was not interfering with flow sensing or subsequent processes. Both *bicc1* MOs gave virtually identical results, fulfilling yet another criterion for the controlled use of MOs<sup>30</sup>. Importantly, parallel LoF of *bicc1* and *dand5* in left sLRO cells rescued *pitx2* expression (Fig. 3A), which fits a scenario where Bicc1 acts downstream of flow and upstream of flow-mediated *dand5* repression.

We, therefore, analyzed the expression of the flow target *dand5* in post-flow *bicc1* morphants. We observed a strong downregulation of *dand5* mRNA (Fig. 3B, C), instead of the expected loss of *dand5* repression and blocked mRNA decay. This effect was not restricted to left sLRO cells as right-sided MO injections equally led to *dand5* mRNA reduction (Fig. 3C). In pre-flow stages, *dand5* was also downregulated (Supplementary Fig. 3G). Importantly, *dand5* expression was restored in *bicc1* morphants by co-injecting *bicc1* rescue mRNAs, demonstrating specificity (Fig. 3B, C). Injecting *bicc1* mRNA alone or with MOs boosted *dand5* mRNA expression in left or right sLRO cells (Fig. 3B, C), which hinted towards an enhanced *dand5* mRNA stability or expression. Overall, the *bicc1* MO phenotype on *dand5* mRNA clearly resembled the results obtained when the *dand5* 3'-UTR was targeted by the m-tpMO (Fig. 2D, E; Supplementary Fig. 2A). However, loss of *dand5* mRNA by *bicc1* LoF was not congruent with observed effects on *pitx2*, i.e., no ectopic right-sided induction but the loss of left-sided *pitx2*, suggesting that additional factors were affected.

To explore this further, we monitored *myo1d* and confirmed that the positioning and the somitic identity of sLRO cells were



unaltered in *bicc1* morphants, (Supplementary Fig. 3H), excluding a general failure in specification or morphogenesis. We then analyzed *nodal1* in sLRO cells. Like *dand5*, *nodal1* expression was substantially reduced in *bicc1* morphants at pre- and post-flow stages (Fig. 3D, E; Supplementary Fig. 3I). The effect was specific because *nodal1* expression was rescued by co-injections of *bicc1* mRNAs (Fig. 3D, E), suggesting that this effect contributed to the observed LR defects, i.e., loss of *pitx2* expression. Bic1 regulation

of *nodal* mRNA has not been reported previously. Taken together, Bic1 controls the expression of both key effectors of symmetry breaking independent of leftward flow.

**Bic1 ensures *gdf3* mRNA translation and thereby *nodal1* expression.** Previous reports suggested that *nodal1* is regulated by Gdf3 signaling in sLRO cells<sup>31</sup> and that *gdf3* is post-

**Fig. 2 Bicc1 responsive element (Bicc1RE) of the *dand5* 3'-UTR is required for LR asymmetry.** **A** Uninjected control (co), m-tpMO, or d-tpMO-injected embryos showed left, bilateral, or absent *pitx2* expression, respectively. Lateral views (left and right) of embryos are presented. Arrowheads mark *pitx2*-positive lateral plate mesoderm. **B** Quantification of *pitx2* results of m-tpMO-treated specimens. **C** Quantification of *pitx2* asymmetry by d-tpMO injections. Note administration of *dand5* TPMO together with d-tpMOs restored wt *pitx2* expression. **D** Diminished *dand5* mRNA expression by left-sided and right-sided m-tpMO injections compared with control. **E** Quantification of *dand5* expression at post-flow stages (st.20) following m-tpMO treatment. **F** Quantification of *dand5* expression in pre-flow specimens injected with m-tpMO. **G** Wildtype *dand5* repression in control (co) and left- or right-sided d-tpMO injected specimens. **H** Quantification of *dand5* asymmetry. Note flow-induced *dand5* mRNA decay was observed in controls and following d-tpMO application. **I** Quantification of *dand5* staining of pre-flow specimens (st.16) following d-tpMO injections. MO pmol/embryo: m-tpMO (L or S, 0.8); d-tpMO (L or S, 1). Asterisks in **D** and **G** mark injected side. Scale bars in **D** and **G** represent 100  $\mu$ m. Numbers (n) in **B**, **C**, **E**, **F**, **H**, and **I** represent analyzed specimens from more than three independent experiments. Statistical analyses were done with one-sided Pearson's chi-square test, which was adjusted for multiple comparisons by Bonferroni (**B**, **C**) or Bonferroni-Holm (**E**, **F**, **H**, **I**). *p* values and listing of individual experiments can be found in the source data file. n.s. not significant  $p > 0.05$ ; \*\*highly significant  $p < 0.01$ ; \*\*\*very highly significant  $p < 0.001$ ; st. stage; a anterior; l left; r right; p posterior.

transcriptionally regulated<sup>32</sup>. To test whether *gdf3* might be regulated by Bicc1, a luciferase reporter containing the *gdf3* 3'-UTR (361 bp S allele) was analyzed in the AC assay. AC cells are devoid of endogenous *gdf3* expression. Translation of *gdf3* reporter mRNA was significantly repressed by Bicc1 (Fig. 4A). Unlike *dand5* and *nodal1*, *gdf3* mRNA in sLRO cells was not altered in *bicc1* SBMOs injected specimens (Fig. 4B, C). *nodal1* mRNA was diminished in *gdf3* morphants leading to impaired *pitx2* asymmetry (Supplementary Fig. 4), suggesting that Bicc1 could act on *gdf3* translation in vivo. If loss of *nodal1* mRNA in *bicc1* morphants was owing to impaired Gdf3 signaling, *nodal1* expression should be restored by *gdf3* GoF. Co-injecting *bicc1* SBMOs and *gdf3* mRNA in the left sLRO lineage indeed rescued *nodal1* expression as well as *pitx2* asymmetry (Fig. 4 D, E and F, G respectively), demonstrating that Bicc1 enabled Gdf3-dependent *nodal1* expression. Thus, in pre-flow stages, Bicc1 seems to be required for securing the interplay of secreted key factors (Nodal1/Gdf3/Dand5) until positional information is provided by leftward flow which represses *dand5*.

**Bicc1 acts in a context-dependent manner with sub-regions of the Bicc1RE.** To provide further evidence that Bicc1 regulation of *dand5* is relayed through the Bicc1RE, we tested for functional cooperation of *bicc1* SBMOs with tpMOs. Consequently, we used single L- or S-specific *bicc1* SBMOs which, separately, did not impact on *pitx2*, *dand5*, and *nodal1* expression, in combination with suboptimal dosages of tpMOs (Fig. 5A–D; Supplementary Fig. 3B, 4A–C). Right-sided injection of low dose m-tpMO (S or L) together with a single *bicc1* SBMO (S or L) resulted in ectopic right-sided LPM induction of *pitx2* (Fig. 5A; Supplementary Fig. 5A), mimicking treatments with high dose m-tpMO (Fig. 2A, B). Accordingly, double morphants showed reduced *dand5* expression on the injected side (Fig. 5B, C). These results suggested that in early neurulae *dand5* mRNA stability depends on (a) Bicc1 and (b) the accessibility of the medial sub-region of the Bicc1RE.

Next, we performed alike experiments with d-tpMOs, to prove the involvement of Bicc1 in post-flow *dand5* regulation. Indeed, left-sided injections of low doses of d-tpMO together with allele-specific *bicc1* SBMO prevented *pitx2* induction in the left LPM (Fig. 5D; Supplementary Fig. 5B). Importantly, *nodal1* expression in sLRO cells was normal (Supplementary Fig. 5C), unlike in *bicc1* morphants (Fig. 3D, E). We, therefore, concluded that flow-induced *dand5* translational repression required Bicc1 activity, which merged on the distal sub-region of the Bicc1RE. Taken together, the cooperation experiments of *bicc1* SBMOs and tpMOs underscore a dual role of Bicc1 on flow independent *dand5* mRNA stability or its flow-induced translational repression. Intriguingly, both Bicc1 functions converge on a small 3'-UTR sequence, the Bicc1RE.

**Bicc1 and Dicer interact in post-transcriptional *dand5* regulation.** Several reports have shown Bicc1 regulation of miRs, small RNAs that bind specific 3'-UTRs and thereby tag the mRNA for translational repression and decay. The RNase III enzyme Dicer processes precursor miRs in the cytoplasm and, together with Ago2, assembles the RNA-induced silencing complex RISC<sup>33</sup>. In the kidney, Bicc1 acted downstream of Dicer1 to transfer target mRNAs unto Ago2, which cleaves or blocks their translation in a miR-dependent manner<sup>22</sup>. To begin exploring the possible role of miRs in *dand5* regulation, we analyzed the expression of *dicer1*. *dicer1* mRNA was expressed in somites and notochord at flow-stage (st. 18; Fig. 6A). *dicer1* mRNA was found specifically in sLRO cells, excluding the cLRO cells in-between and the lateral endodermal cells flanking the LRO (Fig. 6A, A'). Two MOs that targeted translation (TBMO1<sup>34</sup>; TBMO2) through conserved sequences of both S- and L-alleles were used to knockdown *dicer1*. Targeting the left side of the LRO (C2-lineage) inhibited *pitx2* expression in the left LPM (Fig. 6B). Wildtype phenotypes upon right-sided MO injections argue against MO toxicity and off-target effects (Fig. 6B). A parallel knockdown of *dand5* on the left rescued wt *pitx2* expression (Fig. 6B; S6A), further supporting MO-specificity. In addition, western blot analysis confirmed the efficacy of the designed *dicer1* TPMO2 (Supplementary Fig. 6B). In mouse embryos, *Dicer* was also required for Nodal cascade asymmetry. Induced conditional deletion of *Dicer* from the mouse LRO prevented the expression of *Nodal* mRNA in the left LPM (Fig. 6C).

Analyzing earlier stages of laterality determination, left-sided downregulation of *Dand5* mRNA levels at post-flow stages was compromised in mouse *Dicer* mutants and *Xenopus dicer1* morphants (Fig. 6D, E, F). This finding was conserved in zebrafish. In wt 10 somite stage (ss) embryos, *dand5* was repressed on the left side of Kupffer's vesicle (KV), whereas no repression was observed in maternal zygotic *dicer* mutants (MZ*dicer*; Fig. 6G). At the wt KV *dand5* mRNA fades away at 14 ss and is absent at 18 ss (Supplementary Fig. 6C; source data file). Although MZ*dicer* mutants showed some developmental delay, *dand5* expression was retained as late as 24hpf, which was monitored by ISH (Figure S6C) and RNAseq (Fig. 6H; Supplementary Fig. 6D, E). Loss of *dand5* repression upon *dicer* LoF could be caused by the absence of flow or represent a specific function on *dand5* regulation. Previous reports have shown that miRs control motile ciliogenesis<sup>35,36</sup>. In agreement with this, ciliation of multiciliated cells in the *Xenopus* epidermis was impaired in *dicer1* morphants (Supplementary Fig. 6H). When *dicer1* MOs were targeted to flow-generating LRO cells (C1-lineage), ciliation was unaltered in morphants (Supplementary Fig. 6F, F', G), demonstrating that *dicer* acted downstream of flow and upstream of *dand5* repression, like *bicc1*. Next, we investigated whether *dicer1* and *bicc1* acted in the same pathway in flow-sensing cells. When injecting *bicc1* SBMOs (targeting



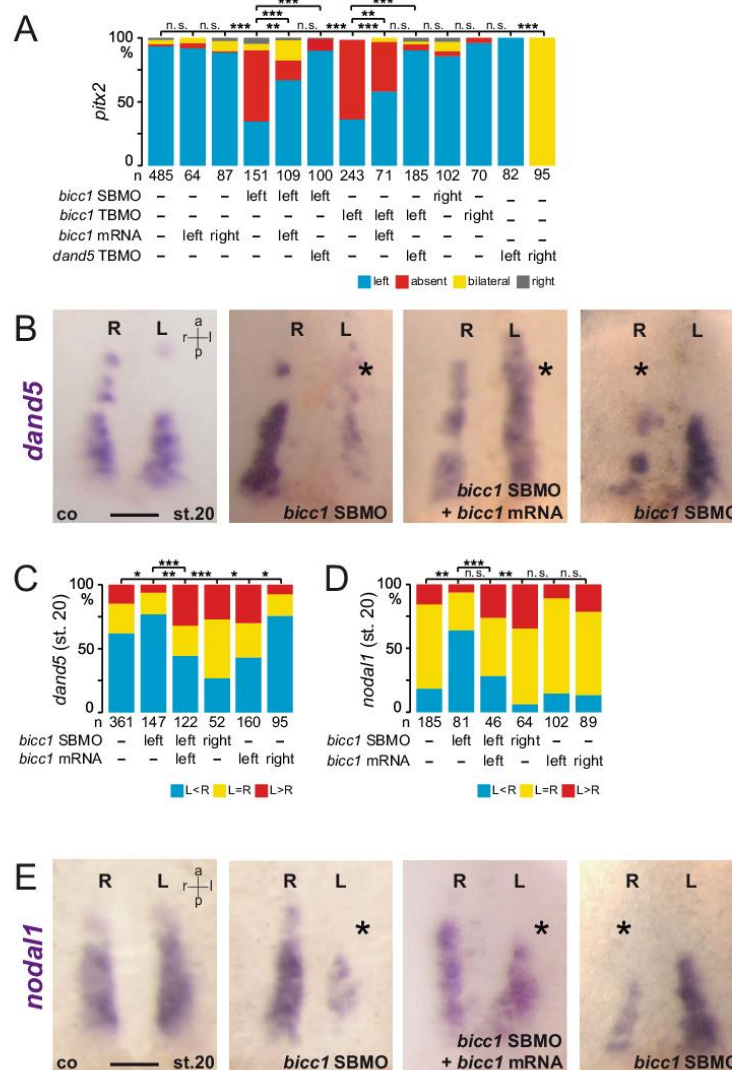


**Fig. 3** *Bicc1*-dependent *dand5* and *nodal1* expression in sLRO cells. **A** Absence of left LPM *pitx2* expression in *bicc1* morphants, unilaterally injected on the left, was rescued by parallel knockdown of *dand5*. Specificity of TBMO or SBMO was shown by co-injecting rescue mRNAs, i.e., mouse *bicc1* or *Xenopus bicc1*, respectively. Note *dand5* knockdown on the right efficiently induced *pitx2* expression, as published. **B** Loss of *dand5* mRNA at post-flow stages (st. 20) following left- and right-sided *bicc1* SBMO injections. Controls (co) showed wt expression. *dand5* expression was restored by co-injecting *bicc1* rescue mRNA. Note enhanced *dand5* staining in rescued specimens. **C** Quantification of *dand5* expression after knockdown of *bicc1*. The effect was observed in the left and right sLRO cells. **D** Downregulation of *nodal1* in *bicc1* morphants. **D** Quantification of results. **E** Wt specimens show bilateral *nodal1* mRNA. Left or right *bicc1* SBMO injections reduced *nodal1*, which was restored by adding rescue *bicc1* mRNA. MO pmol/embryo: *bicc1* SBMO (L and S, each 1); *bicc1* TBMO, (L and S, each 1); *dand5* TPMO (0.5). Asterisks in **B** and **E** mark the injected side. Numbers (n) in **A**, **C**, and **D** represent analyzed specimens from more than three independent experiments. Statistical analyses were done with one-sided Pearson's chi-square test, which was adjusted for multiple comparisons by Bonferroni (**B**) or Bonferroni-Holm (**C**, **D**). n.s. not significant  $p > 0.05$ ; \* significant,  $p < 0.05$ ; \*\* highly significant  $p < 0.01$ ; \*\*\*, very highly significant  $p < 0.001$ . *p* values and listing of individual experiments can be found in the source data file. st., stage. Scale bars in **B** and **E** represent 100 μm.

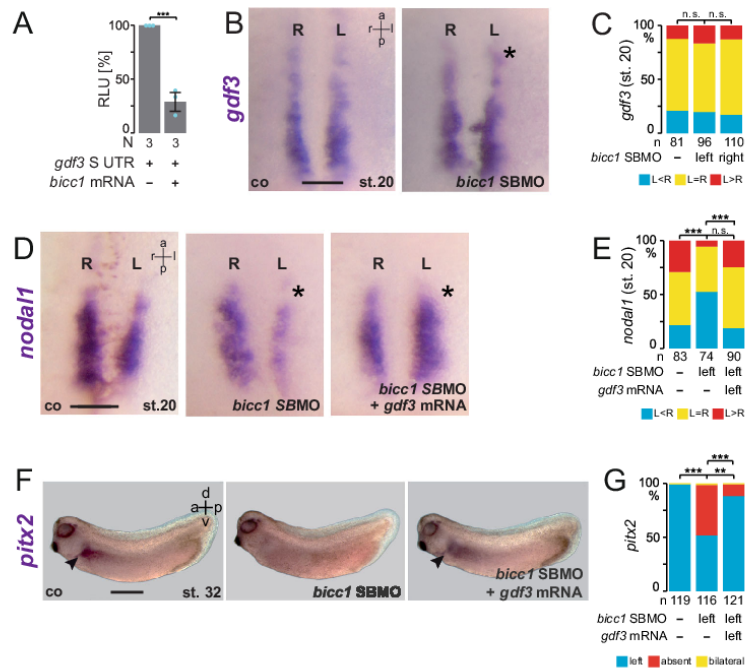


**Fig. 4** Bic1 indirectly regulates nodal1 expression via Gdf3 signaling. **A** Animal cap assay using a luciferase reporter mRNA which contained *gdf3* 3'-UTR sequences. Translation of *gdf3* reporter was efficiently blocked by co-injecting *bic1* mRNA. N represents the number of independent experiments. A pool of 10 animal caps was analyzed per experiment and treatment. The result from reporter mRNA alone served as a reference and was set to 100% RLU. Relative values of single experiments are depicted as blue dots. Data of three experiments are presented as mean value (bar)  $\pm$  standard deviation (error bar, SD). Statistical analyses were done with a one-sided Student's *t* test for two independent means using the values of three individual experiments. **B** *gdf3* mRNA was not affected by *bic1* LoF. **C** Quantification of *gdf3* expression in *bic1* morphants at the LRO margin. **D** *gdf3* GoF rescues *nodal1* expression in *bic1* morphants. Representative *nodal1* staining in left sLRO cells is shown for control (co), *bic1* morphant, and rescued specimens. **E** Quantification of the *bic1* MO rescue of *nodal1* expression by *gdf3*. **F, G** Left-asymmetric *pitx2* expression (arrowhead) is restored in *bic1* morphants by co-injecting *gdf3* mRNA. MO pmol/embryo: *bic1* SBMO (L and S, each 1). Asterisks in **B** and **D** mark injected side. Numbers (n) in **C**, **E**, and **G** represent analyzed specimens from more than independent experiments. Statistical analyses were done with one-sided Pearson's chi-square test, which was adjusted for multiple comparisons by Bonferroni-Holm (**C**, **E**) or Bonferroni (**G**). n.s. not significant,  $p > 0.05$ ; \*\* highly significant  $p < 0.01$ ; \*\*\*, very highly significant  $p < 0.001$ . *p*-values, mean values, SD and listing of individual experiments can be found in the source data file. Scale bars in **B** and **D** represent 100  $\mu$ m and in **F** 1 mm. RLU relative luciferase units, st. stage, a anterior, l left, r right, p posterior, d dorsal, v ventral.

S- or L-alleles) separately, wt *pitx2* induction in the left LPM was observed (Fig. 6I; Supplementary Fig. 3B). Co-injection of either *bic1*.S- or L-SBMO and *dicer1* MO blocked *pitx2* expression in ~70% of cases (Fig. 6I), demonstrating that *bic1* and *dicer1* synergize to mediate *dand5* repression.

Finally, we wondered whether *pkd2*, one of two published active components in the flow sensor<sup>37,38</sup>, acted in the same pathway. Our recent demonstration of an earlier (likely maternal) Pkd2 function in the specification and morphogenesis of the LRO prevented us from investigating this question in the context of LR axis formation in the embryo itself<sup>28</sup>. In zebrafish, however, zygotic *pkd2* mutants and morphants display randomization of *nodal* (*southpaw*), *lefty* and *pitx2*, but are reported to have normal KV ciliation and morphology<sup>39,40</sup>, suggesting a role for Pkd2 in flow sensing. In agreement with this, *dand5* mRNA repression was not observed in *pkd2* mutant and morphant zebrafish embryos (Fig. 7A, B), likely being causative for misregulation of the Nodal cascade in these backgrounds<sup>39</sup>. To test a potential

interplay between *pkd2* and *bic1* in the process of *dand5* repression, we returned to the *Xenopus* AC assay (Fig. 1A). In order to record additive effects of *pkd2*, we attenuated the Bic1-mediated repression of the *dand5* reporter by lowering the concentration of co-injected *bic1* mRNA, such that reporter activity was only repressed to ~40% of wt-level (Fig. 7C). Upon co-injection of full-length *pkd2* mRNA, reporter activity was further repressed to under 20% (Fig. 7C). *pkd2* mRNA alone, however, increased the reporter mRNA's expressivity fourfold. Because *pkd2* is maternally expressed in animal tissue, like *dand5*, we tested this interaction further by co-injecting *pkd2* MO, the specificity of which we showed previously<sup>17,41</sup>. Loss of *pkd2* partially rescued *bic1*-mediated repression of the *dand5* reporter (Fig. 7C), which again is contrasted in a *bic1* free set up, where *pkd2* is required for efficient translation. Therefore, these experiments underscore a scenario in which an upstream ion-channel Pkd2 is able to modulate Bic1 function during post-transcriptional regulation of *dand5*.

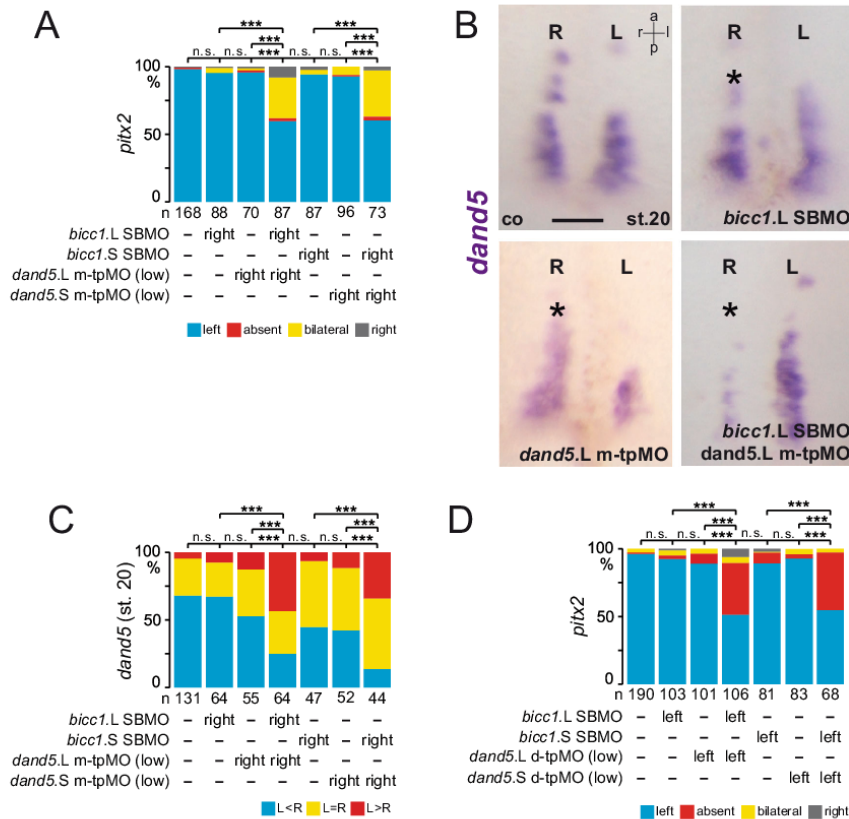


**Fig. 5** *Bicc1* regulates *dand5* mRNA through distinct regions of the *Bicc1RE*. **A** Quantification of right-sided *pitx2* induction by co-injecting a low, ineffective m-tpMO dosage with single allele-specific *bicc1* SBMO. Controls (co), m-tpMO (S or L, low), or allele (S or L) specific *bicc1* SBMO alone showed wt *pitx2* asymmetry. **B** Co-injecting m-tpMO (low) with *bicc1* TPMO (L or S) impacted *dand5* mRNA stability. Treatment with low concentrations of m-tpMO, single allele-specific *bicc1* TPMO, and uninjected co showed wt *dand5* expression at post-flow stages. **C** Quantification of *dand5* expression. **D** Quantification of *pitx2* asymmetry. Only in combination both suboptimal dosages of d-tpMO (low) or single allele-specific *bicc1* SBMO (S or L) prevented left *pitx2* expression. Wt expression was found in controls (co) and in embryos that were left-sided injected with one MO alone. MO pmol/embryo: *bicc1* SBMO (L or S, 1); m-tpMO low (L or S, 0.4); d-tpMO low (L or S, 0.5). Asterisks in **B** mark injected side. Numbers (n) in **A**, **C**, and **D** represent analyzed specimens from more than independent experiments. Statistical analyses were done with one-sided Pearson's chi-square test, which was adjusted for multiple comparisons by Bonferroni (**A**, **D**) or Bonferroni-Holm (**C**). n.s., not significant  $p > 0.05$ ; \*\*\*, very highly significant  $p < 0.001$ . *p* values and listing of individual experiments can be found in the source data file. Scale bar in **B** represents 100  $\mu$ m. st. stage, a anterior, l left, r right, p posterior.

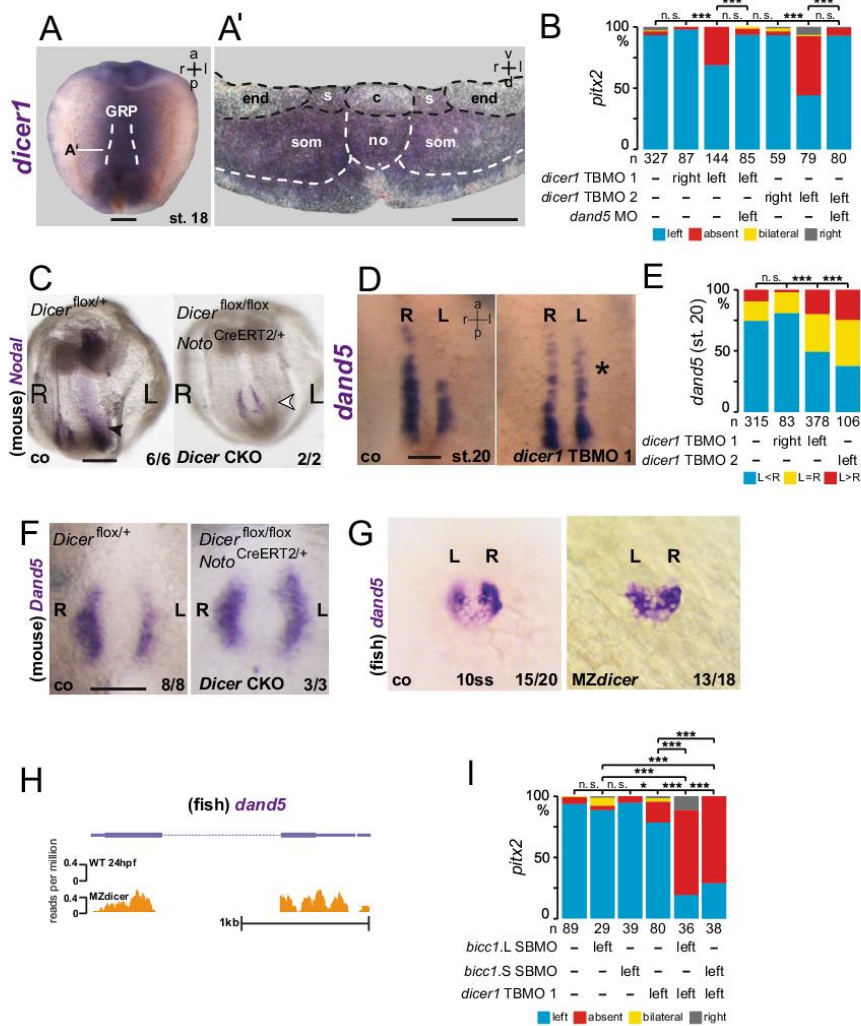
In summary, data presented here demonstrate that the proximal *dand5* 3'-UTR contains regulatory sequences, which allow the RNA-binding protein *Bicc1* and the miR-processing enzyme *Dicer* to execute flow-dependent *dand5* repression. Thereby this *Bicc1RE* likely reflects the downstream target of calcium released by *Pkd2* in sensing of leftward flow at the left LRO margin.

## Discussion

We have identified a minimal 139 nt sequence in the *dand5* 3'-UTR, which was sufficient to mediate *Bicc1*-dependent post-transcriptional regulation. This *Bicc1RE* contains two sub-regions, medial and distal, which represent two distinct regulatory entities in a pre- and post-flow setting. In pre-flow stages, free

access to the medial sub-region and a sufficient amount of *Bicc1* protein was required to maintain *dand5* mRNA expression. In this context, *Bicc1* might protect *dand5* against premature mRNA decay and ensures *Dand5* protein synthesis. However, observed LR defects in *bicc1* morphants were to a great extent caused by loss of *nodal1* expression, which so far has not been reported in other organisms. We identified an additional potential *Bicc1* target, the Tg $\beta$  ligand *gdf3*. This was evidenced by the efficient repression of the *gdf3* 3'-UTR reporter mRNA by *Bicc1* (Fig. 4A). However, *gdf3* mRNA expression, unlike *dand5* and *nodal1*, was not impaired by *bicc1* LoF indicating that in this case, *Bicc1* acted on translation only. *Gdf3* is required for efficient Nodal diffusion and therefore LR patterning<sup>16,31,42,43</sup>. In *Xenopus* sLRO cells an additional *gdf3* function was reported, suggesting that *Gdf3* signaling is upstream of *nodal1* transcription<sup>32</sup>, which





we validated in this study (Supplementary Fig. S4A, B). This finding was underscored by our observation that *gdf3* over-expression restored *nodal1* expression in *bicc1* morphants. Currently, there is no evidence of such a mechanism in other vertebrates and it likely reflects a frog-specific feature. We propose a pre-flow situation in which Bic1 safeguards the expression of *dand5* and *gdf3* in a post-transcriptional manner. Thus, it indirectly influences *nodal1* transcription via Gdf3 signal transduction (Fig. 8). In the embryonic kidney of *Xenopus*, a comparable protective Bic1 function was shown for *pkd2*<sup>17</sup>. Such a scenario should be relevant to ensure an at least equimolar equilibrium of the inhibitor Dand5 and its targets in sLRO cells. In addition, Bic1 control of *gdf3* limits or prevents ectopic Nodal signaling and premature Nodal/Gdf3 diffusion until flow sensing. Early Bic1 functions impeded the analysis of flow-dependent *dand5* mRNA regulation, but we were able to show several lines

of evidence that Bic1 serves as the critical mediator of flow sensing and primarily blocks *dand5* translation. (1) Rescue of *pitx2* asymmetry in *bicc1* morphants by *dand5* knockdown demonstrated that even when *dand5* and *nodal1* were strongly reduced, *dand5* was not repressed in absence of Bic1. (2) Using our d-tpMOs, we separated *dand5* mRNA decay from translation inhibition: left-sided, flow-dependent *dand5* mRNA reduction was still observed in d-tpMO morphants (Fig. 2G, H), whereas left nodal cascade induction was inhibited (Fig. 2A, C). (3) Bic1 dosage and availability of distal sequences of the Bic1IRE cooperated in flow-dependent *dand5* repression and left *pitx2* LPM induction, without any effects on *dand5* mRNA stability (Fig. 5D; Supplementary Fig. 5D). (4) The accompanying manuscript by Minegishi et al.<sup>44</sup> demonstrates Bic1 binding to the mouse *Dand5* 3'-UTR and identified specific binding motifs. Intriguingly, we found alike sequences in the Bic1IRE, which apparently

**Fig. 6 Dicer interacts with Bicc1 in *dand5* repression.** **A** Expression of *dicer1* in sensory (s) LRO cells (N = 3; n = 30) of the frog (GRP; gastrocoel roof plate). Whole-mount in situ hybridizations of stage 18 dorsal explant with a *dicer1*-specific antisense RNA probe. (A') The transverse histological section (indicated in **A**) reveals mRNA expression in sLRO cells, somites (som), and deep cells of the notochord (no), but absence of signals from central (c) flow-generating LRO and lateral endodermal cells (end). **B** Quantification of MO-mediated inhibition of *dicer*. Note knockdown in left, but not right sLRO cells prevented *pitx2* asymmetry in the left LPM, which was rescued by co-injecting *dand5* MO. **C** mRNA expression of *nodal* in control (*Dicer<sup>flax/+</sup>*) and *dicer* conditional knockout (*Dicer<sup>flax/flax</sup> Noto<sup>CreERT2/+</sup>*) mouse embryos at E8.0. Note that *Nodal* asymmetry in the left LPM (arrowhead) was lost in mutants. **D** Absence of flow-induced *dand5* mRNA decay at the left LRO margin in post-flow *dicer1* morphants (st. 20). Representative dorsal explants of wt (left) and *dicer1* morphant (right) specimens hybridized with a *dand5* antisense RNA probe. **E** Quantification of *dand5* results. **F** Flow-induced *Dand5* mRNA downregulation in left crown cells of the murine node was lost in *Dicer* conditional knockout (*Dicer<sup>flax/flax</sup> Noto<sup>CreERT2/+</sup>*) mouse embryos at E7.5. **G** Lack of *dand5* repression in 10 somite stage (ss) MZ*dicer* mutant zebrafish embryos. **H** Absence of *dand5* mRNA by RNAseq reads in 24hpf wt zebrafish embryos, but maintenance in MZ*dicer* mutants. **I** *bicc1* and *dicer1* interact in LR asymmetry. Wt *pitx2* expression upon isolated left-sided injections of allele-specific *bicc1* SBMOs and moderate effects upon *dicer1* TBMO1 injection. Asymmetric *pitx2* was significantly inhibited by co-injecting *dicer1* and *bicc1* MOs. MO pmol/embryo: *dicer1* TBMO1 (1.5); *dicer1* TBMO2 (1); *bicc1* TBMO (L or S, each 1); *bicc1* SBMO (L or S, each 1). Asterisks in **D** mark injected side. Numbers (n) in **B**, **E**, and **I** represent analyzed specimens from three independent experiments. Statistical analyses were done with one-sided Pearson's chi-square test, which was adjusted for multiple comparisons by Bonferroni (**B**, **I**) or Bonferroni-Holm (**E**). n.s. not significant  $p > 0.05$ ; \* significant,  $p < 0.05$ ; \*\*\*, very highly significant  $p < 0.001$ . *p* values and listing of individual experiments can be found in the source data file. Scale bars in **A**, **A'**, **C**, **F**, and **D** represent 100  $\mu$ m. st. stage, a anterior, d dorsal, l left, r right, v ventral, p posterior.

were located within dS-tpMO or next to dL-tpMO target sequences that specifically impair translational repression in *Xenopus* (Figure S1B). In addition, deleting the distal 36 nucleotides of the Bicc1RE, which contains the site, renders the *dand5* reporter mRNA insensitive to Bicc1 (Fig. 1D). Based on the conserved nature of *dand5* as the flow target, the finding in mouse should also apply to *Xenopus*. Potential sites were also found in the *gdf3* 3'-UTR, underscoring their relevance. (5) Both Bicc1 and Dicer are well known for post-transcriptional regulation and they functionally interacted in flow-induced *dand5* repression (Fig. 6I). (6) The flow sensor *pkd2* was able to modulate Bicc1 properties on *dand5* translational inhibition, suggesting that calcium could serve as the switch from a safeguarding pre-flow to a modified inhibitory post-flow Bicc1 function.

Our work, together with complementing analyses in the mouse (cf.<sup>44</sup>), constitutes a conceptual advance in our understanding of symmetry breaking, namely the flow-dependent activation of the RNA-binding protein Bicc1 to repress *dand5* translation on the left LRO margin in a Dicer-dependent manner. Based on our analyses, we suggest a model schematically depicted in Fig. 8. In the pre-flow scenario, Bicc1 protects *dand5* mRNA in a bilateral symmetric manner, which is relayed by the medial sub-region of the Bicc1RE. Thereby, *Dand5* synthesis and *Nodal* inhibition are secured. During flow, left-sided Pkd2 channel activation results in a cytoplasmic  $Ca^{2+}$  signal, which has been described in mouse and zebrafish<sup>10,11,38,45,46</sup>. It represents the intracellular second messenger of the initially extracellular flow signal. In zebrafish, transient activation of CaMK-II downstream of asymmetric  $Ca^{2+}$  is required in the LRO for asymmetric *Nodal* cascade induction and correct development of organ situs<sup>47</sup>. We hypothesize that Bicc1 gets functionally modified (Bicc1\*) by Pkd2 and potentially  $Ca^{2+}$ , which alters Bicc1 properties from initial *dand5* mRNA stabilization to translation inhibition, followed by mRNA decay (Fig. 8). How this molecular switch is achieved remains unclear. In *Drosophila*, Bicc1 phosphorylation has been reported and therefore  $Ca^{2+}$ -dependent phosphorylation might lead to functional changes<sup>48</sup>. Then again, under certain conditions, Bicc1 is thought to form polymeric complexes. Recently it was speculated that monomeric or polymeric Bicc1 aggregates may act differentially on post-transcriptional regulation. It was proposed that in left sLRO cells Bicc1 polymerization might be induced in a *pkd2*/ $Ca^{2+}$ -dependent manner that blocks *dand5* translation, whereas on the right side only low molecular Bicc1 complexes are present, allowing *Dand5* synthesis<sup>49</sup>. So far, we do not have any evidence of how Bicc1 is modified by the leftward flow. However, our analysis demonstrated that the functional switch is accompanied by a differential requirement of relevant sub-regions in the 3'-UTR

of *dand5*. This finding may be very useful in the future to map crucial Bicc1 domains and sequences for *dand5* inhibition.

In evolutionary terms, the *pkd2/bicc1/dicer* module is functionally conserved from zebrafish to mammals. In mouse and *Xenopus*, a proximal element of the *dand5* 3'-UTR is required and sufficient for flow-mediated mRNA decay and translational inhibition, respectively, which is dependent on Bicc1 and Dicer (cf.<sup>44</sup>). Whether or not miRs are involved in Dicer1-mediated *dand5* repression remains open. The analysis of the proximal regions of various vertebrate *dand5* 3'-UTR sequences, which show the highest degree of conservation, using different miR-target prediction tools, detects only a few potential miR-binding sites, with low probabilities in all cases. However, miR-133 may be relevant, because members of this family are specific for muscle development and expressed in somites and sLRO cells have somitic fate<sup>8,50–52</sup>. A conserved target site was detected in the Bicc1RE of *X. laevis* S- and L-alleles and the human proximal *dand5* 3'-UTR (Figure S1B; Supplementary Fig. 7A). It remains to be seen whether one of the four family members in *Xenopus* is involved in Bicc1-mediated *dand5* mRNA stability and post-flow repression. Interestingly, Bicc1 regulates its own expression in a post-transcriptional manner<sup>53</sup>. A highly conserved miR-133-binding site in 3'-UTRs of vertebrate *bicc1* genes (Supplementary Fig. 7A, B, C) may suggest that a Bicc1/miR-133 module has been adapted to the regulation of *dand5* in somitic/sLRO cells. Alternatively, Dicer may act miR-independently through one of its described non-canonical mechanisms<sup>54</sup>.

In conclusion, our work identified Bicc1 and Dicer as two factors downstream of leftward flow sensing. The exact nature of Bicc1's modifications and interactions with the *dand5* Bicc1RE in a pre-flow and post-flow setting remains to be solved.

## Methods

**Image processing.** Imagej (1.48i), Acrobat Illustrator (cs6), and Acrobat Photoshop (cs6) were used for image processing.

**Plasmid construction.** The *mbicc1*-CS2+ construct was a gift from Oliver Wessely (Cleveland, OH, United States).

For in vitro synthesis of mRNA using the Ambion sp6 message kit, the plasmids were linearized with NotI.

Firefly luciferase reporter mRNAs that contained the *gdf3* mRNA 3'-UTR (GenBank: BC073508.1) or the 3'-UTR of the *dand5*L mRNA or the *dand5*S mRNA the Ambion T7 message kit were used and the plasmids were linearized with BamHI.

Supplemental Table 2 lists all primers with sequences used in the context of this work.

**RT-PCR.** RT-PCR was conducted using either the L or S isoform-specific primer for intron 2 or intron 1, respectively, and an isoform-specific reverse primer in

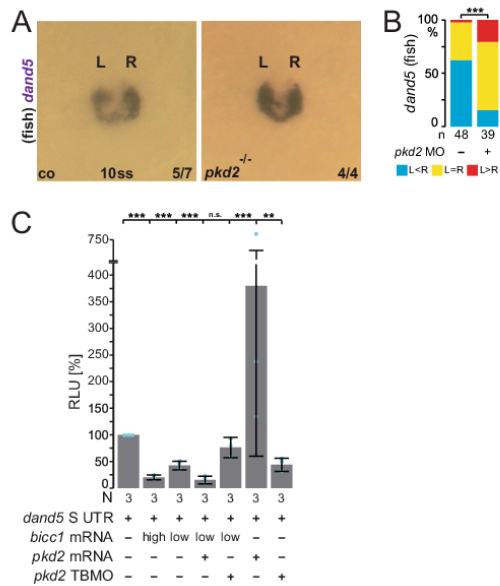


**Fig. 7 Pkd2 function modifies Bicc1-mediated translational repression of *dand5*.** **A** Absence of *dand5* repression in maternal zygotic (MZ) *pkd2* mutant zebrafish at 10 somite stage (ss). **B** Quantification of *dand5* asymmetry in controls (co) and *pkd2* morphant (1–4 ng) zebrafish. Asymmetry was determined by picture analysis using ImageJ. Number (n) represents the number of analyzed specimens. Statistical analyses were done with one-sided Pearson's chi-square test. **C** Animal cap luciferase reporter assay of full-length *dand5* 3'-UTR (cf. Figure 1A). The reporter construct was injected as mRNA either alone or in combination with high or low dose *bicc1* mRNA, *pkd2* mRNA or *pkd2* TBMO. Gradual repression upon co-injection of high or low concentrations of *bicc1* mRNA was observed. Administering only *pkd2* mRNA or *pkd2* TBMO (1 pmol) efficiently blocked or boosted luciferase expression, respectively. The data further indicate that in AC cells endogenous *dand5* mRNA is post-transcriptionally regulated in a Pkd2-dependent manner. In the presence of a lower amount of *bicc1* mRNA high-level, strong repression was achieved when *pkd2* mRNA was co-injected, or further diminished upon knockdown of *pkd2* using TBMO. N represents the number of independent experiments. A pool of 10 animal caps was analyzed per experiment and treatment. The results from reporter mRNA alone served as reference and were set to 100% RLU. Relative values of single experiments are depicted as blue dots. Data of three experiments are presented as mean value (bar)  $\pm$  standard deviation (error bar, SD). Statistical analyses were done with a one-sided Student's *t* test for two independent means (Bonferroni corrected) using the values of three individual experiments. *p* values, values for individual experiments, mean values, and standard deviations are found in the source data file. n.s. not significant,  $p < 0.05$ ; \*\* highly significant  $p < 0.01$ ; \*\*\*, very highly significant  $p < 0.001$ , RLU relative luciferase units, *Luc* luciferase.

exon 5 with 38 cycles. The listing of individual primers used in this work can be found in Supplemental Table 2.

**Morpholinos.** Supplemental Table 1 lists all MOs used with references to previous validations or proof of specificity in the context of this work.

**Xenopus frogs and embryos.** Animals were handled in accordance with German regulations (Tierschutzgesetz) and approved by the Regional Council Stuttgart

(A379/12 Zo, 'Molekulare Embryologie', V340/17 ZO and V349/18 ZO, 'Xenopus Embryonen in der Forschung').

*Xenopus* embryos obtained in vitro fertilization were maintained in 0.1 $\times$  modified Barth medium<sup>55</sup> and staged according to ref.<sup>56</sup>. During injections, embryos were kept in 1 $\times$  modified Barth medium with 2% Ficoll. To specifically target the sensory cells of the GRP for all experiments except for the luciferase assay, we injected them into the dorsal marginal side (left or right; C2-lineage). For luciferase assays, embryos were injected twice into the animal blastomeres at the four-cell stage with a luciferase *dand5* 3'-UTR construct, alone or together with a *bicc1* construct. Animal cap tissue was dissected at stage 10 (cf. Figure 1A for a schematic depiction of the procedure). Following injections, all embryos were transferred to 0.1 modified Barth medium.

**Zebrafish.** Established husbandry protocols were adhered to, and experimental protocols were conducted, in accordance with the Princeton University Institutional Animal Care and Use Committee (IACUC) guidelines. Zebrafish strains utilized include *pkd2/cup*<sup>ts321</sup><sup>39</sup> and *dicer1*<sup>bu715</sup><sup>57</sup>. The *pkd2* AUG MO is described in ref.<sup>39</sup>. Embryos were staged according to ref.<sup>58</sup>. Embryos were raised at 28 °C and processed for injections. For all knockdowns, a morpholino mixture of ~1.8 nl was injected into the yolk of one-cell stage embryos. All morpholino mixtures contained Danicau's Buffer and 0.5 mg/ml phenol red.

Embryos were fixed at the 10 ss stage in 4% paraformaldehyde (PFA) overnight at 4 °C. These embryos were washed with PBST (1 $\times$  PBS containing 0.1% Tween 20), dechorionated, transitioned to 100% methanol, and stored at -20 °C for at least 1 day. The transition to methanol was done by performing 5-minute washes in 75% 1 $\times$  PBST:25% methanol, 50% 1 $\times$  PBST:50% methanol, 25% 1 $\times$  PBST:75% methanol, and 100% methanol. The embryos were then transitioned to 1 $\times$  PBST by performing 5 min washes in 25% 1 $\times$  PBST:75% methanol, 50% 1 $\times$  PBST:50% methanol, and 75% 1 $\times$  PBST:25% methanol. Embryos were then washed four times in 1 $\times$  PBST with 5 min per wash. Somite stage embryos were incubated for 1 min in 1 $\times$  PBST containing 0.01 mg/ml Proteinase K (Sigma Aldrich, P2308) followed by a 20 min incubation in 1 $\times$  PBST containing 4% PFA. These embryos were then washed five more times in 1 $\times$  PBST with 5 min per wash. Blastula and gastrula stage embryos did not undergo this Proteinase K treatment, extra fixation with 4% PFA, or the extra five washes with 1 $\times$  PBST. Embryos were incubated in HYB (50% formamide, 5 $\times$  SSC, 500  $\mu$ g/ml torula yeast RNA, 50  $\mu$ g/ml heparin 0.1% Tween 20, and 9 mM Citric Acid (pH 6.0)) for 2 h at 68 °C. Embryos were then incubated overnight in HYB containing an ISH probe at 68 °C. The next day, embryos were washed at 68 °C in HYB, 75% HYB: 25% 1 $\times$  SSC, 50% HYB: 50% 1 $\times$  SSC, 25% HYB: 75% 1 $\times$  SSC, and 1 $\times$  SSC for 10 min each wash. Embryos were then washed twice in 0.1 $\times$  SSC for 30 min each wash. The remaining washes were performed at room temperature. Embryos were washed in 75% 0.1 $\times$  SSC: 25% 1 $\times$  PBST, 50% 0.1 $\times$  SSC: 50% 1 $\times$  PBST, 25% 0.1 $\times$  SSC: 75% 1 $\times$  PBST, and 1 $\times$  PBST for 5 min each wash. Next, embryos were incubated on a rocker for 2 h in 1 $\times$  PBST containing 2 mg/ml bovine serum albumin (BSA) and 2% normal sheep serum (NSS). Embryos were then incubated overnight on a rocker in 1 $\times$  PBST containing 2 mg/ml BSA, 2% NSS, and 1:3500 of Anti-Digoxigenin-AP (Roche, 11093274910). The next day, the embryos were washed quickly in 1 $\times$  PBST followed by six additional 15 min 1 $\times$  PBST washes on a rocker. Embryos were then washed three times in NTMT (0.1 M Tris-Cl pH 9.5, 0.1 M NaCl, 0.05 M MgCl<sub>2</sub>, 0.1% Tween 20) and stained with 5  $\mu$ l of NBT (Roche, 11383213001) and 3.75  $\mu$ l BCIP (Roche, 11383221001) per 1 ml of NTMT. Staining was stopped by washing the embryos three times with NTMT, a 5 min wash with 1 $\times$  PBST, and a 4 °C overnight incubation in 1 $\times$  PBST containing 4% PFA. The embryos were then transitioned to methanol using the same four-step PBST:methanol washes listed above. Embryos were stored at -20 °C or cleared in 2:1 Benzyl Benzoate: Benzyl Alcohol prior to imaging. Canada Balsam containing 10% methyl salicylate was used to mount cleared embryos on a slide. RNA ISH staining was visualized using a Leica DMRA2 microscope and images were acquired using a Leica DFC450 C camera. The following probes were used for the ISHs: *dand5*.

**ImageJ RNA ISH image analysis of Zebrafish embryos.** Pictures taken of the U-shaped *dand5* domain were cropped in Adobe Photoshop into equal-sized regions of interest corresponding to the left and right sides of the domain. The center of the domain was used as the midline for generating the left and right domains, and the entire staining area was included in the subsequent quantification analysis. "Subtract Background" in ImageJ 1.48i was used to remove unwanted background signals and images were inverted such that a darker stain, relating to more RNA presence, would yield a higher intensity. A ratio was obtained by dividing the right intensity by the left intensity. In this analysis, a right-biased *dand5* domain would have a ratio of 1.1 or higher, a left-biased *dand5* domain would have a ratio of 0.9 or lower, and an equal *dand5* domain would have a ratio between 0.9 and 1.1. At each stage and condition noted, the indicated number of embryos examined is mentioned as the *n* value. To minimize any image saturation bias, RNA in situ staining reactions were carefully monitored and stopped when the *dand5* domain was first evident.

**RNAseq.** Raw reads were mapped to the zebrafish GRCz11 genome using STAR version 2.7.3a<sup>59</sup> with the following non-default parameters: --alignEndsType



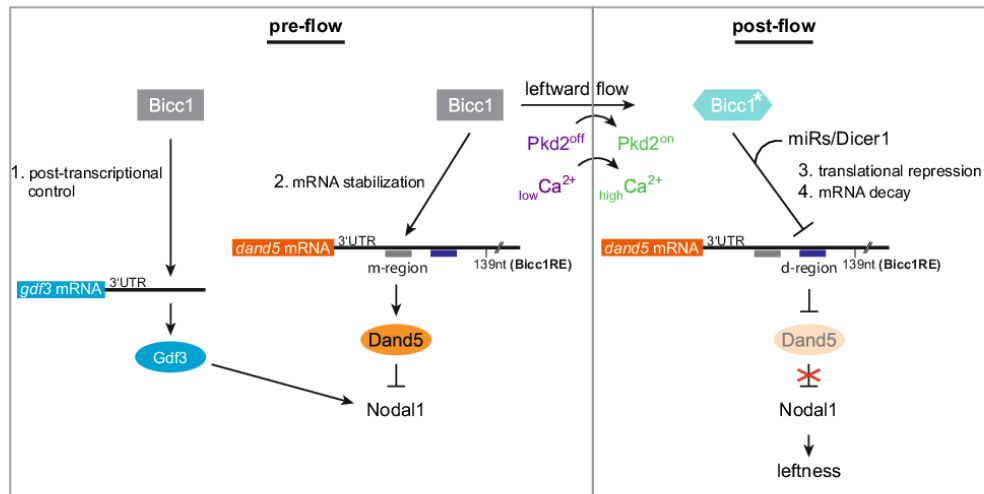


**Fig. 8 Two modes of Bicc1-dependent post-transcriptional regulation of *gdf3* and *dand5* in flow sensor cells at the *Xenopus* left-right organizer.** In the early neurula pre-flow stages, Bicc1 has two functions. Bicc1 assures *gdf3* mRNA translation and thereby indirectly ensures *nodal1* transcription by Gdf3 signaling. Simultaneously Bicc1 mediates *dand5* mRNA stability via the medial (m) sub-region of the BiccIRE. Thus, Dand5 protein levels are sustained on both sides, keeping Nodal in tight repression. Leftward flow activates the Pkd2 channel in left flow sensor cells, resulting in an asymmetric calcium signal. In post-flow stages, a calcium-dependent mechanism activates/modifies Bicc1 to become a repressor of *dand5* translation, which is relayed by the distal (d) sub-region of the BiccIRE. Subsequently, *dand5* mRNA gets degraded in a Dicer1 (miR) dependent manner. Attenuated Dand5 expression lifts repression of Nodal and defines leftness by induction of the LPM Nodal signaling cascade. For details, see text.

--Local --outFilterMultimapNmax 1000 --seedSearchStartLmax 30 --sjdbScore 2 --outMultimapOrder Random. Genomic sequence indices for STAR were built using exon-junction coordinates from Ensembl r92<sup>60</sup>. Read counts per protein-coding gene were computed by summing the total number of reads overlapping the gene annotation by at least 10 nucleotides. All reads were used and contributed for 1/(number of mapping loci) to the gene counts. Per gene annotation was obtained by concatenating all Ensembl isoforms together. A total number of reads mapping to protein-coding genes and their lengths were used to normalize to RPKM (Reads Per Kilobase per Million mapped reads). For comparison, the average RPKMs of the following house-keeping genes were calculated: *actb1* (Actin, beta 1; cytoskeletal), *arpc2* (Actin related protein complex; cytoskeletal), *ef2a* (Eukaryotic translation initiation factor 2 A; translation), *ddx39b* (DEAD box polypeptide 39B; RNA splicing), *pabpn1* (Poly(A) binding protein, nuclear 1; RNA splicing), and *rps6* (Ribosomal protein S6; ribosomal protein). LabxDB<sup>61</sup> was employed to manage sequencing samples.

**Immunofluorescence staining.** For immunofluorescence staining, embryos were fixed in 4% PFA for 1 h at RT on a rocking platform, followed by 2 washes in 1× PBS<sup>-</sup> for 15 min each. For staining of LRO explants, embryos were dissected using a scalpel into anterior and posterior halves. Posterior halves (LRO explants) were collected and transferred to a 24-well plate and washed twice for 15 min in PBS<sup>-</sup>. LRO explants and whole embryos were blocked for 2 h at RT in CAS-Block diluted 1:10 in PBS<sup>-</sup>. The blocking reagent was replaced by an antibody solution (anti-acetylated tubulin antibody, diluted 1:700 in CAS-Block; c2181 Sigma) and incubated overnight at 4 °C. In the morning, the antibody solution was removed and explants/embryos were washed twice for 15 min in PBS<sup>-</sup>. The secondary antibody (diluted 1:1000 in CAS-Block; c2181 Sigma) was added together with Phalloidin (1:200) and incubated for a minimum of 3 h at RT. Before photo documentation, embryos or explants were briefly washed in PBS<sup>-</sup> and transferred onto a microscope slide.

**Western blot.** Embryos were lysed with 10 µl/embryo RIPA buffer (radio immuno precipitation assay buffer) and centrifuged at maximum speed for 15 min at 4 °C and the supernatant was transferred into a new tube. The supernatant was boiled with 1× Laemmli Loading Buffer for 5 min at 95 °C. Probes were transferred to a 4–20% sodium dodecyl sulfate (SDS) gel (BIO RAD Mini-PROTEAN TGX Gels) and gel ran for 1 h at 120 V on a BIO RAD Mini-PROTEAN Tetra System. SDS Gel and nitrocellulose membrane were equilibrated in blotting buffer for 30 min and blotted for 1 h at 350 mA. The membrane was dissected and blocked (5% milk powder in Tbs<sub>1</sub>) for 1 h at room temperature. Incubation with primary antibodies (monoclonal anti-α-tubulin produced in mouse, Sigma Aldrich T9026, 1:3000;

monoclonal anti-Dicer1 produced in mouse, BioLegend MMS5130, 1:100) overnight at 4 °C. Membranes were washed in blocking solution (5% milk powder in Tbs<sub>1</sub>) and incubated with 2° antibody (Anti-Mouse IgG-peroxidase, Sigma Aldrich A9044, 1:80,000) for 3 h at room temperature. Antibody was removed and membranes were washed with Tbs<sub>1</sub> and developed using Pierce ECL Western Blotting Substrate (ThermoScientific, #362109) and recorded with an exposure time of 600 µs. Uncropped blots can be found in the source data file.

**Luciferase assay.** Luciferase reporter assays were carried out using the Promega Dual-Luciferase<sup>®</sup> Reporter Assay System. Animal cap tissue, derived from 10 embryos per treatment, was transferred into a 1.5 ml Eppendorf tube, and the 0.1× MBSH buffer was removed, leaving the tissue moistened. The tissue was lysed and homogenized in 100 µl 1× passive lysis buffer by pipetting the suspension up and down, followed by 15 min incubation at RT. The lysate was centrifuged for 2 min at 21,951 × g and the upper phase was transferred into a new tube. The lysate was re-centrifuged and two 25 µl aliquots (technical duplicates) of each sample were transferred into a 96-well plate. 75 µl 1× Luciferase assay substrate was added through the GloMax<sup>®</sup> Explorer System and luminescence was determined. This step was repeated with 75 µl 1× Stop and Glow reagents. To calculate the relative luciferase units (RLU [%]), the ratio between luciferase and Renilla values was calculated and correlated to the wt control, which was set to 100%. Each sample was measured twice to validate the technical aspect of testing. In order to be valid, the technical replicates should have almost identical values, which was true in all our experiments.

**Statistics and reproducibility.** Statistical calculations of marker gene expression patterns and cilia distribution were performed using one-sided Pearson's chi-square test in statistical R. Adjustments for multiple comparisons were done by Bonferroni (*pitx2* expression) or Bonferroni–Holm (*nodal1* and *dand5* expression) corrections. For the statistical calculation of ciliation, a Wilcoxon–Match-Pair test was used (statistical R-3.0.1). Statistical calculations of the luciferase assays were done with a one-sided student's *t* test for two independent means in statistical R. Bonferroni corrections were implemented when multiple comparisons were conducted. At least three independent successful biological replicates (embryo batches) were used for each experimental setup. The source data file depicts all individual experiments/data points, mean values with standard deviations, and *p* values.

**Mouse strains.** All mouse experiments were performed in accordance with guidelines of the RIKEN Center for Biosystems Dynamics Research (BDR) and under an institutional license (A2016-01-6). Mice were maintained in the animal

facility of the RIKEN Center for BDR. Noto-Cre<sup>ERT2</sup> mice were described in ref. <sup>62</sup>, Dicer<sup>lox</sup> mice in ref. <sup>63</sup> (JAX stock #006001). Expression of the Noto-Cre<sup>ERT2</sup> transgene in embryos was induced by oral administration of tamoxifen (Sigma) in corn oil to pregnant mice at a dose of 5 mg both 24 and 12 h before the late headfold stage.

**WISH analysis in mouse.** WISH was performed according to standard procedures with digoxigenin-labeled riboprobes specific for Nodal or Dand5 mRNA<sup>64</sup>.

**Reporting summary.** Further information on research design is available in the Nature Research Reporting Summary linked to this article.

#### Data availability

The authors declare that the main data supporting the findings of this study are available within the article and its Supplementary Information files. Source data are provided with this paper.

Received: 13 January 2020; Accepted: 11 August 2021;

Published online: 16 September 2021

#### References

- Blum, M. & Ott, T. Animal left-right asymmetry. *Curr. Biol.* **28**, R301–R304 (2018).
- Shiratori, H. & Hamada, H. TGFβ signaling in establishing left-right asymmetry. *Semin. Cell Dev. Biol.* **32**, 80–84 (2014).
- Blum, M. & Ott, T. The power of strain: organizing left-right cilia. *Dev. Cell* **45**, 277–279 (2018).
- Blum, M. et al. Xenopus, an ideal model system to study vertebrate left-right asymmetry. *Dev. Dyn.* **238**, 1215–1225 (2009).
- Little, R. B. & Norris, D. P. Right, left and cilia: How asymmetry is established. *Semin. Cell Dev. Biol.* **110**, 11–18 (2021).
- Guimier, A. et al. MMP21 is mutated in human heterotaxy and is required for normal left-right asymmetry in vertebrates. *Nat. Genet.* **47**, 1260–1263 (2015).
- Hamada, H. & Tam, P. Diversity of left-right symmetry breaking strategy in animals. *Fl000Research* **9**; <https://doi.org/10.12688/f1000research.21670.1> (2020).
- Shook, D. R., Majer, C. & Keller, R. Pattern and morphogenesis of presumptive superficial mesoderm in two closely related species, *Xenopus laevis* and *Xenopus tropicalis*. *Dev. Biol.* **270**, 163–185 (2004).
- Pennekamp, P. et al. The ion channel polycystin-2 is required for left-right axis determination in mice. *Curr. Biol.* **12**, 938–943 (2002).
- Mizuno, K. et al. Role of Ca<sup>2+</sup> transients at the node of the mouse embryo in breaking of left-right symmetry. *Sci. Adv.* **6**, eaba1195 (2020).
- Yuan, S., Zhao, L., Brueckner, M. & Sun, Z. Intraciliary calcium oscillations initiate vertebrate left-right asymmetry. *Curr. Biol.* **25**, 556–567 (2015).
- Schweickert, A. et al. The nodal inhibitor Coco is a critical target of leftward flow in *Xenopus*. *Curr. Biol.* **20**, 738–743 (2010).
- Nakamura, T. et al. Fluid flow and interlinked feedback loops establish left-right asymmetric decay of Cer2 mRNA. *Nature communications* **3**, 1322 (2012).
- Hojo, M. et al. Right-elevated expression of charon is regulated by fluid flow in medaka Kupffer's vesicle. *Dev. Growth Differ.* **49**, 395–405 (2007).
- Tanaka, C., Sakuma, R., Nakamura, T., Hamada, H. & Saijoh, Y. Long-range action of Nodal requires interaction with GDF1. *Genes Dev.* **21**, 3272–3282 (2007).
- Pelliccia, J. L., Jindal, G. A. & Burdine, R. D. Gdf3 is required for robust Nodal signaling during germ layer formation and left-right patterning. *eLife* **6**; <https://doi.org/10.7554/eLife.28635> (2017).
- Tran, U. et al. The RNA-binding protein bicaudal C regulates polycystin 2 in the kidney by antagonizing miR-17 activity. *Development* **137**, 1107–1116 (2010).
- Zhang, Y. et al. Bicaudal-C spatially controls translation of vertebrate maternal mRNAs. *RNA* **19**, 1575–1582 (2013).
- Zhang, Y., Park, S., Blaser, S. & Sheets, M. D. Determinants of RNA binding and translational repression by the Bicaudal-C regulatory protein. *J. Biol. Chem.* **289**, 7497–7504 (2014).
- Maisonneuve, C. et al. Bicaudal C, a novel regulator of Dvl signaling abutting RNA-processing bodies, controls cilia orientation and leftward flow. *Development* **136**, 3019–3030 (2009).
- Rothé, B. et al. Biccl1 polymerization regulates the localization and silencing of bound mRNA. *Mol. Cell. Biol.* **35**, 3339–3353 (2015).
- Piazzon, N., Maisonneuve, C., Guilleret, I., Rotman, S. & Constam, D. B. Biccl1 links the regulation of cAMP signaling in polycystic kidneys to microRNA-induced gene silencing. *J. Mol. Cell. Biol.* **4**, 398–408 (2012).
- Wessely, O. & Robertis, E. Mde The *Xenopus* homologue of Bicaudal-C is a localized maternal mRNA that can induce endoderm formation. *Development* **127**, 2053–2062 (2000).
- Bell, E., Muñoz-Sanjuán, I., Altmann, C. R., Vonica, A. & Brivanlou, A. H. Cell fate specification and competence by Coco, a maternal BMP, TGFβ and Wnt inhibitor. *Development* **130**, 1381–1389 (2003).
- Moulton, J. D. Using morpholinos to control gene expression. *Curr. Protoc. Nucleic Acid Chem.* **68**, 30.1 (2017).
- Moody, S. A. Fates of the blastomeres of the 32-cell-stage *Xenopus* embryo. *Dev. Biol.* **122**, 300–319 (1987).
- Tingler, M. et al. Symmetry breakage in the frog *Xenopus*: role of Rab11 and the ventral-right blastomere. *Genesis* **52**, 588–599 (2014).
- Vick, P. et al. Flow on the right side of the gastrocoel roof plate is dispensable for symmetry breakage in the frog *Xenopus laevis*. *Dev. Biol.* **331**, 281–291 (2009).
- Bowes, J. B. et al. Xenbase: gene expression and improved integration. *Nucleic Acids Res.* **38**, D607–D612 (2010).
- Blum, M., Robertis, E. M., de Wallingford, J. B. & Niehrs, C. Morpholinos: antisense and sensibility. *Dev. Cell* **35**, 145–149 (2015).
- Vonica, A. & Brivanlou, A. H. The left-right axis is regulated by the interplay of Coco, Xnr1 and derrière in *Xenopus* embryos. *Dev. Biol.* **303**, 281–294 (2007).
- Vonica, A., Rosa, A., Arduini, B. L. & Brivanlou, A. H. APOBEC2, a selective inhibitor of TGFβ signaling, regulates left-right axis specification during early embryogenesis. *Dev. Biol.* **350**, 13–23 (2011).
- Bartel, D. P. Metazoan microRNAs. *Cell* **173**, 20–51 (2018).
- Agrawal, R., Tran, U. & Wessely, O. The miR-30 miRNA family regulates *Xenopus* pronephros development and targets the transcription factor Xlim1/Lhx1. *Development* **136**, 3927–3936 (2009).
- Song, R. et al. miR-34/49 miRNAs are required for motile ciliogenesis by repressing cpi10. *Nature* **510**, 115–120 (2014).
- Marcet, B. et al. Control of vertebrate multiciliogenesis by miR-449 through direct repression of the Delta/Notch pathway. *Nat. Cell Biol.* **13**, 693–699 (2011).
- Yoshida, S. et al. Cilia at the node of mouse embryos sense fluid flow for left-right determination via Pkd2. *Science* **338**, 226–231 (2012).
- Yoshida, S. & Hamada, H. Roles of cilia, fluid flow, and Ca<sup>2+</sup> signaling in breaking of left-right symmetry. *Trends Genet.* **30**, 10–17 (2014).
- Schottenfeld, J., Sullivan-Brown, J. & Burdine, R. D. Zebrafish curly up encodes a Pkd2 ortholog that restricts left-side-specific expression of southpaw. *Development* **134**, 1605–1615 (2007).
- Biggrove, B. W., Snarr, B. S., Emrazian, A. & Yost, H. J. Polaris and Polycystin-2 in dorsal forerunner cells and Kupffer's vesicle are required for specification of the zebrafish left-right axis. *Dev. Biol.* **287**, 274–288 (2005).
- Vick, P. et al. An early function of polycystin-2 for left-right organizer induction in *Xenopus*. *iScience* **2**, 76–85 (2018).
- Rankin, C. T., Bunton, T., Lawler, A. M. & Lee, S. J. Regulation of left-right patterning in mice by growth/differentiation factor-1. *Nat. Genet.* **24**, 262–265 (2000).
- Montague, T. G., Gagnon, J. A. & Schier, A. F. Conserved regulation of Nodal-mediated left-right patterning in zebrafish and mouse. *Development* **145**, dev171090 (2018).
- Minegishi, K. et al. Fluid flow-induced left-right asymmetric decay of Dand5 mRNA in the mouse embryo requires Biccl1-Ccr4 RNA degradation complex. *Nat. Commun.* **12**, 4071 (2021).
- McGrath, J., Somlo, S., Makova, S., Tian, X. & Brueckner, M. Two populations of node monocilia initiate left-right asymmetry in the mouse. *Cell* **114**, 61–73 (2003).
- Takao, D. et al. Asymmetric distribution of dynamic calcium signals in the node of mouse embryo during left-right axis formation. *Dev. Biol.* **376**, 23–30 (2013).
- Francscatto, L., Rothschild, S. C., Myers, A. L. & Tomber, R. M. The activation of membrane targeted CaMK-II in the zebrafish Kupffer's vesicle is required for left-right asymmetry. *Development* **137**, 2753–2762 (2010).
- Hara, M. et al. Identification of PNG kinase substrates uncovers interactions with the translational repressor TRAL in the oocyte-to-embryo transition. *eLife* **7**; <https://doi.org/10.7554/eLife.33150> (2018).
- Rothé, B., Gagnieux, C., Leal-Esteban, L. C. & Constam, D. B. Role of the RNA-binding protein Bicaudal-C1 and interacting factors in cystic kidney diseases. *Cell Signal.* **68**, 109499 (2020).
- Chen, J.-F. et al. The role of microRNA-1 and microRNA-133 in skeletal muscle proliferation and differentiation. *Nat. Genet.* **38**, 228–233 (2006).
- Sweetman, D. et al. Specific requirements of MRFs for the expression of muscle specific microRNAs, miR-1, miR-206 and miR-133. *Dev. Biol.* **321**, 491–499 (2008).
- Tani, S., Kuraku, S., Sakamoto, H., Inoue, K. & Kusakabe, R. Developmental expression and evolution of muscle-specific microRNAs conserved in vertebrates. *Evol. Dev.* **15**, 293–304 (2013).

53. Chicoine, J. et al. Bicaudal-C recruits CCR4-NOT deadenylase to target mRNAs and regulates oogenesis, cytoskeletal organization, and its own expression. *Dev. Cell* **13**, 691–704 (2007).
54. Pong, S. K. & Gullerova, M. Noncanonical functions of microRNA pathway enzymes - Drosha, DGCR8, Dicer and Ago proteins. *FEBS Lett.* **592**, 2973–2986 (2018).
55. Sive, H. L., Grainger, R. M. & Harland, R. M. *Xenopus laevis* keller explants. *Cold Spring Harb. Protocols* **2007**, pdb.prot4749 (2007).
56. Nieuwkoop, P. D. & Faber, J. (eds). Normal table of *Xenopus laevis* (Daudin). A systematical and chronological survey of the development from the fertilized egg till the end of metamorphosis (Garland Pub, 1994).
57. Giraldez, A. J. et al. MicroRNAs regulate brain morphogenesis in zebrafish. *Science* **308**, 833–838 (2005).
58. Kimmel, C. B., Ballard, W. W., Kimmel, S. R., Ullmann, B. & Schilling, T. F. Stages of embryonic development of the zebrafish. *Dev. Dyn.* **203**, 253–310 (1995).
59. Dobin, A. et al. STAR: ultrafast universal RNA-seq aligner. *Bioinformatics* **29**, 15–21 (2013).
60. Yates, A. D. et al. Ensembl 2020. *Nucleic Acids Res.* **48**, D682–D688 (2020).
61. Vejnar, C. E. & Giraldez, A. J. LabxDB: versatile databases for genomic sequencing and lab management. *Bioinformatics* **36**, 4530–4531 (2020).
62. Ukita, K. et al. Wnt signaling maintains the notochord fate for progenitor cells and supports the posterior extension of the notochord. *Mech. Dev.* **126**, 791–803 (2009).
63. Harfe, B. D., McManus, M. T., Mansfield, J. H., Hornstein, E. & Tabin, C. J. The RNaseIII enzyme Dicer is required for morphogenesis but not patterning of the vertebrate limb. *Proc. Natl. Acad. Sci. USA* **102**, 10898–10903 (2005).
64. Wilkinson, D. G. & Nieto, M. A. Detection of messenger RNA by in situ hybridization to tissue sections and whole mounts. *Methods Enzymol.* **225**, 361–373 (1993).
65. Tisler, M., Schweickert, A. & Blum, M. *Xenopus*, an ideal model organism to study laterality in conjoined twins. *Genesis* **55**, e22993 (2017).
66. Tingler, M. et al. A conserved role of the unconventional myosin 1d in laterality determination. *Curr. Biol.* **28**, 810–81.e3 (2018).

### Acknowledgements

We thank M. Montino for performing initial *Bicc1* experiments in *Xenopus* during his diploma thesis. Technical assistance was given by E. Schuster. S. Mai helped with critical proofreading. O. Wessely provided the full-length mouse *bicc1* construct. We thank H. Sasaki for *Noto<sup>CreERT2</sup>* mice and Philip Johnson for zebrafish husbandry. M.G. was the recipient of a Ph.D. fellowship from the Landesgraduiertenförderung Baden-Württemberg. Work in the Blum lab was supported by DFG grant BL285/9-2. Work in the Sheets lab was supported by the National Institute of Child Health and Human Development of the National Institutes of Health under award number R01HD091921. Work in the Hamada lab was supported by grants from the Ministry of Education, Culture, Sports, Science, and Technology (MEXT) of Japan (no. 17H01435) and from Core Research for Evolutional Science and Technology (CREST) of the Japan Science and Technology Agency (no. JPMJCR13W5) to H.H.; by a Grant-in-Aid (No. 18K14725) for Early-Career Scientists from the Japan Society for the Promotion of Science (JSPS), a Kakehashi grant from BDR-Otsuka Pharmaceutical Collaboration Center, and a research grant (no. 2018M-018) from the Kato Memorial Bioscience Foundation to K.M. Work in the Giraldez lab was supported by the National Institute of General Medical Sciences of the National Institutes of Health under award number

R35GM12258003. Work in the Burdine lab was supported by the National Institute of Child Health and Human Development of the National Institutes of Health under grant number T32GM007388, and a United Negro College Fund/Merck Graduate Science Research Dissertation Fellowship to JCM. The content is solely the responsibility of the authors and does not necessarily represent the official views of the National Institutes of Health.

### Author contributions

Experiments in *Xenopus* were performed by M.M. (*bicc1*, *dicer*), M.G. (*dicer*), M.D. (part of AC assays), M.T. (western, *dicer1* IP), and P.V. (initial *bicc1* work). Zebrafish experiments were conducted by R.D.B., V.G., D.S.H., J.C.M., and J.L.P., RNAseq by V.Y. and C.V. The conditional *dicer* knockout mouse was generated and analyzed by K.M. A.S., M.B., H.H., R.D.B., A.J.G., and M.S. conceptualized and supervised experiments, which were analyzed by all authors. Both M.B. and A.S. wrote and equally contributed to the manuscript with suggestions from all authors.

### Funding

Open Access funding enabled and organized by Projekt DEAL.

### Competing interests

The authors declare no competing interests.

### Additional information

**Supplementary information** The online version contains supplementary material available at <https://doi.org/10.1038/s41467-021-25464-z>.

**Correspondence** and requests for materials should be addressed to Axel Schweickert

**Peer review information** *Nature Communications* thanks Oliver Wessely and the other, anonymous, reviewer(s) for their contribution to the peer review of this work.

**Reprints and permission information** is available at <http://www.nature.com/reprints>

**Publisher's note** Springer Nature remains neutral with regard to jurisdictional claims in published maps and institutional affiliations.

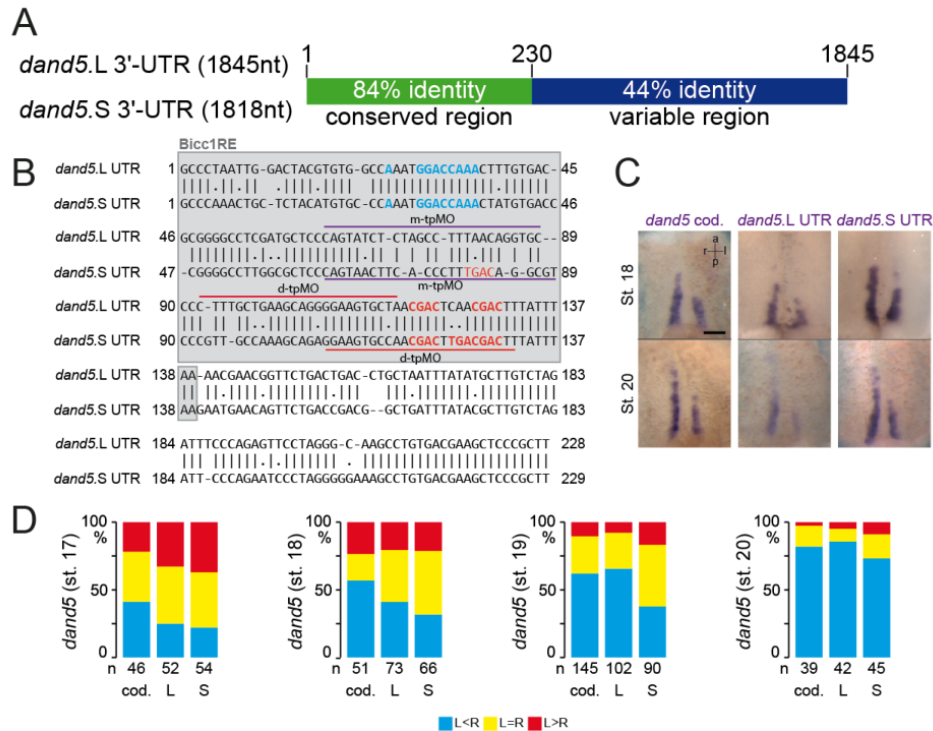


**Open Access** This article is licensed under a Creative Commons Attribution 4.0 International License, which permits use, sharing, adaptation, distribution and reproduction in any medium or format, as long as you give appropriate credit to the original author(s) and the source, provide a link to the Creative Commons license, and indicate if changes were made. The images or other third party material in this article are included in the article's Creative Commons license, unless indicated otherwise in a credit line to the material. If material is not included in the article's Creative Commons license and your intended use is not permitted by statutory regulation or exceeds the permitted use, you will need to obtain permission directly from the copyright holder. To view a copy of this license, visit <http://creativecommons.org/licenses/by/4.0/>.

© The Author(s) 2021



## Supplementary Materials

Supplementary Figure 1. Characterization of *dand5* 3'-UTRs

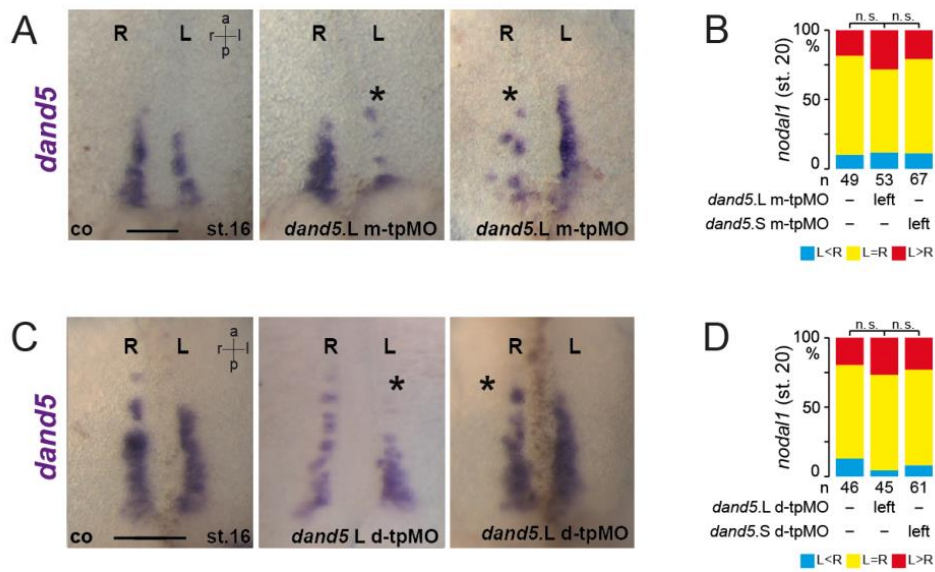
(A) Conservation of 3'-UTR sequences between S- and L-alloalles of *X. laevis*.

(B) Sequence alignment of the proximal 228 respective 229 nucleotides of *dand5* 3'-UTRs of S- and L-alloalleles. Minimal Bicc1 responsive element (Bicc1RE) is indicated by a grey background. The positions of the m-tpMOs and d-tpMOs are marked by blue and red lines, respectively. Two to three (S-UTR) potential Bicc1 binding motifs (based on <sup>1</sup>) are highlighted in red. Putative miR133 interaction site is indicated by blue letters.

(C) Representative dorsal explants of stage 18 (top row) and stage 20 (bottom row) embryos hybridized with antisense RNA probes specific for the *dand5* coding sequence (left), or the 3'-UTRs of *dand5* S- (middle) and L-allele (right).

(D) Quantification of results of a time course analysis from stage 17-20. Following *in situ* hybridization and visual judgement, scoring was carried out according to <sup>2</sup> i.e. bilateral symmetric (L=R), left stronger than right (L>R) or vice versa (L<R). n in the x-axis represent number of embryos analyzed

Scale bar in (C) represents 100  $\mu$ m. st., stage; a, anterior; l, left; r, right; p, posterior. Listing of individual experiments can be found in the source data file.



**Supplementary Figure 2. *dand5* and *nodal1* expression in tpMO injected embryos.**

(A) *dand5* expression in pre-flow stage 16 of controls, left- or right-sided m-tpMO injections.

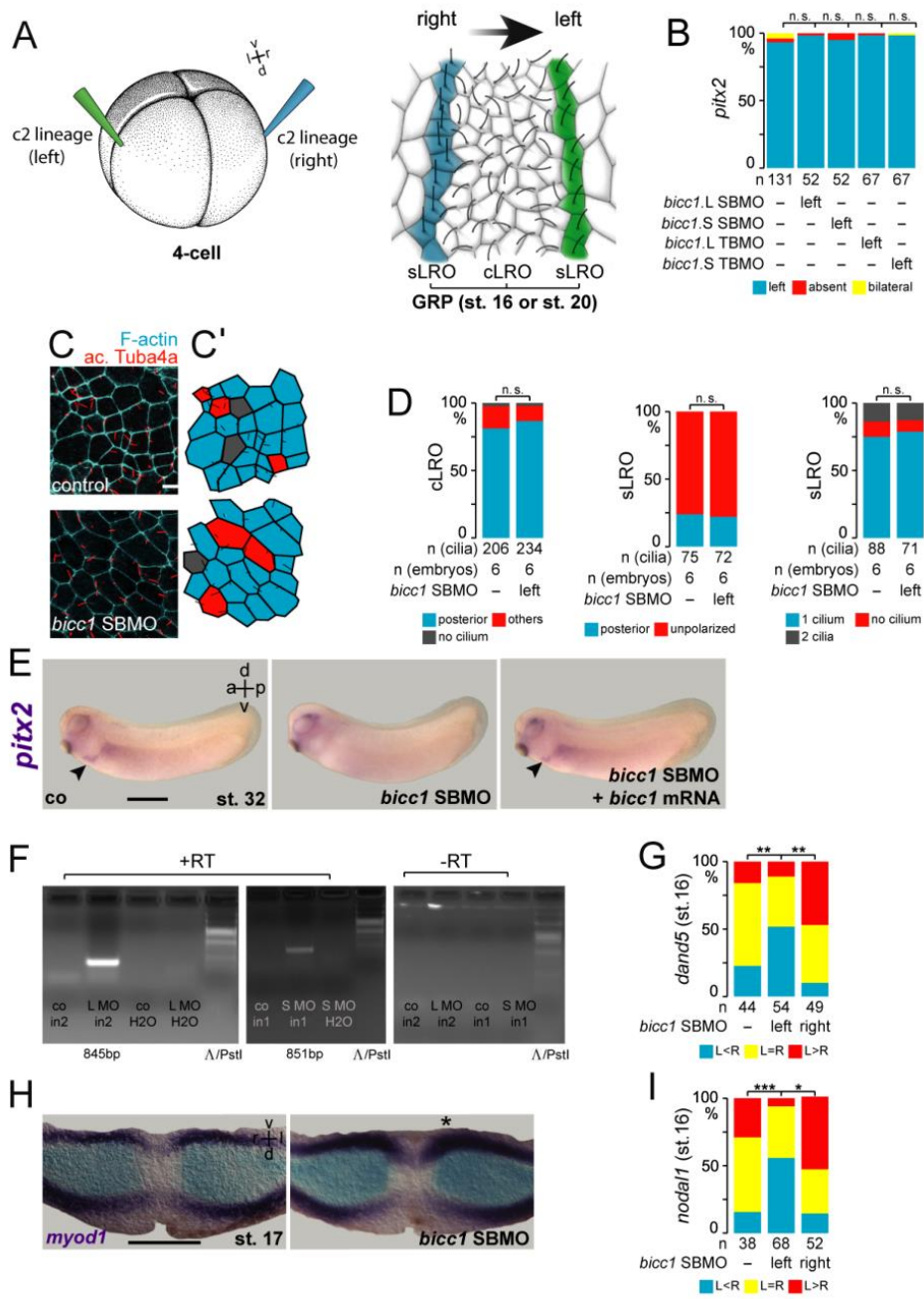
Note that irrespective of which half was targeted, *dand5* mRNA was reduced.

(B) Quantification of *nodal1* expression at stage 20 of wt controls and left-sided m-tpMO injected embryos. No effect on *nodal1* mRNA by m-tpMO treatment.

(C) Wt *dand5* expression following injections of d-tpMO in pre-flow specimens (st. 16).

(D) Quantification of *nodal1* mRNA signals. Note no difference at stage 20 between wt controls and left-sided d-tpMO injections.

MO pmol/embryo: m-tpMO (L or S, 0.8); d-tpMO (L or S, 1). Asterisks in (A and C) mark injected side. Numbers (n) represent analyzed specimens from >3 independent experiments. st., stage; a, anterior; l, left; r, right; p, posterior; n.s., not significant. Scale bars in (A and C) represents 100  $\mu$ m. p-values and listing of individual experiments can be found in the source data file. Statistical analyses were done with a one-sided Pearson's chi-square test (Boniferroni-Holm corrected).



**Supplementary Figure 3. Characterization of *bicc1* morphants**

(A) Schematic depiction of injection scheme at the 4-cell stage to target specifically left (green) or right (blue) flow sensing cells at the gastrocoel roof plate (GRP; left-right organizer, LRO), which is shown as a dorsal explant of the archenteron at stage 19 Adapted from <sup>3</sup> and <sup>4</sup>.

(B) Quantification of allele specific *bicc1* knockdowns. Note individual L or S MO (TB or SB; 1 pmol/embryo) has no effect on *pitx2* asymmetry.

(C) Unaltered LRO ciliation in *bicc1* morphants. Representative dorsal explants of control and *bicc1* morphant specimens are stained with anti- ac. tubulin (red) and phalloidin (F-actin, green). (C') Cartoon of the assessment of cilia polarization.

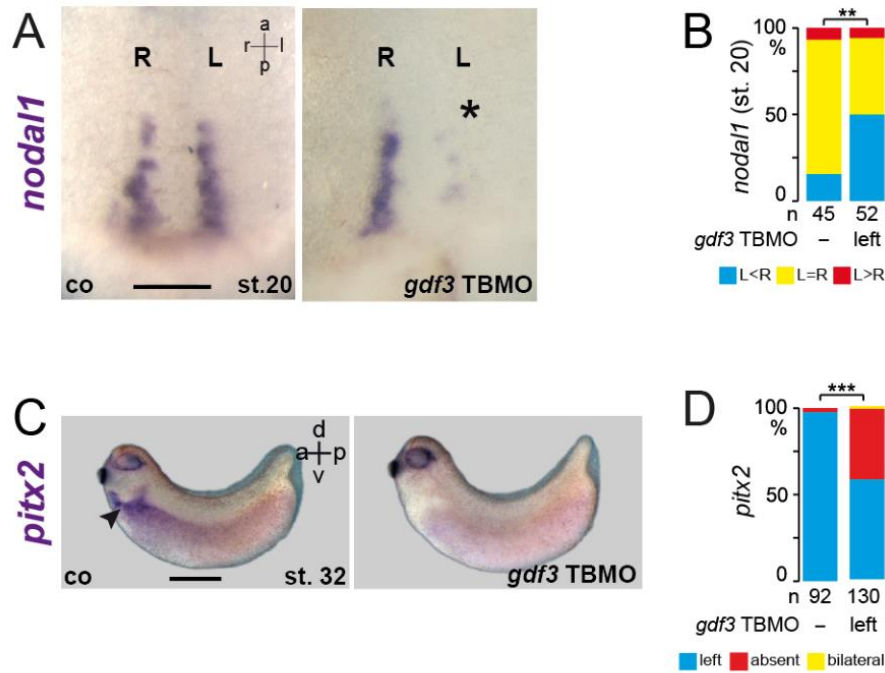
(D) Quantification of ciliary parameters in *bicc1* morphants (1 pmol). Note cilia polarization of flow generating cLRO and targeted flow sensing lateral sLRO cells was not affected by *bicc1* LoF. Ciliation of sLRO cells was not altered either.

(E) *pitx2* expression in representative control (co), *bicc1* morphant and specimen in which both SBMOs (L and S) and a full-length *bicc1* mRNA not targeted by the MOs were co-injected.

(F) RT-PCR on stage 18 embryos which were injected with *bicc1* SBMOs (L or S) showing intron retention (intron2, in2) or intron1, in1), respectively. No PCR products were found in negative control samples where reverse transcriptase was omitted (-RT).

(G, I) Quantification of *dand5* and *nodal1* expression in *bicc1* morphants at pre-flow stage 16. Both *dand5* and *nodal1* mRNA were strongly reduced by *bicc1* knockdown, irrespective of which side was targeted. (see Figure 2D,E).

(H) Expression of *myoD* at stage 17 showed that fate and morphogenesis of lateral sLRO was not affected by *bicc1* LoF. MO pmol/embryo: *bicc1* SBMO (L and S, each 1); *bicc1* SBMO (L or S, 1). Numbers (n) in (B, D, G and I) represent analyzed specimens from >3 independent experiments. st., stage; a, anterior; l, left; r, right; p, posterior; d, dorsal; v, ventral; n.s., not significant; \*\*\*, very highly significant,  $p < 0.001$ ; \*\*, highly significant,  $p < 0.01$ . Asterisk in (H) marks injected side. Scale bars represent in (E) 1mm, in (H) 100  $\mu\text{m}$  and in (C) 10  $\mu\text{m}$ . p-values and listing of individual experiments can be found in the source data file. Statistical analyses were done with two-sided student t-test for 2 independent means (D, Boniferroni corrected) or with a one-sided Pearson's chi-square test (B, G and I, Boniferroni-Holm corrected).



**Supplementary Figure 4. *nodal1* transcription in sLRO cells requires Gdf3 signaling.**

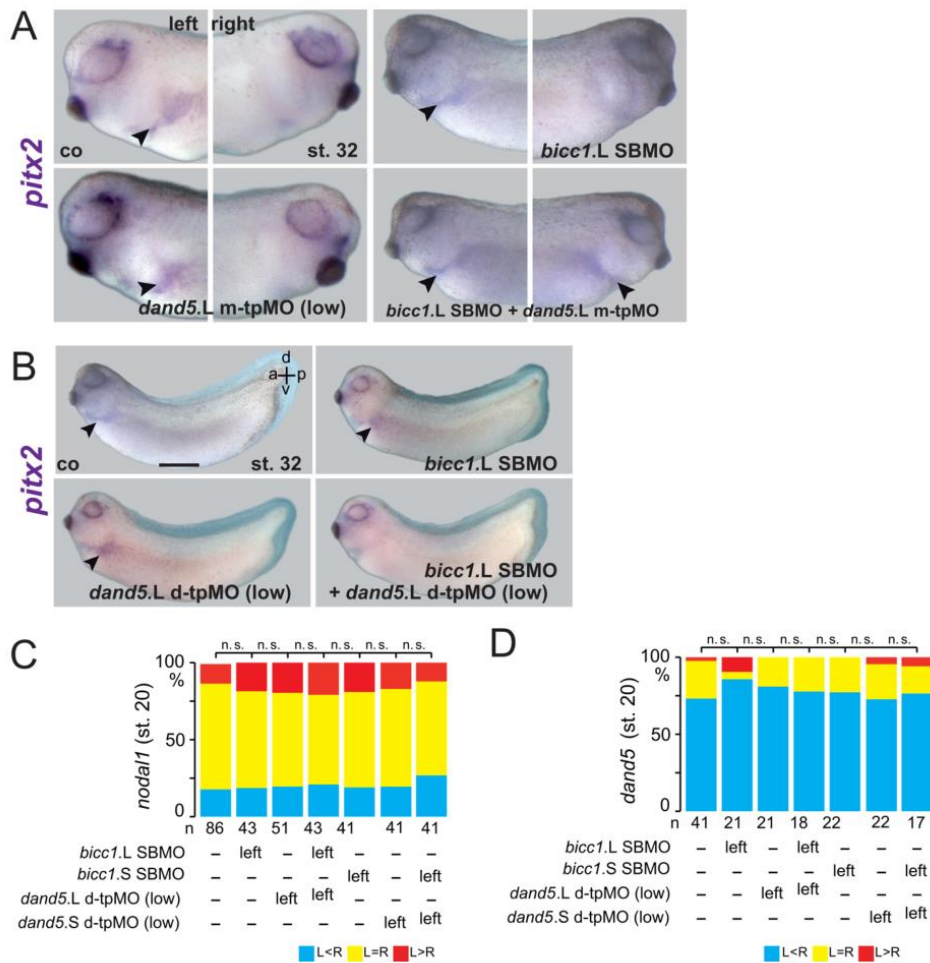
(A) *nodal1* sLRO expression at stage 20 in controls (co) and *gdf3* TBMO (0,3 pmol/embryo) unilaterally left injected specimens. Note reduced *nodal1* staining on the targeted side.

(B) Quantification of *nodal1* signals.

(C) *pitx2* asymmetry in the LPM was lost when *gdf3* MO was injected on the left.

(D) Quantification of *pitx2* expression in co and *gdf3* morphants.

Numbers (n) in (B and D) represent analyzed specimens from >3 independent experiments. Statistical analyses were done with a one-sided Pearson's chi-square test. n.s., not significant; \*\*\*, very highly significant,  $p < 0.001$ ; \*\*, highly significant,  $p < 0.01$ . p-values and listing of individual experiments can be found in the source data file. Asterisk in (A) marks injected side. Scale bars represent in (A) represents 100  $\mu$ m and in (C) 1 mm. st., stage; a, anterior; l, left; r, right; p, posterior; d, dorsal; v, ventral;



**Supplementary Figure 5. *pitx2* expression, but not *nodal1* transcription is altered by a combined treatment with low dose tpMO and single allele specific *bicc1* knockdown.**

(A) Controls (co) as well as right sided injections of single L allele specific *bicc1* SBMO or low dose of m-tpMO have no effect. Combining both MOs induces ectopic *pitx2*.

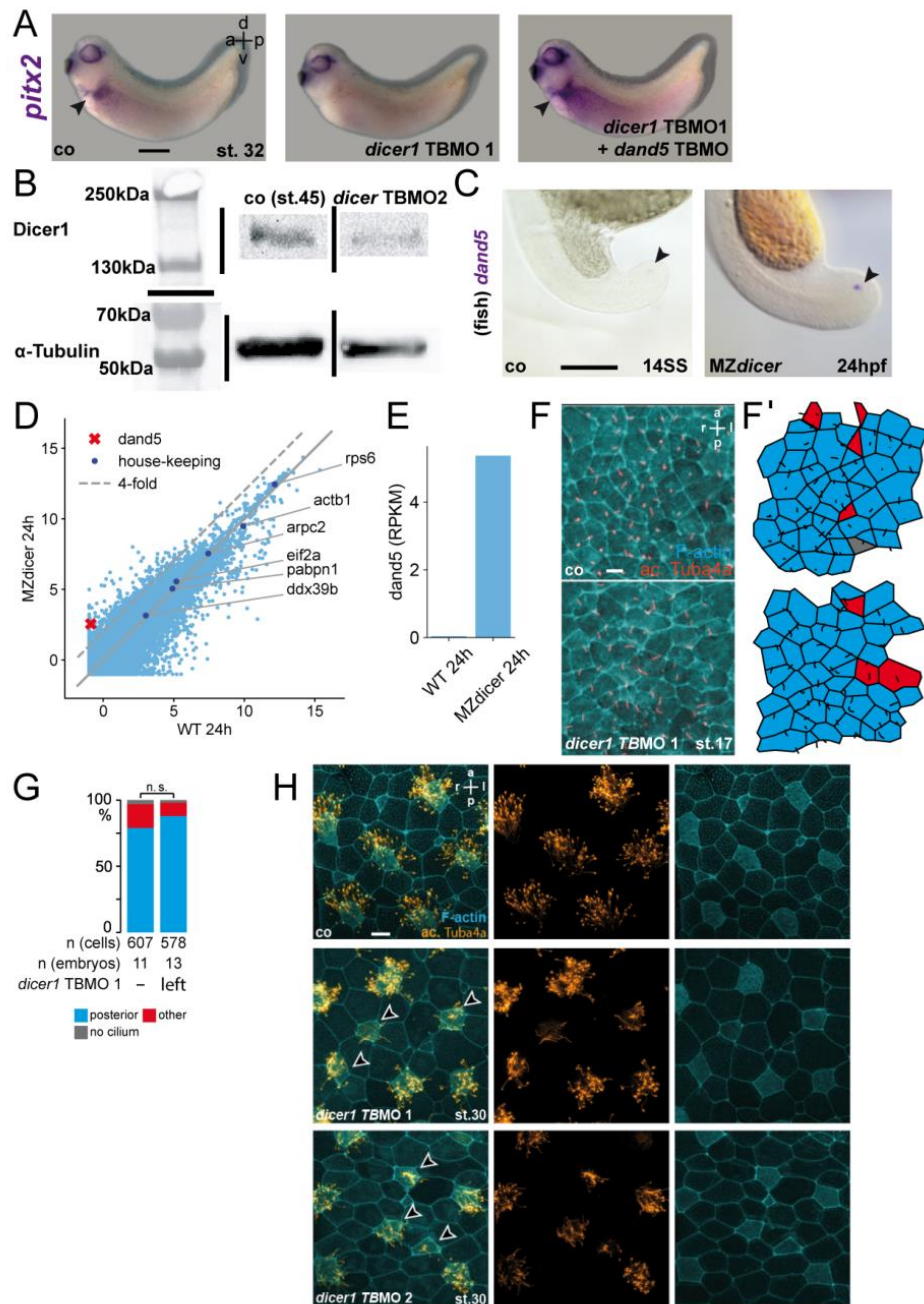
(B) Injecting a mix of L allele specific *bicc1* SBMO and reduced d-tpMO concentrations into the left lineage results in loss of *pitx2* asymmetry. Individual MOs are ineffective.

(C) Quantification of *nodal1* mRNA expression at the LRO. Controls (co) did not differ from specimens which were injected with low dosages of d-tpMO (L or S) or allele specific *bicc1* SBMO (L or S; 1 pmol). This was also true for embryos where both MOs were co-injected.

(D) No effect on *dand5* asymmetry by left sided injections of low dosages of d-tpMO (L or S) or allele specific *bicc1* SBMO (L or S; 1 pmol) or in combination.



MO pmol/embryo: *bicc1* SBMO (L or S, 1); m-tpMO low (L or S, 0.4); d-tpMO low (L or S, 0.5). Scale bar in (B) represents 1 mm. Arrowheads in (A and B) point to *pitx2* positive LPMs. Numbers (n) in (C) and (D) represent analyzed specimens from  $\geq 3$  independent experiments. Statistical analyses were done with a one-sided Pearson's chi-square test (Boniferroni-Holm corrected). n.s., not significant;  $p > 0.05$ . p-values and listing of individual experiments can be found in the source data file. st., stage; a, anterior; p, posterior; d, dorsal; v, ventral; n.s., not significant.

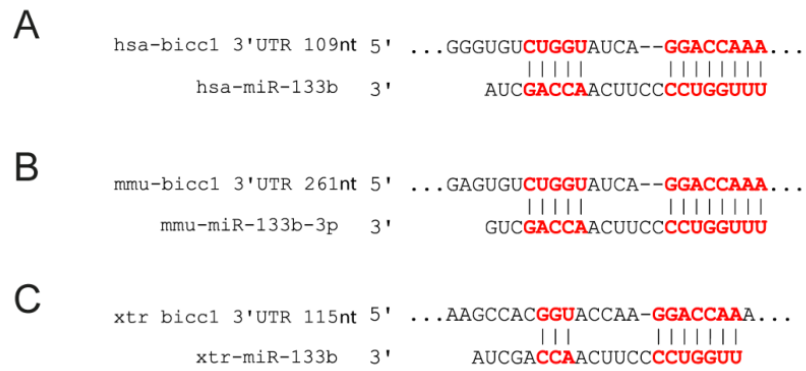


**Supplementary Figure 6. *dicer1* acts in post-flow stages during *Xenopus* LR axis formation.**

(A) Loss of *pitx2* expression in the left LPM (arrowhead) of st. 32 *dicer1* morphants was rescued by parallel knockdown of *dand5*.

## 2. Original research chapter

- (B) Western blot demonstrates *dicer1* TPMO2 (1 pmol) specificity. Proteins of controls and *dicer1* morphants at st. 45 were isolated and an anti-Dicer1 antibody was used for detection. Note strong signal reduction of Dicer1 in morphants. Anti-tubulin staining served as loading control.
- (C) Sustained *dand5* expression in *dicer* mutant fish at 24hpf. Note *dand5* mRNA was basically absent in wt fish at 14 somite stage (SS), in contrast to 24hpf MZ*dicer* mutants. Arrowhead marks faint (co.) or strong (MZ*dicer*) *dand5* staining. Since KV was not specifically targeted, we cannot rule out indirect effects of *dicer* loss on *dand5* asymmetry.
- (D) Scatter-plot comparing the expression of protein-coding genes in wt with their expression in MZ*dicer* zebrafish embryos at 24hpf (scale: log<sub>2</sub> RPKM+0.5 on both axis). *Dand5* gene is marked by red cross. The dashed line represents a 4-fold increase. RPKM; Reads per kilo base per million mapped reads. Six housekeeping genes are highlighted and were not affected in *dicer* mutants.
- (E) Bar-plot comparing *dand5* gene expression in wt (left) with its expression in MZ*dicer* zebrafish embryos at 24hpf. RPKM values wt: 0.040 and MZ*dicer*: 5.4.
- (F) Wt LRO morphology and ciliation in *dicer1* morphants at st. 17 compared to un-injected control specimen, as shown by IF using an anti ac. Tuba4a antibody (red) and counterstaining of actin using phalloidin (blue). (F') Cartoon shows the assessment of cilia polarization.
- (G) Quantification of cilia polarization in *dicer1* morphants. Statistical analyses were done with two-sided student t-test for 2 independent means. n represents number of cells or embryos which were analyzed.
- (H) Dicer1 is required for ciliogenesis of epidermal multi-ciliated cells. Cilia and subcortical actin were stained by immunofluorescence (IF) using an antibody against acetylated tubulin (ac. Tuba4a; orange) and Phalloidin (blue) for F-actin. Compared to controls (co) cilia were substantially shortened upon *dicer1* TPMO1 or TPMO2 injection. Arrowheads point to targeted cells.
- MO pmol/embryo: *dicer1* TBMO1 (1,5); *dicer1* TBMO2 (1); *dand5* TPMO (0,5). Scale bars in (A) represents 1 mm in (C) 200  $\mu$ m and in (F, H) 10  $\mu$ m. st., stage; a, anterior; l, left; r, right; p, posterior; d, dorsal; v, ventral; n.s., not significant. p-values and listing of individual experiments can be found in the source data file.



**Supplementary Figure 7. Conserved miR-133 binding sites in the *bicc1* 3'UTR.**

Targetscan analysis <sup>5,6</sup> predicts miR133 hybridization to the human (A; hsa), mouse (B; mmu) and *Xenopus tropicalis* (C; xtr) *bicc1* 3'UTR. Nucleotide (nt) position of 3'UTR where the seed sequence starts is indicated.

## 2. Original research chapter

Name	Sequence 5'– 3'	pmol/Embryo	Specificity	Origin
m-tpMO L	GCACCTGTTAAAGGCTAGAGATACT	High 0.8 Low 0.4		This work
m-tpMO S	ACGCCTGTCAAAGGGTGAAGTTACT	High 0.8 Low 0.4		This work
d-tpMO L	TAGCACTTCCCCTGCTTCAGCAAAG	High 1 Low 0.5	<i>dand5</i> MO rescue	This work
d-tpMO S	AAGTCGTCAAAGTCGTTGGCACTTCC	High 1 Low 0.5	<i>dand5</i> MO rescue	This work
<i>bicc1</i> -SPMO1 L	GGGAATAGACTCACCTGTAACATT	High 1 Low 0.5	RT PCR; <i>bicc1</i> mRNA / <i>dand5</i> MO rescue	This work
<i>bicc1</i> -SPMO2 S	CCCAACAAGCAAGCTCTTACCTTCT	High 1 Low 0.5	RT PCR; <i>bicc1</i> mRNA / <i>dand5</i> MO rescue	This work
<i>bicc1</i> TBMO1 L	CCATTGTGCTACTGCCGCGCTAAC	1		<sup>7</sup> (xBic-C-MO2)
<i>bicc1</i> TBMO2 S	TAGACTCGCACTGAGCCGCCATTCT	1		<sup>7</sup> (xBic-C-MO1)
<i>dand5</i> -TBMO	CTGGTGGCCTGGAACAACAGCATGT	0.5		<sup>8</sup> (Coco1-MO)
<i>gdf3</i> -TBMO	CACAACCTCTGCCATGTTGACTTCTC	0.3		<sup>8</sup> (derrière-MO)
<i>dicer1</i> -TBMO1	TGCAGGGCTTTCATAAATCCAGTGA	1.5		<sup>9</sup>
<i>dicer1</i> -TBMO2	CATGAGCTGAAGTCCTGCCATGC	1	Western Blot / <i>dand5</i> MO rescue	This work
<i>pkd2</i> TBMO	GCCACTATCTCTCAATCATCTCCG	1		<sup>10</sup>
zfPkd2 TBMO	AGGACGAACGCGACTGGAGCTCATC	1-4ng		<sup>11</sup>

Supplementary table 1. Morpholino oligomers used.

Primer name	Sequence 5'– 3'
<i>dand5.L</i> 3'-UTR forward primer	GCCCTAATTGGACTACGTGTGGCC
<i>dand5.L</i> 3'-UTR reverse primer	GCAGGACAATATAAAAAACATGAGGC
<i>gdf3</i> 3'-UTR forward primer	ATAGATCTGTTTGCTTTGGAGATTGTTCTC
<i>gdf3</i> 3'-UTR reverse primer	ATAGATCTGGGTAAATCACATTTATTTCC
<i>bicc1.L</i> forward primer	GCCACCCCTTCTCTTACTAAACA
<i>bicc1.L</i> reverse primer	CTCTGCTTGGTTATTCCTGTTGGAGT
<i>bicc1.S</i> forward primer	GTGTTGAATTCTACTCACGAGGGAA
<i>bicc1.S</i> reverse primer	CTCGGCTTGGTTATTCCTATTGGAA

Supplementary table 2. PCR primers used.

## References

- Minegishi, K. *et al.* Fluid flow-induced left-right asymmetric decay of Dand5 mRNA in the mouse embryo requires Bicc1-Ccr4 RNA degradation complex. *Nature communications* (In Press).
- Schweickert, A. *et al.* The nodal inhibitor Coco is a critical target of leftward flow in *Xenopus*. *Current Biology* **20**, 738–743; 10.1016/j.cub.2010.02.061 (2010).
- Tisler, M., Schweickert, A. & Blum, M. *Xenopus*, an ideal model organism to study laterality in conjoined twins. *Genesis: the Journal of Genetics and Development* **55**, 55:e22993; <https://doi.org/10.1002/dvg.22993> (2017)
- Blum, M. & Ott, T. Animal left-right asymmetry. *Current Biology* **28**, 301-304; <https://doi.org/10.1016/j.cub.2018.02.0735>. Lewis, B. P., Burge, C. B. & Bartel, D. P. Conserved seed pairing, often flanked by adenosines, indicates that thousands of human genes are microRNA targets. *Cell* **120**, 15–20; 10.1016/j.cell.2004.12.035 (2005).
- Friedman, R. C., Farh, K. K.-H., Burge, C. B. & Bartel, D. P. Most mammalian mRNAs are conserved targets of microRNAs. *Genome research* **19**, 92–105; 10.1101/gr.082701.108 (2009).
- Maisonneuve, C. *et al.* Bicaudal C, a novel regulator of Dvl signaling abutting RNA-processing bodies, controls cilia orientation and leftward flow. *Development* **136**, 3019–3030; 10.1242/dev.038174 (2009).
- Vonica, A. & Brivanlou, A. H. The left-right axis is regulated by the interplay of Coco, Xnr1 and derriere in *Xenopus* embryos. *Developmental biology* **303**, 281–294; 10.1016/j.ydbio.2006.09.039 (2007).
- Agrawal, R., Tran, U. & Wessely, O. The miR-30 miRNA family regulates *Xenopus* pronephros development and targets the transcription factor Xlim1/Lhx1. *Development* **136**, 3927–3936; 10.1242/dev.037432 (2009).
- Tran, U. *et al.* The RNA-binding protein bicaudal C regulates polycystin 2 in the kidney by antagonizing miR-17 activity. *Development* **137**, 1107–1116; 10.1242/dev.046045 (2010).



11. Schottenfeld, J., Sullivan-Brown, J. & Burdine, R. D. Zebrafish curly up encodes a Pkd2 ortholog that restricts left-side-specific expression of southpaw. *Development* **134**, 1605–1615; 10.1242/dev.02827 (2007).



**2H**

		<b>dand5 probe</b>								Bonferroni-Holm corrections p-values
		L<R	L=R	L>R	L-R	L-R	L-R	L-R	n	
	co (st.20)	20	5			133			226	
	dand5 L d-t-pMO (left injection)	11	4			26			41	1
	dand5 S d-t-pMO (left injection)	11	3	1		36			70	1
	co (st.20)	6	7	1		25			49	1
	dand5 L d-t-pMO (left injection)	7	5	1		49			90	1
	dand5 S d-t-pMO (left injection)	9	11	3						
	co (st.20)	8	6	1						
	dand5 L d-t-pMO (left injection)	8	4	1						
	dand5 S d-t-pMO (left injection)	5	4	2						
	co (st.20)	22	6							
	dand5 L d-t-pMO right injection)	20	4	1						
	co (st.20)	9	7	1						
	dand5 L d-t-pMO right injection)	8	5	1						
	co (st.20)	12	20	5						
	dand5 L d-t-pMO right injection)	8	19	4						
	co (st.20)	24	6	1						
	dand5 S d-t-pMO right injection)	17	5	2						
	co (st.20)	17	13	1						
	dand5 S d-t-pMO right injection)	15	15	2						
	co (st.20)	15	10	3						
	dand5 S d-t-pMO right injection)	17	14	3						

**2I**

		<b>dand5 probe</b>								Bonferroni-Holm corrections p-values
		L<R	L=R	L>R	L-R	L-R	L-R	L-R	n	
	co st.16	6	9	3						
	dand5 L d-t-pMO (left injection)	7	12	1						
	dand5 L d-t-pMO (right injection)	8	20	3						
	co st.16	2	14	1						
	dand5 L d-t-pMO (left injection)	4	25	1						
	dand5 L d-t-pMO (right injection)	4	23	1						
	co st.16	2	12	2						
	dand5 L d-t-pMO (left injection)	2	8	2						
	dand5 L d-t-pMO (right injection)	3	6	2						
	co st.16	4	27	2						
	dand5 L d-t-pMO (left injection)	4	24	4						
	dand5 L d-t-pMO (right injection)	7	25	5						
	co st.16	5	16	1						
	dand5 S d-t-pMO (left injection)	6	22	1						
	dand5 S d-t-pMO (right injection)	6	23	4						
	co st.16	6	24	4						
	dand5 S d-t-pMO (left injection)	2	23	7						
	dand5 S d-t-pMO (right injection)	6	23	2						
	co st.16	5	20	3						
	dand5 S d-t-pMO (left injection)	5	20	9						
	dand5 S d-t-pMO (right injection)	9	23	2						

		<b>dand5 probe</b>						Bonferroni-Holm corrections p-values
		L<R	L>R	L-R	L-R	L-R	n	
	co (st.16)	31	122	169				
	dand5 L d-t-pMO (left injection)	17	69	94				1.
	dand5 L d-t-pMO (right injection)	22	74	110				1.
	dand5 S d-t-pMO (left injection)	13	67	94				1.
	dand5 S d-t-pMO (right injection)	24	71	99				1.

3C		damd5 probe		Bonferroni-Holm corrections p-values	
		Rp-L	Rc-L	Rp-L	Rc-L
co (sr.20)	17	4	1		
bicc1 SBMO (left injection)	12	7			
bicc1 SBMO (right injection)	8	3	6		
co (sr.20)	5				
bicc1 SBMO (left injection)	11				
bicc1 SBMO (right injection)	7	6	2		
co (sr.20)	13	4	1		
bicc1 SBMO (left injection)	17	6			
bicc1 SBMO (right injection)	2	15	6		
co (sr.20)	43	12	9		
bicc1 SBMO (left injection)	22	4	1		
bicc1 SBMO + bicc1 mRNA (left injection)	24	12	18		
co (sr.20)	13	13	3		
bicc1 SBMO (left injection)	36	8	5		
bicc1 SBMO + bicc1 mRNA (left injection)	15	10	11		
co (sr.20)	19	10	4		
bicc1 SBMO (left injection)	15	0	10		
bicc1 SBMO + bicc1 mRNA (left injection)	44	22	10		
co (sr.20)	21	17	31		
bicc1 mRNA (left injection)	41	10	5		
bicc1 mRNA (right injection)	51	6	15		
co (sr.20)	38	11	19		
bicc1 mRNA (left injection)	12	2	6		
bicc1 mRNA (right injection)	16	8	6		
co (sr.20)	9	15	8		
bicc1 mRNA (left injection)	15	4	1		
bicc1 mRNA (right injection)	15	4	1		
co (sr.20)	224				
bicc1 SBMO (left injection)	113				
bicc1 SBMO + bicc1 mRNA (left injection)	54				
bicc1 SBMO (right injection)	14				
bicc1 mRNA (left injection)	69				
bicc1 mRNA (right injection)	72				
		Rp-L	Rc-L	n	
		224	53	361	
		113	84	147	0.034
		54	25	79	0.0046
		14	29	43	0
		69	24	93	0.0117
		72	16	88	0.034
					0.00001

3D		nodal1 probe		Bonferroni-Holm corrections p-values	
		Rp-L	Rc-L	Rp-L	Rc-L
co (sr.20)	4	7	2		
bicc1 SBMO (left injection)	13	5	1		
bicc1 SBMO (right injection)	1	7	5		
co (sr.20)	6	10	4		
bicc1 SBMO (left injection)	15	7	2		
bicc1 SBMO + bicc1 mRNA (left injection)	4	12	4		
bicc1 SBMO (right injection)	1	12	8		
co (sr.20)	3	6	1		
bicc1 SBMO (left injection)	11	5	1		
bicc1 SBMO + bicc1 mRNA (left injection)	5	4	6		
bicc1 SBMO (right injection)	2	19	9		
co (sr.20)	2	43			
bicc1 mRNA (left injection)	2	43			
bicc1 mRNA (right injection)	8	24	10		
co (sr.20)	7	18	6		
bicc1 mRNA (left injection)	6	16	9		
bicc1 mRNA (right injection)	7	20	8		
co (sr.20)	6	15	5		
bicc1 mRNA (left injection)	6	13	9		
bicc1 mRNA (right injection)	6	12	4		
co (sr.20)	13	7	1		
bicc1 SBMO (left injection)	4	5	2		
bicc1 SBMO + bicc1 mRNA (left injection)	4	5	2		
		Rp-L	Rc-L	n	
		34	29	185	
		52	24	81	.0057
		13	21	46	1.
		4	38	22	0.0094
		15	76	11	102
		12	58	19	89
					0.000537

**Figure 4A**

Luc-Biccl1/Luc For individual experiments >>  
 derriere5 UTR Luciferase 0.385039 0.15526 0.32563

	Mean	SD	p values compared to control
	0.288643	0.113	0.000248

4C		<i>gdj3</i> probe		Bonferroni-Holm corrections p-values	
	R=L	R=L	R=L	n	
co (st.20)	4	4			
biccl1 SBMO (left injection)	3	4			
biccl1 SBMO (right injection)	2	4			
co (st.20)	1	7			
biccl1 SBMO (left injection)	2	7			
biccl1 SBMO (right injection)	2	6			
co (st.20)	6	4			
biccl1 SBMO (left injection)	5	9			
biccl1 SBMO (right injection)	4	8			
co (st.20)	2	13			
biccl1 SBMO (left injection)	4	13			
biccl1 SBMO (right injection)	1	23			
co (st.20)	2	16			
biccl1 SBMO (left injection)	2	18			
biccl1 SBMO (right injection)	4	17			
co (st.20)	2	10			
biccl1 SBMO (left injection)	3	10			
biccl1 SBMO (right injection)	6	19			
			co (st.20)	81	
			biccl1 SBMO (left injection)	17	54
			biccl1 SBMO (right injection)	19	61
				77	14
					1.
					1.

4E		<i>nodal1</i> probe		Bonferroni-Holm corrections p-values	
	R=L	R=L	R=L	n	
co (st.20)	4	9			
biccl1 SBMO (left injection)	6	5			
biccl1 SBMO + <i>gdj3</i> mRNA (left injection)	4	26			
co (st.20)	3	8			
biccl1 SBMO (left injection)	7	7			
biccl1 SBMO + <i>gdj3</i> mRNA (left injection)	4	10			
co (st.20)	6	12			
biccl1 SBMO (left injection)	12	9			
biccl1 SBMO + <i>gdj3</i> mRNA (left injection)	3	5			
co (st.20)	5	12			
biccl1 SBMO (left injection)	14	10			
biccl1 SBMO + <i>gdj3</i> mRNA (left injection)	6	10			
			co (st.20)	83	
			biccl1 SBMO (left injection)	18	41
			biccl1 SBMO + <i>gdj3</i> mRNA (left injection)	39	31
				17	51
					22
					0
					0.631

4G		<i>pix2</i> probe		Bonferroni corrections p-values	
	wt	bilateral	absent	n	
co	26				
biccl1 SBMO (left injection)	13	2			
biccl1 SBMO + derriere mRNA (left injection)	28	4			
co	33				
biccl1 SBMO (left injection)	10				
biccl1 SBMO + derriere mRNA (left injection)	27				
co	32				
biccl1 SBMO (left injection)	21				
biccl1 SBMO + derriere mRNA (left injection)	27				
co	27				
biccl1 SBMO (left injection)	16				
biccl1 SBMO + derriere mRNA (left injection)	25				
			wt	118	
			co	60	119
			biccl1 SBMO	2	54
			biccl1 SBMO + derriere mRNA	1	13
					121
					0
					0.0089
					0.00001



**Figure 5A**

wt		piX2 probe		right		Benferroni corrections	
absent	bi	absent	bi	absent	bi	n	p-value
48	2	1	4	2	0	1	1.00001
30	2	1	4	2	0	1	1.00001
22	2	1	4	2	0	1	1.00001
11	2	1	4	2	0	1	1.00001
3	2	1	4	2	0	1	1.00001
31	2	1	4	2	0	1	1.00001
30	2	1	4	2	0	1	1.00001
15	1	1	11	2	2	7	0.00001
25	1	1	11	2	2	7	0.00001
18	1	1	11	2	2	7	0.00001
18	1	1	11	2	2	7	0.00001
19	1	1	11	2	2	7	0.00001
23	1	1	11	2	2	7	0.00001
6	1	1	9	2	2	7	0.00001
31	2	1	9	2	2	7	0.00001
19	2	1	9	2	2	7	0.00001
30	2	1	9	2	2	7	0.00001
29	2	1	9	2	2	7	0.00001
32	2	1	9	2	2	7	0.00001
36	2	1	9	2	2	7	0.00001
23	2	1	9	2	2	7	0.00001

**5C**

wt		dams probe		right		Benferroni-Holm corrections	
absent	bi	absent	bi	absent	bi	n	p-value
12	3	1	13	3	4	131	0.0044
7	3	1	13	3	4	131	0.0044
8	3	1	13	3	4	131	0.0044
20	2	1	13	3	4	131	0.0044
21	4	1	11	2	2	47	0.00001
13	6	1	11	2	2	47	0.00001
15	30	1	11	2	2	44	0.00001
5	30	1	11	2	2	44	0.00001
6	7	2	7	2	2	15	0.00001
7	7	2	7	2	2	15	0.00001
11	7	1	7	1	1	15	0.00001
6	5	1	7	1	1	15	0.00001
7	6	2	7	2	2	15	0.00001
18	6	5	7	5	5	15	0.00001
10	8	2	7	2	2	15	0.00001
9	11	2	7	2	2	15	0.00001
5	2	2	7	2	2	15	0.00001
13	5	2	7	2	2	15	0.00001
10	4	2	7	2	2	15	0.00001
5	5	4	7	4	4	15	0.00001

**5D**

wt		piX2 probe		right		Benferroni corrections	
absent	bi	absent	bi	absent	bi	n	p-value
22	4	1	4	3	5	100	0.00001
26	1	1	4	3	5	100	0.00001
18	1	1	4	3	5	100	0.00001
24	4	1	4	3	5	100	0.00001
20	1	1	4	3	5	100	0.00001
20	1	1	4	3	5	100	0.00001
19	1	1	4	3	5	100	0.00001
19	1	1	4	3	5	100	0.00001
19	1	1	4	3	5	100	0.00001
31	7	1	4	3	5	100	0.00001
24	1	1	4	3	5	100	0.00001
24	5	1	4	3	5	100	0.00001
16	6	1	4	3	5	100	0.00001
27	4	1	4	3	5	100	0.00001
10	6	1	4	3	5	100	0.00001
26	1	1	4	3	5	100	0.00001
17	1	1	4	3	5	100	0.00001
12	8	1	4	3	5	100	0.00001
38	1	1	4	3	5	100	0.00001
30	1	1	4	3	5	100	0.00001
13	2	2	4	3	5	100	0.00001

6E	<i>damd5</i> probe			Bonferroni-Holm corrections p-values
	L<R	L=R	L>R	
co (st.>20)	15	7	0	
dicer1 TBMO1 (left injection)	5	7	0	
dicer1 TBMO1 (right injection)	20	2	1	
dicer1 TBMO1 (left injection)	11	10	2	
co (st.>20)	38	0	1	
dicer1 TBMO1 (left injection)	64	15	6	
co (st.>20)	3	5	0	
dicer1 TBMO1 (left injection)	2	6	8	
co (st.>20)	23	4	1	
dicer1 TBMO1 (left injection)	67	58	33	
co (st.>20)	21	16	3	
dicer1 TBMO1 (left injection)	2	8	2	
co (st.>20)	10	3	1	
dicer1 TBMO1 (left injection)	12	5	0	
co (st.>20)	21	2	0	
dicer1 TBMO1 (left injection)	17	4	3	
co (st.>20)	13	5	7	
dicer1 TBMO1 (left injection)	4	4	12	
co (st.>20)	24	1	5	
dicer1 TBMO2 (left injection)	14	17	10	
co (st.>20)	21	3	4	
dicer1 TBMO2 (left injection)	12	10	6	
co (st.>20)	25	2	6	
dicer1 TBMO2 (left injection)	14	13	10	

6F	<i>Damd5</i> probe			n
	L<R	L=R	L>R	
Mouse 8.0	R>L	R=L	R<L	
WT	8		3	
Dicer CKO				

6G	<i>damd5</i> probe			p-values compared to control
	L<R	L=R	L>R	
Zebrafish				
WT	15	5	20	
Medicer	5	13	1	0.0059665

6I	<i>pix2</i> probe			Bonferroni corrections p-values
	wt	absent	bilateral	
co	13		right	
bicc1.SBMO (left injection)	18	1		
dicer1 TBMO1 (left injection)	17			
bicc1.SBMO+dicer1 TBMO1 (left injection)	1	13		
co	12			
bicc1.SBMO (left injection)	19	1		
dicer1 TBMO1 (left injection)	20	2		
bicc1.SBMO+dicer1 TBMO1 (left injection)	6	14		
co	30	1		
bicc1.LSBMO (left injection)	13			
dicer1 TBMO1 (left injection)	12	4	1	
bicc1.LSBMO+dicer1 TBMO1 (left injection)	3	11	1	
co	31	2		
bicc1.SBMO (left injection)	13	4		
dicer1 TBMO1 (left injection)	14	6	2	
bicc1.LSBMO+dicer1 TBMO1 (left injection)	4	14	3	

6J	<i>pix2</i> probe			n	Bonferroni corrections p-values
	wt	absent	bilateral		
co	86	3	0	89	
bicc1.SBMO (left injection)	37	2	0	39	
dicer1 TBMO1 (left injection)	63	12	3	80	
bicc1.SBMO+dicer1 TBMO1 (left injection)	11	27	0	38	0.00001
co	26	1	0	29	
bicc1.LSBMO (left injection)	7	25	4	36	0.00001

**Figure 7A**

<i>dand5</i> probe					
Zebrafish	L>R	L=R	L<R	L<R	n
WT	1	1	5	5	7
heterozygous	1	2	5	5	8
null mutant		4			4

**7B**

<i>dand5</i> probe					
Zebrafish	L>R	L=R	L<R	L<R	n
WT	1	17	30	30	48
pkd2 MO	8	25	6	6	39

p-values compared to control  
1,4552E-05

**7C**

Dand5 UTR Luciferase	Luc+/Luc For individual experiments>>			Mean	SD	Bonferroni corrections p values
bicc1 mRNA	0,1523	0,23112	0,2166	0,20000667	0,04194821	0,0001
bicc1 mRNA (low)	0,4452458	0,33784789	0,48967	0,42425456	0,07805743	0,0006
bicc1 mRNA (low) + pkd2 mRNA	0,0752231	0,2200858	0,1666	0,15396964	0,07325261	0,0001
bicc1 mRNA (low) + pkd2 TBMO	0,90912924	0,56591475	0,7789	0,764648	0,19200437	0,2033
pkd2 mRNA	7,6974	1,329	2,363636	3,7966787	3,4175047	0,0001
pkd2 TBMO	0,53727393	0,47828019	0,30085578	0,4388033	0,12305366	0,0042

Supplementary Figure 1D

<i>dand5</i> coding probe				<i>dand5</i> coding probe			
Stage	R>L	R=L	L>R	st.17	R>L	R=L	L>R
17	1	3	2	17	19	17	10
17	6	4	1	18	29	10	12
17	5	5	3	19	90	40	15
17	7	5	4	20	32	6	1
18	7	1	2		R>L	R=L	L>R
18	6	3	1	17	12	22	20
18	6	1		18	21	31	14
18	5	3	5	19	34	41	15
18	5	2	4	20	33	8	4
19	7	4	1		R>L	R=L	L>R
19	17	5	2	17	13	22	17
19	10	4	2	18	30	28	15
19	10	3	2	19	67	27	8
19	11	6	2	20	36	4	2
19	20	10	3				
19	15	8	3				
20	9	1					
20	10	2					
20	8	2					
20	5	1	1				
<i>dand5</i> S UTR probe				<i>dand5</i> S UTR probe			
Stage	R>L	R=L	L>R	st.17	R>L	R=L	L>R
17	1		5				
17	4	13	6				
17	1	1	6				
17	3	4	3				
17	3	4					
18	10	6	4				
18	3	3	2				
18	2	6	0				
18	4	8	4				
18	1	4	1				
18	1	4	3				
19	0	5	4				
19	5	9	1				
19	2	1	1				
19	9	9	3				
19	10	9	4				
19	8	8	2				
20	8	4	2				
20	7	1	1				
20	8	2					
20	7	1	0				
20	3		1				
<i>dand5</i> L UTR probe				<i>dand5</i> L UTR probe			
Stage	R>L	R=L	L>R	st.17	R>L	R=L	L>R
17		3	3				
17	4	8	5				
17	2	3	1				
17	4	5	2				
17	3	3	6				
18	7	8	1				
18	1	7	2				
18	2	0	2				
18	12	8	1				
18	6	5	1				
18	2	0	8				
19	10	0	1				
19	2	2	2				
19	5	1	0				
19	9	5	1				
19	10	5	1				
19	12	6	2				
19	8	2					
19	11	6	1				
20	3	0	0				
20	12	1	1				
20	6	1					
20	8	1	1				
20	7	1					

**Supplementary Figure 2B**

	<i>nodal1</i> probe			L<R	L=R	L>R	n	Bonferroni-Holm corrections p-values
	L<R	L=R	L>R					
co (st.20)	1	9	4					
dand5 L m-tpMO (right injection)	2	8	9				49	0.7937
dand5 S m-tpMO (right injection)	2	6	5				67	0.7937
co (st.20)	3	15	4					
dand5 L m-tpMO (right injection)	4	10	6					
dand5 S m-tpMO (right injection)	2	18	4					
co (st.20)	1	11	1					
dand5 L m-tpMO (right injection)	2	22	4					
dand5 S m-tpMO (right injection)	2	12	2				53	0.7937

**2D**

	<i>nodal1</i> probe			L<R	L=R	L>R	n	Bonferroni-Holm corrections p-values
	L<R	L=R	L>R					
co (st.20)	1	11	1					
dand5 S d-tpMO (left injection)	2	23	5				46	0.6882
dand5 L d-tpMO (left injection)	2	12	2				61	0.597
co (st.20)	2	9	3					
dand5 S d-tpMO (left injection)	1	6	4					
dand5 L d-tpMO (left injection)	3	11	5					
co (st.20)	2	13	5					
dand5 S d-tpMO (left injection)	2	14	6					

**Supplementary Figure 3B**

	<i>pix2</i> probe		bilateral	absent	n	p-values
	wt	co				
bic1.1.SBMO(left injection)	27	2	1	1	69	
bic1.5.SBMO(left injection)	18	1	1	1	64	
co	20	1	1	1	67	1.
bic1.1.SBMO(right injection)	19	1	1	0	67	1.
bic1.5.SBMO(right injection)	19	1	1	2	52	1.
co	18	1	2	3	52	1.
bic1.1.SBMO(left injection)	18	2	0	0		
bic1.5.SBMO(left injection)	21	1	0	0		
co	16	1	1	1		
bic1.1.SBMO(right injection)	20	1	1	1		
bic1.5.SBMO(right injection)	14	1	1	1		

**3D LRO cells**

	posterior		no cilium		others		wt	bic1.1.SBMO(left injection)	bic1.5.SBMO(left injection)	posterior	no cilium	others	wt	bic1.1.SBMO(right injection)	bic1.5.SBMO(right injection)	posterior	no cilium	others	n	p-values compared to control
	wt	co	wt	co	wt	co														
Embryo 1	26	1	3	3	24	3	24	3	3	203	5	3	238	5	3	203	5	3	238	0.265277
Embryo 2	32	1	7	7	32	1	32	1	6	18	6	6	18	6	6	18	6	6	18	
Embryo 3	28	1	8	8	32	1	38	1	3	16	3	3	16	3	3	16	3	3	16	
Embryo 4	24	1	7	7	30	1	30	1	4	14	4	4	14	4	4	14	4	4	14	
Embryo 5	24	2	6	6	30	1	30	1	7	14	7	7	14	7	7	14	7	7	14	
Embryo 6	24	2	6	6	30	1	30	1	7	14	7	7	14	7	7	14	7	7	14	

**somatic LRO cells**

	posterior		no cilium		2 cilia		wt	bic1.1.SBMO(left injection)	bic1.5.SBMO(left injection)	posterior	no cilium	2 cilia	wt	bic1.1.SBMO(right injection)	bic1.5.SBMO(right injection)	posterior	no cilium	2 cilia	n	p-values compared to control
	wt	co	wt	co	wt	co														
Embryo 1	3	12	13	13	3	3	3	3	3	18	18	18	18	18	18	18	18	18	18	0.798308
Embryo 2	5	14	12	12	4	4	4	4	4	12	12	12	12	12	12	12	12	12	12	
Embryo 3	4	11	7	7	4	4	4	4	7	7	7	7	7	7	7	7	7	7	7	
Embryo 4	4	11	7	7	4	4	4	4	7	7	7	7	7	7	7	7	7	7	7	
Embryo 5	2	6	12	12	3	3	3	3	12	12	12	12	12	12	12	12	12	12	12	
Embryo 6	2	6	12	12	3	3	3	3	12	12	12	12	12	12	12	12	12	12	12	
Embryo 7	1	1	1	1	1	1	1	1	1	1	1	1	1	1	1	1	1	1	1	
Embryo 8	11	1	3	3	12	2	12	2	2	2	2	2	2	2	2	2	2	2	2	
Embryo 9	20	3	2	2	9	1	9	1	1	1	1	1	1	1	1	1	1	1	1	
Embryo 10	14	1	4	4	13	0	13	0	0	0	0	0	0	0	0	0	0	0	0	
Embryo 11	8	3	1	1	8	1	8	1	1	1	1	1	1	1	1	1	1	1	1	

**3G**

	<i>dand5</i> probe		RcL	RcL	n	p-values
	wt	co				
co	2	9	2	2	10	
bic1.1.SBMO(left injection)	1	3	9	9	27	
bic1.5.SBMO(right injection)	1	3	9	9	27	
co	2	9	2	2	10	
bic1.1.SBMO(left injection)	1	4	7	7	21	
bic1.5.SBMO(right injection)	1	4	7	7	21	
co	2	9	2	2	10	
bic1.1.SBMO(left injection)	10	7	4	4	38	
bic1.5.SBMO(right injection)	10	7	4	4	38	
co	3	14	7	7	52	
co	2	4	4	4	16	
bic1.1.SBMO(left injection)	12	11	2	2	44	
bic1.5.SBMO(right injection)	3	2	8	8	54	0.0098
co	3	11	6	6	49	0.0094
bic1.1.SBMO(left injection)	14	9	2	2	68	
bic1.5.SBMO(right injection)	2	11	10	10	68	
co	1	6	1	1	52	
bic1.1.SBMO(left injection)	12	5	11	11	52	



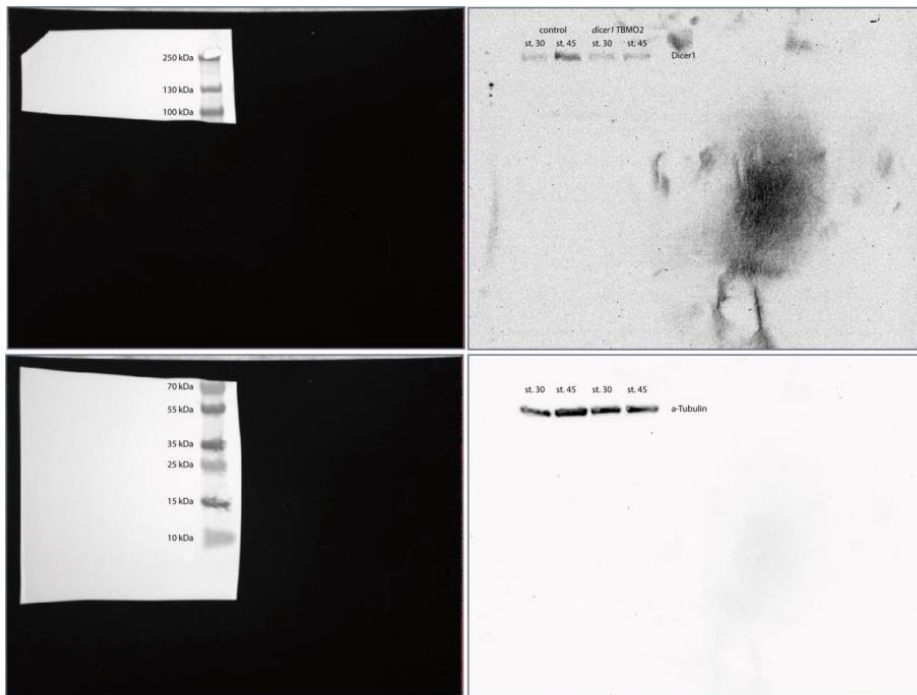
Supplementary Figure 4B		<i>nodal1</i> probe				p-values compared to control		
	R>L	R=L	R<L		R>L	R=L	R<L	n
co (st.20)	1	6	3		7	35	3	45
gdf3 TBMO (left injection)	8	3	2		26	23	3	52
co (st.20)	2	11			4,66666667	23,33333333	2	0,001515
gdf3 TBMO (left injection)	9	4	1		15	13,2692308	1,73076923	
co (st.20)	4	18						
gdf3 TBMO (left injection)	9	16						

4D		<i>pitx2</i> probe				p-values compared to control		
	wt	bilateral	absent	right	wt	bilateral	absent	n
co	31				90	0	2	92
gdf3 TBMO (left injection)	26		13		75	2	53	130
co	33		2					
gdf3 TBMO (left injection)	31	2	30					
co	26		10					
gdf3 TBMO (left injection)	18							







Source data to supplementary figure 6: Western blot was cut (after running) for photo documentation purposes. stage, st.

### 2.3 Author's contribution

#### **“A novel role of the organizer gene Goosecoid as an inhibitor of Wnt/PCP-mediated convergent extension in *Xenopus* and mouse”**

(Scientific reports 7, Article 43010, 2017)

Bärbel Ulmer, Melanie Tingler, Sabrina Kurz, Markus Maerker, Philipp Andre, Dina Mönch, Marina Campione, Kirsten Deißler, Mark Lewandoski, Thomas Thumberger, Axel Schweickert, Abraham Fainsod, Herbert Steinbeißer, Martin Blum

I was involved in the process of revision, by performing microinjections with *gsc* constructs, analysing gastrulation and neurulation phenotypes, performing *gsc* gene analyses and editing and finalizing the manuscript.

#### **“A Conserved Role of the Unconventional Myosin1d in Laterality Determination”**

(Current Biology, Vol. 28, Issue 5, 2018)

Melanie Tingler, Sabrina Kurz, Markus Maerker, Tim Ott, Franziska Fuhl, Axel Schweickert, Janine M. LeBlanc-Straceski, Stéphane Noselli, Martin Blum

I performed part of the luciferase assays and was involved in the process of revision, by performing microinjections with *myo1d* MO and mRNA, analysing the expression of LR marker genes, editing and finalizing the manuscript.

**“Bicc1 and Dicer regulate left-right patterning through post-transcriptional control of the Nodal-inhibitor Dand5”**

(Nature Communications **12**, 5482)

Markus Maerker, Maike Getwan, Megan E. Dowdle, Jason C. McSheene, Vanessa Gonzalez, José L. Pelliccia, Danielle S. Hamilton, Valeria Yartseva, Melanie Tingler, Katsura Minegishi, Philipp Vick, Antonio J. Giraldez, Hiroshi Hamada, Rebecca D. Burdine, Michael D. Sheets, Martin Blum and Axel Schweickert

I was involved in the conceptualization of the study and writing of the manuscript. I designed the figures and performed most of the *X. laevis* experiments except for partial animal cap assays (Michael D. Sheets and Megan E. Dowdle), partial initial Dicer experiments (Maike Getwan), *dicer* MO skin IF and Western Blot (Melanie Tingler) and initial Bicc experiments (Philipp Vick).

Stuttgart 6.4.2021

**Place and Date**



**Signature (apl. Prof. Dr. Axel Schweickert)**



### 3. Discussion

#### 3.1 The novel function of *gsc* during the evolution of vertebrates

While *gsc* has been investigated for about three decades now, its early function as SO gene was enigmatic as no developmental defects occur after LOF (Rivera-Pérez et al., 1995; Yamada et al., 1995). Surprisingly its impact and importance can be seen upon GOF at the ventral side of the vertebrate embryo, which results in a secondary axis formation. This is also true for non-vertebrate *gsc* constructs. In contrast to that, overexpression of *gsc* in the dorsal side leads to severe gastrulation and neurulation defects, which was only true for vertebrate (mouse, *Xenopus*; (Ulmer, 2008; Ulmer, 2012) *gsc*. This effect could be explained with Gsc as a negative regulator of the Wnt/PCP pathway. This was proven in various contexts like in a Dsh2 membrane recruitment assay and rescue experiments via GOF of PCP components. More specifically, Gsc inhibits CE resulting in gastrulation and neurulation defects. A *gsc* gene comparison showed a high conservation concerning the homeodomain (HD) and the GEH/ En homology region 1 (eh-1), but no other specific conservation among *gsc* genes in the animal kingdom (Jiménez, Verrijzer and Ish-Horowicz, 1999). Interestingly among invertebrates and vertebrates distinct conserved regions were determined. Of special interest were two conserved regions in vertebrate *gsc* genes, named as X (67-81 amino acids [AA] long) and Y domain (36-38 AA long), directly up- and downstream enclosing the HD. Of special interest was that the chephalochordate amphioxus and the jawless ancestral lamprey fish do not have these conserved regions, directly linking these conserved regions to the evolutionary origin of cranial head development of chordates (Shimeld and Donoghue, 2012; Yu, 2010). Blitz and colleagues could also show in *Xenopus tropicalis* (Gray, 1864) that head structures were severely reduced upon loss of *gsc* (Blitz, Fish and Cho, 2016). This could be explained by the function of Gsc, which represses *tbxt* in the early SO. This in fact restricts the expression of *tbxt* to the notochord and thereby separates the axial mesoderm into head and trunk. In the notochord *tbxt* regulates *wnt11*/PCP dependent CE to lengthen the embryo, in comparison to the migratory properties of the *gsc* positive prechordal plate which later forms on cranial structures (Artinger et al., 1997; Latinkić and Smith, 1999; Tada and Smith, 2000). It remains to be seen if this effect is cell autonomous or non-cell autonomous: The inner ear cortical hair cells (stereocilia) in *gsc* knockout (KO) mice were disturbed in a cell non-autonomous way, while in the animal cap assays the Dsh localization was disturbed in an autonomous way. It further remains an open question whether these two identified domains/regions (X and Y) or only one of them are important for the new function of Gsc. It is possible that they interact with or without other factors to repress PCP signaling or that one of them is more of general structural importance to enable this new evolutionary module for Gsc to form the AP and DV axis.

### 3.2 Myo1d: An ancestral effector of the cytoskeleton based mechanism for the LR axis determination

Myo1d is an unconventional ATP dependent actin filament binding Myosin. This motor protein, which is usually important to transport cargo like vesicles along the actin cytoskeleton, was found to have PCP defects but no LR axis defects in rats. This was due to mispolarization of the PCP core component Van Gough like 2 (Vangl2; (Foth, Goedecke and Soldati, 2006; Hegan et al., 2015; Morgan, Heintzelman and Mooseker, 1995; Sokac and Bement, 2000). In this study we showed that *myo1d* LOF leads to LR axis failure in a PCP dependent manner in *X. laevis*. Upon *myo1d* LOF ciliation of the cLRO cells was disturbed (shortened, unpolarized) resulting in an aberrant flow and consequently a bilateral activation of the Nodal signaling cascade. This was also true in fish, speaking for a conserved role of Myo1D as regulator for PCP signaling and overall LR axis determination in vertebrates (Juan et al., 2018). While for vertebrates it has been established that the LR axis is ancestrally broken by a cilia dependent flow mechanism with a downstream nodal signaling cascade, this is not as clear for invertebrates.

Snails and nematodes break the bilateral symmetry very early, during the first and third cleavage respectively. This mechanism is actin/spindle based and results in an asymmetric cell arrangement. In snails this results in the handedness of the shell and the inner organs by nodal activation without a ciliary leftward flow (Abe and Kuroda, 2019; Grande and Patel, 2009; Meshcheryakov and Belousov, 1975; Okumura et al., 2008; Wood, 1991). In snails it involves the actin modulator Diaphanous related formin 1 (*dia1*), and in nematodes the formin homologue CYK-1 and actomyosin flows (Abe and Kuroda, 2019; Naganathan et al., 2014; Pimpale et al., 2020). In comparison to that, the derived embryogenesis of flies includes a syncytium (one cell and up to 12 nuclei), and therefore lost the early mechanism of LR determination. Interestingly in *D. melanogaster*, like in vertebrates, a *myo1d* orthologous gene *myo31DF* and a delayed LR axis mechanism was adapted. The genital plate and the hindgut rotate in a dextral/clockwise manner, which is important for fertility and a right inner organ arrangement (Meshcheryakov and Belousov, 1975; Okumura et al., 2008; Spéder, Adám and Noselli, 2006). Taken together protostomes show an actomyosin based LR axis determination mechanism. A Nodal signaling based mechanism in contrast was shown only for lophotrochozoa (snails) but not for ecdysozoa (nematodes and flies).

Interestingly, a concept in biology called “deep homology”, seems to fit the LR axis determination in bilateria well. It describes the reuse of processes, mechanisms and structures in the development of animals, suggesting an actin based mechanism as ancestral mode for LR axis determination in bilateria (Shubin, Tabin and Carroll, 2009). Vertebrates adapted a cilia/flow/sensor module to the pre-existing actomyosin module for their

development. Remarkably derived vertebrates like the chick do not have a cilia/flow based mechanism. Rather the LRO cells rotate leftward resulting in an asymmetric nodal signaling cascade. This is a cytoskeleton based mechanism, and therefore may be a more ancestral mode of breaking the LR axis symmetry (Davison et al., 2016; Gros et al., 2009; Naganathan et al., 2014; Shibazaki, Shimizu and Kuroda, 2004).

Taken together this work links the actin based LR breakage of protostomes with the adapted cilia/flow/sensor module of deuterostomes. It identifies Myo1d as key component of an actin/cytoskeleton based ancestral LR axis breaking mechanism of bilateria.

### 3.3 Bicc1 as key regulator of LR axis determinants

The critical step during the determination of the LR axis in vertebrates is the flow dependent downregulation of the Nodal antagonist *dand5*. This includes flow-sensing by the cation channel Pkd2 and Ca<sup>2+</sup> spikes. But more downstream effectors which lead to the degradation of *dand5* mRNA are unknown (Schweickert et al., 2017; Takao et al., 2013; Yoshiba et al., 2012; Yuan et al., 2015). In this study we showed that *dand5* is post-transcriptionally regulated through Bicc1. This was shown in *ex vivo* animal cap assays through protein activity as well as *in vivo* on the level of *dand5* and *pitx2* mRNA. Notably, this regulation occurs in a small proximal region of the *dand5* 3'UTR which can be divided into two subregions. These regions were analysed *ex vivo* and *in vivo* with target protector morpholino oligomers (tpMO): small antisense RNA oligomers which bind to a specific mRNA region and thereby prevent the interaction with e.g. RNA binding proteins (Moulton, 2017). The more proximal subregion could be identified as generally important for Bicc1 dependent *dand5* stabilization, while the more distal region seems to be important for Bicc1 dependent downregulation of *dand5* translation. The importance of the proximal 3'UTR of *dand5* as Bicc1 target during LR axis determination was also verified in mouse (Minegishi et al., 2020). It is known that Bicc1 as RNA binding protein regulates mRNA positively as well as negatively in a context dependent manner. Like for *dand5* the exact mechanism of this is poorly understood (Leal-Esteban et al., 2018; Park et al., 2016; Rothé et al., 2020; Tran et al., 2010; Zhang et al., 2013). While there were explanatory approaches through recruiting of e.g. CCR4-NOT (de- acetylation) or homodimerization vs heterodimerization of Bicc1 proteins, there is a strong connection with miRs which was researched in our paper (Chicoine et al., 2007; Minegishi et al., 2020; Piazzon et al., 2012; Rothé et al., 2020). Bicc1 can associate with p-bodies and is involved in the transfer of mature miRs from Dicer to Ago (Lasko, 2012; Maisonneuve et al., 2009; Piazzon et al., 2012). In line with that, LOF of *dicer* led to absence of *pitx2* due to absence of flow induced *dand5* repression/decay and interacted with the LOF of *bicc1*. As prerequisite of a miR induced repression, UTRs of mRNAs are normally searched for evolutionary conserved seed sequences, which are

essential for miR binding (Bartel, 2018). But conserved seed sequences are rare among the 3'UTRs of vertebrate *dand5*, which may be attributed to the fact that Dand5 proteins and orthologs are very different - not only on the level of base pairs of both the UTRs and the coding sequence, but also on the AA level (Human to mouse 62% AA identity; human to *X. laevis* just 34%). We also showed that *dand5* mRNA degradation *in vivo* as well as Bicc1 dependent translational repression *ex vivo* is Pkd2, supposable  $Ca^{2+}$ , dependent. Interestingly Bicc1 and Pkd2 act together in the kidney too, an interaction also involving miRs (Piazzon et al., 2012; Tran et al., 2010). Bicc1 can be functionally changed through phosphorylation in other contexts which could also be the case in LR axis determination. Remarkably Bicc1 is also phosphorylated through  $Ca^{2+}$ /calmodulin-dependent protein kinase II (CaMK II), which is also a downstream target of Pkd2 in the LPM (Bernet, 2015; Hara et al., 2018). Such a functional change of Bicc1 can be the switch from stabilization to the translational repression of *dand5* triggered by the flow induced  $Ca^{2+}$  signal. Therefore this could happen through the two subregions of the proximal *dand5* 3'UTR. This is also in line with the described *dand5* mRNA translocalization in the left sLRO cells in post-flow stages, as RNA translocalization often means a change of translational manner and/or protein destination (Hesketh, 1996; Keene, 2007; Nakamura et al., 2012; Simmonds et al., 2001; Wilhelm and Vale, 1993). Additionally to the Bicc1 dependent regulation of *dand5*, *nodal1* is stabilized by Bicc1 too. Interestingly, in contrast to the direct regulation of *dand5*, this is an indirect regulation through *gdf3*. Like *dand5*, *gdf3* is regulated through its 3'UTR, which is necessary for the *nodal1* expression in the sLRO cells and the transfer and activation of the Nodal signaling cascade in the left LPM (Pelliccia, Jindal and Burdine, 2017; Rankin et al., 2000; Vonica et al., 2011; Vonica and Brivanlou, 2007). Notably, miRs are also important to control various steps of Nodal signaling, which could be important for this function of Bicc1 too (Martello et al., 2007; Syeda, Kirchhof and Fabritz, 2017). Our data leads to a model where Bicc1 secures an inhibition of the Nodal signaling cascade prior to flow through securing *dand5* expression and regulating *nodal1* through *gdf3*. Then the leftward fluid flow triggers a Pkd2 dependent  $Ca^{2+}$  signal and CaMK II phosphorylates Bicc1. This leads to a functional change of Bicc1 resulting in translocation, translational repression and degradation of *dand5*. The de-repressed Nodal1 is then transmitted to the left LPM and starts the Nodal signaling cascade. Whether this involves miRs or Dicer interacts in a non-canonical mechanism can only be answered with further studies (Pong and Gullerova, 2018).

While protostomes seem to lack *dand5*, deuterostomes have recruited *dand5* to their Nodal module. Additionally, the mechanism of an asymmetric regulation of an antagonist of the Nodal signaling cascade to break LR symmetry is incorporated into the development of deuterostomes (Kenny et al., 2014; Namigai, Kenny and Shimeld, 2014; Tisler et al., 2016). For this mechanism, a repressor of the antagonist Dand5 was obligatory: Bicc1. This study

and the Hamada lab could show that *Bicc1*'s function is evolutionary conserved at least in tetrapoda, but most likely beyond together with the need of a tightly controlled *Dand5* (Minegishi et al., 2020).

#### **3.4 Conclusion**

The purpose of these comprehensive studies was to functionally characterize the genes *myo1d* and *bicc1* for their role in the LR body axis and *gsc* for its role in the AP and DV body axes development in vertebrates. These functions were also set in an evolutionary context of newly adapted mechanisms.

The transcriptional repressor *Gsc*, which is expressed in the primary embryonic organizer, was mainly known for its ability to induce a secondary axis across the animal kingdom. In this study, a novel function of *Gsc* (regulating Wnt/PCP signaling) was discovered in vertebrates. It was also successfully mapped to two newly discovered *Gsc* sequences/domains, which are conserved in vertebrates.

In case of *Myosin1d* it was shown that novel functions to determine LR axis development often rely on modifications of pre-existing mechanisms. Therefore the actin based motor protein and an actomyosin mechanism for LR axis determination was adapted to the newly evolved cilia/flow based mechanism breaking LR symmetry.

The RNA binding protein *Bicc1* was initially described as an important factor for PCP/Wnt dependent polarization of cLRO cilia in regards to the LR axis determination. In this study *Bicc1* was re-evaluated describing a novel function regulating LRO determinants in sLRO cells, connecting *Bicc1* to several important key factors during LR axis determination. This highlights the importance of a tightly controlled *Dand5* level during LR breakage.

## References

- Abe, M; Kuroda, R. (2019): The development of CRISPR for a mollusc establishes the formin *Lsdia1* as the long-sought gene for snail dextral/sinistral coiling. *Development* **146**.
- Agrawal, R; Tran, U; Wessely, O. (2009): The miR-30 miRNA family regulates *Xenopus* pronephros development and targets the transcription factor *Xlim1/Lhx1*. *Development* **136**: 3927–3936.
- Ahrens, M.J; Li, Y; Jiang, H; Dudley, A.T. (2009): Convergent extension movements in growth plate chondrocytes require *gpi*-anchored cell surface proteins. *Development* **136**: 3463–3474.
- Antic, D; Stubbs, J.L; Suyama, K; Kintner, C; Scott, M.P; Axelrod, J.D. (2010): Planar cell polarity enables posterior localization of nodal cilia and left-right axis determination during mouse and *Xenopus* embryogenesis. *PLoS one* **5**: e8999.
- Artinger, M; Blitz, I; Inoue, K; Tran, U; Cho, K.W. (1997): Interaction of *gooseoid* and *brachyury* in *Xenopus* mesoderm patterning. *Mechanisms of Development* **65**: 187–196.
- Assoian, R.K; Komoriya, A; Meyers, C.A; Miller, D.M; Sporn, M.B. (1983): Transforming growth factor-beta in human platelets. Identification of a major storage site, purification, and characterization. *Journal of Biological Chemistry* **258**: 7155–7160.
- Axelrod, J.D; Miller, J.R; Shulman, J.M; Moon, R.T; Perrimon, N. (1998): Differential recruitment of *Dishevelled* provides signaling specificity in the planar cell polarity and *Wingless* signaling pathways. *Genes & development* **12**: 2610–2622.
- Babiarz, J.E; Ruby, J.G; Wang, Y; Bartel, D.P; Blelloch, R. (2008): Mouse ES cells express endogenous shRNAs, siRNAs, and other Microprocessor-independent, Dicer-dependent small RNAs. *Genes & development* **22**: 2773–2785.
- Bae, S; Reid, C.D; Kessler, D.S. (2011): *Siamois* and *Twin* are redundant and essential in formation of the Spemann organizer. *Developmental biology* **352**: 367–381.
- Bartel, D.P. (2018): Metazoan MicroRNAs. *Cell* **173**: 20–51.
- Becker, K; Bluhm, A; Casas-Vila, N; Dinges, N; Dejung, M; Sayols, S; Kreutz, C; Roignant, J.-Y; Butter, F; Legewie, S. (2018): Quantifying post-transcriptional regulation in the development of *Drosophila melanogaster*. *Nature communications* **9**: 4970.
- Bellaïche, Y; Gho, M; Kaltschmidt, J.A; Brand, A.H; Schweisguth, F. (2001): *Frizzled* regulates localization of cell-fate determinants and mitotic spindle rotation during asymmetric cell division. *Nature cell biology* **3**: 50–57.
- Bell, E; Muñoz-Sanjuán, I; Altmann, C.R; Vonica, A; Brivanlou, A.H. (2003): Cell fate specification and competence by *Coco*, a maternal BMP, TGFbeta and Wnt inhibitor. *Development* **130**: 1381–1389.
- Belo, J.A; Bouwmeester, T; Leyns, L; Kertesz, N; Gallo, M; Follettie, M; Robertis, E.M. de (1997): *Cerberus-like* is a secreted factor with neuralizing activity expressed in the anterior primitive endoderm of the mouse gastrula. *Mechanisms of Development* **68**: 45–57.
- Bénazéraf, B; Pourquié, O. (2013): Formation and segmentation of the vertebrate body axis. *Annual review of cell and developmental biology* **29**: 1–26.



- Bernet, F.U. (2015): Regulation of the mRNA silencing activity of Bicaudal-C. *Swiss*.
- Bilic, J; Huang, Y.-L; Davidson, G; Zimmermann, T; Cruciat, C.-M; Bienz, M; Niehrs, C. (2007): Wnt induces LRP6 signalosomes and promotes dishevelled-dependent LRP6 phosphorylation. *Science* **316**: 1619–1622.
- Bisgrove, B.W; Snarr, B.S; Emrazian, A; Yost, H.J. (2005): Polaris and Polycystin-2 in dorsal forerunner cells and Kupffer's vesicle are required for specification of the zebrafish left-right axis. *Developmental biology* **287**: 274–288.
- Blitz, I.L; Fish, M.B; Cho, K.W.Y. (2016): Leapfrogging: primordial germ cell transplantation permits recovery of CRISPR/Cas9-induced mutations in essential genes. *Development (Cambridge, England)* **143**: 2868–2875.
- Blumberg, B; Wright, C.V; Robertis, E.M. de; Cho, K.W. (1991): Organizer-specific homeobox genes in *Xenopus laevis* embryos. *Science* **253**: 194–196.
- Blum, M; Gaunt, S.J; Cho, K.W; Steinbeisser, H; Blumberg, B; Bittner, D; Robertis, E.M. de (1992): Gastrulation in the mouse The role of the homeobox gene goosecoid. *Cell* **69**: 1097–1106.
- Blum, M; Andre, P; Muders, K; Schweickert, A; Fischer, A; Bitzer, E; Bogusch, S; Beyer, T; van Straaten, Henny W M; Viebahn, C. (2007): Ciliation and gene expression distinguish between node and posterior notochord in the mammalian embryo. *Differentiation; research in biological diversity* **75**: 133–146.
- Blum, M; Schweickert, A; Vick, P; Wright, C.V.E; Danilchik, M.V. (2014a): Symmetry breakage in the vertebrate embryo: when does it happen and how does it work? *Developmental biology* **393**: 109–123.
- Blum, M; Feistel, K; Thumberger, T; Schweickert, A. (2014b): The evolution and conservation of left-right patterning mechanisms. *Development* **141**: 1603–1613.
- Blum, M; Robertis, E.M. de; Wallingford, J.B; Niehrs, C. (2015): Morpholinos: Antisense and Sensibility. *Developmental Cell* **35**: 145–149.
- Blum, M; Ott, T. (2018a): Animal left-right asymmetry. *Current Biology* **28**: R301-R304.
- Blum, M; Ott, T. (2018b): The Power of Strain: Organizing Left-Right Cilia. *Developmental Cell* **45**: 277–279.
- Blum, M; Ott, T. (2018c): *Xenopus*: An Undervalued Model Organism to Study and Model Human Genetic Disease. *Cells, tissues, organs* **205**: 303–313.
- Bolker, J.A. (1993): Gastrulation and mesoderm morphogenesis in the white sturgeon. *The Journal of experimental zoology* **266**: 116–131.
- Boorman, C.J; Shimeld, S.M. (2002): The evolution of left-right asymmetry in chordates. *BioEssays: news and reviews in molecular, cellular and developmental biology* **24**: 1004–1011.
- Boskovski, M.T; Yuan, S; Pedersen, N.B; Goth, C.K; Makova, S; Clausen, H; Brueckner, M; Khokha, M.K. (2013): The heterotaxy gene GALNT11 glycosylates Notch to orchestrate cilia type and laterality. *Nature* **504**: 456–459.

Boucher, D.M; Schäffer, M; Deissler, K; Moore, C.A; Gold, J.D; Burdsal, C.A; Meneses, J.J; Pedersen, R.A;

Blum, M. (2000): goosecoid expression represses Brachyury in embryonic stem cells and affects craniofacial development in chimeric mice. *The International journal of developmental biology* **44**: 279–288.

Bowes, J.B; Snyder, K.A; Segerdell, E; Jarabek, C.J; Azam, K; Zorn, A.M; Vize, P.D. (2010): Xenbase: gene expression and improved integration. *Nucleic acids research* **38**: D607-12.

Brannon, M; Gomperts, M; Sumoy, L; Moon, R.T; Kimelman, D. (1997): A beta-catenin/XTcf-3 complex binds to the siamois promoter to regulate dorsal axis specification in *Xenopus*. *Genes & development* **11**: 2359–2370.

Bregues, M; Teixeira, D; Parker, R. (2005): Movement of eukaryotic mRNAs between polysomes and cytoplasmic processing bodies. *Science* **310**: 486–489.

Broun, M; Sokol, S; Bode, H.R. (1999): Cngsc, a homologue of goosecoid, participates in the patterning of the head, and is expressed in the organizer region of Hydra. *Development* **126**: 5245–5254.

Bryja, V; Andersson, E.R; Schambony, A; Esner, M; Bryjová, L; Biris, K.K; Hall, A.C; Kraft, B; Cajanek, L; Yamaguchi, T.P; Buckingham, M; Arenas, E. (2009): The extracellular domain of Lrp5/6 inhibits noncanonical Wnt signaling in vivo. *Molecular biology of the cell* **20**: 924–936.

Burt, D.W. (1992): Evolutionary grouping of the transforming growth factor- $\beta$  superfamily. *Biochemical and Biophysical Research Communications* **184**: 590–595.

Burt, D.W; Law, A.S. (1994): Evolution of the transforming growth factor-beta superfamily. *Progress in Growth Factor Research* **5**: 99–118.

Cai, X; Hagedorn, C.H; Cullen, B.R. (2004): Human microRNAs are processed from capped, polyadenylated transcripts that can also function as mRNAs. *RNA* **10**: 1957–1966.

Campbell, E.P; Quigley, I.K; Kintner, C. (2016): Foxn4 promotes gene expression required for the formation of multiple motile cilia. *Development* **143**: 4654–4664.

Carreira-Barbosa, F; Concha, M.L; Takeuchi, M; Ueno, N; Wilson, S.W; Tada, M. (2003): Prickle 1 regulates cell movements during gastrulation and neuronal migration in zebrafish. *Development* **130**: 4037–4046.

Chen, J.-F; Mandel, E.M; Thomson, J.M; Wu, Q; Callis, T.E; Hammond, S.M; Conlon, F.L; Wang, D.-Z. (2006): The role of microRNA-1 and microRNA-133 in skeletal muscle proliferation and differentiation. *Nature genetics* **38**: 228–233.

Chicoine, J; Benoit, P; Gamberi, C; Paliouras, M; Simonelig, M; Lasko, P. (2007): Bicaudal-C recruits CCR4-NOT deadenylase to target mRNAs and regulates oogenesis, cytoskeletal organization, and its own expression. *Developmental Cell* **13**: 691–704.

Chien, Y.-H; Srinivasan, S; Keller, R; Kintner, C. (2018): Mechanical Strain Determines Cilia Length, Motility, and Planar Position in the Left-Right Organizer. *Developmental Cell* **45**: 316-330.e4.

- Cho, K.W; Blumberg, B; Steinbeisser, H; Robertis, E.M. de (1991): Molecular nature of Spemann's organizer The role of the *Xenopus* homeobox gene goosecoid. *Cell* **67**: 1111–1120.
- Christian, J.L; Moon, R.T. (1993): Interactions between Xwnt-8 and Spemann organizer signaling pathways generate dorsoventral pattern in the embryonic mesoderm of *Xenopus*. *Genes & development* **7**: 13–28.
- Clements, D; Taylor, H.C; Herrmann, B.G; Stott, D. (1996): Distinct regulatory control of the Brachyury gene in axial and non-axial mesoderm suggests separation of mesoderm lineages early in mouse gastrulation. *Mechanisms of Development* **56**: 139–149.
- Conlon, F.L; Smith, J.C. (1999): Interference with brachyury function inhibits convergent extension, causes apoptosis, and reveals separate requirements in the FGF and activin signalling pathways. *Developmental biology* **213**: 85–100.
- Coutelis, J.-B; González-Morales, N; Géminard, C; Noselli, S. (2014): Diversity and convergence in the mechanisms establishing L/R asymmetry in metazoa. *EMBO reports* **15**: 926–937.
- Danilov, V; Blum, M; Schweickert, A; Campione, M; Steinbeisser, H. (1998): Negative autoregulation of the organizer-specific homeobox gene goosecoid. *The Journal of biological chemistry* **273**: 627–635.
- Davidson, L.A; Keller, R.E. (1999): Neural tube closure in *Xenopus laevis* involves medial migration, directed protrusive activity, cell intercalation and convergent extension. *Development* **126**: 4547–4556.
- Davison, A; McDowell, G.S; Holden, J.M; Johnson, H.F; Koutsovoulos, G.D; Liu, M.M; Hulpiau, P; van Roy, F; Wade, C.M; Banerjee, R; Yang, F; Chiba, S; Davey, J.W; Jackson, D.J; Levin, M; Blaxter, M.L. (2016): Formin Is Associated with Left-Right Asymmetry in the Pond Snail and the Frog. *Current Biology* **26**: 654–660.
- Dickmeis, T; Aanstad, P; Clark, M; Fischer, N; Herwig, R; Mourrain, P; Blader, P; Rosa, F; Lehrach, H; Strähle, U. (2001): Identification of nodal signaling targets by array analysis of induced complex probes. *Developmental dynamics* **222**: 571–580.
- Dixon Fox, M; Bruce, A.E.E. (2009): Short- and long-range functions of Goosecoid in zebrafish axis formation are independent of Chordin, Noggin 1 and Follistatin-like 1b. *Development* **136**: 1675–1685.
- Dobin, A; Davis, C.A; Schlesinger, F; Drenkow, J; Zaleski, C; Jha, S; Batut, P; Chaisson, M; Gingeras, T.R. (2013): STAR: ultrafast universal RNA-seq aligner. *Bioinformatics* **29**: 15–21.
- Domingo, C; Keller, R. (1995): Induction of notochord cell intercalation behavior and differentiation by progressive signals in the gastrula of *Xenopus laevis*. *Development* **121**: 3311–3321.
- Duncan, A.R; Khokha, M.K. (2016): *Xenopus* as a model organism for birth defects Congenital heart disease and heterotaxy. *Seminars in cell & developmental biology* **51**: 73–79.
- Durston, A.J. (2015): Time, space and the vertebrate body axis. *Seminars in cell & developmental biology* **42**: 66–77.
- Eastman, Q; Grosschedl, R. (1999): Regulation of LEF-1/TCF transcription factors by Wnt and other signals. *Current Opinion in Cell Biology* **11**: 233–240.

- Edlund, A.F; Davidson, L.A; Keller, R.E. (2013): Cell segregation, mixing, and tissue pattern in the spinal cord of the *Xenopus laevis* neurula. *Developmental dynamics* **242**: 1134–1146.
- Eimon, P.M; Harland, R.M. (2002): Effects of heterodimerization and proteolytic processing on *Derrière* and *Nodal* activity: implications for mesoderm induction in *Xenopus*. *Development* **129**: 3089–3103.
- Elinson, R.P; Rowning, B. (1988): A transient array of parallel microtubules in frog eggs Potential tracks for a cytoplasmic rotation that specifies the dorso-ventral axis. *Developmental biology* **128**: 185–197.
- Ewald, A.J; Peyrot, S.M; Tyszka, J.M; Fraser, S.E; Wallingford, J.B. (2004): Regional requirements for Dishevelled signaling during *Xenopus* gastrulation: separable effects on blastopore closure, mesendoderm internalization and archenteron formation. *Development* **131**: 6195–6209.
- Fainsod, A; Steinbeisser, H; Robertis, E.M. de (1994): On the function of BMP-4 in patterning the marginal zone of the *Xenopus* embryo. *The EMBO Journal* **13**: 5015–5025.
- Fan, M.J; Sokol, S.Y. (1997): A role for *Siamois* in Spemann organizer formation. *Development* **124**: 2581–2589.
- Faure, S; Lee, M.A; Keller, T; Dijke, P. ten; Whitman, M. (2000): Endogenous patterns of TGFbeta superfamily signaling during early *Xenopus* development. *Development* **127**: 2917–2931.
- Feiguin, F; Hannus, M; Mlodzik, M; Eaton, S. (2001): The Ankyrin Repeat Protein Diego Mediates Frizzled-Dependent Planar Polarization. *Developmental Cell* **1**: 93–101.
- Fernandez-Gonzalez, R; Simoes, S.d.M; Röper, J.-C; Eaton, S; Zallen, J.A. (2009): Myosin II dynamics are regulated by tension in intercalating cells. *Developmental Cell* **17**: 736–743.
- Ferreiro, B; Artinger, M; Cho, K; Niehrs, C. (1998): Antimorphic goosecooids. *Development* **125**: 1347–1359.
- Fletcher, R.B; Baker, J.C; Harland, R.M. (2006): FGF8 spliceforms mediate early mesoderm and posterior neural tissue formation in *Xenopus*. *Development* **133**: 1703–1714.
- Foth, B.J; Goedecke, M.C; Soldati, D. (2006): New insights into myosin evolution and classification. *Proceedings of the National Academy of Sciences of the United States of America* **103**: 3681–3686.
- Francescato, L; Rothschild, S.C; Myers, A.L; Tombes, R.M. (2010): The activation of membrane targeted CaMK-II in the zebrafish Kupffer's vesicle is required for left-right asymmetry. *Development* **137**: 2753–2762.
- Funa, N.S; Schachter, K.A; Lerdrup, M; Ekberg, J; Hess, K; Dietrich, N; Honoré, C; Hansen, K; Semb, H. (2015):  $\beta$ -Catenin Regulates Primitive Streak Induction through Collaborative Interactions with SMAD2/SMAD3 and OCT4. *Cell stem cell* **16**: 639–652.
- Gans, C; Northcutt, R.G. (1983): Neural crest and the origin of vertebrates: a new head. *Science* **220**: 268–273.
- Gan, X.-q; Wang, J.-y; Xi, Y; Wu, Z.-l; Li, Y.-p; Li, L. (2008): Nuclear Dvl, c-Jun, beta-catenin, and TCF form a complex leading to stabilization of beta-catenin-TCF interaction. *The Journal of cell biology* **180**: 1087–1100.

- Gao, B; Song, H; Bishop, K; Elliot, G; Garrett, L; English, M.A; Andre, P; Robinson, J; Sood, R; Minami, Y; Economides, A.N; Yang, Y. (2011): Wnt signaling gradients establish planar cell polarity by inducing Vangl2 phosphorylation through Ror2. *Developmental Cell* **20**: 163–176.
- Gao, C; Chen, Y.-G. (2010): Dishevelled: The hub of Wnt signaling. *Cellular signalling* **22**: 717–727.
- Gaunt, S.J; Blum, M; Robertis, E.M. de (1993): Expression of the mouse goosecoid gene during mid-embryogenesis may mark mesenchymal cell lineages in the developing head, limbs and body wall. *Development* **117**: 769–778.
- Gawantka, V; Delius, H; Hirschfeld, K; Blumenstock, C; Niehrs, C. (1995): Antagonizing the Spemann organizer Role of the homeobox gene Xvent-1. *The EMBO Journal* **14**: 6268–6279.
- Gerhart, J. (1999): Pieter Nieuwkoop's contributions to the understanding of meso-endoderm induction and neural induction in chordate development. *The International journal of developmental biology* **43**: 605–613.
- Germain, S; Howell, M; Esslemont, G.M; Hill, C.S. (2000): Homeodomain and winged-helix transcription factors recruit activated Smads to distinct promoter elements via a common Smad interaction motif. *Genes & development* **14**: 435–451.
- Gilbert, S.F., Barresi, M.J.F. (2020): *Developmental biology*, International twelfth edition ed.
- Giraldez, A.J; Cinalli, R.M; Glasner, M.E; Enright, A.J; Thomson, J.M; Baskerville, S; Hammond, S.M; Bartel, D.P; Schier, A.F. (2005): MicroRNAs regulate brain morphogenesis in zebrafish. *Science* **308**: 833–838.
- Giraldez, A.J; Mishima, Y; Rihel, J; Grocock, R.J; van Dongen, S; Inoue, K; Enright, A.J; Schier, A.F. (2006): Zebrafish MiR-430 promotes deadenylation and clearance of maternal mRNAs. *Science* **312**: 75–79.
- González-Morales, N; Géminard, C; Lebreton, G; Cerezo, D; Coutelis, J.-B; Noselli, S. (2015): The Atypical Cadherin Dachsh Controls Left-Right Asymmetry in *Drosophila*. *Developmental Cell* **33**: 675–689.
- Goriely, A; Stella, M; Coffinier, C; Kessler, D; Mailhos, C; Dessain, S; Desplan, C. (1996): A functional homologue of goosecoid in *Drosophila*. *Development* **122**: 1641–1650.
- Gorny, A.-K; Steinbeisser, H. (2012): Brachet's cleft: a model for the analysis of tissue separation in *Xenopus*. *Wiley interdisciplinary reviews. Developmental biology* **1**: 294–300.
- Goto, T; Keller, R. (2002): The planar cell polarity gene strabismus regulates convergence and extension and neural fold closure in *Xenopus*. *Developmental biology* **247**: 165–181.
- Grande, C; Patel, N.H. (2009): Nodal signalling is involved in left-right asymmetry in snails. *Nature* **457**: 1007–1011.
- Grimes, D.T; Burdine, R.D. (2017): Left-Right Patterning: Breaking Symmetry to Asymmetric Morphogenesis. *Trends in genetics* **33**: 616–628.
- Gros, J; Feistel, K; Viebahn, C; Blum, M; Tabin, C.J. (2009): Cell movements at Hensen's node establish left/right asymmetric gene expression in the chick. *Science* **324**: 941–944.

- Gros, J; Hu, J.K.-H; Vinegoni, C; Feruglio, P.F; Weissleder, R; Tabin, C.J. (2010): WNT5A/JNK and FGF/MAPK pathways regulate the cellular events shaping the vertebrate limb bud. *Current Biology* **20**: 1993–2002.
- Gubb, D; Green, C; Huen, D; Coulson, D; Johnson, G; Tree, D; Collier, S; Roote, J. (1999): The balance between isoforms of the prickle LIM domain protein is critical for planar polarity in *Drosophila* imaginal discs. *Genes & development* **13**: 2315–2327.
- Guimier, A; Gabriel, G.C; Bajolle, F; Tsang, M; Liu, H; Noll, A; Schwartz, M; El Malti, R; Smith, L.D; Klena, N.T; Jimenez, G; Miller, N.A; Oufadem, M; Moreau de Bellaing, A; Yagi, H; Saunders, C.J; Baker, C.N; Di Filippo, S; Peterson, K.A; Thiffault, I; Bole-Feysot, C; Cooley, L.D; Farrow, E.G; Masson, C; Schoen, P; Deleuze, J.-F; Nitschké, P; Lyonnet, S; Pontual, L. de; Murray, S.A; Bonnet, D; Kingsmore, S.F; Amiel, J; Bouvagnet, P; Lo, C.W; Gordon, C.T. (2015): MMP21 is mutated in human heterotaxy and is required for normal left-right asymmetry in vertebrates. *Nature genetics* **47**: 1260–1263.
- Habas, R; Kato, Y; He, X. (2001): Wnt/Frizzled Activation of Rho Regulates Vertebrate Gastrulation and Requires a Novel Formin Homology Protein Daam1. *Cell* **107**: 843–854.
- Hamada, H; Tam, P. (2020): Diversity of left-right symmetry breaking strategy in animals. *F1000Research* **9**.
- Hara, M; Lourido, S; Petrova, B; Lou, H.J; Stetina, J.R. von; Kashevsky, H; Turk, B.E; Orr-Weaver, T.L. (2018): Identification of PNG kinase substrates uncovers interactions with the translational repressor TRAL in the oocyte-to-embryo transition. *eLife* **7**.
- Hardin, J; Keller, R. (1988): The behaviour and function of bottle cells during gastrulation of *Xenopus laevis*. *Development* **103**: 211–230.
- Harfe, B.D; McManus, M.T; Mansfield, J.H; Hornstein, E; Tabin, C.J. (2005): The RNaseIII enzyme Dicer is required for morphogenesis but not patterning of the vertebrate limb. *Proceedings of the National Academy of Sciences of the United States of America* **102**: 10898–10903.
- Hartwell, K.A; Muir, B; Reinhardt, F; Carpenter, A.E; Sgroi, D.C; Weinberg, R.A. (2006): The Spemann organizer gene, *Goosecoid*, promotes tumor metastasis. *Proceedings of the National Academy of Sciences of the United States of America* **103**: 18969–18974.
- Hegan, P.S; Ostertag, E; Geurts, A.M; Mooseker, M.S. (2015): Myosin Id is required for planar cell polarity in ciliated tracheal and ependymal epithelial cells. *Cytoskeleton* **72**: 503–516.
- Hesketh, J.E. (1996): Sorting of messenger RNAs in the cytoplasm: mRNA localization and the cytoskeleton. *Experimental cell research* **225**: 219–236.
- He, X; Saint-Jeannet, J.P; Woodgett, J.R; Varmus, H.E; Dawid, I.B. (1995): Glycogen synthase kinase-3 and dorsoventral patterning in *Xenopus* embryos. *Nature* **374**: 617–622.
- He, X; Semenov, M; Tamai, K; Zeng, X. (2004): LDL receptor-related proteins 5 and 6 in Wnt/beta-catenin signaling: arrows point the way. *Development* **131**: 1663–1677.
- Hikasa, H; Sokol, S.Y. (2013): Wnt signaling in vertebrate axis specification. *Cold Spring Harbor perspectives in biology* **5**: a007955.



- Hojo, M; Takashima, S; Kobayashi, D; Sumeragi, A; Shimada, A; Tsukahara, T; Yokoi, H; Narita, T; Jindo, T; Kage, T; Kitagawa, T; Kimura, T; Sekimizu, K; Miyake, A; Setiamarga, D; Murakami, R; Tsuda, S; Ooki, S; Kakihara, K; Naruse, K; Takeda, H. (2007): Right-elevated expression of charon is regulated by fluid flow in medaka Kupffer's vesicle. *Development, growth & differentiation* **49**: 395–405.
- Houliston, E; Elinson, R.P. (1991): Patterns of microtubule polymerization relating to cortical rotation in *Xenopus laevis* eggs. *Development* **112**: 107–117.
- Hozumi, S; Maeda, R; Taniguchi, K; Kanai, M; Shirakabe, S; Sasamura, T; Spéder, P; Noselli, S; Aigaki, T; Murakami, R; Matsuno, K. (2006): An unconventional myosin in *Drosophila* reverses the default handedness in visceral organs. *Nature* **440**: 798–802.
- Hubstenberger, A; Courel, M; Bénard, M; Souquere, S; Ernoult-Lange, M; Chouaib, R; Yi, Z; Morlot, J.-B; Munier, A; Fradet, M; Daunesse, M; Bertrand, E; Pierron, G; Mozziconacci, J; Kress, M; Weil, D. (2017): P-Body Purification Reveals the Condensation of Repressed mRNA Regulons. *Molecular Cell* **68**: 144-157.e5.
- Jaffe, A.B; Hall, A. (2005): Rho GTPases: biochemistry and biology. *Annual review of cell and developmental biology* **21**: 247–269.
- Jiménez, G; Verrijzer, C.P; Ish-Horowicz, D. (1999): A conserved motif in goosecoid mediates groucho-dependent repression in *Drosophila* embryos. *Molecular and cellular biology* **19**: 2080–2087.
- Jones-Rhoades, M.W; Bartel, D.P; Bartel, B. (2006): MicroRNAs and their regulatory roles in plants. *Annual review of plant biology* **57**: 19–53.
- Juan, T; Géminard, C; Coutelis, J.-B; Cerezo, D; Polès, S; Noselli, S; Fürthauer, M. (2018): Myosin1D is an evolutionarily conserved regulator of animal left-right asymmetry. *Nature communications* **9**: 1942.
- Kantarci, H; Gerberding, A; Riley, B.B. (2016): Spemann organizer gene Goosecoid promotes delamination of neuroblasts from the otic vesicle. *Proceedings of the National Academy of Sciences of the United States of America* **113**: E6840-E6848.
- Karpinka, J.B; Fortriede, J.D; Burns, K.A; James-Zorn, C; Ponferrada, V.G; Lee, J; Karimi, K; Zorn, A.M; Vize, P.D. (2015): Xenbase, the *Xenopus* model organism database; new virtualized system, data types and genomes. *Nucleic acids research* **43**: D756-63.
- Keene, J.D. (2007): RNA regulons: coordination of post-transcriptional events. *Nature reviews. Genetics* **8**: 533–543.
- Keller, J.B; Miksis, M. (1980): Bubble oscillations of large amplitude. *The Journal of the Acoustical Society of America* **68**: 628–633.
- Keller, P.J; Schmidt, A.D; Wittbrodt, J; Stelzer, E.H.K. (2008): Reconstruction of zebrafish early embryonic development by scanned light sheet microscopy. *Science* **322**: 1065–1069.
- Keller, R; Tibbetts, P. (1989): Mediolateral cell intercalation in the dorsal, axial mesoderm of *Xenopus laevis*. *Developmental biology* **131**: 539–549.
- Keller, R; Winklbauer, R. (1992): Cellular basis of amphibian gastrulation. *Current topics in developmental biology* **27**: 39–89.

- Keller, R; Davidson, L; Edlund, A; Elul, T; Ezin, M; Shook, D; Skoglund, P. (2000): Mechanisms of convergence and extension by cell intercalation. *Philosophical transactions of the Royal Society of London. Series B, Biological sciences* **355**: 897–922.
- Keller, R; Shook, D; Skoglund, P. (2008): The forces that shape embryos: physical aspects of convergent extension by cell intercalation. *Physical biology* **5**: 15007.
- Keller, R.E; Schoenwolf, G.C. (1977): An SEM study of cellular morphology, contact, and arrangement, as related to gastrulation in *Xenopus laevis*. *Wilhelm Roux's archives of developmental biology* **182**: 165–186.
- Kelly, M; Chen, P. (2007): Shaping the mammalian auditory sensory organ by the planar cell polarity pathway. *The International journal of developmental biology* **51**: 535–547.
- Kenny, N.J; Namigai, E.K.O; Dearden, P.K; Hui, J.H.L; Grande, C; Shimeld, S.M. (2014): The Lophotrochozoan TGF- $\beta$  signalling cassette - diversification and conservation in a key signalling pathway. *The International journal of developmental biology* **58**: 533–549.
- Khokha, M.K; Chung, C; Bustamante, E.L; Gaw, L.W.K; Trott, K.A; Yeh, J; Lim, N; Lin, J.C.Y; Taverner, N; Amaya, E; Papalopulu, N; Smith, J.C; Zorn, A.M; Harland, R.M; Grammer, T.C. (2002): Techniques and probes for the study of *Xenopus tropicalis* development. *Developmental dynamics* **225**: 499–510.
- Kiecker, C; Niehrs, C. (2001): A morphogen gradient of Wnt/beta-catenin signalling regulates anteroposterior neural patterning in *Xenopus*. *Development* **128**: 4189–4201.
- Kimelman, D; Xu, W. (2006): beta-catenin destruction complex: insights and questions from a structural perspective. *Oncogene* **25**: 7482–7491.
- Kirsch, K; Zeke, A; Tőke, O; Sok, P; Sethi, A; Sebő, A; Kumar, G.S; Egri, P; Póti, Á.L; Gooley, P; Peti, W; Bento, I; Alexa, A; Reményi, A. (2020): Co-regulation of the transcription controlling ATF2 phosphoswitch by JNK and p38. *Nature communications* **11**: 5769.
- Komiya, Y; Habas, R. (2008): Wnt signal transduction pathways. *Organogenesis* **4**: 68–75.
- Koos, D.S; Ho, R.K. (1998): The *nieuwkoid* gene characterizes and mediates a *Nieuwkoop*-center-like activity in the zebrafish. *Current Biology* **8**: 1199–1206.
- Kubo, H; Shiga, K; Harada, Y; Iwao, Y. (2010): Analysis of a sperm surface molecule that binds to a vitelline envelope component of *Xenopus laevis* eggs. *Molecular reproduction and development* **77**: 728–735.
- Kühl, M; Geis, K; Sheldahl, L.C; Pukrop, T; Moon, R.T; Wedlich, D. (2001): Antagonistic regulation of convergent extension movements in *Xenopus* by Wnt/ $\beta$ -catenin and Wnt/Ca<sup>2+</sup> signaling. *Mechanisms of Development* **106**: 61–76.
- Kulkarni, M; Ozgur, S; Stoecklin, G. (2010): On track with P-bodies. *Biochemical Society transactions* **38**: 242–251.
- Kwan, K.M; Kirschner, M.W. (2003): *Xbra* functions as a switch between cell migration and convergent extension in the *Xenopus* gastrula. *Development* **130**: 1961–1972.

- Larabell, C.A; Torres, M; Rowning, B.A; Yost, C; Miller, J.R; Wu, M; Kimelman, D; Moon, R.T. (1997): Establishment of the dorso-ventral axis in *Xenopus* embryos is presaged by early asymmetries in beta-catenin that are modulated by the Wnt signaling pathway. *The Journal of cell biology* **136**: 1123–1136.
- Lartillot, N; Le Gouar, M; Adoutte, A. (2002): Expression patterns of fork head and goosecoid homologues in the mollusc *Patella vulgata* supports the ancestry of the anterior mesendoderm across Bilateria. *Development genes and evolution* **212**: 551–561.
- Lasko, P. (2012): mRNA localization and translational control in *Drosophila* oogenesis. *Cold Spring Harbor perspectives in biology* **4**.
- Latinkić, B.V; Umbhauer, M; Neal, K.A; Lerchner, W; Smith, J.C; Cunliffe, V. (1997): The *Xenopus* Brachyury promoter is activated by FGF and low concentrations of activin and suppressed by high concentrations of activin and by paired-type homeodomain proteins. *Genes & development* **11**: 3265–3276.
- Latinkić, B.V; Smith, J.C. (1999): Goosecoid and mix.1 repress Brachyury expression and are required for head formation in *Xenopus*. *Development* **126**: 1769–1779.
- Leal-Esteban, L.C; Rothé, B; Fortier, S; Isenschmid, M; Constam, D.B. (2018): Role of Bicaudal C1 in renal gluconeogenesis and its novel interaction with the CTLH complex. *PLoS genetics* **14**: e1007487.
- LeBlanc-Straceski, J.M; Sokac, A; Bement, W; Sobrado, P; Lemoine, L. (2009): Developmental expression of *Xenopus* myosin 1d and identification of a myo1d tail homology that overlaps TH1. *Development, growth & differentiation* **51**: 443–451.
- Lee, J.-Y; Harland, R.M. (2007): Actomyosin contractility and microtubules drive apical constriction in *Xenopus* bottle cells. *Developmental biology* **311**: 40–52.
- Lee, Y; Jeon, K; Lee, J.-T; Kim, S; Kim, V.N. (2002): MicroRNA maturation: stepwise processing and subcellular localization. *The EMBO Journal* **21**: 4663–4670.
- Lewandoski, M. (2001): Conditional control of gene expression in the mouse. *Nature reviews. Genetics* **2**: 743–755.
- Little, R.B; Norris, D.P. (2021): Right, left and cilia: How asymmetry is established. *Seminars in cell & developmental biology* **110**: 11–18.
- Lohr, J.L; Danos, M.C; Yost, H.J. (1997): Left-right asymmetry of a nodal-related gene is regulated by dorsoanterior midline structures during *Xenopus* development. *Development* **124**: 1465–1472.
- Luu, O; Nagel, M; Wacker, S; Lemaire, P; Winklbauer, R. (2008): Control of gastrula cell motility by the Goosecoid/Mix.1/ Siamois network: basic patterns and paradoxical effects. *Developmental dynamics* **237**: 1307–1320.
- MacDonald, B.T; Tamai, K; He, X. (2009): Wnt/beta-catenin signaling: components, mechanisms, and diseases. *Developmental Cell* **17**: 9–26.
- Machikhin, A.S; Volkov, M.V; Burlakov, A.B; Khokhlov, D.D; Potemkin, A.V. (2020): Blood Vessel Imaging at Pre-Larval Stages of Zebrafish Embryonic Development. *Diagnostics* **10**.

- Ma, H; Lin, Y; Zhao, Z.-A; Lu, X; Yu, Y; Zhang, X; Wang, Q; Li, L. (2016): MicroRNA-127 Promotes Mesendoderm Differentiation of Mouse Embryonic Stem Cells by Targeting Left-Right Determination Factor 2. *The Journal of biological chemistry* **291**: 12126–12135.
- Mailhos, C; André, S; Mollereau, B; Goriely, A; Hemmati-Brivanlou, A; Desplan, C. (1998): Drosophila Goosecoid requires a conserved heptapeptide for repression of paired-class homeoprotein activators. *Development* **125**: 937–947.
- Maisonneuve, C; Guilleret, I; Vick, P; Weber, T; Andre, P; Beyer, T; Blum, M; Constam, D.B. (2009): Bicaudal C, a novel regulator of Dvl signaling abutting RNA-processing bodies, controls cilia orientation and leftward flow. *Development* **136**: 3019–3030.
- Malone, C.D; Hannon, G.J. (2009): Small RNAs as guardians of the genome. *Cell* **136**: 656–668.
- Manes, M.E; Elinson, R.P. (1980): Ultraviolet light inhibits grey crescent formation on the frog egg. *Wilhelm Roux's archives of developmental biology* **189**: 73–76.
- Marcet, B; Chevalier, B; Luxardi, G; Coraux, C; Zaragosi, L.-E; Cibois, M; Robbe-Sermesant, K; Jolly, T; Cardinaud, B; Moreilhon, C; Giovannini-Chami, L; Nawrocki-Raby, B; Birembaut, P; Waldmann, R; Kodjabachian, L; Barbry, P. (2011): Control of vertebrate multiciliogenesis by miR-449 through direct repression of the Delta/Notch pathway. *Nature cell biology* **13**: 693–699.
- Marjoram, L; Wright, C. (2011): Rapid differential transport of Nodal and Lefty on sulfated proteoglycan-rich extracellular matrix regulates left-right asymmetry in *Xenopus*. *Development* **138**: 475–485.
- Martello, G; Zacchigna, L; Inui, M; Montagner, M; Adorno, M; Mamidi, A; Morsut, L; Soligo, S; Tran, U; Dupont, S; Cordenonsi, M; Wessely, O; Piccolo, S. (2007): MicroRNA control of Nodal signalling. *Nature* **449**: 183–188.
- Matus, D.Q; Pang, K; Marlow, H; Dunn, C.W; Thomsen, G.H; Martindale, M.Q. (2006): Molecular evidence for deep evolutionary roots of bilaterality in animal development. *Proceedings of the National Academy of Sciences of the United States of America* **103**: 11195–11200.
- McCulloch, C.A; Tenenbaum, H.C. (1986): Dexamethasone induces proliferation and terminal differentiation of osteogenic cells in tissue culture. *The Anatomical record* **215**: 397–402.
- McDowell, G.S; Lemire, J.M; Paré, J.-F; Cammarata, G; Lowery, L.A; Levin, M. (2016): Conserved roles for cytoskeletal components in determining laterality. *Integrative biology : quantitative biosciences from nano to macro* **8**: 267–286.
- McGrath, J; Somlo, S; Makova, S; Tian, X; Brueckner, M. (2003): Two Populations of Node Monocilia Initiate Left-Right Asymmetry in the Mouse. *Cell* **114**: 61–73.
- McKendry, R; Hsu, S.C; Harland, R.M; Grosschedl, R. (1997): LEF-1/TCF proteins mediate wnt-inducible transcription from the *Xenopus* nodal-related 3 promoter. *Developmental biology* **192**: 420–431.
- Medina, A; Reintsch, W; Steinbeisser, H. (2000): *Xenopus* frizzled 7 can act in canonical and non-canonical Wnt signaling pathways Implications on early patterning and morphogenesis. *Mechanisms of Development* **92**: 227–237.
- Meinhardt, H. (2006): Primary body axes of vertebrates: generation of a near-Cartesian coordinate system and the role of Spemann-type organizer. *Developmental dynamics* **235**: 2907–2919.

- Meno, C; Shimono, A; Saijoh, Y; Yashiro, K; Mochida, K; Ohishi, S; Noji, S; Kondoh, H; Hamada, H. (1998): *lefty-1* Is Required for Left-Right Determination as a Regulator of *lefty-2* and *nodal*. *Cell* **94**: 287–297.
- Meshcheryakov, V.N; Beloussov, L.V. (1975): Asymmetrical rotations of blastomeres in early cleavage of gastropoda. *Wilhelm Roux's archives of developmental biology* **177**: 193–203.
- Metcalfe, C; Bienz, M. (2011): Inhibition of GSK3 by Wnt signalling--two contrasting models. *Journal of cell science* **124**: 3537–3544.
- Minegishi, K; Rothé, B; Komatsu, K.R; Ono, H; Ikawa, Y; Nishimura, H; Miyashita, E; Takaoka, K; Bando, K; Kiyonari, H; Yamamoto, T; Saito, H; Constam, D.B; Hamada, H. (2020): Fluid flow-induced left-right asymmetric decay of *Dand5* mRNA in the mouse embryo requires *Bicc1-Ccr4* RNA degradation complex. *bioRxiv*.
- Mizuno, K; Shiozawa, K; Katoh, T.A; Minegishi, K; Ide, T; Ikawa, Y; Nishimura, H; Takaoka, K; Itabashi, T; Iwane, A.H; Nakai, J; Shiratori, H; Hamada, H. (2020): Role of  $Ca^{2+}$  transients at the node of the mouse embryo in breaking of left-right symmetry. *Science advances* **6**: eaba1195.
- Montague, T.G; Gagnon, J.A; Schier, A.F. (2018): Conserved regulation of *Nodal*-mediated left-right patterning in zebrafish and mouse. *Development* **145**.
- Moody, S.A. (1987): Fates of the blastomeres of the 32-cell-stage *Xenopus* embryo. *Developmental biology* **122**: 300–319.
- Moran, Y; Fredman, D; Praher, D; Li, X.Z; Wee, L.M; Rentzsch, F; Zamore, P.D; Technau, U; Seitz, H. (2014): Cnidarian microRNAs frequently regulate targets by cleavage. *Genome research* **24**: 651–663.
- Morgan, N.S; Heintzelman, M.B; Mooseker, M.S. (1995): Characterization of myosin-IA and myosin-IB, two unconventional myosins associated with the *Drosophila* brush border cytoskeleton. *Developmental biology* **172**: 51–71.
- Moulton, J.D. (2017): Using Morpholinos to Control Gene Expression. *Current protocols in nucleic acid chemistry* **68**: 4.30.1.
- Munnamalai, V; Fekete, D.M. (2013): Wnt signaling during cochlear development. *Seminars in cell & developmental biology* **24**: 480–489.
- Nagai, K; Ishida, T; Hashimoto, T; Harada, Y; Ueno, S; Ueda, Y; Kubo, H; Iwao, Y. (2009): The Sperm-surface glycoprotein, SGP, is necessary for fertilization in the frog, *Xenopus laevis*. *Development, growth & differentiation* **51**: 499–510.
- Naganathan, S.R; Fürthauer, S; Nishikawa, M; Jülicher, F; Grill, S.W. (2014): Active torque generation by the actomyosin cell cortex drives left-right symmetry breaking. *eLife* **3**: e04165.
- Nakamura, T; Saito, D; Kawasumi, A; Shinohara, K; Asai, Y; Takaoka, K; Dong, F; Takamatsu, A; Belo, J.A; Mochizuki, A; Hamada, H. (2012): Fluid flow and interlinked feedback loops establish left-right asymmetric decay of *Cerl2* mRNA. *Nature communications* **3**: 1322.
- Nakamura, T; Hamada, H. (2012): Left-right patterning: conserved and divergent mechanisms. *Development* **139**: 3257–3262.

- Nakayama, T; Blitz, I.L; Fish, M.B; Odeleye, A.O; Manohar, S; Cho, K.W.Y; Grainger, R.M. (2014): Cas9-based genome editing in *Xenopus tropicalis*. *Methods in enzymology* **546**: 355–375.
- Namigai, E.K.O; Kenny, N.J; Shimeld, S.M. (2014): Right across the tree of life: the evolution of left-right asymmetry in the Bilateria. *Genesis* **52**: 458–470.
- Newport, J; Kirschner, M. (1982): A major developmental transition in early *Xenopus* embryos I. characterization and timing of cellular changes at the midblastula stage. *Cell* **30**: 675–686.
- Nguyen, T.A; Jo, M.H; Choi, Y.-G; Park, J; Kwon, S.C; Hohng, S; Kim, V.N; Woo, J.-S. (2015): Functional Anatomy of the Human Microprocessor. *Cell* **161**: 1374–1387.
- Niehrs, C; Keller, R; Cho, K.W; Robertis, E.M. de (1993): The homeobox gene goosecoid controls cell migration in *Xenopus* embryos. *Cell* **72**: 491–503.
- Niehrs, C. (2012): The complex world of WNT receptor signalling. *Nature reviews. Molecular cell biology* **13**: 767–779.
- Nieuwkoop, P.D., Faber, J. (Eds.) (1994): Normal table of *Xenopus laevis* (Daudin) A systematical and chronological survey of the development from the fertilized egg till the end of metamorphosis. New York, Garland Pub.
- Ninomiya, H; Elinson, R.P; Winklbauer, R. (2004): Antero-posterior tissue polarity links mesoderm convergent extension to axial patterning. *Nature* **430**: 364–367.
- Nonaka, S; Tanaka, Y; Okada, Y; Takeda, S; Harada, A; Kanai, Y; Kido, M; Hirokawa, N. (1998): Randomization of Left–Right Asymmetry due to Loss of Nodal Cilia Generating Leftward Flow of Extraembryonic Fluid in Mice Lacking KIF3B Motor Protein. *Cell* **95**: 829–837.
- Nusse, R; Varmus, H. (2012): Three decades of Wnts: a personal perspective on how a scientific field developed. *The EMBO Journal* **31**: 2670–2684.
- Ocaña, O.H; Coskun, H; Minguillón, C; Murawala, P; Tanaka, E.M; Galcerán, J; Muñoz-Chápuli, R; Nieto, M.A. (2017): A right-handed signalling pathway drives heart looping in vertebrates. *Nature* **549**: 86–90.
- Ohkawara, B; Niehrs, C. (2011): An ATF2-based luciferase reporter to monitor non-canonical Wnt signaling in *Xenopus* embryos. *Developmental dynamics* **240**: 188–194.
- Okada, Y; Hirokawa, N. (1999): A processive single-headed motor: kinesin superfamily protein KIF1A. *Science* **283**: 1152–1157.
- Okamura, K; Hagen, J.W; Duan, H; Tyler, D.M; Lai, E.C. (2007): The mirtron pathway generates microRNA-class regulatory RNAs in *Drosophila*. *Cell* **130**: 89–100.
- Oki, S; Hashimoto, R; Okui, Y; Shen, M.M; Mekada, E; Otani, H; Saijoh, Y; Hamada, H. (2007): Sulfated glycosaminoglycans are necessary for Nodal signal transmission from the node to the left lateral plate in the mouse embryo. *Development* **134**: 3893–3904.
- Okumura, T; Utsuno, H; Kuroda, J; Gittenberger, E; Asami, T; Matsuno, K. (2008): The development and evolution of left-right asymmetry in invertebrates: lessons from *Drosophila* and snails. *Developmental dynamics* **237**: 3497–3515.

- Onichtchouk, D; Gawantka, V; Dosch, R; Delius, H; Hirschfeld, K; Blumenstock, C; Niehrs, C. (1996): The Xvent-2 homeobox gene is part of the BMP-4 signalling pathway controlling correction of controlling dorsoventral patterning of *Xenopus* mesoderm. *Development* **122**: 3045–3053.
- Ossipova, O; Chu, C.-W; Fillatre, J; Brott, B.K; Itoh, K; Sokol, S.Y. (2015a): The involvement of PCP proteins in radial cell intercalations during *Xenopus* embryonic development. *Developmental biology* **408**: 316–327.
- Ossipova, O; Chuykin, I; Chu, C.-W; Sokol, S.Y. (2015b): Vangl2 cooperates with Rab11 and Myosin V to regulate apical constriction during vertebrate gastrulation. *Development* **142**: 99–107.
- Papanayotou, C; Benhaddou, A; Camus, A; Perea-Gomez, A; Jouneau, A; Mezger, V; Langa, F; Ott, S; Sabéran-Djoneidi, D; Collignon, J. (2014): A novel nodal enhancer dependent on pluripotency factors and smad2/3 signaling conditions a regulatory switch during epiblast maturation. *PLoS biology* **12**: e1001890.
- Paré, A.C; Vichas, A; Fincher, C.T; Mirman, Z; Farrell, D.L; Mainieri, A; Zallen, J.A. (2014): A positional Toll receptor code directs convergent extension in *Drosophila*. *Nature* **515**: 523–527.
- Park, J.-i; Ji, H; Jun, S; Gu, D; Hikasa, H; Li, L; Sokol, S.Y; McCrea, P.D. (2006): Frd3 links Dishevelled to the p120-catenin/Kaiso pathway: distinct catenin subfamilies promote Wnt signals. *Developmental Cell* **11**: 683–695.
- Park, M; Moon, R.T. (2002): The planar cell-polarity gene *stbm* regulates cell behaviour and cell fate in vertebrate embryos. *Nature cell biology* **4**: 20–25.
- Park, S; Blaser, S; Marchal, M.A; Houston, D.W; Sheets, M.D. (2016): A gradient of maternal Bicaudal-C controls vertebrate embryogenesis via translational repression of mRNAs encoding cell fate regulators. *Development* **143**: 864–871.
- Park, T.J; Gray, R.S; Sato, A; Habas, R; Wallingford, J.B. (2005): Subcellular localization and signaling properties of dishevelled in developing vertebrate embryos. *Current Biology* **15**: 1039–1044.
- Park, T.J; Haigo, S.L; Wallingford, J.B. (2006): Ciliogenesis defects in embryos lacking inturned or fuzzy function are associated with failure of planar cell polarity and Hedgehog signaling. *Nature genetics* **38**: 303–311.
- Parry, D.A; Logan, C.V; Stegmann, A.P.A; Abdelhamed, Z.A; Calder, A; Khan, S; Bonthron, D.T; Clowes, V; Sheridan, E; Ghali, N; Chudley, A.E; Dobbie, A; Stumpel, Constance T R M; Johnson, C.A. (2013): SAMS, a syndrome of short stature, auditory-canal atresia, mandibular hypoplasia, and skeletal abnormalities is a unique neurocristopathy caused by mutations in *Goosecoid*. *American journal of human genetics* **93**: 1135–1142.
- Paterson, H.F; Self, A.J; Garrett, M.D; Just, I; Aktories, K; Hall, A. (1990): Microinjection of recombinant p21rho induces rapid changes in cell morphology. *The Journal of cell biology* **111**: 1001–1007.
- Pelliccia, J.L; Jindal, G.A; Burdine, R.D. (2017): *Gdf3* is required for robust Nodal signaling during germ layer formation and left-right patterning. *eLife* **6**.



- Pennekamp, P; Karcher, C; Fischer, A; Schweickert, A; Skryabin, B; Horst, J; Blum, M; Dworniczak, B. (2002): The Ion Channel Polycystin-2 Is Required for Left-Right Axis Determination in Mice. *Current Biology* **12**: 938–943.
- Petersen, C.P; Reddien, P.W. (2009): Wnt signaling and the polarity of the primary body axis. *Cell* **139**: 1056–1068.
- Piazzon, N; Maisonneuve, C; Guilleret, I; Rotman, S; Constam, D.B. (2012): Bicc1 links the regulation of cAMP signaling in polycystic kidneys to microRNA-induced gene silencing. *Journal of molecular cell biology* **4**: 398–408.
- Piccolo, S; Sasai, Y; Lu, B; Robertis, E.M. de (1996): Dorsoventral Patterning in *Xenopus* Inhibition of Ventral Signals by Direct Binding of Chordin to BMP-4. *Cell* **86**: 589–598.
- Piccolo, S; Agius, E; Lu, B; Goodman, S; Dale, L; Robertis, E.M. de (1997): Cleavage of Chordin by Xolloid Metalloprotease Suggests a Role for Proteolytic Processing in the Regulation of Spemann Organizer Activity. *Cell* **91**: 407–416.
- Piccolo, S; Agius, E; Leyns, L; Bhattacharyya, S; Grunz, H; Bouwmeester, T; Robertis, E.M. de (1999): The head inducer Cerberus is a multifunctional antagonist of Nodal, BMP and Wnt signals. *Nature* **397**: 707–710.
- Pimpale, L.G; Middelkoop, T.C; Mietke, A; Grill, S.W. (2020): Cell lineage-dependent chiral actomyosin flows drive cellular rearrangements in early *Caenorhabditis elegans* development. *eLife* **9**.
- Pong, S.K; Gullerova, M. (2018): Noncanonical functions of microRNA pathway enzymes - Drosha, DGCR8, Dicer and Ago proteins. *FEBS letters* **592**: 2973–2986.
- Prager, A; Hagenlocher, C; Ott, T; Schambony, A; Feistel, K. (2017): hmmr mediates anterior neural tube closure and morphogenesis in the frog *Xenopus*. *Developmental biology* **430**: 188–201.
- Putnam, N.H; Butts, T; Ferrier, D.E.K; Furlong, R.F; Hellsten, U; Kawashima, T; Robinson-Rechavi, M; Shoguchi, E; Terry, A; Yu, J.-K; Benito-Gutiérrez, E.L; Dubchak, I; Garcia-Fernández, J; Gibson-Brown, J.J; Grigoriev, I.V; Horton, A.C; Jong, P.J. de; Jurka, J; Kapitonov, V.V; Kohara, Y; Kuroki, Y; Lindquist, E; Lucas, S; Osoegawa, K; Pennacchio, L.A; Salamov, A.A; Satou, Y; Sauka-Spengler, T; Schmutz, J; Shin-I, T; Toyoda, A; Bronner-Fraser, M; Fujiiyama, A; Holland, L.Z; Holland, P.W.H; Satoh, N; Rokhsar, D.S. (2008): The amphioxus genome and the evolution of the chordate karyotype. *Nature* **453**: 1064–1071.
- Qian, D; Jones, C; Rzadzinska, A; Mark, S; Zhang, X; Steel, K.P; Dai, X; Chen, P. (2007): Wnt5a functions in planar cell polarity regulation in mice. *Developmental biology* **306**: 121–133.
- Rankin, C.T; Bunton, T; Lawler, A.M; Lee, S.J. (2000): Regulation of left-right patterning in mice by growth/differentiation factor-1. *Nature genetics* **24**: 262–265.
- Rankin, S.A; Kormish, J; Kofron, M; Jegga, A; Zorn, A.M. (2011): A gene regulatory network controlling *hhx* transcription in the anterior endoderm of the organizer. *Developmental biology* **351**: 297–310.
- Reissmann, E; Jörnvall, H; Blokzijl, A; Andersson, O; Chang, C; Minchiotti, G; Persico, M.G; Ibáñez, C.F; Brivanlou, A.H. (2001): The orphan receptor ALK7 and the Activin receptor ALK4 mediate signaling by Nodal proteins during vertebrate development. *Genes & development* **15**: 2010–2022.

- Rivera-Pérez, J.A; Mallo, M; Gendron-Maguire, M; Gridley, T; Behringer, R.R. (1995): Goosecoid is not an essential component of the mouse gastrula organizer but is required for craniofacial and rib development. *Development* **121**: 3005–3012.
- Rothbacher, U; Laurent, M.N; Deardorff, M.A; Klein, P.S; Cho, K.W; Fraser, S.E. (2000): Dishevelled phosphorylation, subcellular localization and multimerization regulate its role in early embryogenesis. *The EMBO Journal* **19**: 1010–1022.
- Rothé, B; Leal-Esteban, L.C; Bernet, F; Urfer, S; Doerr, N; Weimbs, T; Iwaszkiewicz, J; Constam, D.B. (2015): Bicc1 Polymerization Regulates the Localization and Silencing of Bound mRNA. *Molecular and cellular biology* **35**: 3339–3353.
- Rothé, B; Gagnieux, C; Leal-Esteban, L.C; Constam, D.B. (2020): Role of the RNA-binding protein Bicaudal-C1 and interacting factors in cystic kidney diseases. *Cellular signalling* **68**: 109499.
- Ruby, J.G; Jan, C.H; Bartel, D.P. (2007): Intronic microRNA precursors that bypass Drosha processing. *Nature* **448**: 83–86.
- Saka, Y; Smith, J.C. (2001): Spatial and temporal patterns of cell division during early *Xenopus* embryogenesis. *Developmental biology* **229**: 307–318.
- Sampath, K; Cheng, A.M; Frisch, A; Wright, C.V. (1997): Functional differences among *Xenopus* nodal-related genes in left-right axis determination. *Development* **124**: 3293–3302.
- Sander, V; Reversade, B; Robertis, E.M. de (2007): The opposing homeobox genes Goosecoid and Vent1/2 self-regulate *Xenopus* patterning. *The EMBO Journal* **26**: 2955–2965.
- Schier, A.F. (2003): Nodal signaling in vertebrate development. *Annual review of cell and developmental biology* **19**: 589–621.
- Schlessinger, K; Hall, A; Tolwinski, N. (2009): Wnt signaling pathways meet Rho GTPases. *Genes & development* **23**: 265–277.
- Schneider, S; Steinbeisser, H; Warga, R.M; Hausen, P. (1996):  $\beta$ -catenin translocation into nuclei demarcates the dorsalizing centers in frog and fish embryos. *Mechanisms of Development* **57**: 191–198.
- Schottenfeld, J; Sullivan-Brown, J; Burdine, R.D. (2007): Zebrafish curly up encodes a Pkd2 ortholog that restricts left-side-specific expression of southpaw. *Development* **134**: 1605–1615.
- Schroeder, T.E. (1970): Neurulation in *Xenopus laevis*. An analysis and model based upon light and electron microscopy. *Journal of embryology and experimental morphology* **23**: 427–462.
- Schroeder, T.E. (1973): Cell Constriction Contractile Role of Microfilaments in Division and Development. *American Zoologist* **13**: 949–960.
- Schulte-Merker, S; Hammerschmidt, M; Beuchle, D; Cho, K.W; Robertis, E.M. de; Nüsslein-Volhard, C. (1994): Expression of zebrafish goosecoid and no tail gene products in wild-type and mutant no tail embryos. *Development* **120**: 843–852.
- Schweickert, A; Weber, T; Beyer, T; Vick, P; Bogusch, S; Feistel, K; Blum, M. (2007): Cilia-driven leftward flow determines laterality in *Xenopus*. *Current Biology* **17**: 60–66.

- Schweickert, A; Vick, P; Getwan, M; Weber, T; Schneider, I; Eberhardt, M; Beyer, T; Pachur, A; Blum, M. (2010): The nodal inhibitor Coco is a critical target of leftward flow in *Xenopus*. *Current Biology* **20**: 738–743.
- Schweickert, A; Ott, T; Kurz, S; Tingler, M; Maerker, M; Fuhl, F; Blum, M. (2017): Vertebrate Left-Right Asymmetry: What Can Nodal Cascade Gene Expression Patterns Tell Us? *Journal of cardiovascular development and disease* **5**.
- Schwenk, F; Baron, U; Rajewsky, K. (1995): A cre-transgenic mouse strain for the ubiquitous deletion of loxP-flanked gene segments including deletion in germ cells. *Nucleic acids research* **23**: 5080–5081.
- Seifert, J.R.K; Mlodzik, M. (2007): Frizzled/PCP signalling: a conserved mechanism regulating cell polarity and directed motility. *Nature reviews. Genetics* **8**: 126–138.
- Seilliez, I; Thisse, B; Thisse, C. (2006): FoxA3 and gooseoid promote anterior neural fate through inhibition of Wnt8a activity before the onset of gastrulation. *Developmental biology* **290**: 152–163.
- Shabalina, S.A; Koonin, E.V. (2008): Origins and evolution of eukaryotic RNA interference. *Trends in ecology & evolution* **23**: 578–587.
- Shapira, E; Marom, K; Yelin, R; Levy, A; Fainsod, A. (1999): A role for the homeobox gene *Xvex-1* as part of the BMP-4 ventral signaling pathway. *Mechanisms of Development* **86**: 99–111.
- Shapira, E; Marom, K; Levy, V; Yelin, R; Fainsod, A. (2000): The *Xvex-1* antimorph reveals the temporal competence for organizer formation and an early role for ventral homeobox genes. *Mechanisms of Development* **90**: 77–87.
- Shibazaki, Y; Shimizu, M; Kuroda, R. (2004): Body handedness is directed by genetically determined cytoskeletal dynamics in the early embryo. *Current Biology* **14**: 1462–1467.
- Shih, J; Keller, R. (1992): The epithelium of the dorsal marginal zone of *Xenopus* has organizer properties. *Development* **116**: 887–899.
- Shimeld, S.M; Donoghue, P.C.J. (2012): Evolutionary crossroads in developmental biology: cyclostomes (lamprey and hagfish) *Development* **139**: 2091–2099.
- Shindo, A; Wallingford, J.B. (2014): PCP and septins compartmentalize cortical actomyosin to direct collective cell movement. *Science* **343**: 649–652.
- Shindo, A; Inoue, Y; Kinoshita, M; Wallingford, J.B. (2019): PCP-dependent transcellular regulation of actomyosin oscillation facilitates convergent extension of vertebrate tissue. *Developmental biology* **446**: 159–167.
- Shiratori, H; Hamada, H. (2014): TGF $\beta$  signaling in establishing left-right asymmetry. *Seminars in cell & developmental biology* **32**: 80–84.
- Shook, D.R; Majer, C; Keller, R. (2004): Pattern and morphogenesis of presumptive superficial mesoderm in two closely related species, *Xenopus laevis* and *Xenopus tropicalis*. *Developmental biology* **270**: 163–185.
- Shubin, N; Tabin, C; Carroll, S. (2009): Deep homology and the origins of evolutionary novelty. *Nature* **457**: 818–823.

- Shyamala, K; Yanduri, S; Girish, H.C; Murgod, S. (2015): Neural crest: The fourth germ layer. *Journal of oral and maxillofacial pathology* **19**: 221–229.
- Silva, A.C; Filipe, M; Kuerner, K.-M; Steinbeisser, H; Belo, J.A. (2003): Endogenous Cerberus activity is required for anterior head specification in *Xenopus*. *Development* **130**: 4943–4953.
- Simmonds, A.J; dosSantos, G; Livne-Bar, I; Krause, H.M. (2001): Apical Localization of wingless Transcripts Is Required for Wingless Signaling. *Cell* **105**: 197–207.
- Sindelka, R; Abaffy, P; Qu, Y; Tomankova, S; Sidova, M; Naraine, R; Kolar, M; Peuchen, E; Sun, L; Dovichi, N; Kubista, M. (2018): Asymmetric distribution of biomolecules of maternal origin in the *Xenopus laevis* egg and their impact on the developmental plan. *Scientific reports* **8**: 8315.
- Sive, H.L; Grainger, R.M; Harland, R.M. (2007): *Xenopus laevis* Keller Explants. *Cold Spring Harbor Protocols* **2007**: pdb.prot4749.
- Smithers, L.E; Jones, C. (2002): *Xhex*-expressing endodermal tissues are essential for anterior patterning in *Xenopus*. *Mechanisms of Development* **119**: 191–200.
- Sokac, A.M; Bement, W.M. (2000): Regulation and expression of metazoan unconventional myosins. *International review of cytology* **200**: 197–304.
- Sokol, S.Y. (2016): Mechanotransduction During Vertebrate Neurulation. *Current topics in developmental biology* **117**: 359–376.
- Song, R; Walentek, P; Sponer, N; Klimke, A; Lee, J.S; Dixon, G; Harland, R; Wan, Y; Lishko, P; Lize, M; Kessel, M; He, L. (2014): miR-34/449 miRNAs are required for motile ciliogenesis by repressing cp110. *Nature* **510**: 115–120.
- Spéder, P; Adám, G; Noselli, S. (2006): Type ID unconventional myosin controls left-right asymmetry in *Drosophila*. *Nature* **440**: 803–807.
- Spemann, H; Mangold, H. (1924): über Induktion von Embryonalanlagen durch Implantation artfremder Organisatoren. *Archiv für Mikroskopische Anatomie und Entwicklungsmechanik* **100**: 599–638.
- Steinbeisser, H; Fainsod, A; Niehrs, C; Sasai, Y; Robertis, E.M. de (1995): The role of *gsc* and BMP-4 in dorsal-ventral patterning of the marginal zone in *Xenopus*: a loss-of-function study using antisense RNA. *The EMBO Journal* **14**: 5230–5243.
- Strutt, D. (2003): Frizzled signalling and cell polarisation in *Drosophila* and vertebrates. *Development* **130**: 4501–4513.
- Stubbs, J.L; Oishi, I; Izpisua Belmonte, J.C; Kintner, C. (2008): The forkhead protein Foxj1 specifies node-like cilia in *Xenopus* and zebrafish embryos. *Nature genetics* **40**: 1454–1460.
- Sulik, K; Dehart, D.B; Iangaki, T; Carson, J.L; Vrablic, T; Gesteland, K; Schoenwolf, G.C. (1994): Morphogenesis of the murine node and notochordal plate. *Developmental dynamics* **201**: 260–278.
- Sweetman, D; Goljanek, K; Rathjen, T; Oustanina, S; Braun, T; Dalmay, T; Münsterberg, A. (2008): Specific requirements of MRFs for the expression of muscle specific microRNAs, miR-1, miR-206 and miR-133. *Developmental biology* **321**: 491–499.

- Syeda, F; Kirchhof, P; Fabritz, L. (2017): PITX2-dependent gene regulation in atrial fibrillation and rhythm control. *The Journal of physiology* **595**: 4019–4026.
- Tabin, C.J; Vogan, K.J. (2003): A two-cilia model for vertebrate left-right axis specification. *Genes & development* **17**: 1–6.
- Tada, M; Smith, J.C. (2000): Xwnt11 is a target of *Xenopus* Brachyury: regulation of gastrulation movements via Dishevelled, but not through the canonical Wnt pathway. *Development (Cambridge, England)* **127**: 2227–2238.
- Tahinci, E; Symes, K. (2003): Distinct functions of Rho and Rac are required for convergent extension during *Xenopus* gastrulation. *Developmental biology* **259**: 318–335.
- Taira, M; Jamrich, M; Good, P.J; Dawid, I.B. (1992): The LIM domain-containing homeo box gene *Xlim-1* is expressed specifically in the organizer region of *Xenopus* gastrula embryos. *Genes & development* **6**: 356–366.
- Takao, D; Nemoto, T; Abe, T; Kiyonari, H; Kajiura-Kobayashi, H; Shiratori, H; Nonaka, S. (2013): Asymmetric distribution of dynamic calcium signals in the node of mouse embryo during left-right axis formation. *Developmental biology* **376**: 23–30.
- Takeuchi, M; Nakabayashi, J; Sakaguchi, T; Yamamoto, T.S; Takahashi, H; Takeda, H; Ueno, N. (2003): The prickle-Related Gene in Vertebrates Is Essential for Gastrulation Cell Movements. *Current Biology* **13**: 674–679.
- Tanaka, C; Sakuma, R; Nakamura, T; Hamada, H; Saijoh, Y. (2007): Long-range action of Nodal requires interaction with GDF1. *Genes & development* **21**: 3272–3282.
- Tani, S; Kuraku, S; Sakamoto, H; Inoue, K; Kusakabe, R. (2013): Developmental expression and evolution of muscle-specific microRNAs conserved in vertebrates. *Evolution & development* **15**: 293–304.
- Taylor, J; Abramova, N; Charlton, J; Adler, P.N. (1998): Van Gogh: a new *Drosophila* tissue polarity gene. *Genetics* **150**: 199–210.
- Tessmar-Raible, K. (2003): Emerging systems Between vertebrates and arthropods, the Lophotrochozoa. *Current Opinion in Genetics & Development* **13**: 331–340.
- Theisen, H; Purcell, J; Bennett, M; Kansagara, D; Syed, A; Marsh, J.L. (1994): dishevelled is required during wingless signaling to establish both cell polarity and cell identity. *Development* **120**: 347–360.
- Thompson, H; Shaw, M.K; Dawe, H.R; Shimeld, S.M. (2012): The formation and positioning of cilia in *Ciona intestinalis* embryos in relation to the generation and evolution of chordate left-right asymmetry. *Developmental biology* **364**: 214–223.
- Tingler, M; Ott, T; Tözser, J; Kurz, S; Getwan, M; Tisler, M; Schweickert, A; Blum, M. (2014): Symmetry breakage in the frog *Xenopus*: role of Rab11 and the ventral-right blastomere. *Genesis* **52**: 588–599.
- Tisler, M; Wetzel, F; Mantino, S; Kremnyov, S; Thumberger, T; Schweickert, A; Blum, M; Vick, P. (2016): Cilia are required for asymmetric nodal induction in the sea urchin embryo. *BMC developmental biology* **16**: 28.

- Torres, M.A; Yang-Snyder, J.A; Purcell, S.M; DeMarais, A.A; McGrew, L.L; Moon, R.T. (1996): Activities of the Wnt-1 class of secreted signaling factors are antagonized by the Wnt-5A class and by a dominant negative cadherin in early *Xenopus* development. *The Journal of cell biology* **133**: 1123–1137.
- Tözser, J; Earwood, R; Kato, A; Brown, J; Tanaka, K; Didier, R; Megraw, T.L; Blum, M; Kato, Y. (2015): TGF- $\beta$  Signaling Regulates the Differentiation of Motile Cilia. *Cell reports* **11**: 1000–1007.
- Tran, U; Zakin, L; Schweickert, A; Agrawal, R; Döger, R; Blum, M; Robertis, E.M. de; Wessely, O. (2010): The RNA-binding protein bicaudal C regulates polycystin 2 in the kidney by antagonizing miR-17 activity. *Development* **137**: 1107–1116.
- Ukita, K; Hirahara, S; Oshima, N; Imuta, Y; Yoshimoto, A; Jang, C.-W; Oginuma, M; Saga, Y; Behringer, R.R; Kondoh, H; Sasaki, H. (2009): Wnt signaling maintains the notochord fate for progenitor cells and supports the posterior extension of the notochord. *Mechanisms of Development* **126**: 791–803.
- Ulmer, B.M. (2008): Die Rolle des Homeoboxgens *Goosecoid* im PCP-Signalweg. Universität Hohenheim.
- Ulmer, B.M. (2012): *Goosecoid* and *Calponin* : two new regulators of the PCP-pathway. Universität Hohenheim.
- Urry, L.A., Cain, M.L., Wasserman, S.A., Minorsky, P.V., Reece, J. (2019): *Campbell Biologie*, 11., aktualisierte Auflage ed.
- Usui, T; Shima, Y; Shimada, Y; Hirano, S; Burgess, R.W; Schwarz, T.L; Takeichi, M; Uemura, T. (1999): Flamingo, a Seven-Pass Transmembrane Cadherin, Regulates Planar Cell Polarity under the Control of Frizzled. *Cell* **98**: 585–595.
- Valles, J.M; Wasserman, Sarah R R M; Schweidenback, C; Edwardson, J; Denegre, J.M; Mowry, K.L. (2002): Processes that occur before second cleavage determine third cleavage orientation in *Xenopus*. *Experimental cell research* **274**: 112–118.
- van den Bosch, M.H; Blom, A.B; Sloetjes, A.W; Koenders, M.I; van de Loo, Fons A; van den Berg, Wim B; van Lent, P.L; van der Kraan, Peter M (2015): Induction of Canonical Wnt Signaling by Synovial Overexpression of Selected Wnts Leads to Protease Activity and Early Osteoarthritis-Like Cartilage Damage. *The American journal of pathology* **185**: 1970–1980.
- Vandenberg, L.N; Levin, M. (2013): A unified model for left-right asymmetry? Comparison and synthesis of molecular models of embryonic laterality. *Developmental biology* **379**: 1–15.
- Vejnar, C.E; Giraldez, A.J. (2020): LabxDB: versatile databases for genomic sequencing and lab management. *Bioinformatics* **36**: 4530–4531.
- Vick, P; Schweickert, A; Weber, T; Eberhardt, M; Mencl, S; Shcherbakov, D; Beyer, T; Blum, M. (2009): Flow on the right side of the gastrocoel roof plate is dispensable for symmetry breakage in the frog *Xenopus laevis*. *Developmental biology* **331**: 281–291.
- Vick, P; Kreis, J; Schneider, I; Tingler, M; Getwan, M; Thumberger, T; Beyer, T; Schweickert, A; Blum, M. (2018): An Early Function of Polycystin-2 for Left-Right Organizer Induction in *Xenopus*. *iScience* **2**: 76–85.

- Vincent, J.-P; Oster, G.F; Gerhart, J.C. (1986): Kinematics of gray crescent formation in *Xenopus* eggs The displacement of subcortical cytoplasm relative to the egg surface. *Developmental biology* **113**: 484–500.
- Vincent, J.-P; Gerhart, J.C. (1987): Subcortical rotation in *Xenopus* eggs An early step in embryonic axis specification. *Developmental biology* **123**: 526–539.
- Vladar, E.K; Antic, D; Axelrod, J.D. (2009): Planar cell polarity signaling: the developing cell's compass. *Cold Spring Harbor perspectives in biology* **1**: a002964.
- Vonica, A; Brivanlou, A.H. (2007): The left-right axis is regulated by the interplay of *Coco*, *Xnr1* and *derrière* in *Xenopus* embryos. *Developmental biology* **303**: 281–294.
- Vonica, A; Gumbiner, B.M. (2007): The *Xenopus* Nieuwkoop center and Spemann-Mangold organizer share molecular components and a requirement for maternal Wnt activity. *Developmental biology* **312**: 90–102.
- Vonica, A; Rosa, A; Arduini, B.L; Brivanlou, A.H. (2011): APOBEC2, a selective inhibitor of TGF $\beta$  signaling, regulates left-right axis specification during early embryogenesis. *Developmental biology* **350**: 13–23.
- Walentek, P; Schneider, I; Schweickert, A; Blum, M. (2013): Wnt11b is involved in cilia-mediated symmetry breakage during *Xenopus* left-right development. *PloS one* **8**: e73646.
- Wallingford, J.B; Rowning, B.A; Vogeli, K.M; Rothbächer, U; Fraser, S.E; Harland, R.M. (2000): Dishevelled controls cell polarity during *Xenopus* gastrulation. *Nature* **405**: 81–85.
- Wallingford, J.B; Goto, T; Keller, R; Harland, R.M. (2002): Cloning and expression of *Xenopus* Prickle, an orthologue of a *Drosophila* planar cell polarity gene. *Mechanisms of Development* **116**: 183–186.
- Wallingford, J.B; Fraser, S.E; Harland, R.M. (2002): Convergent Extension. *Developmental Cell* **2**: 695–706.
- Wallingford, J.B; Harland, R.M. (2002): Neural tube closure requires Dishevelled-dependent convergent extension of the midline. *Development* **129**: 5815–5825.
- Wang, J; Bai, Y; Li, N; Ye, W; Zhang, M; Greene, S.B; Tao, Y; Chen, Y; Wehrens, X.H.T; Martin, J.F. (2014): Pitx2-microRNA pathway that delimits sinoatrial node development and inhibits predisposition to atrial fibrillation. *Proceedings of the National Academy of Sciences of the United States of America* **111**: 9181–9186.
- Wang, Y; Nathans, J. (2007): Tissue/planar cell polarity in vertebrates: new insights and new questions. *Development* **134**: 647–658.
- Weaver, C; Kimelman, D. (2004): Move it or lose it: axis specification in *Xenopus*. *Development* **131**: 3491–3499.
- Wessely, O; Robertis, E.M. de (2000): The *Xenopus* homologue of Bicaudal-C is a localized maternal mRNA that can induce endoderm formation. *Development* **127**: 2053–2062.
- Wilhelm, J.E; Vale, R.D. (1993): RNA on the move: the mRNA localization pathway. *The Journal of cell biology* **123**: 269–274.



- Wilkinson, D.G; Nieto, M.A. (1993): Detection of messenger RNA by in situ hybridization to tissue sections and whole mounts. *Methods in enzymology* **225**: 361–373.
- Willert, K; Nusse, R. (2012): Wnt proteins. *Cold Spring Harbor perspectives in biology* **4**: a007864.
- Winklbauer, R. (1990): Mesodermal cell migration during *Xenopus* gastrulation. *Developmental biology* **142**: 155–168.
- Winklbauer, R; Schürfeld, M. (1999): Vegetal rotation, a new gastrulation movement involved in the internalization of the mesoderm and endoderm in *Xenopus*. *Development* **126**: 3703–3713.
- Wood, W.B. (1991): Evidence from reversal of handedness in *C. elegans* embryos for early cell interactions determining cell fates. *Nature* **349**: 536–538.
- Xie, M; Steitz, J.A. (2014): Versatile microRNA biogenesis in animals and their viruses. *RNA biology* **11**: 673–681.
- Yamada, G; Mansouri, A; Torres, M; Stuart, E.T; Blum, M; Schultz, M; Robertis, E.M. de; Gruss, P. (1995): Targeted mutation of the murine goosecoid gene results in craniofacial defects and neonatal death. *Development* **121**: 2917–2922.
- Yamada, T. (1994): Caudalization by the amphibian organizer: brachyury, convergent extension and retinoic acid. *Development* **120**: 3051–3062.
- Yang, J; Tan, C; Darken, R.S; Wilson, P.A; Klein, P.S. (2002): Beta-catenin/Tcf-regulated transcription prior to the midblastula transition. *Development* **129**: 5743–5752.
- Yang, Y; Mlodzik, M. (2015): Wnt-Frizzled/planar cell polarity signaling: cellular orientation by facing the wind (Wnt) *Annual review of cell and developmental biology* **31**: 623–646.
- Yan, Y.-T; Liu, J.-J; Luo, Y; E, C; Haltiwanger, R.S; Abate-Shen, C; Shen, M.M. (2002): Dual roles of Cripto as a ligand and coreceptor in the nodal signaling pathway. *Molecular and cellular biology* **22**: 4439–4449.
- Yao, J; Kessler, D.S. (2001): Goosecoid promotes head organizer activity by direct repression of *Xwnt8* in Spemann's organizer. *Development* **128**: 2975–2987.
- Yasuo, H; Lemaire, P. (2001): Role of Goosecoid, *Xnot* and Wnt antagonists in the maintenance of the notochord genetic programme in *Xenopus* gastrulae. *Development* **128**: 3783–3793.
- Yates, A.D; Achuthan, P; Akanni, W; Allen, J; Allen, J; Alvarez-Jarreta, J; Amode, M.R; Armean, I.M; Azov, A.G; Bennett, R; Bhai, J; Billis, K; Boddu, S; Marugán, J.C; Cummins, C; Davidson, C; Dodiya, K; Fatima, R; Gall, A; Giron, C.G; Gil, L; Grego, T; Haggerty, L; Haskell, E; Hourlier, T; Izuogu, O.G; Janacek, S.H; Juettemann, T; Kay, M; Lavidas, I; Le, T; Lemos, D; Martinez, J.G; Maurel, T; McDowall, M; McMahan, A; Mohanan, S; Moore, B; Nuhn, M; Oheh, D.N; Parker, A; Parton, A; Patricio, M; Sakthivel, M.P; Abdul Salam, A.I; Schmitt, B.M; Schuilenburg, H; Sheppard, D; Sycheva, M; Szuba, M; Taylor, K; Thormann, A; Threadgold, G; Vullo, A; Walts, B; Winterbottom, A; Zadissa, A; Chakiachvili, M; Flint, B; Frankish, A; Hunt, S.E; Ilesley, G; Kostadima, M; Langridge, N; Loveland, J.E; Martin, F.J; Morales, J; Mudge, J.M; Muffato, M; Perry, E; Ruffier, M; Trevanion, S.J; Cunningham, F; Howe, K.L; Zerbino, D.R; Flicek, P. (2020): Ensembl 2020. *Nucleic acids research* **48**: D682–D688.

Ybot-Gonzalez, P; Savery, D; Gerrelli, D; Signore, M; Mitchell, C.E; Faux, C.H; Greene, N.D.E; Copp, A.J. (2007): Convergent extension, planar-cell-polarity signalling and initiation of mouse neural tube closure. *Development* **134**: 789–799.

Yeo, C.-Y; Whitman, M. (2001): Nodal Signals to Smads through Cripto-Dependent and Cripto-Independent Mechanisms. *Molecular Cell* **7**: 949–957.

Yoshida, S; Shiratori, H; Kuo, I.Y; Kawasumi, A; Shinohara, K; Nonaka, S; Asai, Y; Sasaki, G; Belo, J.A; Sasaki, H; Nakai, J; Dworniczak, B; Ehrlich, B.E; Pennekamp, P; Hamada, H. (2012): Cilia at the node of mouse embryos sense fluid flow for left-right determination via Pkd2. *Science* **338**: 226–231.

Yoshida, S; Hamada, H. (2014): Roles of cilia, fluid flow, and Ca<sup>2+</sup> signaling in breaking of left-right symmetry. *Trends in genetics* **30**: 10–17.

Yost, C; Farr, G.H; Pierce, S.B; Ferkey, D.M; Chen, M.M; Kimelman, D. (1998): GBP, an Inhibitor of GSK-3, Is Implicated in *Xenopus* Development and Oncogenesis. *Cell* **93**: 1031–1041.

Yuan, S; Zhao, L; Brueckner, M; Sun, Z. (2015): Intraciliary calcium oscillations initiate vertebrate left-right asymmetry. *Current Biology* **25**: 556–567.

Yu, J.-K.S. (2010): The evolutionary origin of the vertebrate neural crest and its developmental gene regulatory network--insights from amphioxus. *Zoology* **113**: 1–9.

Zeke, A; Misheva, M; Reményi, A; Bogoyevitch, M.A. (2016): JNK Signaling: Regulation and Functions Based on Complex Protein-Protein Partnerships. *Microbiology and molecular biology reviews* **80**: 793–835.

Zhang, J; Houston, D.W; King, M.L; Payne, C; Wylie, C; Heasman, J. (1998): The Role of Maternal VegT in Establishing the Primary Germ Layers in *Xenopus* Embryos. *Cell* **94**: 515–524.

Zhang, Y; Forinash, K.D; McGivern, J; Fritz, B; Dorey, K; Sheets, M.D. (2009): Spatially restricted translation of the xCR1 mRNA in *Xenopus* embryos. *Molecular and cellular biology* **29**: 3791–3802.

Zhang, Y; Cooke, A; Park, S; Dewey, C.N; Wickens, M; Sheets, M.D. (2013): Bicaudal-C spatially controls translation of vertebrate maternal mRNAs. *RNA* **19**: 1575–1582.

Zhang, Y; Park, S; Blaser, S; Sheets, M.D. (2014): Determinants of RNA binding and translational repression by the Bicaudal-C regulatory protein. *The Journal of biological chemistry* **289**: 7497–7504.

Zheng, H; Ying, H; Yan, H; Kimmelman, A.C; Hiller, D.J; Chen, A.-J; Perry, S.R; Tonon, G; Chu, G.C; Ding, Z; Stommel, J.M; Dunn, K.L; Wiedemeyer, R; You, M.J; Brennan, C; Wang, Y.A; Ligon, K.L; Wong, W.H; Chin, L; DePinho, R.A. (2008): p53 and Pten control neural and glioma stem/progenitor cell renewal and differentiation. *Nature* **455**: 1129–1133.

Zhou, X; Sasaki, H; Lowe, L; Hogan, B.L; Kuehn, M.R. (1993): Nodal is a novel TGF-beta-like gene expressed in the mouse node during gastrulation. *Nature* **361**: 543–547.

### Internet addresses

<http://wnt.stanford.edu>: february 26, 2021

## Curriculum vitae

### Personal data

Name: Markus Ferdinand Maerker  
 Place of birth: Stuttgart Bad-Cannstatt, Germany  
 Date of birth: 24.07.1990  
 Place of residence: 73230 Kirchheim unter Teck / Ötlingen, Germany  
 Nationality: German

### Education and scientific career

06/2016 – 06/2021 Doctoral student at the University of Hohenheim, Germany in the group of Prof. Dr. Martin Blum, Institute of Biology, Department of Zoology  
 10/2010 – 05/2016 Study of biology at the University of Hohenheim (1.2), Germany  
 B. Sc. and M. Sc. thesis in the group of Prof. Dr. Martin Blum  
 Title Master thesis: Heterologe Funktionsanalyse des humanen 5-Hydroxytryptamin 3 D Rezeptors (5-HT3D) und dessen Wnt inhibitorischen Domäne in *Xenopus laevis*. (1.0)  
 Title Bachelor thesis: Expressionsmusteranalyse im Modellorganismus *Xenopus laevis* und Erstellung eines molekularen Stammbaumes für PARK2 co-regulated gene like (PACRGL). (1.0)  
 09/2007 – 06/2010 Käthe-Kollwitz High-School with biotechnical background (2.1)  
 Esslingen, Germany

### Internships

12/2014 – 03/2015 Department of Zoology, Herpetology,  
 Supervisor PD. Dr. Alexander Kupfer  
 State Museum of Natural History Stuttgart, Germany  
 03/2015 – 06/2015 Institute of Biology, Department of Zoology 190z,  
 Supervisor apl. Prof. Dr. Axel Schweickert  
 University of Hohenheim, Germany

### Qualifications

03/2017 Laboratory Animal Course Category B, University of Hohenheim,  
 Germany  
 07/2016 Seminar: "Aquatische Modellsysteme", University of Ulm, Germany  
 12/2015 Seminar: "*Xenopus* als Modellorganismus", University of Ulm,  
 Germany  
 08/2014 Course: Cytogenetics, University of Hohenheim, Germany

**Conference participations**

- 11/2020 6<sup>th</sup> German *Xenopus* Meeting, University of Munich, Germany
- 12/2019 5<sup>th</sup> German *Xenopus* Meeting, University of Freiburg, Germany  
**Talk:** Symmetry breakage in *Xenopus laevis* through post-transcriptional repression of *dand5*
- 10/2019 6<sup>th</sup> Tri-Regional Stem Cell and Developmental Biology Meeting, University of Strasbourg, France
- 06/2019 2<sup>nd</sup> European Amphibian Club, University of Halle-Wittenberg, Germany  
**Talk:** Symmetry breakage in *Xenopus laevis* through post-transcriptional repression of *dand5*
- 12/2018 4<sup>th</sup> German *Xenopus* Meeting, University of Hohenheim, Germany  
**Talk:** A novel function of the RNA binding protein Bicaudal C during L/R axis determination
- 08/2018 17<sup>th</sup> International *Xenopus* Conference, University of Washington, USA  
**Poster:** How miRNAs and bicC contribute to the *dand5* regulation in the GRP during left-right determination in *Xenopus laevis*  
**Funding:** DAAD travel and congress grant
- 06/2017 1<sup>st</sup> European Amphibian Club, University of Rennes; France  
**Poster:** A novel role of the organizer gene Goosecoid as an inhibitor of Wnt/PCP-mediated convergent extension in *Xenopus* and mouse
- 12/2016 3<sup>rd</sup> German *Xenopus* Meeting, University of Hohenheim, Germany  
**Poster:** The human serotonin type 3 receptor (5-HTR3): A possible interactant with the canonical Wnt pathway.
- 10/2015 2<sup>nd</sup> German *Xenopus* Meeting, Karlsruhe Institute of Technology, Germany
- 10/2013 1<sup>st</sup> German *Xenopus* Meeting, University of Hohenheim, Germany

**Publications**

- 09/2021 **Maerker M.**, Getwan M., Dowdle M. E., McSheene J. C., Gonzalez V., Pelliccia J. L., Hamilton D. S., Yartseva V., Tingler M., Minegishi K., Vick P., Giraldez A. J., Hamada H., Burdine R. D., Sheets M. D., Blum M. and Schweickert A. (2021). *Bicc1* and *Dicer* regulate left-right patterning through post-transcriptional control of the Nodal-inhibitor *Dand5*. *Nature communications* **12**, 5482
- 03/2018 Tingler M., Kurz S., **Maerker M.**, Ott T., Fuhl F., Schweickert A., LeBlanc-Staceski J. M., Noselli S. and Blum M. (2018). A conserved role of the unconventional myosin 1D in laterality determination. *Current Biology*, Vol. 28, Issue 5
- 12/2017 Schweickert A., Ott T., Kurz S., Tingler M., **Maerker M.**, Fuhl F. and Blum M. (2017). Vertebrate Left-Right Asymmetry: What Can Nodal Cascade Gene Expression Patterns Tell Us? *Journal of Cardiovascular Development and Disease*, Vol. 5, Issue 1
- 02/2017 Ulmer B., Tingler M., Kurz S., **Maerker M.**, Andre P., Mönch D., Campione M., Deißler K., Lewandoski M., Thumberger T., Schweickert A., Fainsod A., Steinbeißer H., Blum M. (2017). A novel role of the organizer gene *Gooseoid* as an inhibitor of Wnt/PCP-mediated convergent extension in *Xenopus* and mouse. *Scientific Reports*, Vol. 7
- 10/2016 **Maerker M.**, Reinhard S., Pogoda P., Kupfer A. (2016). Sexual size dimorphism in the viviparous caecilian amphibian *Geotrypetes seraphini seraphini* (Gymnophiona: Dermophiidae) including an updated overview of sexual dimorphism in caecilian amphibians. *Amphibia-Reptilia*, Vol. 37, pp 291–299

Kirchheim/Teck, 20.09.2021

**Place and Date****Signature**

## Danksagung

Zu aller erst möchte ich **Prof. Dr. Martin Blum** für sein Vertrauen und seine Unterstützung danken. Dies ermöglichte mir während meiner ganzen Promotion das selbstständige wissenschaftliche Arbeiten zu erlernen und interessante Meetings zu besuchen.

**Prof. Dr. Axel Schweickert** möchte ich für seine stetige Unterstützung in allen Fragen der Wissenschaft danken. Die zahllosen spannenden wissenschaftliche Diskussionen ermöglichten mir meinen Wissenschaftsgeist zu formen und sicher durch die Zeit der Promotion zu kommen.

**Prof. Dr. Heinz Breer** danke ich für seine stetige Bereitschaft meine, so wie viele andere, Dissertationen unseres Institutes zu begutachten.

**Dr. Silke Schmalholz** und **Dr. Annegret Bäuerle** möchte ich danken für den Office-Rückhalt, auch schon während des Studiums, und für das Ertragen meiner Papierkram-Phobie.

Für jedwege Laborassistenz möchte ich allen technischen Assistenten des Institutes ganz herzlich danken (auch ehemalige: ja Anna I. ich habe dich nicht vergessen). Mein großer Dank gilt vor allem **Susanne Bogusch**, **Elisabeth Schuster** und **Sebastian Vogel** die mir geholfen haben die Corona Pandemie/das Bicc Paper zu überstehen.

**Paul Bregner** und **Daniel Winkler** möchte ich hiermit für ihre Unterstützung an der Froschfront danken und für den ein oder anderen Exkurs über die Tierhaltung hinaus.

Meinen aktuellen und ehemaligen wissenschaftlichen Kollegen möchte ich danken für die gemeinsame Zeit, die gemeinsam erlebten Konferenzen und dem wissenschaftlichen Input und daraus entstandenen zahlreichen wissenschaftlichen Diskussionen. Insbesondere gilt mein Dank **Melanie Tingler**, **Tim Ott**, **Philipp Vick**, **Jennifer Kreis**, **Franziska Fuhl** und **Kerstin Feistel**. Vielen Dank für die gemeinsame Zeit, die Unterstützung auch in schweren Situationen und die vielen gemeinsam erlebten Grillabende.

Dann möchte ich noch meiner Familie und meinen außer universitären Freunden für ihre Unterstützung in allen Lebenslagen danken. Ohne dieses Vertrauen und den stetigen Rückhalt wäre weder das Studium noch die anschließene Promotion möglich gewesen. Vielen Dank!

Ein großes Dankeschön möchte ich hiermit noch meiner Freundin **Sabrina Mai** ausdrücken, die mir in jeder Lebenslage immer zur Seite stand und ohne die diese Zeit deutlich trister gewesen wäre.